Bolted Connections Between Open Section Beams and Box Columns

by

John Edward France

A thesis submitted to the
Department of Civil and Structural Engineering
in partial fulfilment of the requirements for the degree of:

Doctor of Philosophy

University of Sheffield
January 1997

With thanks to my mum and late dad.

To the memory of;

Alan France (1933-1995, aged 61), Dad
Denis John France (1928-1994, aged 65), Uncle
Lindsey Jade France (1992-1996, aged 4), Niece

Contents

List of tables

List of Figures

Acknowledgements

I would like to thank my supervisors, Dr Buick Davison and Dr Patrick Kirby for their guidance and support throughout my time at Sheffield. Their enthusiasm for the project proved to be invaluable when difficulties were encountered.

I would like to thank the whole of the department for making my stay at Sheffield a pleasant one. There are some special thanks required to the technical staff who helped in the development of the project, notably Mr Shaun Walters and Shane Smith, who constructed the test rig for the project. Also, sincere thanks to Roger Grace, Mick Moore, Jonathan Wood and Andy Marshall, for their general help. A special thank you must also be given to the skill of John Webster, who played an immeasurable part in welding the specimens together and keeping the project on time.

Funding for the project was through British Steel Tube and Pipes who sponsored me and provided the steel for the project. Thanks are gratefully acknowledge to both Eddie Hole and Noel Yeomans, for backing the project.

Declaration

Except where specific reference has been made to the work of others, this thesis is the result of my own work. No part of this thesis has been submitted to any University or other educational establishment for a degree, Diploma or other qualification.

JOHN EDWARD FRANCE

Summary

This thesis reports on the full scale testing of joints comprised of open section beams, bolted to square closed formed columns (SHS) using the novel Flowdrill blind bolting connector. Twenty-six joints were constructed using Flowdrill connectors. In addition six stand alone tests were conducted on endplates. Three joint tests were also conducted using a rival Hollo-bolt connector, in which the joint geometry was nominally identical to those of the Flowdrill joints. Thus a total of thirty-five cantilevered joint tests of member configurations typically found in building frames were conducted.

Only welded endplates were examined in the programme of joint tests which included-partial depth (flexible), flush and extended endplate details. These particular details enabled the full range of both connection stiffness and strength in typical simple and rigid construction to be examined. The aim of the project was to investigate the joint's semi-rigid behaviour, and the acceptability of the flowdrill connector as a method to site bolt the beam to the column rather than using the welded solution commonly associated with closed formed columns.

From the experimental moment-rotation data collected during the tests, a proposed joint model for both the flush and extended endplate details was developed to predict its full non linear behaviour. The model provides guidance on the joint's rotation limit and ultimate design capacity. It assumes that the endplate of the joint is rigid and provides only a limited contribution to the joints overall rotation for its effect to be ignored in the model; the principal failure of all the joints being severe column face deformation. Although the capacity of the connector was not in the original aim of the investigation, an assessment on the published capacities has been conducted for completeness.

As well as providing design guidance for these type of joints, the thesis also presents the results of a parametric study into sub-frame behaviour using the actual joint responses from the test data. The findings suggest that the restraint afforded by the connection on stocky columns in sub-frame arrangements do not outweigh the disadvantages of the moment transfer. A further study on the economics of using tubular columns has also been included. This shows only a marginal increase in cost to that using equivalent open sections, when the advantages of reduced fire protection are included in the pricing.

Notation

b_0	SHS column face width
b_1	Bolt cross centres
b_2	Endplate width
d	Distance from top row of bolts to joints axis of rotation
e_1	Distance from edge of SHS to bolt
e_2	Distance from edge of SHS to endplate
f_y	Yield stress of steel
F_c	Design compression zone resistance of column face derived from yield line pattern
F_t	Design tension zone resistance of bolt group derived from capacity of column face.
$F_{t,str}$	Design tension zone resistance of bolt group derived from capacity of column face allowing for strain hardening and membrane effects.
h	Distance from top row of bolts to bottom of endplate
K_i	Initial stiffness
K_p	Post yield stiffness (membrane stiffness)
L_c	Column system length
m_p	Plastic moment capacity of column wall
m_{p-par}	Plastic column capacity of wall for yield lines developed parallel to axis of column
m_{p-per}	Plastic column capacity of wall for yield lines developed perpendicular to axis of column
$M_{j,expt}$	Moment capacity determined from experimental test
$M_{j,Rd}$	Design ultimate moment resistance of joint
$M_{j,Sd}$	Arbitrary moment developed at joint
P_1	Projection of yield line model based on bolt pitch
P_{cr}	Euler column buckling capacity
P_{pin}	Predicted numerical column capacity with pin ended restraint
P_{sr}	Predicted numerical column capacity with semi-rigid connections incorporated within the sub-frame model
P_{sq}	Squash load of column at yield
t_0	Column wall thickness

$\alpha_{pin} = \frac{P_{sr}}{P_{pin}}$ Alpha pin ratio

$\beta_1 = \frac{b_1}{b_0}$ Ratio of bolt cross centres to column width

$\beta_2 = \frac{b_2}{b_0}$ Ratio of endplate width to column width

ϕ_{cd} Design rotation capacity of joint

ϕ_d Design rotation of joint at $M_{j,Rd}$

ψ Curve fitting parameter

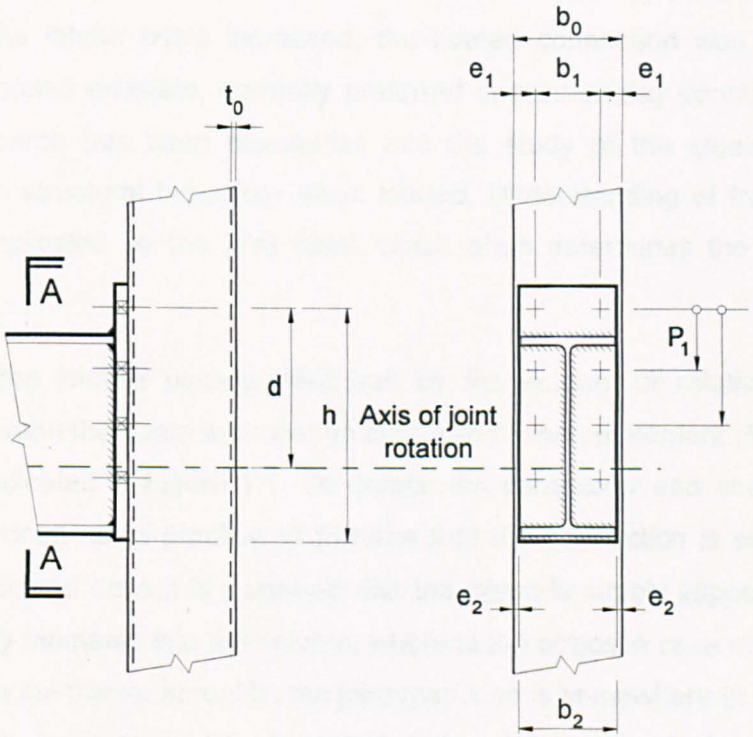

Elevation Section A-A

Joint geometry

Chapter 1

Introduction

The majority of buildings which incorporate a steelwork frame usually consist of open section profiles for both the beam and column members. The popularity of steel framed buildings maybe partly attributed to the ease with which steel members can be pre-fabricated and erected. At the beginning of the 20th century, beam to column connections frequently used the rivet as the connector, requiring access on both sides of the head. As labour costs increased, the riveted connection was abandoned in favour of the bolted endplate, currently preferred in present day construction. During this time, research has been channelled into the study of the steelwork frame to understand the structural behaviour when loaded. Understanding of frame behaviour has been complicated by the joint detail which often determines the distribution of moment.

Behaviour of the joint is usually described by the amount of relative rotation (ϕ) developed between the beam and column centre line, when a moment (M) is applied to the joint, as indicated in Figure 1.1. To reduce the complexity and analysis of frame design, it has been usual practice to assume that the connection is either pinned or rigid. For the pinned case it is assumed that the beam is simply supported and does not transfer any moments into the column, whereas the opposite case of rigid assumes full continuity in the frame. In reality, the joint response is somewhere in between these two extremes, being described as semi-rigid. Figure 1.1 shows a typical joint response for the different categories. Both the extended endplate and fully welded connections are usually assumed to operate as if rigid, whereas the flexible endplate (partial depth) connection is normally assumed to act as a pin.

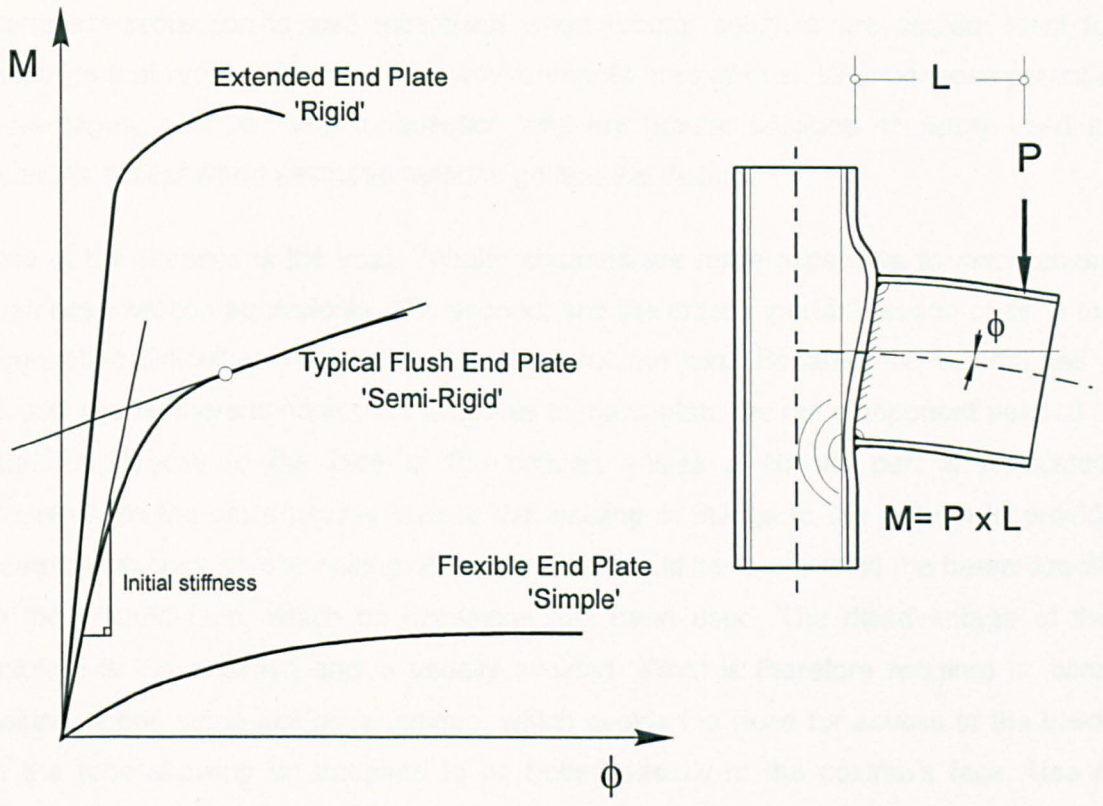

Figure 1.1 Typical moment rotation characteristics of steelwork joints

From the first introduction of the steel frame, the popularity of the open section profile for both the beam and column members has never been in question. The dominance of the profile as a beam member results from the favourable disposition of the section's mass to the extreme fibres of the beam which is suited to developing efficient bending resistance. This cannot be said for the column member under compression where the asymmetrical properties and weakness of the minor axis (compared to that of the major axis), usually produces a buckling type of failure about this axis. It is commonly accepted that the open section column subjected to axial loads for normal storey heights is structurally inefficient when compared to the closed profile of tubular sections.

A natural evolutionary process would lead to a combination of the open section beam and the tubular column. The advantages of using a tubular column section, apart from the obvious gains in structural efficiency, include a smaller area on plan, which not only improves the aesthetics of the building but reduces the cost of any fire protection which needs to be installed. Further benefits relating to fire protection can be achieved when water filled columns are used, providing an exceptional fire rating. Concrete filling can also improve the fire rating and also allows the column load capacity to be increased.

Corrosion protection is also minimised when tubular columns are sealed; ideal for buildings that require clean working environments, free of dust. With all these potential advantages, it is pertinent to question why are tubular sections so rarely used as columns except when aesthetic reasons govern the design.

One of the reasons is the cost. Tubular columns are more expensive to manufacture than open section equivalents. The second, and the most important reason of all, is the connection difficulties incurred at the beam column joint. Because the column has a closed shape, there is no access available to manipulate the nut component needed to site bolt directly to the face of the column unless a special part is fabricated. Connections therefore usually involve the welding of fittings to the column to provide adequate access for site bolting. An alternative would be to site weld the beam directly to the column face, which on occasions has been used. The disadvantage of this solution is the expense and is usually avoided. What is therefore required is 'blind' bolting, a one sided bolting technique, which avoids the need for access to the inside of the tube allowing an endplate to be bolted directly to the column's face. Use of Flowdrill connectors is one such method, where an integral thread is formed into the face of the column, replacing the nut component of the ordinary bolt.

A three year project has been conducted to investigate 'Flowdrilled joints', in which 35 experimental joint tests have been conducted on 'I'-beam to SHS column arrangements with endplates bolted directly to 200x200 SHS columns using flowdrill connectors. The aim of the project was to investigate the joint's suitability for connecting steelwork together and provide sufficient joint characteristic data to enable the development of a proposed moment-rotation joint model developed by the author. The data from the tests has also been used in a Finite Element program to investigate the effect that the joints have on the column collapse load in typical arrangements of sub-frames.

This thesis reports on those tests and the conclusions drawn. Chapter 2 provides background on the flowdrill connector and relevant joint tests conducted with other mechanical blind bolt fasteners. Chapter 3 describes the experimental tests conducted on the simple flowdrill joints with partial depth and flush endplates, with Chapter 4 reporting on the isolated joint tests where identical endplate details used in this programme were tested attached to a rigid base rather than to a column. Chapter 5 provides details of the rigid flowdrill joint tests using the extended endplate. Within this chapter the results of two tests are reported on a rival blind bolt (called 'Hollo-bolt')

enabling a direct comparison to be made with a nominally identical flowdrill joint. Chapter 6 reports on flowdrill joint tests conducted where the column tube was concrete filled. These results are compared directly to nominally identical joint tests of both the simple and rigid categories.

Analytical work to predict the moment-rotation response is reported in Chapter 7, with a review of the response of simple flexible endplates and the contribution of such behaviour, to the joint's overall rotation. The isolated endplate characteristics, reported in Chapter 4, have also been directly compared to predicted response using the EC3 Annex J joint model. Chapter 8, reports on the author's own joint model, where the results have been compared to the joint test data. The results of the sub-frame analysis using the actual joint moment-rotation characteristics have been assessed in chapter 9.

Finally, the economic aspects of using tubular columns have been reported in Chapter 10. This chapter provides a direct comparison of column costs between both the closed and open profiles for a typical building development.

As a final note to avoid undue confusion of terminology, reference has been made to 'tubes', which may cause the reader some concern when the column sections used in the tests are square. Tube is a general word which can describe both geometries. Reference has also been made to SHS which stands for Structural Hollow Section's, a term which can also describe the range of circular sections produced. The correct terminology to use to describe a square section would be RHS (Rectangular Hollow Section). However, in this thesis the term SHS has been commonly used to define Square Hollow Sections. Other terminology which may cause confusion is the use of face and wall. Here the 'face' describes the side to which the beam is connected whilst wall refers to the webs or adjoining faces of the section.

Chapter 2

Background

Previous work on flowdrill joint may be separated into two distinct areas of research: semi-rigid behaviour of open sections and that of tubular construction. These two areas cover extensive investigations on the subject that can be traced back to 1917 [1] with the first joint tests conducted on riveted joints comprising of open sections. It is impossible to cover both of these topics separately in this short chapter, consequently the background has been restricted to the less extensive and more recent work with tubular construction.

2.1 Manufacture of tubular columns

Modern hot finished welded hollow sections are produced using an electric welding resistance technique. This method was originally developed by Babcock & Wilcox Ltd of America. The first tube to be produced in this country using this method was in 1951 by Stuart and Lloyd at their Corby Steel works, now British Steel Tubes & Pipes division.

The modern method of tube manufacture relies on a continuous strip of cold steel fed through a series of rollers which gradually shape the initially flat steel into a circular profile. At this stage the section is circular with the edges ready to be welded together to close the cross section. The electric resistance welding process is now used to weld the profile together. This process uses high frequency radio waves to locally heat up the two edges of the profile as it is fed through at high speed. The edges are then forced together thereby welding into the closed profile. No material is deposited in the welding operation. All sections fabricated are circular with one diameter. To produce the required section size, the tube is heated and passed through another series of rollers which shape and stretch the tube into its final thickness and profile, of either a square, rectangular or circular geometry. A different method has been recently introduced at Corby using the cold formed process of SHS manufacture in which the production is as above but no final heating of the steel is conducted and the section is

left with very high residual stresses from the welding process. Only hot formed SHS columns have been used in the joint tests reported herein.

2.2 Connections in tubular construction

The majority of research conducted into tubular construction has been co-ordinated by CIDECT (Comite International pour le Developpement et l'Etude de la Construction Tubulaire). This organisation was founded in 1962 by tubular manufactures to compile and assess research data into guidelines for design. Their efforts have formed the basis for other design codes [3].

The main area of work covered by CIDECT has concentrated on the development of welded tube to tube joint arrangements more commonly associated with roof trusses and off-shore oil platform jackets. Many research organisations have contributed to the understanding of this type of joint by conducting full scale isolated tests of branch to chord connections [4]. A sizeable portion of tests were conducted at Sheffield. These, together with other research organisations tests are reported in CIDECT Monograph N0. 6 [5]. The recommendations for the ultimate strength of these type of joints were derived from empirical relationships based on experimental evidence.

Other types of connections relate to the beam-column joints of either simple or rigid classifications. These two categories are discussed in the following sections.

2.2.1 'Simple' joints with tubular columns

Typical connection details for simple framing usually adopt a fitting welded to the column which supports the beam and allows clearance for site bolting. Figure 2.1 indicates examples of some of the more common types of simple joints which include the seating angle, web cleats, top and bottom angles or the fin plate (tab plate). A detailed survey of these connections has been conducted by the SCI [6].

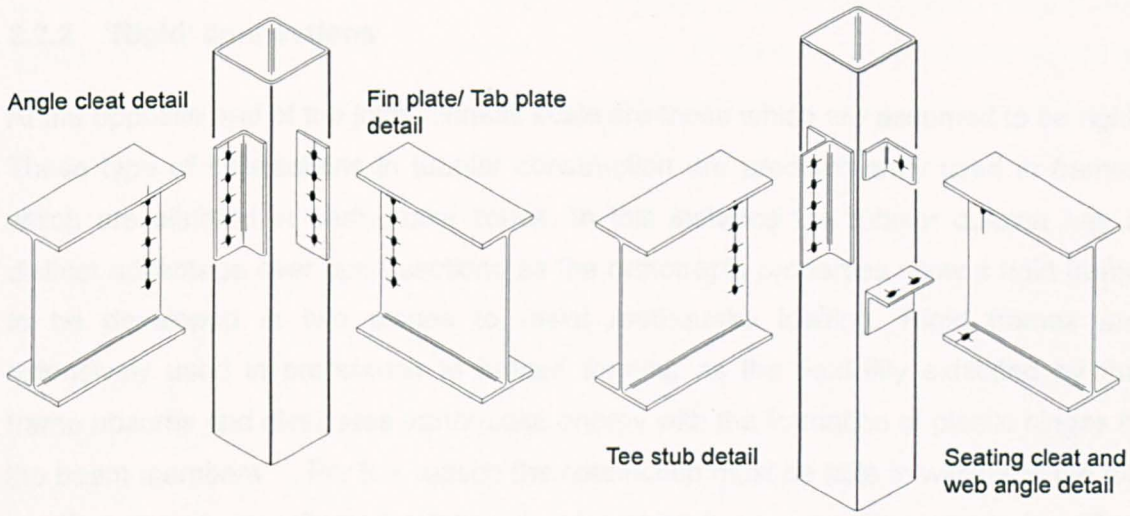

Figure 2.1 Typical existing site bolted simple joint details

Of the connections previously mentioned, the shear tab or fin plate is probably the most frequently used of all because of its simplicity and the ease with which the beam and column can be bolted together. Research into its behaviour was conducted as early as 1966 by White & Fang [7] who observed that the beam's end rotation and fixity under load distorted the column's wall. Subsequent recommendations from the tests suggested that the tab plate was only to be used for secondary connections due to the effect of wall distortion on column capacity. Ales [8] continued with tests on both the shear tab and the through plate (a connection where the plate travels all the way through the hollow section and is welded on both faces), observing similar flexibility, but concluded that the through plate presented a better connection detail with less wall distortion.

Nearly all of the investigations into shear tab performance have been concerned with 'open' section column profiles [9] rather than the SHS. The resulting design methods have then been applied to the SHS assuming a similar performance, in which the wall distortion has little or no effect on column capacity. The only research (since the original tests by White & Fang) which has been conducted into the influence of the connection's performance on column capacity has been through the work of Haslam [10]. In this investigation, eight column assembly tests were conducted. Small tube wall thickness exhibited reduced capacity, although this conclusion is based on a small number of tests.

2.2.2 'Rigid' connections

At the opposite end of the joint stiffness scale are those which are assumed to be rigid. These type of connections in tubular construction are predominantly used in frames which are situated in earthquake zones. In this instance the tubular column has a distinct advantage over open sections as the orthotropic properties allow a rigid frame to be developed in two planes to resist earthquake loading. Rigid frames are extensively used in preference to braced framing as the flexibility exhibited by the frame absorbs and dissipates earthquake energy with the formation of plastic hinges in the beam members [11]. For this reason the connection must be able to withstand the full plastic moment capacity and rotation developed by the beam. Other areas identified where rigid joints could appear are within vierendeel girders (a variation on the rigid frame).

The simplest rigid connections are those where the beam is welded directly to the column face. A number of investigations have been conducted on this type of joint[12,13,14] and both the rigidity and strength of the joint have been found to be dependent on the beam depth and thickness of column wall. One way of increasing the capacity of the joint is to reduce the amount of face flexure of the column. This can be achieved by using beam sizes approaching that of the column width. Such joint tests have been conducted by Mehrotra [15] using tubular beam and column members. The results were reasonable, with expected web buckling of the column cited as the main cause of failure.

Increasing the beam width may at times be impractical. Stiffening of the joint with welded plates is an alternative solution for welded connections. Dawe & Grondin [16] has conducted a number of joint tests where cover plates have been welded to the top flange. Further stiffening of the joints was also introduced by the addition of doubler plates welded to the face of the column to increase the face capacity in flexure. Other ways of increasing the joint capacity has been investigated by Picard & Giroux [17] who used angles strapped either side of the beam. Similar concepts of joint stiffening have employed 'tee' sections welded either side of the beam flange and then onto the column walls [18, 19].

A more common method often adopted to provide the beam's full moment capacity at the joint, is to incorporate a steel diaphragm welded to the top and bottom of the beam[11]. An external or internal diaphragm can be used. External diaphragms require

the plate to be shaped around the column, whereas internal diaphragms require the column to be cut and welded in between. The use of this type of connection provides the best possible rigidity, but with obvious fabrication expense.

2.3 Blind bolting connections

The majority of the frames constructed in the UK are assumed to be pin jointed, relying on simple jointing techniques and flexible endplates. If tubular columns were used then the connections described in section 2.2.1 would usually be adopted. These connections all have one disadvantage; welding fittings to the outside of the column is both costly and the fittings are prone to damage during both transportation and site erection. What is required is a connection technique which allows flexible traditional endplates to be bolted directly to the column face, thereby allowing the column to be drilled normally.

Previous attempts to bolt connections to tubular columns have frequently necessitated the provision of access holes to allow the nut to be tightened from the inside. Both the size and position of the holes severely weakens the section. As a solution, recent attention has been directed towards blind bolted connections which allow the joint to be fastened from the outside.

One blind bolting scheme has been investigated in the joint tests conducted by Kanatani et al[20] in which concrete filled SHS columns incorporated extended endplates bolted on opposite faces of the column. The bolts passed through both endplates, clamping the column in between. The disadvantage of this method was that the connections made at 90 degrees would need to be staggered to avoid the bolts clashing as they passed through the column. Other attempts at blind bolting have concentrated on welding a threaded stud to the column face (similar to the Nelson stud). Maquoi et al[21] has tested a range of joints with threaded studs, using various connection details from web angles to extended endplates. More recently, the technique has been employed by Vandegans[22] on concrete filled tubes. The problem suffered by the stud technique is the damage which can be inflicted on the studs during transportation, similar to that of the fin plates mentioned earlier. The erection of the last beam can also be quite tricky if using a flush endplate detail, as the studs project outside of the column.

Recent attention has been drawn to blind bolting methods which involve no projection beyond the column's exterior. One series of joint tests conducted by Kato[23] used

special nuts which were welded into the column wall, providing a smooth finish to the column exterior. Other methods of forming a connector use mechanical blind bolts, which are specially designed to work with ordinary drilled holes. These bolts are inserted through the endplate and column and expand at the back when tightened from the front, thereby mechanically clamping the endplate to the column face.

The most recent mechanical blind bolts have been the BOM (blind oversized mechanically locked), HSBB (high strength blind bolts) and Ultra-twist fasteners developed by Huck International. The first two bolts work on the principle of a ratchet which pulls a central pin to expand the back. A collar at the front is crimped around the pin to clamp the front. Both the BOM and HSBB bolts have been investigated with extended endplate details [24- 27]. The ultra-twist bolt [28], shown in Figure 2.2, is a more recent development, superseding the other two by removing the complicated ratcheting system and working on the principle of a nut at the front torqued up. Similar endplate joint tests have also been conducted using this bolt [29]. At the other end of the scale another blind bolt has been developed by Lindapter International, called Hollo-bolt, which is considerably simpler than all the other mechanical bolts mentioned. This particular bolt has been tested in this programme of joint tests as a direct comparison to the flowdrill joints and is described later on in the thesis.

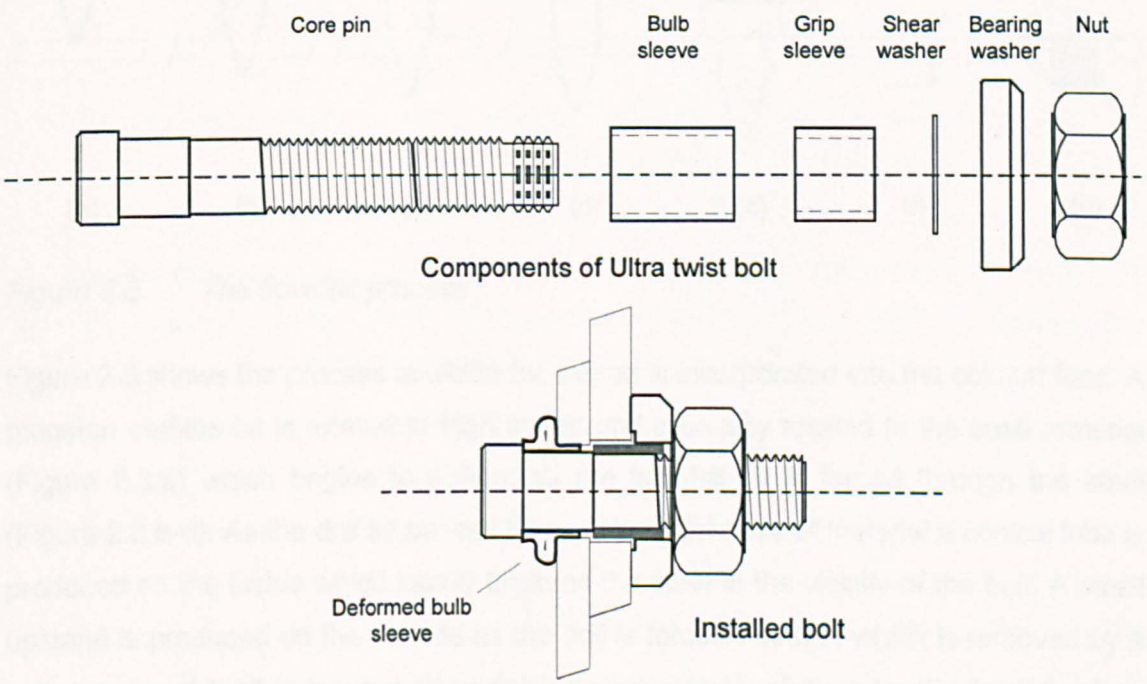

Figure 2.2 Ultra-twist bolt.

2.3.1 Flowdrilling process and previous research

The flowdrill process is a technique which allows a thread to be incorporated into relatively thin steel using a process of thermal drilling which locally displaces metal and increases the thickness sufficiently to permit tapping of a thread into the steel. It was developed in 1923 by Jan Claude de Valliere [30] as an alternative to conventional drilling. Although the concept was successful, practical applications were not forthcoming until almost sixty years later when technical developments made possible the use of tungsten carbide material for the drill bit, machines to generate the complicated profile and diamond grinding wheels for hard materials.

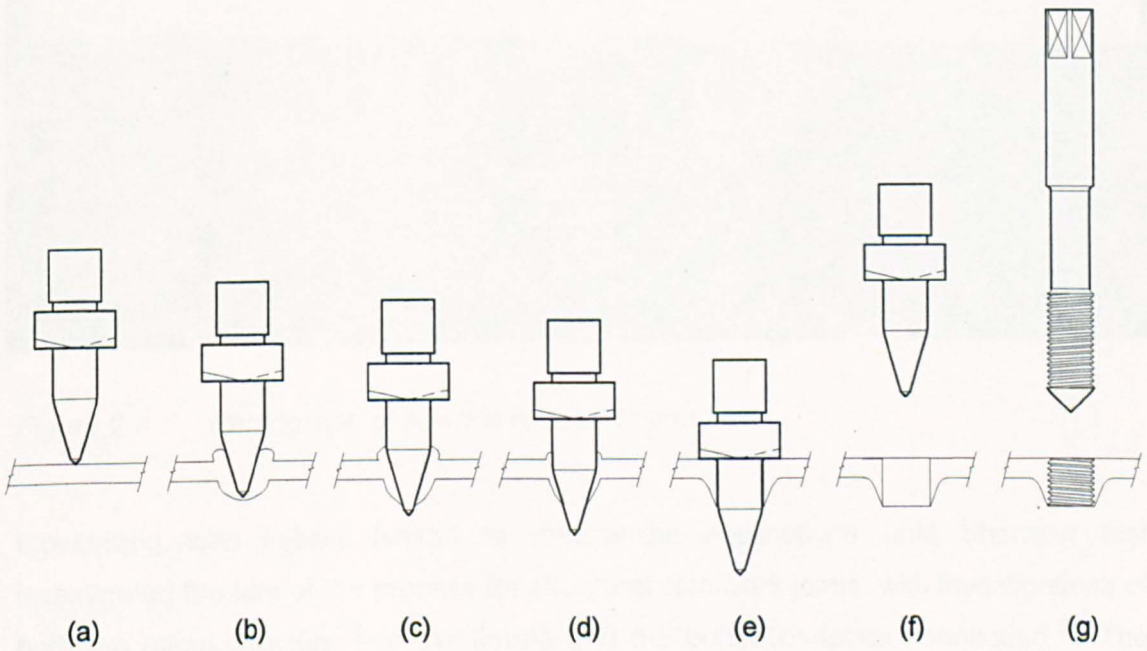

Figure 2.3 The flowdrill process

Figure 2.3 shows the process in which the thread is incorporated into the column face. A tungsten carbide bit is rotated at high speed and gradually applied to the base material (Figure 2.3,a) which begins to soften, as the flowdrill bit is forced through the steel (Figure 2.3,b-d). As the drill bit passes through the thickness of material a conical lobe is produced on the inside which locally thickens the steel in the vicinity of the bolt. A small upstand is produced on the outside as the drill is forced through, which is removed by a cutter on the drill bit to leave a clean finish on the exterior of the tube (Figure 2.3,e,f). A cold formed thread capable of accepting a normal grade 8.8 bolt without any special modifications can now be successfully introduced, (Figure 2.3,g). The process is only

required up to 12.5mm thickness. Greater thicknesses of wall can be drilled and tapped in the normal way. Figure 2.4 shows both the bolt and flowdrill thread.

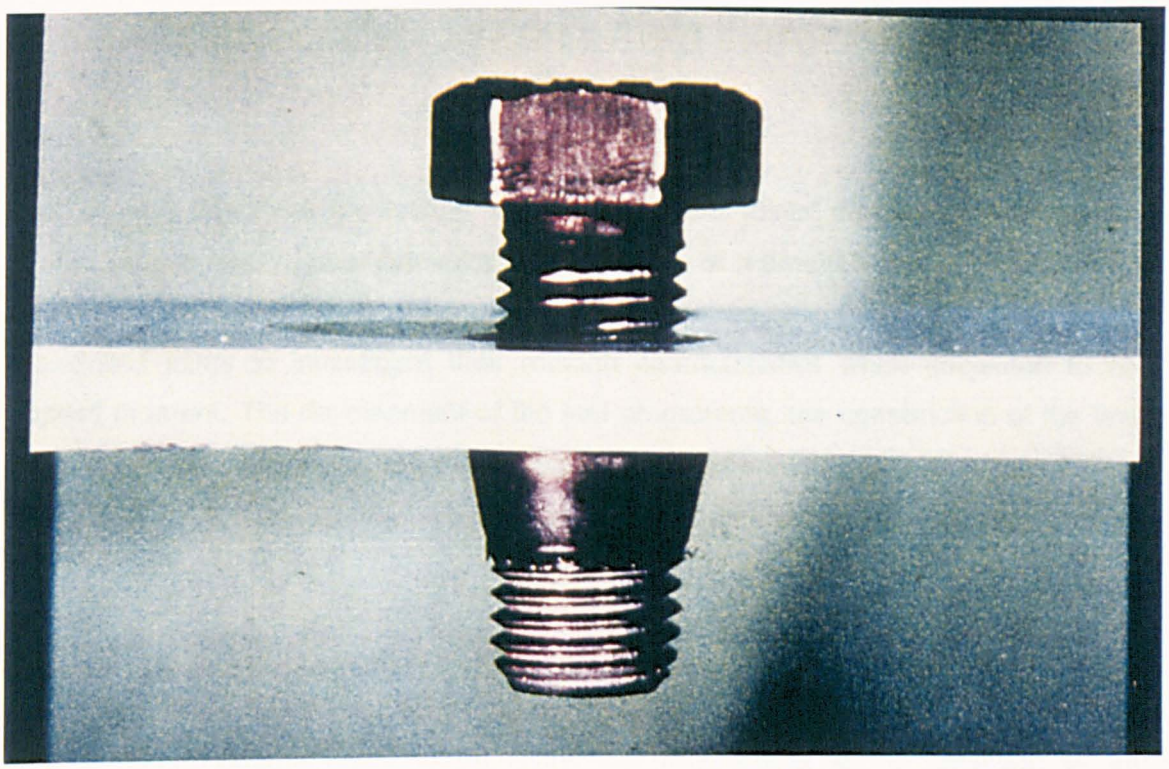

Figure 2.4 Photograph of flowdrill connector and bolt

Flowdrilling was initially limited to mechanical applications until Sherman first investigated the use of the process for structural steelwork joints, with investigations of both the micro-structure [2] of the thread and the bolted endplate connection [31]. The findings by Sherman were promising, suggesting that the bolts could be used with tubular columns. Further work by Banks [32, 33] and Ballerini et al [34, 35] have also investigated extensively the connector's performance. The majority of these projects have concentrated on the connectors performance in shear and tension rather than overall joint behaviour. Relatively few tests of endplate to column connections had been conducted prior to this project. The majority of the tests have been more concerned with 'tee'-stub arrangements that were bolted either side of the column and pulled apart to investigate the tensile capacity of the connector for use in structural integrity checks [33]. The only known tests conducted on the extended endplate and on the flush simple endplate detail have been reported by Yeomans [36, 37]. The extended endplates of Yeoman's joint test programme are described later on in the thesis.

Chapter 3

Experimental tests on simple Flowdrill joints.

This chapter describes the testing of 'simple' flowdrill joints, which are designed as pinned, but in reality usually develop some degree of moment transference between beam and column. A series of joint tests was conducted on a typical range of simple Flowdrilled joints to investigate their rotation characteristics when subjected to an applied moment. The development of the test programme, the construction of the test rig, the test procedure and the instrumentation of the joints are reported on. A final discussion on the variation of joint parameters that influence the overall moment-rotation behaviour is presented.

3.1 Development of an appropriate test programme on simple joints

One of the problems faced in any joint test programme is the selection of an appropriate member size and joint detail suitable for investigation. At first this appeared to be a formidable exercise as the possible combinations of joint geometry is immense, especially since there is little standardisation within the UK steel fabrication industry; a problem which arises from each individual fabricator preferring a particular connection detail.

Fortunately the problems faced with respect to connection details associated with open sections are greatly simplified by the use of the flowdrill connectors and tubular columns. In these instances a reduced combination of joint variants can be established as the connection is not hindered by adjacent details framing into the SHS column. The investigation will sought to investigate the most favourable and least favourable joint constraints that can be imposed onto the column. From this view point it was decided to restrict the series of tests to welded endplates which incorporated only partial depth and flush endplate details. The programme was simplified by the utilisation of only one serial size of tubular column for the overall joint test programme. By adopting these constraints and realising the potential for standard details offered by flowdrill connectors the selection process for the joints emerged.

To help in the selection of the member sizes an economic study (reported on in Chapter 10) was completed on typical buildings that may employ the flowdrill system and more importantly provided some practical significance to the joint tests. It was found that the 200 serial size of SHS column member would represent a typical column in a multi-storey frame. The decision was taken to adopt the 200 section as this particular serial size also provided a large variation of tube wall thickness for the tests. It was also decided to adopt the 356 UB as the benchmark serial beam size. The 356 UB serial size was partly based on the study, but was also guided by the practical aspects associated with the limitations of the jack size, to the future expansion of the study to the rigid joint details and the height restrictions imposed by the lab space to provide the leverarm for the jack.

Preliminary calculations on the joint moment capacity was carried out where yield lines forming in the column face allowed an approximation of jack and leverarm value to ensure failure. A reserve of jack capacity was included in the calculations which allowed for any increase in nominal column yield strength that may be present. This reserve played an important role as the jack capacity used to apply the moment at the joint was overrated because the available hydraulic pump developed only 3000 psi rather than the 5000 psi required to run the jack at full capacity.

3.2 Programme of joint tests

The programme of simple joint tests is shown in Table 3.1. The series of tests was constructed around joint test number '4' which uses the 356 UB attached to the 200 box section with flush endplates. All other parameters examined in Table 3.1 are variants of this joint detail. Details of the simple joints tested referred to in Table 3.1 are shown in Figure 3.1

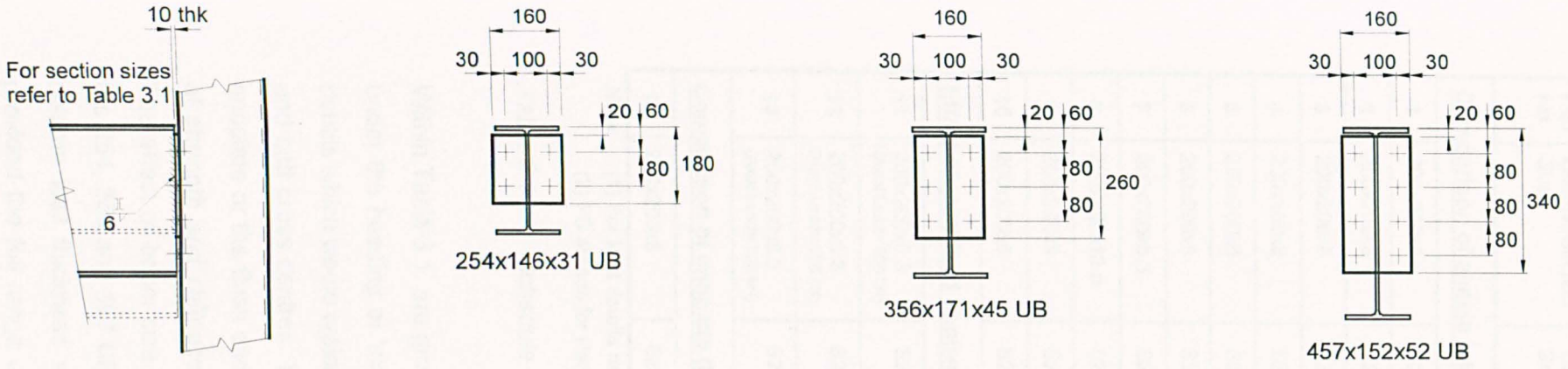

Partial Depth Endplate Details (PD)

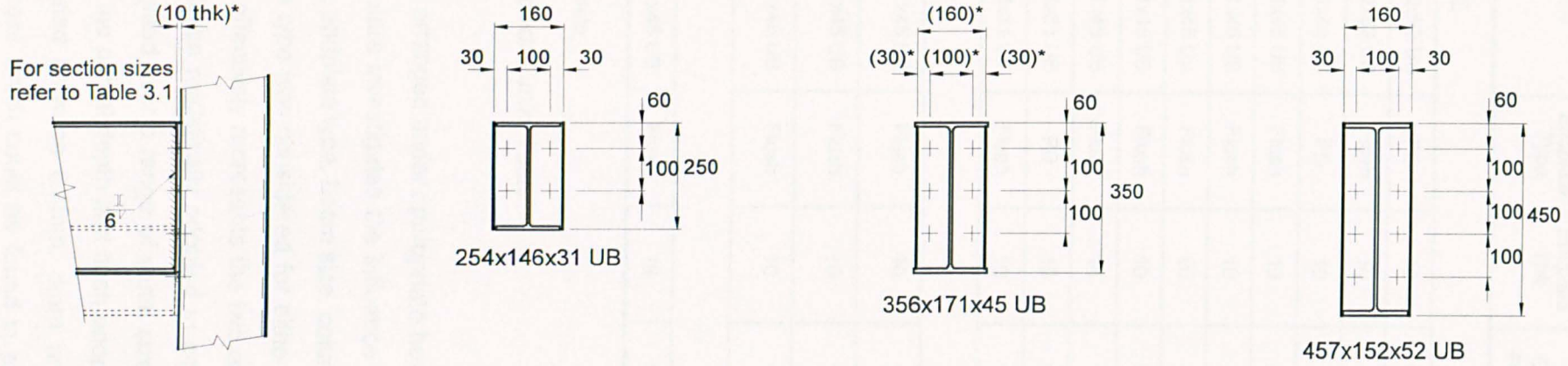

Flush Endplate Details (FE)

NOTES: (1) M20(8.8) bolts used throughout.
(2) Where values are bracketed thus ( )*, refer to table 3.1 for variations to dimensions shown.

Figure 3.1 Details of endplates adopted for Simple Flowdrill joint tests

Test No.	*Column Section Size*	*Steel Grade*	*Beam size*	*Endplate Type*	*Endplate Thk.*	*Bolt Cross-centres*	*Concrete Filled*
Comparison of simple joint parameters							
1	200x200x8	S275	457x152x52 UB	PD	10	100	
2	200x200x8	S275	457x152x52 UB	Flush	10	100	
3	200x200x8	S275	356x171x45 UB	PD	10	100	
4	200x200x8	S275	356x171x45 UB	Flush	10	100	
5	200x200x8	S275	356x171x45 UB	Flush	10	80	
6	200x200x8	S275	356x171x45 UB	Flush	10	120	
7	200x200x6.3	S275	356x171x45 UB	Flush	10	100	
8	200x200x12.5	S275	356x171x45 UB	Flush	15	100	
9	200x200x8	S275	254x146x31 UB	PD	10	100	
10	200x200x8	S275	254x146x31 UB	Flush	10	100	
Effect of axial load applied to SHS							
11	200x200x6.3 (Axial Load= 506 kN)	S275	356x171x45 UB	Flush	10	100	
12	200x200x6.3 (Axial Load= 906 kN)	S275	356x171x45 UB	Flush	10	100	
13	200x200x6.3 (Axial Load= 702 kN)	S275	356x171x45 UB	Flush	10	100	
Comparison of endplate thickness							
18	200x200x8	S275	356x171x45 UB	Flush	15	100	

Note: (1) For joint details refer to Figure 3.1
(2) PD stands for Partial Depth endplate

Table 3.1 Schedule of Simple Flowdrill Joint Tests

Within Table 3.1. are groups of joints arranged under appropriate headings. The group under the heading of 'simple' joint details investigates the influence of various design details which would typically included; endplate type, beam size, column tube thickness and bolt cross centres. The endplate type was considered for either the partial depth endplate or the flush endplate which effectively represents the two extreme conditions of strength and stiffness, which could be realistically adopted in simple joint details. The effect of beam size was investigated over a range of serial sizes which included the 254, 356 and 457 UB's (for both the partial depth and flush endplate details). The column wall thickness was also varied between 6.3mm, 8mm and 12.5mm. This provided the full range of wall thickness which could be found in practical situations

(the 12.5mm wall being the maximum thickness of material where the flowdrill connector is appropriate, material thicknesses greater than this do not require the use of flowdrilling). Another parameter which was varied within this group heading relate to the bolt cross centres where the 80mm, 100mm, and 120mm were examined. The standard bolt cross centre used in the majority of the tests was 100mm.

The other sub-heading in Table 3.1 relates to the effect of column axial load on the joint moment-rotation characteristic. Usually a column is subjected to varying axial loads. It was decided that the influence of such an important parameter needed to be investigated. This was done by varying the ratio of applied compressive stress for each individual test conducted on the smallest serial column size available in the 200 range of SHS using the flush endplate connection. The smallest column size was selected to allow the greatest variation of stress for a given axial load range and allowed the flush endplate connection to induce a more severe deformation of the tube face leading to a worst case combination.

3.3 Test rig development and construction

The two most common joint testing arrangements to be used for joint tests are either the cruciform or cantilevered methods. In the cruciform method of testing two beams are connected to either side of a column and subjected to a central point load as the outer ends of the beams are supported. The advantage of such a method is the simplicity of testing and the ability to acquire two moment-rotation characteristics produced during a single test. The disadvantage is that one side of the joint can be affected by moment shedding [38] if the test apparatus is not perfectly symmetrical. Such a method is simple to construct and use. The second method uses the cantilevered form of arrangement where only one beam is connected to the column. Both of these methods represent the conditions found in steel frames where the cruciform test mimics the geometry imposed by the internal column and the cantilever method simulates the conditions of an edge column detail. The disadvantage of cantilevered testing of the joints is the increased complexity of the testing arrangement and the test rig. However, the test of joint performance is more onerous and allows a full examination of the effect of shear panel deformation.

Because of the requirements to test the joint under large axial loads, practical considerations required the column to be positioned horizontally. The moment that was required at the joint resulted in a large leverarm for the limited jack capacity available.

A test arrangement based on the cantilevered method was used where a separate jack was used to maintain the column load, while the joint moment was applied independently from a hydraulic ram located at a suitable distance from the connection. Figure 3.2 shows sectional elevations of the test rig developed for the simple joint details, showing the arrangement of the two jacks, whilst figure 3.3 shows an overall photograph of the test rig.

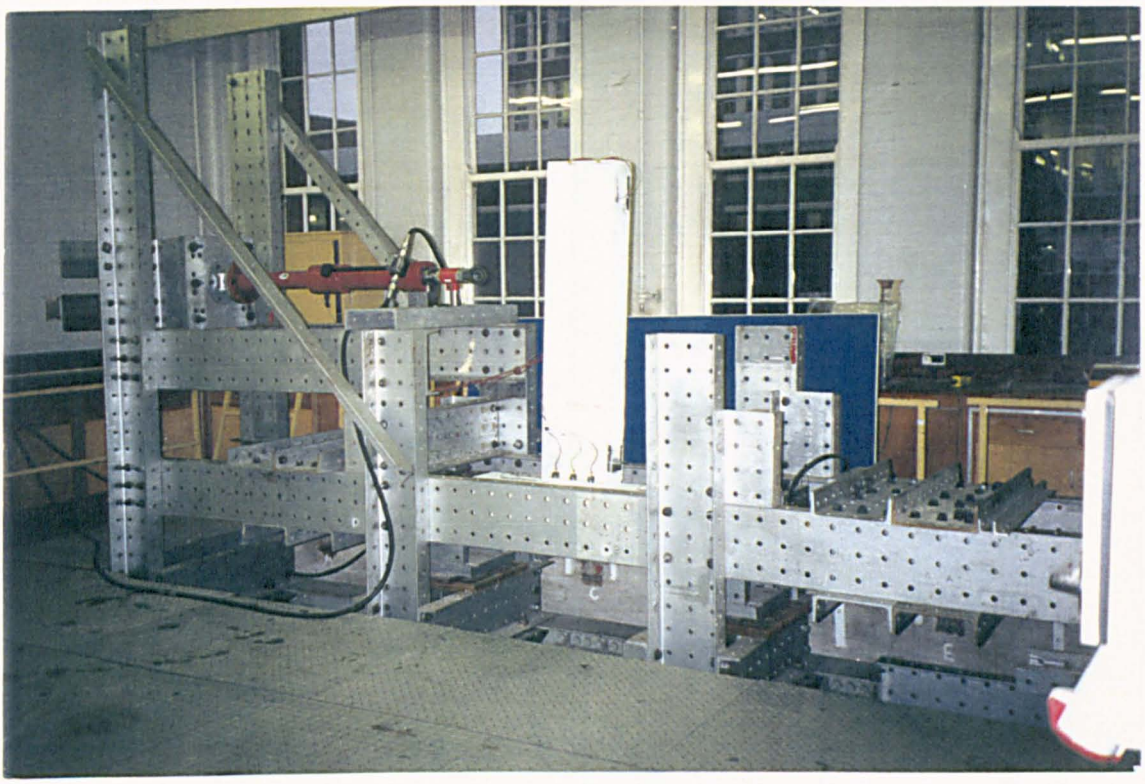

Figure 3.3 Photograph of test rig used with Simple joint details

The test rig was constructed from 305x102 channel sections. Each channel incorporated 22 diameter holes at 100 mm grid spacing and a 50 mm backmark which allowed the sections to be bolted together with M20 HSFG (high strength friction grip) bolts into the arrangement shown. The test rig was built on a strong floor and securely bolted to it. Figure 3.2 illustrates a typical joint test bolted into the test rig and ready for testing. Note that the specimen is at 90 degrees to the position it would normally occupy in a real steel frame. The axial load was applied through a 1000 kN capacity short jack which was under load control. The jack was placed in line with the column between two self straining channels, which enabled the load to be contained by reacting against the endblocks that straddled the two channels at each ends of the column specimen. Spherical seating arrangements were used in the end blocks to ensure that the jack load was applied centrally to the column specimen, with guides used on the cap plates to locate the column accurately into its final alignment.

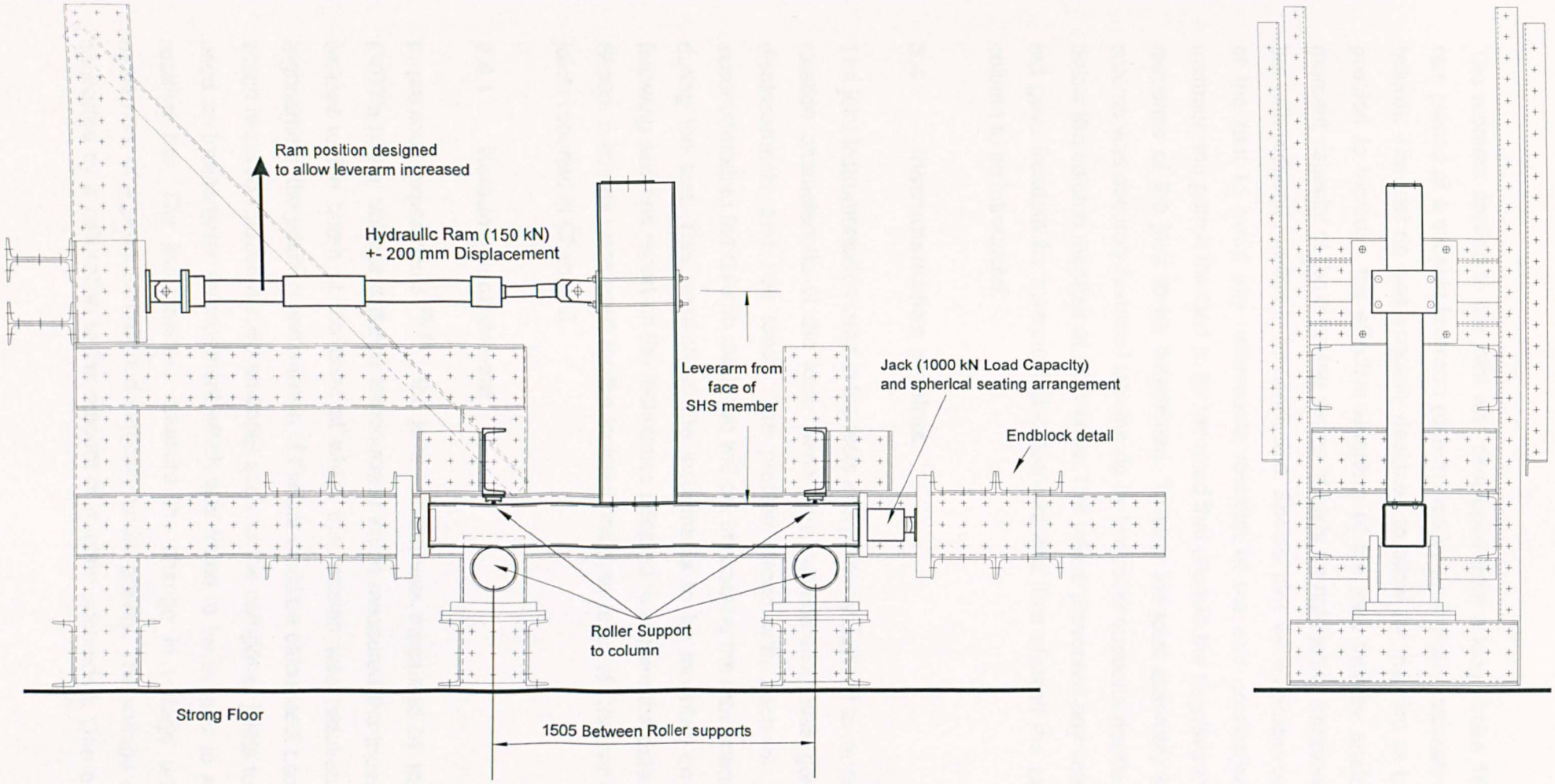

Figure 3.2 Details of test rig and joint arrangement for Simple Flowdrill joint tests

The moment applied to the joint was developed from a long stroke 150 kN hydraulic ram placed at a suitable leverarm (determined by preliminary calculations to generate failure). The test rig was specially designed to allow for the ram to be moved up in position to increase the effective leverarm of the joint thereby enabling the higher moment capacity of the following series of tests on rigid joints (reported in Chapter 5) but with reduced rotation to be conducted. Special pins were constructed at either end of the ram to avoid any undesirable restraint at the end connection to the beam member and permit the load to be reversed that allowed the negative moment-rotation response of the joint to be determined. To stop the joint assembly from lifting, the column was securely fastened into the rig by two roller supports positioned above and below the column member at both ends. The rollers prevented any vertical movement but gave freedom for horizontal displacement and thus allowed the axial load of the column to be introduced.

3.4 Instrumentation of joints

The joint instrumentation used in the tests was primarily devised to record the moment-rotation characteristic of the joint. Secondary consideration was given to the bolt displacements and bolt loads. The problem faced with each of the tests was accommodating the column axial load without obstructing the movement of the column during the test. This required all the instruments to be mounted on the joint. The following sections report on the techniques adopted to acquire the data from the tests. Similar methods were used for the isolated endplate tests of Chapter 4 and the rigid joints reported in Chapter 5.

3.4.1 Rotation measurement

In previous experiments [39, 40], the joint rotation was measured by the use of three LVDT's (linear voltage distance transducers) which measured the movement of a bar welded to the beam at the point at which the rotation was required. From simple trigonometry the position and rotation of the bar could be calculated. Later experiments which required rotation measurements,- such as the composite joints tested by Lam [41] used an inclinometer arrangement which was found to be simpler to set up than the rotation bar. The inclinometers measure the change in voltage arising from the movement of a pendulum aligned vertically under gravity. The voltage change is then converted by a calibration to the amount of rotation subtended. One of the problems

encountered with the inclinometers, and found with other systems which rely on gravity, was that such instruments are prone to fluctuate throughout the test as a result of the dynamic response of the pendulum to vibrations. This problem was solved by Lam [41] who immersed the pendulum in oil to dampen its response to movement. Because of the ease in which the inclinometers can be set up, they were adopted for the flowdrill joint tests.

The Penny and Giles inclinometers used in the joint tests were calibrated over an operating range of 22 degrees. The required joint rotation was the relative rotation of the beam and the column. Therefore one inclinometer was positioned on the centre line of the column while a second inclinometer was located on the centre line of the beam, 125mm from the column face. The relative rotation of the joint was measured as the difference in readings between these two inclinometers.

3.4.2 Bolt displacement measurements

A secondary interest in the tests was an investigation of the component deformations of the joint and an examination of the joint's rotation pivot throughout its loading history. To conduct such investigations, LVDT's were positioned directly over the bolts and attached to the underside of the column, allowing the relative movement of the bolt and hence the face deformation to be monitored. There were also two LVDT's positioned a set distance outside of the beam's flanges to allow for a second check on the overall rotation, in case of failure of the inclinometers but perhaps more importantly to determine the movement of the axis about which the joint was pivoting.

3.4.3 Strain gauged bolts and bolt load measurements

As part of the examination of the joint's component response, attempts were made to determine bolt load during each of the tests. However, the results proved to be disappointing. At the beginning of the project it was assumed, quite wrongly, that the bolt measurement was a relatively simple task of adapting the techniques of strain gauged bolts used in previous investigations [97] into open section beam to column connections. It was subsequently found that the bolt's response under load is significantly more complicated than first envisaged.

The majority of popular bolt force measurement techniques [42] rely on the determination of the bolt elongation. This is done directly by positioning strain gauges on the shank of the bolt or by measuring the elongation of the bolt. An indirect method of bolt force

can be measured by means of a ring load cell. However, to incorporate this into the joint test may entail some modifications to the joint detail (bolt spacing, edge distances etc.). For this reason, only the direct measurement of bolt force was considered for further examination.

Although the idea of measuring bolt elongation under load appeared simple, the reality of achieving this in practice was more difficult than first appeared. A bolt under load will have various amounts of strain at different locations of the bolt. The strain in the threaded area will vary with each bolt as the thread of the bolt connects with the thread of the nut or Flowdrill connector. A complex interaction will also occur directly under the bolt head as the resultant contact changes from either deformation in the joint itself or subsequent local yielding of the washers. The only position which results in a uniform strain is that of the shank of the bolt in between the thread and the bolt head, which has been known to respond linearly at, and above the bolt's proof load.

Three types of bolt load measuring devices were examined at various stages in the joint test programme. The methods assessed comprised; external shank strained gauged bolts, internally strain gauged bolts (adopted for the joint tests) and finally direct measurement of bolt elongation. All the bolts were calibrated in a 100kN load controlled universal testing machine.

3.4.3.1 Externally strained gauged bolts

The first attempt at determining the bolt load was made by positioning three strain gauges (3mm long) on to a M20 bolt, directly under the bolt head. The bolt adopted was fully threaded, requiring the shank diameter to be reduced to provide a smooth surface to locate the strain gauges under the bolt head, as indicated in Figure 3.4(a). This was the only place in which the gauges could be located within the depth of the 10mm thick endplate zone without them suffering damage. The reduction of the bolt's cross sectional area significantly decreased the bolt capacity but was offset by the protection afforded to the gauges as the bolt was bearing in the hole.

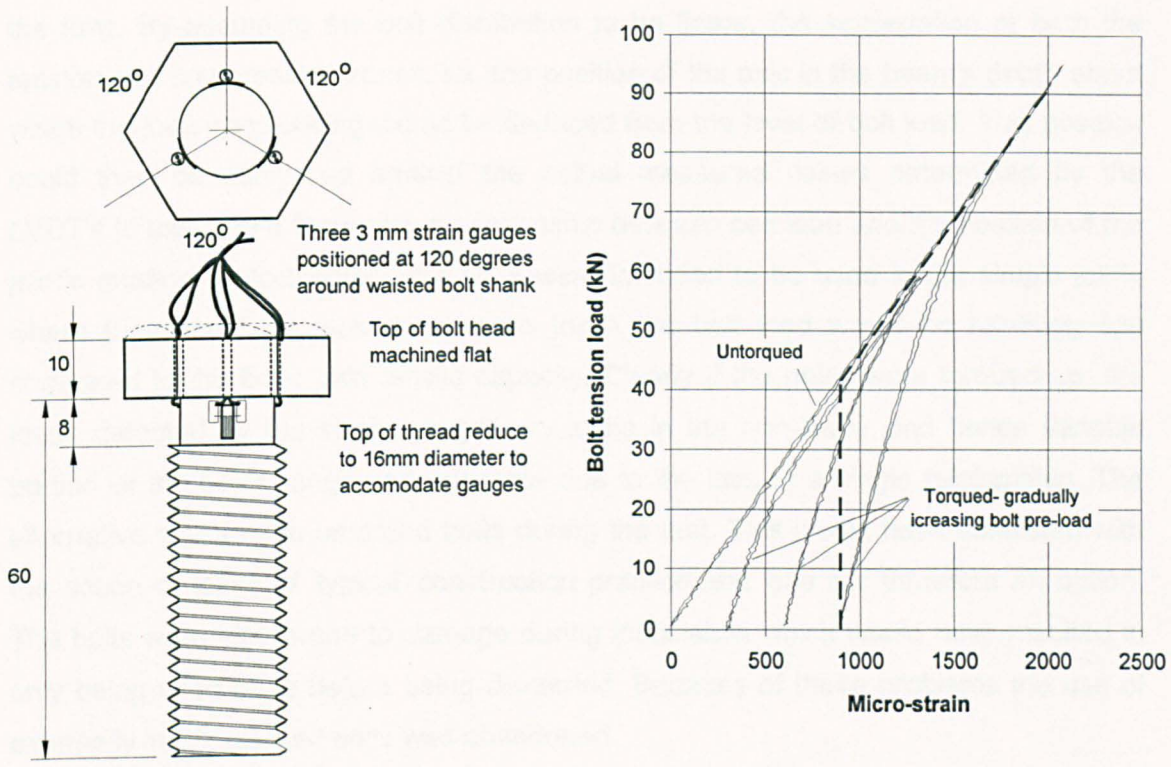

(a) *(b)*

Figure 3.4 *Strain gauge response for externally located gauged bolt under tensile load*

With the bolt untorqued, measured output from the gauges produced a response which was both linear and repeatable. Even with a pack positioned under the head, to induce bending, the average output from all three gauges was the same for that of a bolt without induced bending. Unfortunately problems were encountered when the bolt was torqued to a level that was to be adopted in the actual joint test. A significant non-linear response was encountered at various levels of bolt pre-load, as shown in Figure 3.4(b). The non-linear response of the bolts occurred at relatively low torque levels. In theory when the bolts are pre-loaded, i.e. subjected to an initial torque, the level of strain recorded by the bolt from the initial moment applied to the joint should remain constant, until the connection induces a level of bolt load greater than that from the initial applied torque. After the bolt exceeds this level of load, the load vs. strain plot should reflect that of the untorqued bolt, increasing linearly as shown by the dashed line in Figure 3.4(b). It is evident that the torqued bolts do not respond in this way in practice.

The reason for using the bolts in the joint tests was to determine the movement of the joint's rotation pivot by examining the bolt distribution throughout the loading history of

the joint. By assuming the bolt distribution to be linear, the segregation of both the tension and compression zones, i.e. the position of the axis in the beam's depth about which the joint was rotating, could be deduced from the level of bolt load. This position could then be compared against the actual measured values determined by the LVDT's to examine if there was a relationship between bolt load and the position of the joint's rotation. Unfortunately, the bolts were intended to be used in the simple joints where they could be reused. In these joints the bolt load would be relatively low compared to the bolts own tensile capacity. Clearly if the bolt's were torqued up, the loads detected by the strain gauges would be in the non-linear and hence variable portion of the bolt's range and unusable due to the lack of a single relationship. The alternative was to use untorqed bolts during the test. This would have conflicted with the notion of joints of 'typical' construction practice and was not therefore an option. The bolts were also prone to damage during installation which would have resulted in only being used once before being discarded. Because of these problems the use of externally strain gauged bolts was abandoned.

3.4.3.2 Internally strain gauged bolts

The second method of bolt measurement and the one which was eventually adopted in the joint tests was the internally gauged bolt. This method of bolt load measurement was previously used by both Jenkins et. al. [43] and Owens & Moore [44]. The bolts evaluated were acquired second-hand from BRE who had used them in previous experiments into frame behaviour. Their construction required a small diameter hole to be drilled centrally in the bolt to the point at which the strain is to be measured. The special strain gauge is cemented into place, with the outer wires encased in resin as indicated in Figure 3.5(a). Because of the age and previous use of the bolts, only seven of the twenty-five bolts supplied functioned reliably. The bolts were tested under an applied tensile load which produced a linear response to load when untorqued. The effect of inducing bending in the bolt did not alter the response as the gauge is located on the centre line of the bolt and is unaffected by flexural loading. However, non-linearity of response was once again encountered when the bolts were torqued, as shown in Figure 3.5(b). The severity of the non-linearity was less than with the external strain gauges, as the torque stress experienced by the internal gauge was significantly less than that which would be subjected to the externally mounted strain gauges seen previously.

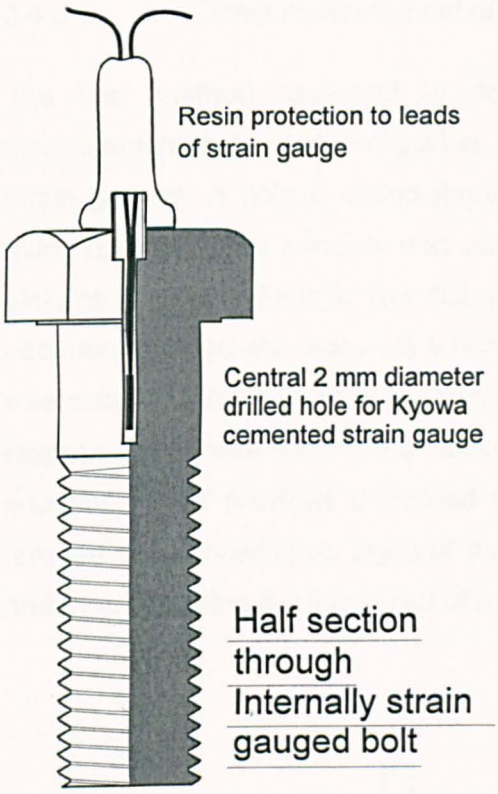

(a)

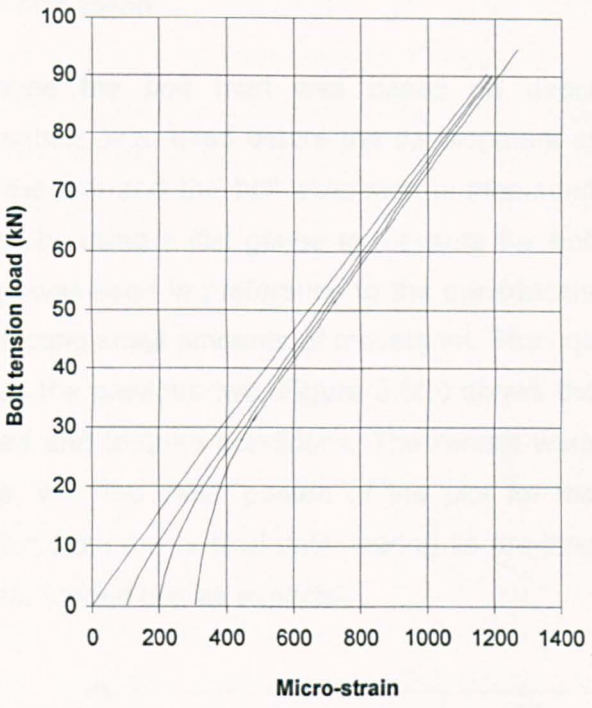

(b)

Figure 3.5 *Strain gauge response for internally located gauged bolt for applied tensile load*

Because of the internally strain gauged bolts reduced sensitivity to torque and their overall robustness, it was decided to use these bolts in preference to the externally strain gauged bolts. The non-linear effect was reduced to a minimum by subjecting the bolts to only 100 micro-strains. The 100 micro-strain value was accepted in preference to a constant torque, as the value of torque usually depends on the friction generated under the bolt head. In this way the same calibration for each bolt could be used.

Earlier it was stated that the results obtained from the joint tests had proved disappointing. The reason for nearly all the poor results stems from the cyclic loading of the joint. As the bolt was loaded and unloaded, the thread underwent local plasticity which resulted in the bolt losing its pre-stress and hence the conditions required to accurately determine the bolt load. These problems are even more severe when using the flowdrill connector compared to that of a normal nut and bolt combination because the integral thread is subjected to far greater deformation as a consequence of the tube face deforming. This problem is further complicated by the low bolt loads developed in the simple joints, which resulted in poor interpretation from the lower range of the bolt's non-linear response, as seen from Figure 3.5(b).

3.4.3.3 Direct measurement of bolt elongation

The final method assessed to determine the bolt load was based on direct measurement of the bolt elongation; a method often used before the development of strain gauges. A hole is drilled through the bolt and the bolt extension is measured using callipers. This principle was adapted by using a dial gauge to measure the bolt elongation (Figure 3.6(a)). The dial gauge was used in preference to the transducers because of its greater accuracy when detecting small amounts of movement. The bolt was subjected to the same test regime as the previous two. Figure 3.6(b) shows the response to tensile force under untorqued and torqued conditions. The results were superior to the previous described tests, with the initial portion of the plot for the torqued bolts showing no signs of deviation from the vertical until nearing its pre-load and then re-joining the linear plot of non pre-loaded bolt as expected.

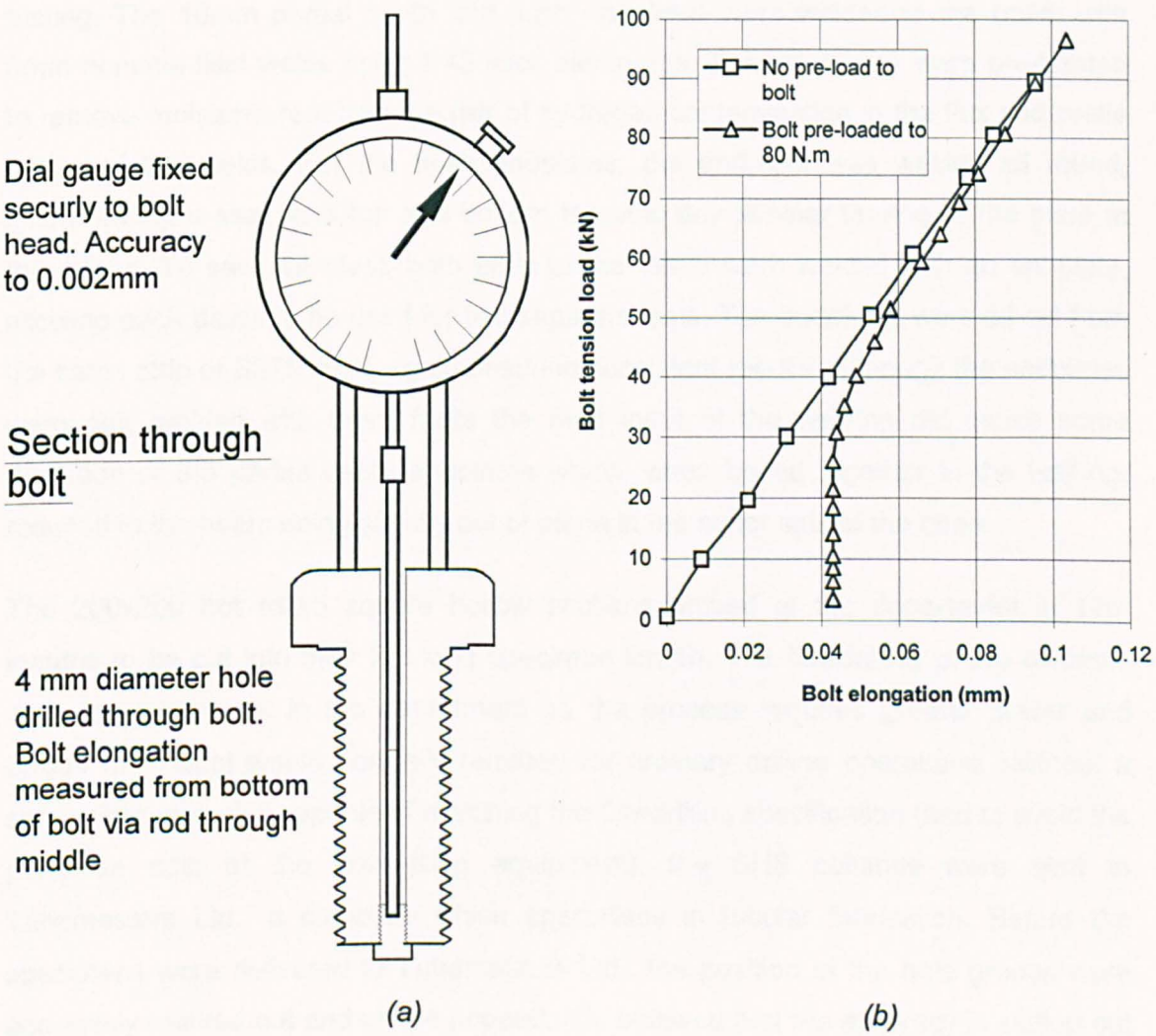

Figure 3.6 Elongation of dial gauged bolt under applied tensile load

Although the dial gauged bolt finally proved successful in determining the bolt load, the success had come too late to be of benefit for the joint test programme described in this thesis. If accurate bolt loads are required then the use of the dial gauge bolt or ring load cell positioned under the bolt head will provide more successful results than the strain gauges which were found to be unduly sensitive to the amount of applied torque.

3.5 Fabrication of test specimens and material properties

All the fabrication of the beam members was completed within the department's technical workshop with the same technician used to weld the endplates to provide consistent quality. In general, the steel used in the tests conformed to S275 (design grade 43) while the M20(8.8) connector was adopted as standard throughout all of the testing. The 10mm partial depth and flush endplates were welded to the beam with 6mm nominal fillet welds using E43 stick electrodes. The electrodes were pre-heated to remove moisture, reducing the risk of hydrogen contamination in the flux and brittle failure of the welds. For the flush endplates, the endplate was welded all round, incorporating a seal weld top and bottom to avoid any laminar tearing of the plate at the edges. To save on steel, both ends of the beam were welded with an endplate, allowing each beam to be used for two separate tests. The endplates were all cut from the same strip of S275 steel, again ensuring consistent results. Although the endplates were only welded with 6mm fillets the heat input of the welding did cause some distortion of the partial depth endplates which, when bolted together in the test rig, resulted in the beam being slightly out of plane in the minor axis of the beam.

The 200x200 hot rolled square hollow sections arrived at the department in 12m lengths to be cut into their 2m long specimen length. The flowdrilling of the columns was not carried out in the department as the process requires greater power and torque than what would normally required for ordinary drilling operations. Without a convenient pillar drill capable of matching the flowdrilling specification (and to avoid the purchase cost of the flowdrilling equipment), the SHS columns were sent to Tubemasters Ltd., a company which specialises in tubular fabrication. Before the specimens were delivered to Tubemasters Ltd., the position of the hole groups were accurately marked out and centre popped. It is believed that the accuracy in setting out of the holes resulted in trouble free assembly of the test specimens. All the holes were deliberately positioned on the opposite face of the weld seam to avoid any possible

interference and inconsistency. This does not affect the overall performance of flowdrilled connectors as the tests conducted by Banks [33] incorporating the flowdrill hole positioned directly over the weld seam revealed no deterioration in the thread's performance.

Section size	Flowdrill		SHS Dimension	
	Depth of thread (mm)	Depth of lobe (mm)	D (mm)	t (mm)
200x200x6.3 SHS	17.8	11.5	199.7	6.4
200x200x8 SHS	20.3	12.3	200.1	8.3
200x200x10 (S275) SHS	22.9	12.9	201.0	10.1
200x200x10 (S355) SHS	23.3	13.3	200.3	10.2
200x200x12.5 SHS	26.5	14.0	200.3	12.9

Table 3.2 SHS Section dimensions and Flowdrill thread depths

After the column specimens had been drilled and returned to the department, a survey was conducted on the depth of hole produced by the flowdrilling, presented in Table 3.2. The depth of the projection is dependent on the diameter of the hole and the thickness of tube wall. During the inspection of the flowdrill holes, the tubular sections were also dimensionally surveyed. The results indicated excellent dimensional tolerance and uniform wall thickness. Average values for each of the tube sizes is also shown in Table 3.2. A full account of the complete survey is presented in Appendix B.

The 200x200 box sections used for the tests were provided by British Steel from their Hartlepool works, accompanied by test certificates for material strength. As an independent check to these results, tensile coupons were removed from the column sections which related to all identifiable batches of steel. No coupon tests were conducted for the beam members or endplates. Table 3.3 provides a summary of the results for the columns used in the simple joint tests. Further information on the coupon tests can be found in Appendix B.

Section size	Steel grade	Tensile coupon tests			British Steel Test Certificates	
		Yield	Young's modulus	UTS(1)	Yield	UTS(1)
		(N/mm^2)	(kN/mm^2)	(N/mm^2)	(N/mm^2)	(N/mm^2)
200x200x6.3 SHS	S275	336	205	479	360	500
200x200x8.0 SHS	S275	318	201	466	331	474
200x200x12.5 SHS	S275	307	207	452	316	484

Notes: (1) UTS- Ultimate tensile strength
(2) All values presented are averaged longitudinal yield stress

Table 3.3 Summary of tensile coupon results and comparison to British Steel test certificates

3.6 Joint test procedure and assembly

In each joint test conducted, the beam and column were painted with white emulsion prior to assembly to highlight areas of yielding, identified by the flaking of the paint from the steel. The jack used to apply the column axial load was fixed to the column prior to being positioned into the test rig. This left the spherical seats to be located after the column had been positioned in the rig. The column specimens were specially detailed to allow adequate clearance for final insertion of the spherical seats. The column was aligned centrally, and the two top channels and rollers were fixed. Packs were inserted at the position of the rollers to take up the slack, although in some of the tests this did not prove to be successful as some movement occurred as the test proceeded.

In all the simple joint tests the beam was craned into position and bolted to the column within the test rig as this was found to be the easiest way of handling the sections. With the beam tested vertically there was sufficient access to bolt and position the beam onto the SHS column. The sequence of bolt tightening was critical as the majority of tests incorporated the strain gauged bolts. In cases where the bolt loads were expected to be high and could result in damage to the bolts, normal grade 8.8 bolts were used instead. As explained above (in section 3.4.3.2), the strain gauged bolts were tightened to a nominal 100 micro-strain, which represented a very low

torque relative to normal practical tightening. The tightening sequence adopted was determined by trial and error because of the subsequent loss of bolt tension when adjacent bolts were tightened. In some instances the bolt force increased, resulting in the need for the bolt to be slackened off. Acceptably accurate bolt forces could be determined when values between 80 and 120 micro-strains were measured.

One of the problems which occurred with the strain gauged bolts was the 'free-ranging' of the signal logged. The bolt signal tended to wander from its initial starting position over a period of time. This was not due to the loss of pre-stress in the bolts as adjacent bolts torqued to the same level of micro-strain were stable, indicating that some of the bolts were unreliable. In the cases where the M20 grade (8.8) bolts were used, a torque wrench was used to 160 N.m.; this value of torque had been previously adopted in other joint test programmes and represented an equivalent tightness of bolt that would normally be adopted if a normal spanner had been used to tighten the bolt. The torque wrench used in this situation added some consistency to the test results.

With the specimen bolted together and the instrumentation positioned around the joint, the 1000 kN column flat jack was used to apply a column axial load of 80 kN to nip the member into place. All the simple joint column members were subjected to this initial load, which removed the original clearance needed to allow the column to be positioned into the rig. The hydraulic ram was then connected to the beam flange. The hydraulic ram was under displacement control, which allowed a safe and controlled failure of the joint. At this stage all the transducers, bolts, inclinometers and jack load cells were zeroed. The data from the instrumentation was recorded during the test by an Orion data logger which was controlled via a PC that allowed two channels of information to be displayed on the screen in real time. All channels were logged at five second intervals.

The loading sequence adopted was a slow cyclic pattern, which gradually increased in load after each cycle. The hydraulic ram first loaded the joint in a positive moment up to a prescribed value where upon the joint was unloaded. The unloading would continue to subject the joint to a negative moment to an equal or slightly less load than the first positive moment generated. Again the joint was unloaded and the moment reversed, increasing past the first moment and so on. The peak values generated defined the outer envelope of the flowdrilled joint's moment-rotation characteristic for positive and negative moment. Nearly all the simple joint tests were conducted in this

way apart from the axially loaded and concrete-filled joints which will be described separately, in section 3.7.6 and Chapter 6.

Half way through the test programme the leverarm to the hydraulic ram was increased to suit the capacity of the joints tested. The leverarm for each of the tests was measured from the centre-line of the ram to the face of the 200x200 column section, as shown in Table 3.4. The moment calculated is therefore that which is developed at the connection and not the centre-line of the column.

Test No.	Leverarm (mm)	Test No.	Leverarm (mm)
1	1007	8	1323
2	1014	9	1006
3	1014	10	1008
4	1010	11	1318
5	1015	12	1318
6	1008	13	1314
7	1009	18	1005

Table 3.4 Leverarm position for hydraulic ram

3.6.1 Review of slow cyclic loading and its effect on overall joint behaviour

The adoption of cyclic loading in previous research projects has usually been restricted to dynamic tests which investigate the behaviour of joints under seismic loading, where the joint is clearly subjected to a positive and negative loading regime. It might be considered that, in the majority of cases in braced frames subjected to only 'static' loading, the joint never realistically develops a negative moment response. There are, however, circumstances when the joint does undergo unloading and reversal of moment. This occurs as the column approaches its collapse load, allowing moment shedding to occur at the column head [98] . The unloading stiffness developed in the joint has been known to provide some degree of restraint to the column to increase the column's capacity.

The importance of the unloading stiffness of joints on the column capacity has been observed through the experimental work of Gent & Milner [98] for rigid frames and

Davison [39] for semi-rigid frames, which has led to the recommendations of Kirby [38] to suggest that joint tests should be conducted under cyclic loading to determine the full joint response under both unloading and negative moment-rotations. The loading should be sufficiently slow for the static moment-rotation characteristic to be defined rather than the dynamic loading condition. Celikag [45] incorporated slow cyclic loading into joint tests to investigate the out-of-plane response of open section joint behaviour. Based on Celikag's experience of completely reversing the load, the technique was subsequently incorporated into these tests

Using slow cyclic loading has an additional advantage as it enables two moment-rotation characteristics to be determined from only one test. The endplates used in the tests were detailed so as to allow the bolt group arrangement to be positioned asymmetrically about the beam's mid-depth. The top bolts are always set a distance 60mm down from the top flange. This resulted in one joint test producing two different moment-rotation envelopes, for the positive and negative joint rotations, with the possibility of interpolating between the two curves for various locations of bolt group details, including that of a bolt group positioned centrally to the web's horizontal axis. Adopting cyclic loading was also advantageous in that the results could be used for unbraced frames subjected to lateral loading. Such sway frames develop 'negative' moments in the joints, contrary to the situation for traditional simple braced frames which rarely involve complete moment reversal.

One problem created by cyclic loading is the accuracy to which the moment-rotation envelope so defined represents that of the monotonic loading and what effect, if any, does the variation of loading sequence have on the joint's performance. To answer this question, consider the plot of the moment-rotation characteristic of joint test no. 2 shown in Figure 3.7. In this instance the positive loading cycle was increased at each loop, whereas the negative load was maintained at the same level of moment (-30 kN.m) for four load cycles. On each load cycle the joint responded by returning to almost the same level of rotation, (noted as point 'Y' in Figure 3.7), even though the joint was subjected to ever-increasing plastic deformation highlighted by the non-linear loading path. From these results it can be concluded that the moment-rotation envelope developed during cyclic loading of the test is unaffected by either alternating plasticity or variation in load sequence. The results are therefore representative of the true 'static' moment-rotation curve of the flowdrill joints.

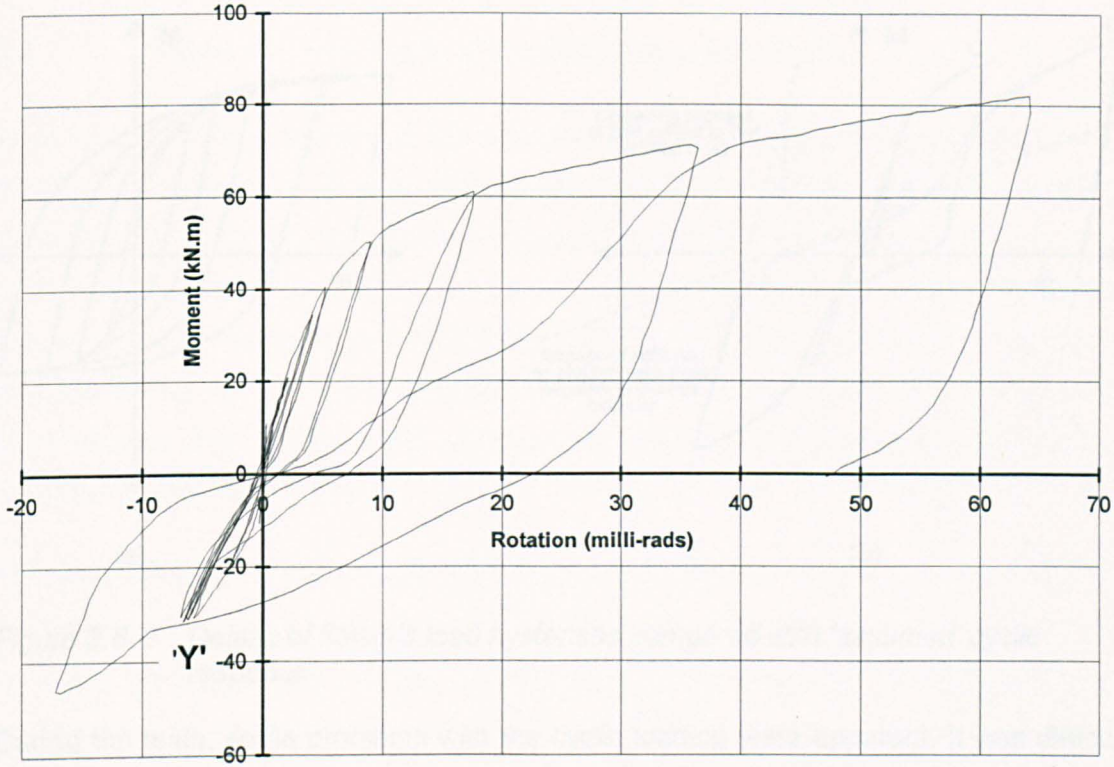

Figure 3.7 *Moment-rotation characteristic of typical flowdrill joint under cyclic loading*

One of the more unusual properties of the joint, discovered by cyclic loading, has concerned it's hysteresis. In traditional seismic joint tests which consist of open section members a moment-rotation hysteresis typical of Figure 3.8(a) has regularly been observed. This contrasts with the results of the flowdrill tests shown typically in Figure 3.8(b). In these instances at relatively high rotations the flowdrill joint mimics the response of the seismic hysteresis by unloading elastically to point A in Figure 3.8(b), equivalent to the initial stiffness of the joint. At this point the stiffness suddenly reduces and travels to point B, cutting across inside the positive moment-rotation envelope, until regaining stiffness at B. The last stage is when the curve gradually increases until sufficient moment has been developed in the joint to allow the curve to rejoin the original path of the moment-rotation envelope at D. This kind of path is typical for all the joint tests and only deviates from this character as a result of the degree of original loading and the severity of load reversal. Only at relatively large rotations does this characteristic of the moment-rotation relationship become apparent.

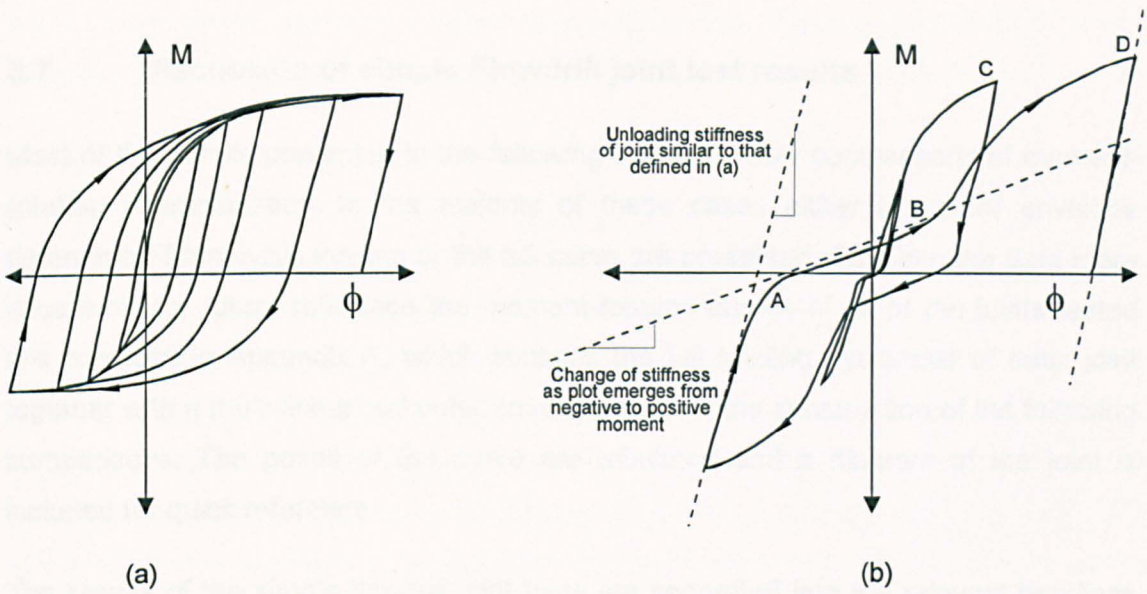

Figure 3.8 Details of flowdrill load hysterises compared with 'assumed' cyclic response

During the tests, some problems with the cyclic loading were apparent. It was difficult to determine if the load hysteresis of the joint had been reloaded sufficiently for the path of the 'monotonic' moment-rotation curve to have been rejoined as indicated by points C and D in Figure 3.8(b). If the test was stopped between these two points then the final recorded point would not be on the monotonic moment-rotation envelope. This occurred on a couple of the tests, with points that indicated an unrealistic value. There was also difficulty encountered on the load level at which to initiate a reversal of joint loading. The decision was made easier by monitoring the moment-rotation curve in real time processing while conducting the test, but difficulty still existed in identifying the load reversals to define with reasonable accuracy the monotonic characteristic whilst gaining information on the important unloading stiffness. Other problems encountered with the cyclic loading were slippage, and subsequent loss of accuracy, from the transducers as the joint passed through its initial starting value.

3.7 Discussion of simple Flowdrill joint test results

Most of the results presented in the following sections show comparisons of moment-rotation characteristics. In the majority of these cases either the outer envelope determined from cyclic loading or the full curve are presented. To make the data more accessible for future reference the moment-rotation curves of all of the joints tested are compiled in Appendix A, which contains the full loading hysteresis of each joint together with a multi-linearised outer envelope used in the construction of the following comparisons. The points of the curve are tabulated and a diagram of the joint is included for quick reference.

The results of the simple flowdrill joint tests are separated into the relevant headings previously grouped in Table 3.1. By reporting the tests in group order there will inevitably be some joints that are described out of the sequence in which they were tested and in some cases, will result in an overlap of the tests as different comparisons will reference similar joints. However, every effort has been made to test the joints in group order rather than the order represented by the numbering system which identifies the Flowdrill joint.

3.7.1 Endplate thickness

Two tests (nos. 4 and 18) were provided in the programme to examine the effect of endplate thickness. At the start of the programme no such tests were envisaged and they were developed out of general concern that the 10 mm thick endplates specified may be too flexible to induce failure in the column face. This was at variance with the aim of the programme which was to investigate the influence of the flexibility of column face as it was deemed to be one of the most critical criteria for these types of joints. With this reasoning, test no. 18 was added to the programme to examine the influence of endplate thickness associated with low column wall thickness, and more importantly to use the results of the test as a trial run for the test rig.

The joint detail for test no. 18 consisted of a 356 beam and a 200x200x8mm SHS column. A 15 mm thick flush endplate was used. No alignment problems were encountered when bolting the specimen together. However, one of the difficulties which did surface through testing the beam in the vertical position was that it was unable to allow the bolts to bear as in normal construction. If tested horizontally, gravity would induce a different natural settlement of the joint, although problems would still

have arisen when negative moment was applied and the resulting change in the direction of shear would have caused slippage of the bolts in the clearance holes.

During the test, the load was reversed four times to define the moment-rotation envelope. The joint detail attained a maximum positive moment of 50 kN.m at 0.049 radians rotation and a maximum negative moment of -40kN.m at -0.043 radians. The test was stopped during the positive moment cycle of the joint due to excessive rotation. At this rotation the test indicated limited further potential increases in moment capacity. The joint failed in a ductile and safe manner, with failure attributed to extensive column face bending. In general, the joint possessed reasonable elastic stiffness and recoverability up to approximately 25 kN.m when significant non-linearity of the joint was exhibited. A high degree of non-linearity was observed in the lower stages of the joint's moment capacity above 20 kN.m due to the flexibility of the 8 mm tube face. Figure 3.9 shows a plot of the outer envelope of the positive moment-rotation characteristics for test no. 18 and test no. 4, which was nominally identical except that the endplate thickness was only 10 mm.

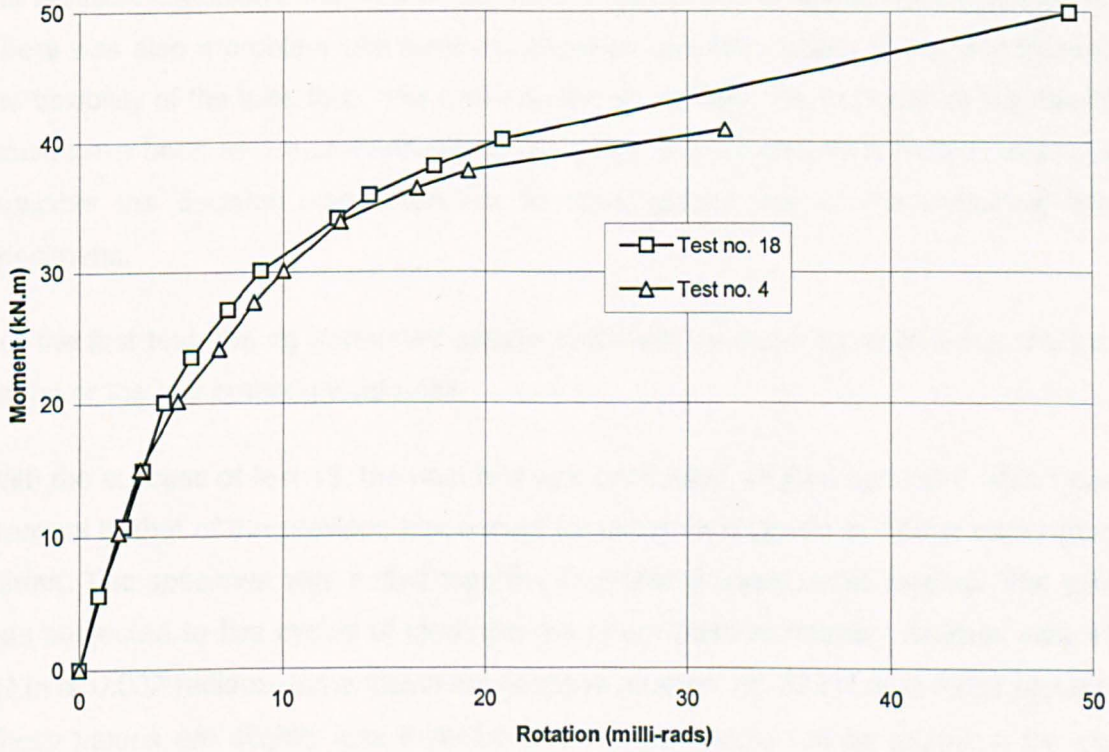

Figure 3.9 Comparison of endplate thickness on simple flush endplates

The specimen was removed from the test rig and the endplate unbolted from the column. Even though the column face had undergone quite large distortions the bolts

were easily removed from the joint. Closer inspection revealed no yielding of the endplate or the beam. Yielding of the column face was extensive, with the flowdrill holes elongated at the top as a result of the SHS face distortions. This caused the top threads of the hole to lose contact with the bolt. Distortion of the column face was confined to the vicinity of the tension bolts and the area directly in line with the beam compression flange. Column yielding was also found to extend into the side webs at the location of the top row of bolts. The inward distortion of the column face at the area of the compression flange stemmed from the use of a relatively small width of endplate. A larger endplate width could have been adopted to reduce flexural action of the face by transferring the compression force from the beam flange directly into the column webs. Outward bulging of the webs also occurred in the compression zone.

As this was the first joint test conducted, the column was strain gauged to determine the distribution of stress in the section. The 10 mm long strain gauges were positioned at specific cross sections in groups of four to determine the moment in the column, with additional gauges positioned adjacent to the joint to detect the onset of plasticity. The results from the strain gauges were disappointing as the relatively short length and the restraint conditions imposed on the column developed a severe moment-gradient. There was also a problem with early plastification occurring locally at the joint through the flexibility of the tube face. The only solution to increase the accuracy of the results would have been to comprehensively strain gauge the column. With limited resources available the decision was taken not to strain gauge any of the remaining test specimens.

For the first test, the rig performed satisfactorily with no major faults in either the test set up or the test procedure adopted.

With the success of test 18, the next test was conducted on joint number 4 which was identical to that of the previous test except for using an endplate of 10mm rather than 15mm. The specimen was bolted together and tested under cyclic loading. The joint was subjected to five cycles of load; the maximum positive moment attained was 41 kN.m at 0.032 radians and a maximum negative moment of -33 kN.m at 0.023 radians. These values are slightly less than for test 18, but should not be mistaken for any deficiency in the joint's rotation capacity, as test no. 4 was stopped at a much earlier stage in the joint's loading history.

Examination of the joint after the test revealed a column distortion pattern very similar to that observed in test no. 18, although slightly less yielding had progressed into the

column webs because of the earlier stoppage of the test. The endplate did however show initial signs of yielding when unbolted.

Figure 3.9 referred to previously shows the positive moment-rotation envelope of both test 18 and test 4. The plot indicates the 10mm endplate joint to have slightly lower stiffness and strength than the 15mm endplate test, which would be expected. However, the results of the two moment-rotation envelopes are very similar, indicating the small contribution that endplate deformation has on the joint's response. Although the 10mm endplate showed signs of yielding, it was adequate in terms of stiffness and strength to cause column face flexibility to be the main cause of the joint's ductility and overall failure. On this basis the 10mm endplate was adopted as the standard thickness for the remaining simple joint tests for the 6.3 and 8.0 mm thickness columns.

3.7.2 Partial depth endplates with beam depth variation

The partial depth endplate was examined over a range of three beam sizes, which were included to investigate the lower levels of joint stiffness attainable with these types of endplates. The partial depth endplate, sometimes referred to as either a header or flexible endplate, is the most likely to be adopted to simulate the characteristics of a simple joint. Endplate connections are a modern-day equivalent to the riveted web angle connection (later bolted) which is known to exhibit similar joint stiffness. The design of the partial depth endplate simulates the pin joint by using a plate of such thickness that its flexibility and strength in relation to the column flange is such that any deformation and yielding is controlled by that of the endplate in bending. The disadvantage of the detail is the susceptibility of the endplate to damage during transportation and frame erection.

The selection and design of the endplates was conducted using the SCI recommendations for simple design [46]. Design guidance refers to the depth of the endplate, which should not be greater than 0.6 times the depth of beam, and a recommended endplate thickness of 10mm. Other guidance on edge and end distances have also been adhered to. In keeping with the aim of determining the most onerous cases for all the details tested, the number of bolts adopted for each of the tests was selected on the basis of the beam supporting relatively high shear loads, which would require the greatest number of bolts in the endplate. Similar bolt cross

centres of 100 mm were carried over from the flush endplates for reasons of direct comparison.

The testing procedure of all the joints in this group differed from others in that cyclic loading was not adopted in the testing. The reason for this was that these joints are primarily designed for shear, and are not capable of sustaining appreciable moments. It would be quite probable that any attempt at cyclic load would have resulted in failure of the joint before the end of the first cycle. Also this type of connection would, under normal circumstances, only be capable of limited negative restraint to the column.

The first partial depth endplate specimen to be tested was joint test number 3. This joint consisted of a 356 beam bolted to a 200x200x8 SHS column with three rows of M20(8.8) bolts. Although the joint was not subjected to cyclic loading it was unloaded to 10 kN.m. The moment of the joint was reapplied, resulting in the tips of the compression flanges of the beam bearing against the face of the box section at a moment of 17 kN.m and rotation of 0.050 radians. The test was stopped when the moment-resistance developed by the joint was 26 kN.m at 0.057 radians. The failure of the joint was attributed to endplate yielding.

Examination of the joint after testing revealed that the endplate had been plastically deformed with the top part of the plate being pulled out and the bottom part being pushed in. Yielding of the endplate had been concentrated along the weld root, with the endplate assuming the shape of single curvature bending with no indication of prying action to the bolts. The column section had yielded around the top row of bolts but no yielding or outward deformation of the tube was observed on the sides of the column section. During the test, the endplate had rotated around the bottom junction of the beam web and endplate, which culminated in yielding of the beam web.

The second test of the group, was joint test no. 9, conducted with the 254 beam and 200x200x8 SHS column. The loading system was similar to test no. 3 with a similar mode of failure. The joint test was stopped at a moment of 18 kN.m and a rotation of 0.103 radians.

The last joint test to be conducted on the partial depth endplates was test no. 1. This involved the largest serial beam size to be used of the three, with a 457 UB bolted to the 200x200x8 SHS column. The joint attained a final moment-resistance of 62 kN.m at 0.076 radians. Again a similar failure was observed to those of the previous two tests. Figure 3.10 shows all three moment-rotation results of the group for comparison

where the increased stiffness attained for each test was dependent on the beam depth.

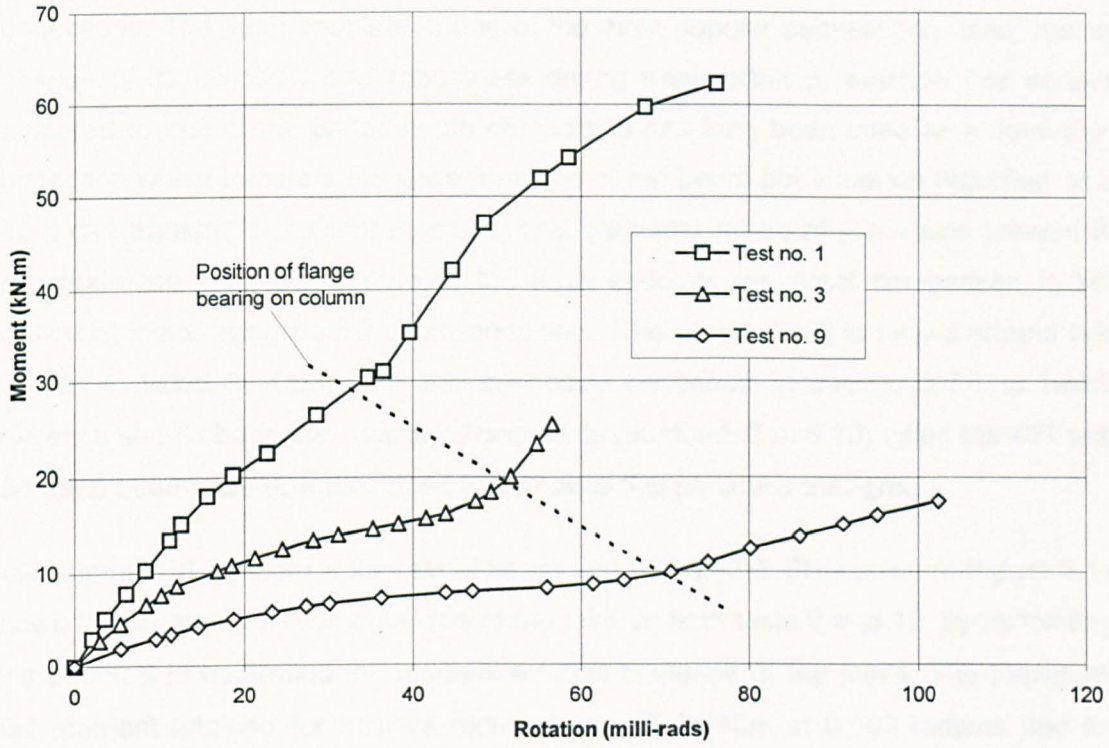

Figure 3.10 Comparison of partial depth endplates for 457, 356, and 254 UB serial size beam depths

One of the interesting features of the plots in Figure 3.10 is the change of stiffness as the compression flange comes into contact with the column. The location at which this occurs differs for each of the three beams, although the rotation level in each instance is substantially beyond the rotation which would typically be generated by a simply supported beam under gravity loads. It must also be pointed out that the moments generated by the joints are very small in comparison to the moment-resistance of the beams. For example the 457x152x52 UB used in the test has a nominal plastic moment capacity of 300 kN.m which, when compared to the joint moment at a typical serviceability rotation of 0.010 radians, generates a moment of 12 kN.m. The acceptability of the connections to simple construction is further underpinned by the criteria given by EC3 [47] which firmly places these joints in the nominally pinned classification for braced simple construction [48].

3.7.3 Flush Endplates with beam depth variation

The majority of the tests which are in the programme are on flush endplate connections. The flush endplate is one of the most popular connections used, mainly because of its simplicity and robustness during transportation, erection and service compared to that of the partial depth endplate. It has long been used as a semi-rigid connection which transfers the shear reaction of the beam but although regarded as a pin, it can transmit significant moment. This particular group of joints was created to investigate the semi-rigid nature of the flush endplate for direct comparison to the equivalent joints using partial depth endplates. The group detail is based around test number 4, listed in Table 3.1 and previously described in section 3.7.1 to which reference should be made. Two additional tests (numbers 2 and 10) using the 457 and 254 deep beams are now described to complete this particular sub-group.

Test number 10 adopted a 254 serial beam and 200x200x8 SHS column. Figure 3.11 shows the moment-rotation envelope of the joint. In both tests 2 and 10, cyclic loading was adopted to determine the moment-rotation envelope of the joints. The maximum joint moment attained for positive moment was 26.2 kN.m at 0.069 radians and for negative moment the test did not exceed -10.2 kN.m at 0.010 radians. Closer inspection of the endplate after the test revealed some yielding at the location of the top row of bolts. The column exhibited large deformation around the top row of bolts but the bottom row appeared undamaged as these bolts were located in the compression zone of the joint. As in test number 4, there was a visible imprint of the compression part of the endplate in the column face where the stiffness of the side walls had attracted the load from the beam. Signs of yielding on the extreme tips of the beam compression flange were visible for the first time in the test programme. The local yielding on the outside tips of the compression flange would in the majority of cases progressively spread inwards towards the web of the section.

The final test in this group, test number 2, adopted a 457 beam bolted onto the 200x200x8 SHS column (refer to Figure 3.1 for detail of endplate). The moment-rotation characteristic for this joint is also shown in Figure 3.11. The maximum moment attained before the test was halted at a recorded positive moment of 82 kN.m at 0.064 radians and a negative moment of -46 kN.m at 0.017 radians. After the test the endplate again showed signs of yielding, with the deformation clearly visible at the top row of bolts. Similar failure conditions which were reported for the previous tests are

also applicable to this one. However, because of the increased moment, the extent of column yielding was observed to be significantly greater, extending down into the web by approximately 25 mm. Slight bulging of the web in the area of the compression flange had also been noted.

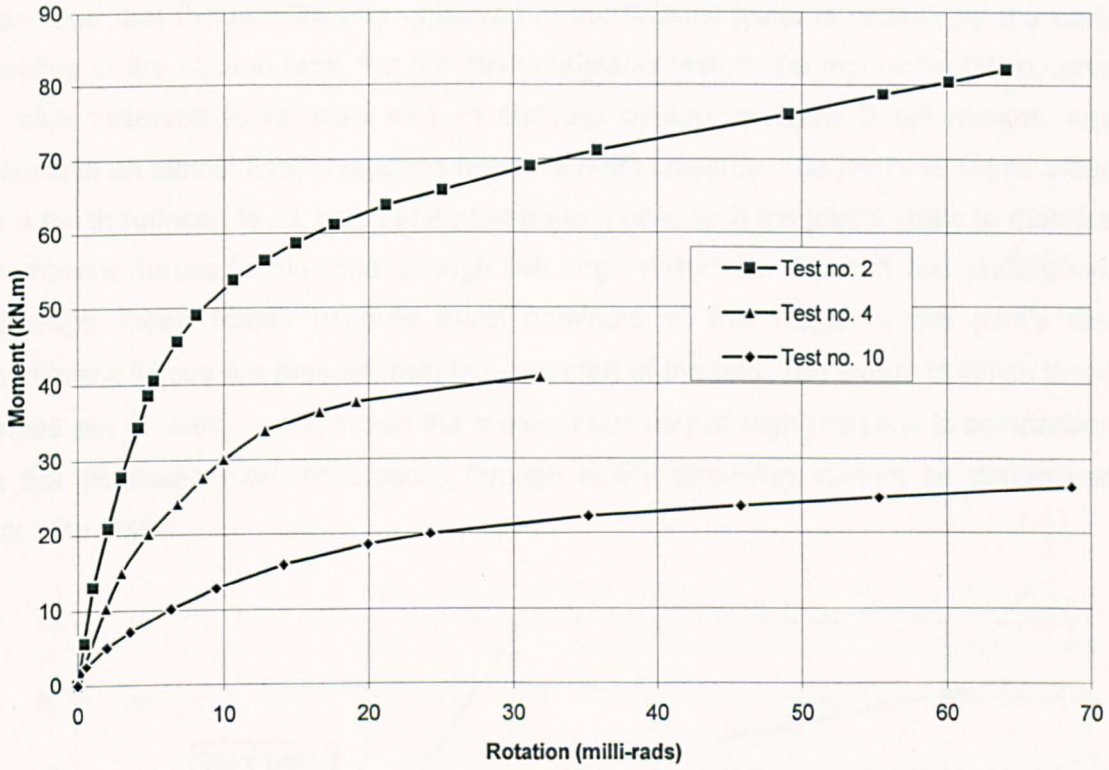

Figure 3.11 Comparison of Flush endplates for 457, 356 and 254 UB serial size beams

Figure 3.11 shows all three of the tests relating to the 254, 356 and 457 serial sections plotted together. It is evident from these comparisons of joint performance that the depth of beam places considerable variation on the initial stiffness and the final ultimate capacity of the joint. Both stiffness and strength are shown to increase with beam depth. If compared against the moment capacity of the tested beam, then the joint's moment capacity is only about 25%; the maximum recorded moments being 27%, 19% and 24% of the nominal plastic moment capacity of the 457, 356, and 254 serial size beams respectively. With such small capacities the use of the flush endplates as moment-resisting joints is unrealistic, although the selection of a thicker endplate would have increased the joint's performance as the 10 mm plate was just flexible enough for it to yield. However, the amount of contribution the endplate deformation has on the performance of the joint was not clear at this stage and is addressed in Chapters 4 and 7.

A second important observation of all the tests has been the non-linear moment-rotation response of the joint from a relatively early stage of the joints loading history. Usually, in traditional open section joints of nominally identical endplate details, the joint characteristic, allows the identification of an initial stiffness that is essentially linear and elastic, and which extends to a high proportion of the joints moment capacity. It is assumed that the non-linearity observed in the flowdrill joints is caused by the early yielding of the column face. For the flush endplates tested, the moment-rotation curve is also observed to radically lose its stiffness at approximately 0.020 radians, and results in an almost linear response from this point onwards. The joint's stiffness, albeit at a much reduced level, has usually been associated with the joint's ability to mobilise membrane forces in the face through the large distortions which it has undergone. Although these forces become more dominant at this stage of the joint's life, membrane forces are present from the very start of the test. The extent to which these forces are present, and increase the moment capacity at high rotations in comparison to the increased moment capacity through strain hardening, cannot be determined from the tests.

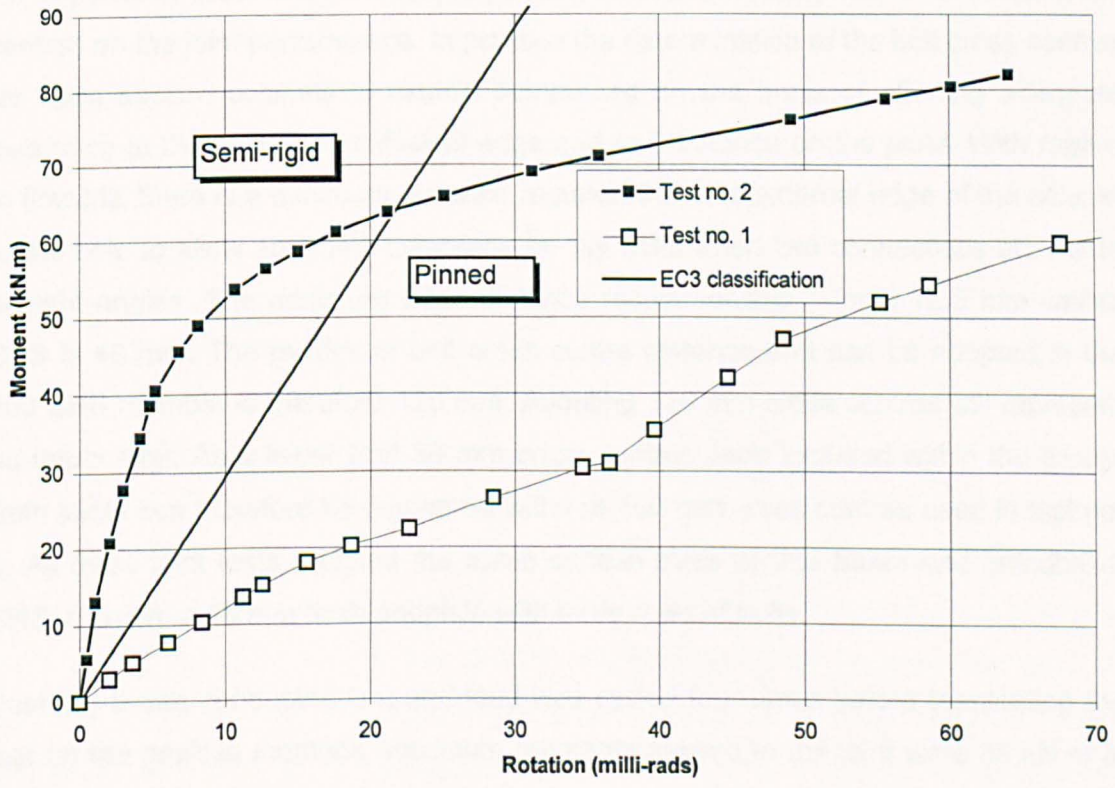

Figure 3.12 *Comparisons between flush and partial depth endplates for the 457 UB serial beam size*

As a comparison to highlight the differences between the two categories of partial depth and flush endplates, Figure 3.12 shows the two plots for both the endplates of the 457 UB serial section. Clearly the responses of the two details immediately contrast in both stiffness and strength. Included on the graph is the plot of EC3 classification system of semi-rigid and pinned categories for a 457x152x52 UB beam which spans 7500 mm. With this relationship the two endplates are immediately segregated; the flush endplate is clearly identified as semi-rigid while the partial depth endplate has been classified as pinned. The classification of the remaining 356 and 254 similarly show the partial depth endplate to be pinned and the flush endplates to be semi-rigid. EC3 thus permits the use of partial depth endplates for simple braced construction. However, it is the author's opinion that the disqualification of the flush endplate simply because it falls outside the category, which is defined by a single line, is not reasonable for a connection which in practice has been shown to work.

3.7.4 Bolt cross centres

An opportunity was taken in the programme to examine the effect of the bolt cross centres on the joint performance. In practice the determination of the bolt cross centres for open section columns is usually determined on the basis of allowing adequate clearance to the bolts, and sufficient edge and end distance on the plate. With regard to flowdrill, there is a minimum distance required from the external edge of the column to the bolt, to allow adequate clearance for the bolts when two connections are made at right angles. The minimum edge distance recommended [49] for a 12.5 mm walled SHS is 40 mm. The maximum bolt cross centre distance that can be adopted in the 200 SHS member is therefore 120 mm. Adopting 120 mm cross centres will represent an upper limit. As a lower limit 80 mm cross centres were included within the group. Both joints can therefore be compared with the 100 mm cross centres used in test no. 4. All three joint tests adopted the same section sizes of 356 beam and 200x200x8 SHS, utilising a 10 mm flush endplate with three rows of bolts.

Test no. 5 was conducted first and load was cycled four times before terminating the test on the positive moment. Maximum moments applied to the joint were 56 kN.m at 0.084 radians and a negative moment of -30kN.m at -0.019 radians. The endplate width was 160mm, the same as that detailed for the 100mm bolt centres. Figure 3.13 shows the moment-rotation curve of test no. 5. Inspection of the joint after the tests revealed little distortion and yielding to the endplate. The majority of the flexibility was

developed from the column face. Outward bulging of the column webs in line with the compression flange of the beam was also observed for this joint test.

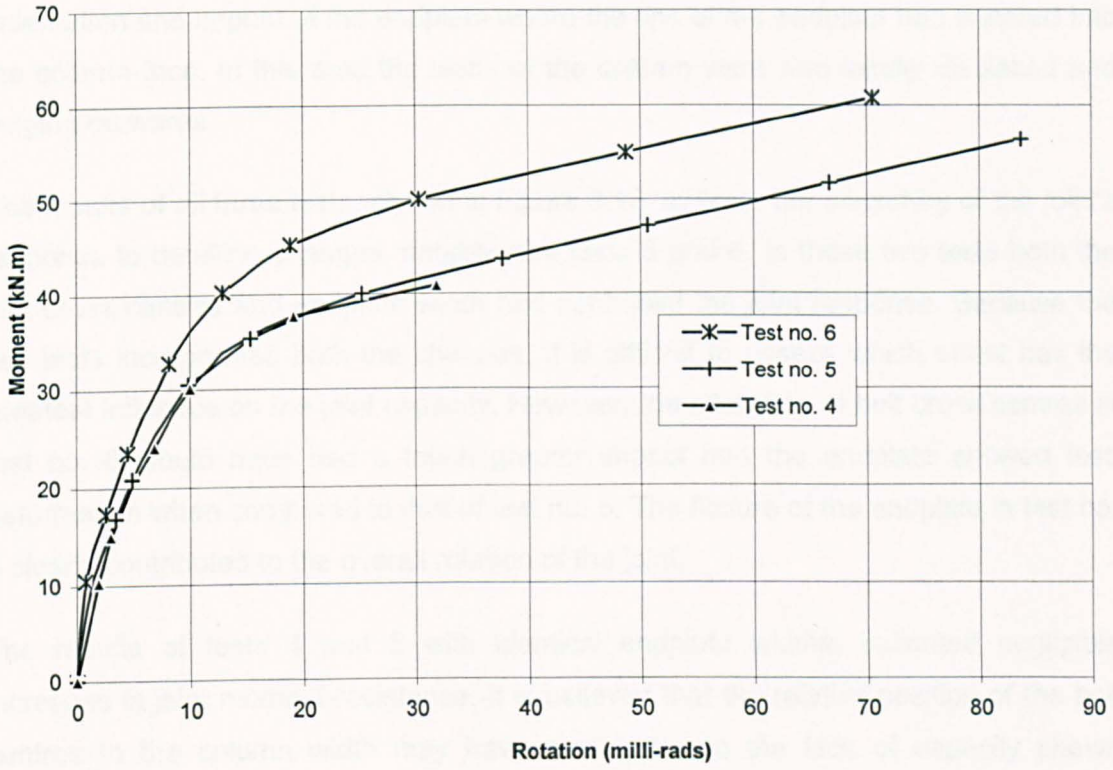

Figure 3.13 Comparisons between 80mm, 100mm and 120mm bolt cross-centres

The test and failure of joint no. 6 incorporating the 120 mm cross centres deviated from the other two tests by having a 180 mm wide endplate instead of 160 mm. This was a direct consequence of accommodating the 120 mm bolt centres and the edge distance required to the bolts. The test adopted cyclic loading, looping five times, but was abruptly halted by the steel packing between the beam and hydraulic ram dislodging from its position. To avoid a recurrence of this, subsequent tests were conducted with the pack welded to the pivot of the ram. The final moments recorded for the positive cycle was 61 kN.m at 0.071 radians and for the negative moment, -41 kN.m at -0.059 radians. The moment-rotation response is shown in Figure 3.13 with the other two tests as comparisons. After the test, the endplate showed severe distortion in single curvature bending with yield lines developing along the weld root. There was also plasticity on the outer edges of the beam compression flange caused by the wider endplate attracting greater stiffness in this area of the joint.

Inspection of the column showed the greatest yielding of the three tests in the area of the top two bolt rows. The yielding at the top bolts had also extended into the web of the column. In the location of the compression zone of the joint there was a significant indentation and imprint of the endplate where the tips of the endplate had sheared into the column face. In this area the webs of the column were also locally displaced and bulging outwards.

The results of all three tests, shown in Figure 3.13, indicate the sensitivity of the joint's response to detailing changes, notably joint tests 5 and 6. In these two tests both the bolt cross centres and endplate width had controlled the joint response. Because the two tests incorporated both the changes, it is difficult to assess which effect has the greatest influence on the joint capacity. However, the alteration of bolt cross centres in test no. 6 would have had a much greater impact had the endplate showed less deformation when compared to that of test no. 5. The flexure of the endplate in test no. 6 clearly contributed to the overall rotation of the joint.

The results of tests 4 and 5 with identical endplate widths, indicated negligible increases in joint moment-resistance. It is believed that the relative position of the bolt centres to the column width may have contributed to the lack of capacity shown between the two joints. In a previous investigation into the tensile capacity of flowdrill bolt groups conducted by Swinden Laboratories [33] (prior to the endplate tests), the effect of bolt cross centre performance was also examined. The bolt groups were subjected to direct tensile loading. These simple tests indicated that the tensile resistance of the bolt group increased as the bolts were positioned closer to the column's webs. The magnitudes of these increases were disproportionate, with only a small increase observed between different bolt cross centres located in the middle of the column face, whereas much greater increases were observed as the bolts moved closer to the column webs. The marginal increase in capacity indicated for the bolt groups located in the centre of the column may explain the small increase in performance for the flush endplate tests 4 and 5.

An interesting point to note from tests 4 and 5, shown in Figure 3.13, is that the last point in test number 4 is plotted below test number 5. The trend of the graph suggests that the 100mm bolt cross centres should attract more moment than the 80mm centres. An explanation for this anomaly is through not subjecting the joint to an adequate increase in moment as stated in section 3.6.1. to enable the load path to rejoin its moment-rotation envelope. This is shown by Figure 3.14 which constructs the

outer moment-rotation characteristic envelope from the cyclically loaded joint. It is difficult to know if the last point has reached the outer envelope of the joint's response. To avoid this occurring for the remaining tests, cyclic loading was adopted only in the initial stages of the joint tests but was avoided near failure.

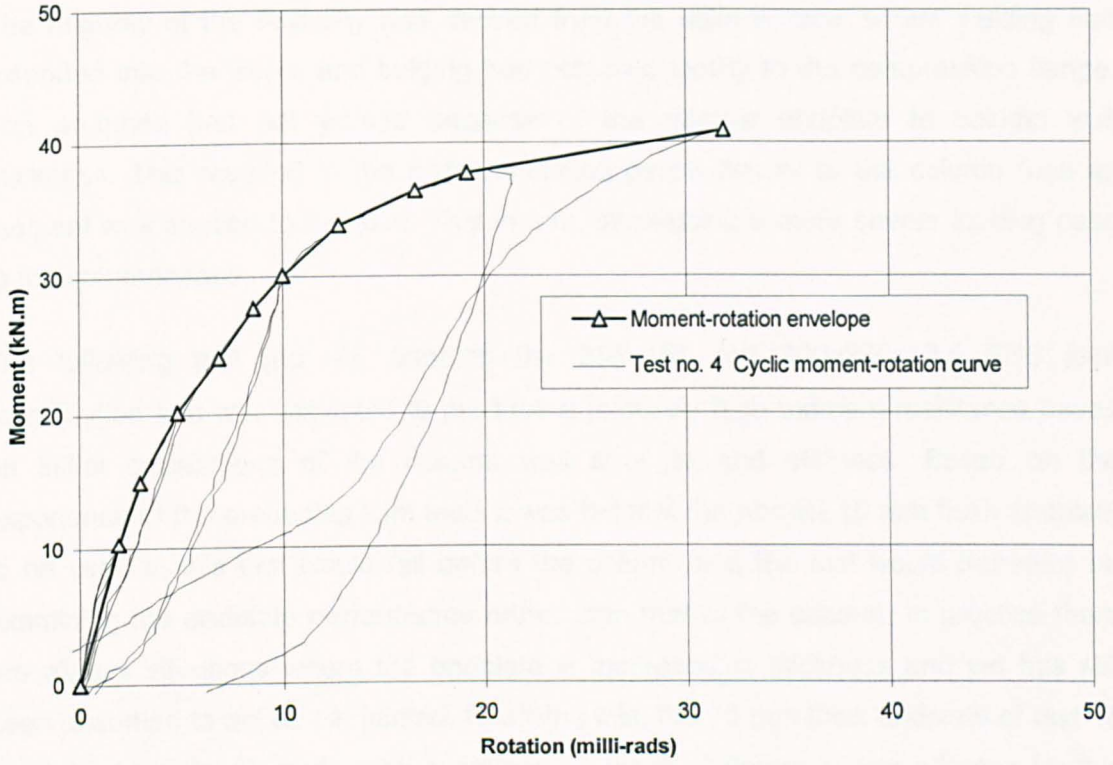

Figure 3.14 *Construction of joint test number 4 moment-rotation envelope from the positive cyclic joint response*

3.7.5 Tube wall thickness

The effect of the thickness of the tube wall was examined for three tests with identical bolt groups incorporating the flush endplate. The SHS section for the 200 serial size offers a range of 6.3 mm, 8 mm, 10 mm, 12.5 mm and 16 mm wall thickness. Two tests using the 6.3 and 12.5 mm tube sizes were conducted to compare directly against test no. 4 of the 8mm walled tube. These joint tests provided an insight into the flexural behaviour of the smallest thickness of wall available to compare against the maximum 12.5 mm thickness for which the flowdrill process is appropriate.

Test no. 7 involved the 356 UB beam attached to the 10mm endplate and bolted to the 200x200x6.3 SHS column. The joint was subjected to three cyclic load reversals before the test was stopped at a maximum positive moment of 34 kN.m at 0.061 radians. The negative moment attained was -19kN.m at -0.020 radians. Examination of the joint revealed that the endplate had not suffered from any visible signs of yielding. The majority of the flexibility was derived from the column face, where yielding had extended into the webs, and bulging had occurred locally to the compression flange. The endplate had not yielded because of the relative endplate to column wall thickness. This resulted in the bolts remaining perpendicular to the column face as moment was applied to the joint. This in turn, introducing a more severe loading case to the columns face.

The following test (no. 8), adopted the 356 UB and 200x200x12.5 SHS joint combination and was expected to produce a relatively high moment-resistance based on initial calculations of the column wall strength and stiffness. Based on the experience of the preceding joint tests it was felt that the normal 10 mm flush endplate to be used in this test would fail before the column and the test would therefore be examining the endplate performance rather than that of the column. In practice there are always situations where the endplate is increased in thickness and yet has still been assumed to act as pin jointed. Realising this, the 15 mm thick endplate of test 18 conducted previously and which sustained no signs of damage, was adopted for this test. The resulting endplate to wall thickness would now provide a more extreme case for the joint to be considered as 'pinned'.

The test was conducted without the strain gauged bolts because of the expected high bolt loads; they were replaced by M20(8.8) x 50 mm long setscrews (fully threaded bolts). The load was applied cyclically, with the jack leverarm increased to 1.3 m to allow for the increased moment-resistance of the joint. The loading was stopped when the moment attained was 123 kN.m at 0.069 radians. The largest negative moment developed was -53.3 kN.m at 0.007 radians. Inspection of the joint after the test showed large deformation and yielding of the endplate. The decision to increase the endplate thickness to 15 mm was therefore felt to be the correct one as evidenced by the severe distortions of both the column face and endplate. The beam compression flange tips were also found to have yielded. Column deformations were also apparent, similar to those of the previous test, except that the yielding around the top bolts was more severe.

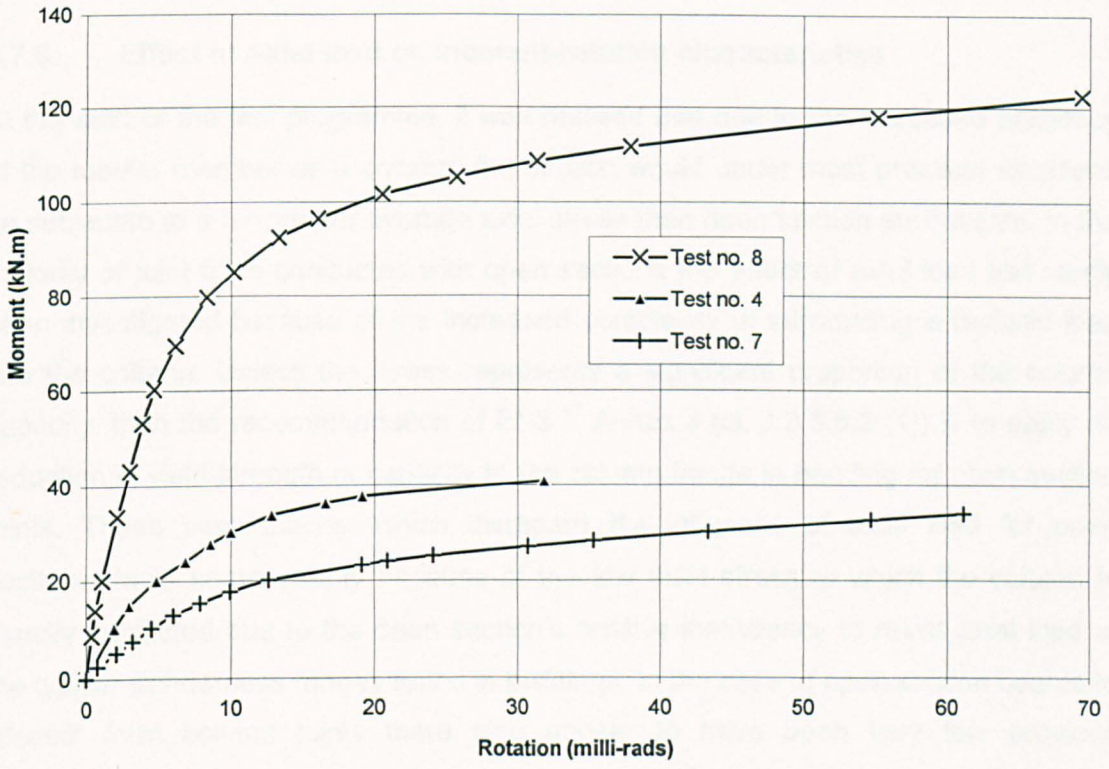

Figure 3.15 Comparison of tube wall thickness for 356 UB flush endplate

Figure 3.15 shows all three moment-rotation characteristics grouped together. The tube wall thickness has a significant effect by increasing the strength and stiffness of the joint as the tube wall increases. These characteristics are put in perspective when considering the nominal plastic moment capacity of the 356x171x45 UB is 213 kN.m. The 123 kN.m for the joint with the 12.5 mm tube highlights the concern that such a connection is placed in the top end of the semi-rigid category. The performance of these joints contrasts clearly with that shown with the bolt cross-centres which only affected joint performance marginally. The selection of tube thickness will in the majority of cases be based on the limits imposed on the column cross section and the degree of load which the column is to support. If the column has a constant cross section throughout the full height of a mullti-storey frame, it is quite probable that the thickness of the tube will be varied for economic reasons. A situation will obviously arise where similar connections will present quite different joint behaviour, unless connection flexibility is determined via the endplate such as the tests conducted with partial depth endplates of section 3.7.2.

3.7.6 Effect of Axial load on moment-rotation characteristics

At the start of the test programme, it was realised that due to the increased efficiency of the tubular member as a column, the section would under most practical situations be subjected to a far greater average axial stress than open section equivalents. In the majority of joint tests conducted with open sections the effect of axial load has rarely been investigated because of the increased complexity of introducing a realistic load into the column. Unless the stress represents a significant proportion of the column capacity, then the recommendation of EC3 [47] Annex J (cl. J.3.5.5.2 (4)) is to apply no reduction in yield strength or capacity to the column flange in bending for open section joints. These assumptions, which disregard the influence of axial load for open sections, have some validity because of the low axial stress to which the column is usually subjected due to the open section's relative inefficiency to resist axial load at the typical slenderness ranges found in buildings. In the case of open section beams to 'closed' form column joints there also appear to have been very few previous experimental tests conducted where axial load has been specifically examined. The only relevant area where the effect of axial load has been investigated is the research conducted under the guidance of CIDECT on pin jointed trusses totally consisting of tubular members.

The CIDECT effort has concentrated on examining the ultimate strength of pin jointed truss connections composed of hollow section members [4]. The main testing parameters investigated were the geometry and composition of the joint. It was found that when a chord of a truss has a relatively high axial load the ultimate capacity of the connection is reduced. A reduction factor applied to the joint is based on the ratio of axial stress developed in the chord and the connection geometry. This formula has been developed for the ultimate strength of the connection and is an empirical equation determined from experimental results. More recent experimental research has been conducted by Zhao & Hancock [50] on the effect of chord bending on tee joints. The findings show that the typical load versus connection deformation becomes flat after the joint has failed, i.e. the membrane and strain hardening effects are reduced in the presence of longitudinal stress. This finding has also been confirmed by Yu & Wardenier [51] with numerical models of joints, which have indicated the reduced membrane stiffness which has in some instance shown to be detrimental after the failure of the joints.

To date, the experimental results available have usually involved test arrangements where the tubular section is subjected to one simple loading case; for example, the tests conducted by Zhao involved the use of tee-joints where the branch member was loaded in compression only. A different situation exists for the flowdrill joint as the column is subjected to a more complex loading arrangement. Here, two yield line mechanisms in both the tension and compression zones develop to produce the joint's moment-resistance. The longitudinal stress is also developed from both the moment of the joint and the axial load introduced into the column. The results from the tests are therefore important in providing a more realistic loading regime of practical significance to the joint's behaviour.

The four axially loaded Flowdrill joint tests adopted nominally identical joint details with the 200x200x6.3 SHS column section being subjected to various levels of applied axial load. The 356 UB beam was adopted with the flush endplate which incorporated three rows of bolts at 100 cross-centres. The use of such a connection was to ensure the greatest possible deformation occurred to the column face. The lighter column section was selected to provide the greatest average axial stress from the 1000 kN jack. Unfortunately the 1000 kN load capacity was not sufficient to induce a squash load failure of the column. The ultimate capacity of the column was found to be 1633 kN based on the tensile coupon strength of the steel of 336 N/mm^2 (this compares to the nominal capacity of 1340 kN). Ideally a 2000 kN jack capacity would have been preferable but would have caused a great deal of difficulty incorporating such a large load into the assembled test rig.

Three tests (no's. 11, 12 and 13) were conducted with substantial axial loads which were compared with test no. 7, for a nominally identical joint detail which was conducted previously with only a nominal 80 kN axial load. The three additional tests were subjected to monotonic loading only, as the presence of cyclic loading may have detracted from the clarity of the moment-rotation characteristic produced during the tests. Also cyclic loading had been shown to produce results with regard to determining the position of the centre of joint rotation, as the loading sequence tended to displace the transducers and provide poor readings.

During all the tests the axial load was applied first via a flat jack and this pressure was maintained constant. The hydraulic ram subsequently applied the moment to the joint which meant that the part of the column remote from the jack was subject to a variation in applied axial load. This variation was however less than 2% of the column squash

load and as such was deemed insignificant. The nominal load levels induced into the columns are shown in Table 3.5. The level of column loads provide increments up to the maximum column load of 906 kN applied by the jack in test no. 12. In the last test conducted (no. 13) there was a problem with the pump in maintaining the load. The pump was replaced, but manual control of the pump's pressure resulted in continual fine adjustments throughout the duration of test. These adjustments caused the inclinometers to fluctuate and resulted in some lack of smoothness as can be seen on page A-14. However the overall results were reasonable, as shown in Figure 3.16 which presents the moment-rotation responses for the four axial load cases listed.

Test No.	Axial load (kN)	Ratio of axial load to squash load
7	80	0.05
11	506	0.31
12	906	0.55
13	702	0.43

Table 3.5 Axial load applied to column member

After each test the joints were inspected. In every test, the endplate had not yielded but the column face had deformed appreciably. The column had yielded similarly to the previous test number 7, in which the top two rows of bolts had pulled the face extensively causing the face to yield around those bolts and into the web. The deformation was so severe that the column member showed signs of inward buckling at the top row of bolts and outward bowing in the compression zone of the joint. The degree of yielding and deformation of the two webs of the column was dependent on the level of axial stress; the greater the stress, the increased amount of yielding. In the worst case the yielding had spread to below the centre-line of the column webs.

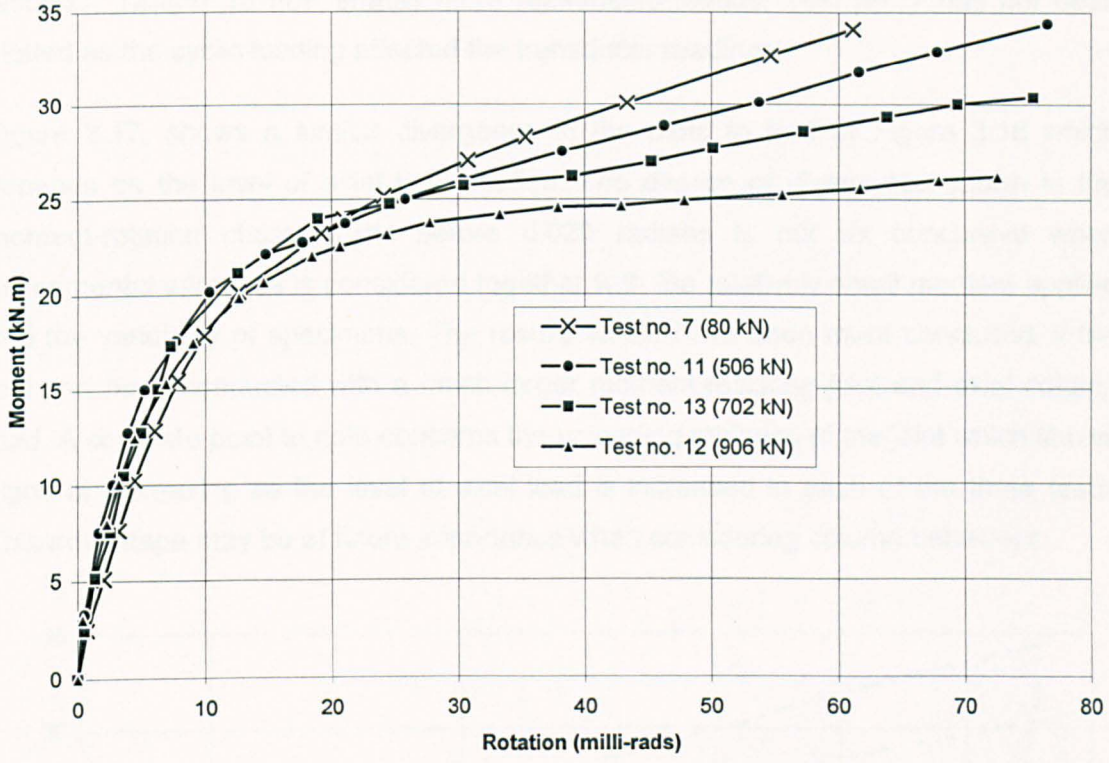

Figure 3.16 *Comparison of moment-rotation characteristics of flush endplates under the presence of column axial loads*

The results of the tests shown in Figure 3.16, clearly indicate the reduced post yield stiffness levels developed at rotations from 0.020 radians onwards. Test no. 12 is especially interesting as the joint stiffness is approaching zero when the average longitudinal stress in the column is at only 55 percent of the yield value. It was disappointing that this was the maximum level of stress that could be developed in the column, which in a practical sense is equivalent to its 'serviceability' load if axial loads are dominant.

The effect of axial load on the joint's stiffness and capacity is clearly apparent after 0.020 radians. What is masked is the effect on joint response prior to these rotations (i.e. at the beginning of the joint's load history). The results from the inclinometers in Figure 3.16 for this area of the moment-rotation response are cluttered, with test no. 7 plotted below the other tests when it was expected to be above. Both cyclic loading and experimental tolerance influencing the data. To provide more clarity for the initial stages of the joints loading, Figure 3.17 shows the same moment-rotations but compiled from the transducers mounted top and bottom of the flanges. In the past the resulting cyclic action had produced poor results but the non-cyclic loading used in

tests 11, 12 and 13 now enable more reasonable results. Test no. 7 has not been plotted as the cyclic loading affected the transducer readings.

Figure 3.17, shows a similar divergence in the plots to that of Figure 3.16 which depends on the level of axial load applied. The degree of divergence shown in the moment-rotation characteristic before 0.020 radians is not as conclusive when experimental tolerance is considered together with the relatively small moment applied and the variability of specimens. The results would have been more conclusive if the test had been conducted with a much larger moment-resisting joint and axial column load. A separate point to note concerns the unloading stiffness of the joint which shows signs of increasing as the level of axial load is increased in each of the three tests. This advantage may be of future importance when considering column behaviour.

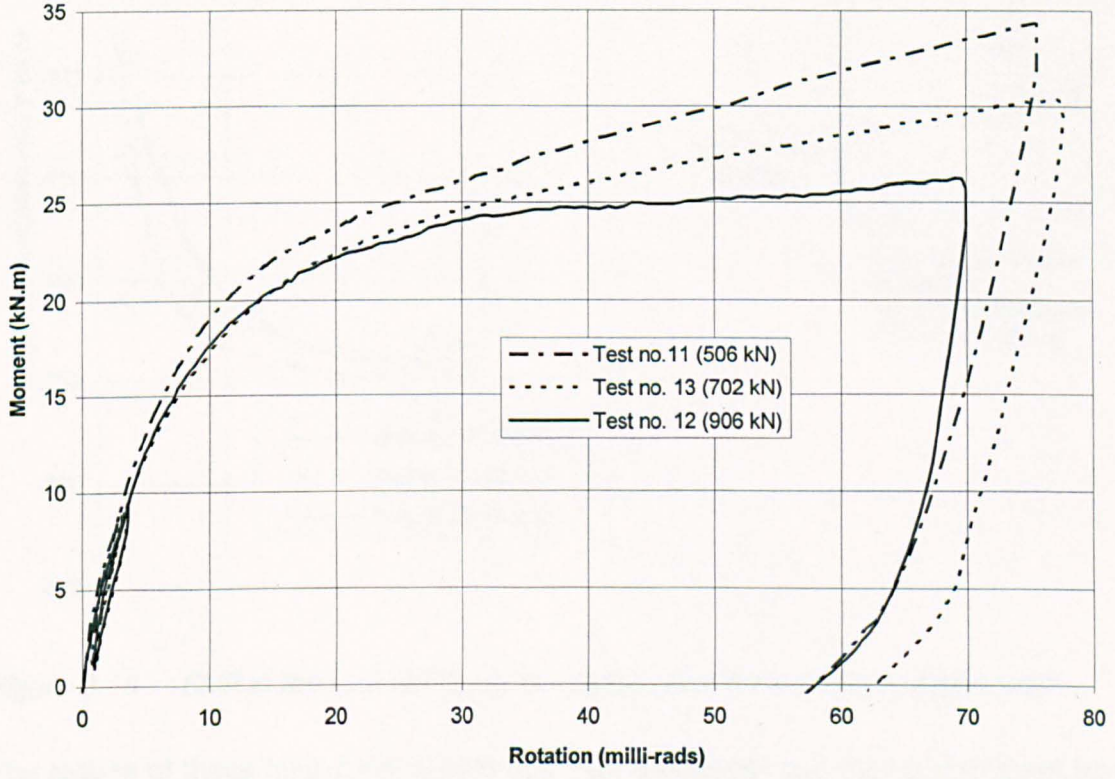

Figure 3.17 Complete moment-rotation response by LVDT's for axial loaded column joint test

The success of measuring top and bottom beam deflections in tests with non-cyclic loading applied also enabled the location of the rotation pivotal axis to be monitored throughout each of the joint tests. Figure 3.18 plots the shift in the joint's axis of rotation along the depth of the section as the positive moment is applied. At small moments the joint rotates about an internal pivot positioned at the top of the endplate

before travelling down the depth of the beam member as applied moment to the joint is increased and plastification of the tube face starts to redistribute the neutral axis of the joint. A final position is reached where the joint is unable to redistributed the applied moment at which condition the joint has clearly failed. Figure 3.18 clearly indicates that the level of stress does not significantly affect the final pivot position of the joint. The average rotation pivot for the joint tests was found to be at an approximate distance of 0.69 times the depth of the section. Obviously this position will depend on the flexibilities of both the tension and compression zone of the joint.

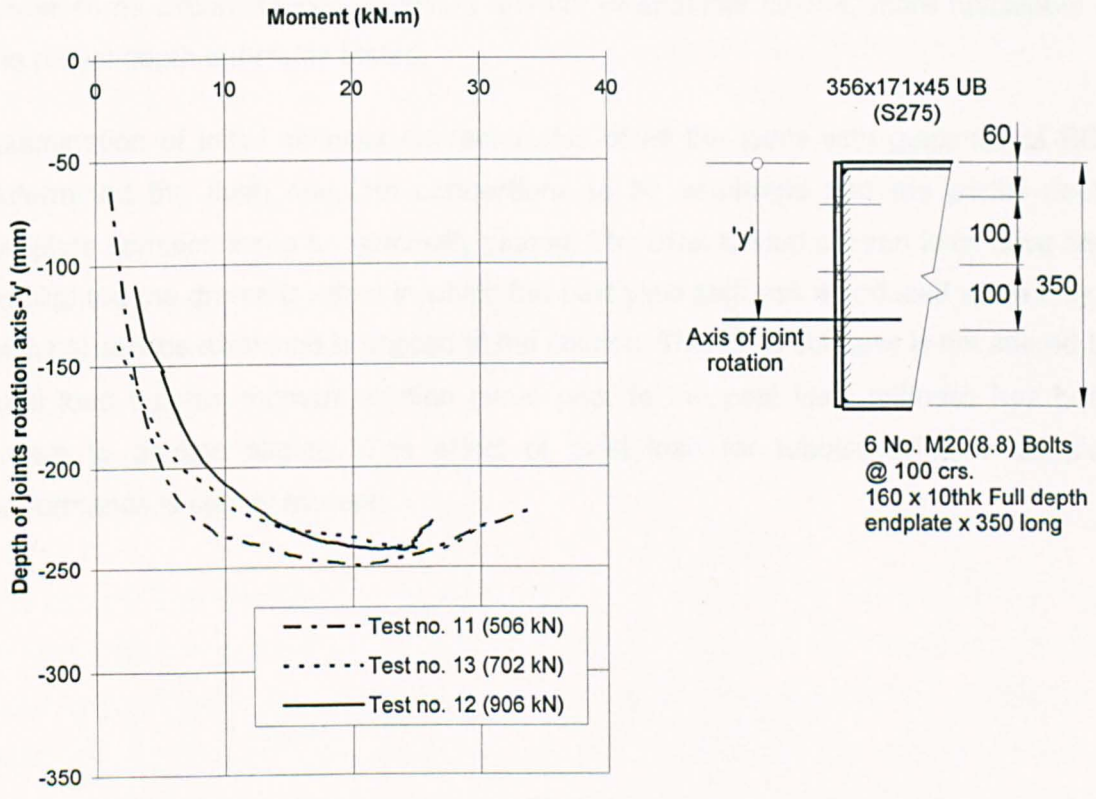

Figure 3.18 Shift in the axis of the joints rotation pivot for axial loaded joint tests

The results of these tests have shown that high axial loads can play a significant part in the behaviour of flowdrill joints; the results clearly indicating the reducing stiffness, after each of the joints had failed as the axial load is increased. The significance of this reduction is that a column which is subjected to normal serviceability loads will result in a joint used for its moment-resistance failing more rapidly than one without high axial load; the beneficial post yield stiffness that would have allowed an added factor of safety to the joint if the column was not loaded has been removed. It is regretted that the joint tests were not conducted over the full column capacity to induce a negative

stiffness. However, the complexity of the test rig to determine the moment-rotation characteristic of the joints under axial load has been worthwhile.

3.8 Chapter summary

The work reported has concentrated on the moment-rotation response of 'simple' flowdrill joints. In all the joints tested none of the connectors showed any signs of bolt pullout. They performed with great ductility, resulting in the tests being stopped because of excessive rotation induced principally by the flexibility of the tube face and, under some circumstances, a limited amount of endplate flexure, more noticeable in the partial depth endplates tested.

Examination of initial stiffness characteristics of all the joints with guidance of EC3 determined the flush endplate connections to be semi-rigid and the partial depth endplate connections to be nominally pinned. The axial loaded column tests have also highlighted the dramatic effect in which the post yield stiffness is reduced when only a nominal service axial load is applied to the column. The initial stiffness is not altered by axial load but the moment-rotation curve prior to the post yield stiffness has been shown to deviate slightly. The effect of axial load for tubular columns on joint performance is clearly evident.

Chapter 4

Experimental tests on isolated endplates

During the testing of the simple joints, reported in Chapter 3, it was evident that the flexibility of the endplate had contributed to the overall joint rotation and, in some instances, both the endplates and tube face had deformed by equal amounts. The degree of joint rotation caused by the endplate contribution had largely depended upon the detail and the relative stiffness of the joint. For example, deformation was clearly visible when partial depth endplates were adopted or when the bolts of simple flush endplates had been located as close as possible to the wall of the tube. To assess the amount of flexibility which the endplate contributes to the overall joint rotation, a series of joint tests was conducted on flush endplates that were nominally identical to those adopted in the flowdrill tests but this time securely bolted to a rigid base. In this way the endplate was tested in isolation.

4.1 Programme of joint tests

The programme consisted of six tests. Four of the joints were identical to the flush endplate details selected from the simple flowdrill joints tested in Chapter 3, and two more were adopted from the rigid series of flowdrill tests reported on in Chapter 5. Although, the rigid tests are reported in the following chapter, it is appropriate that all the separate isolated endplate tests are reported together. The sequence of reporting also reflects the sequence and development of the overall joint test programme. To ensure comparability the same batch of material was used for the endplates as in the flowdrill joint tests. Similarly, nominally identical fabrication was used with regard to weld details and construction. Table 4.1 and Figure 4.1 provide details of the six endplates tested, with the leverarm defining the positions of the jack for each test indicated in Table 4.2. The leverarm distance was again measured from the face of the column to the pivot position of the jack, and the moment was therefore calculated at the column face, similar to all the flowdrill tests conducted previously. Halfway through the testing it was necessary to increase the leverarm for the 'rigid' endplates to allow for their increased moment capacity when using the full capacity of the 100 kN jack.

Hence, a relatively high moment to shear ratio was used for the two rigid endplate tests.

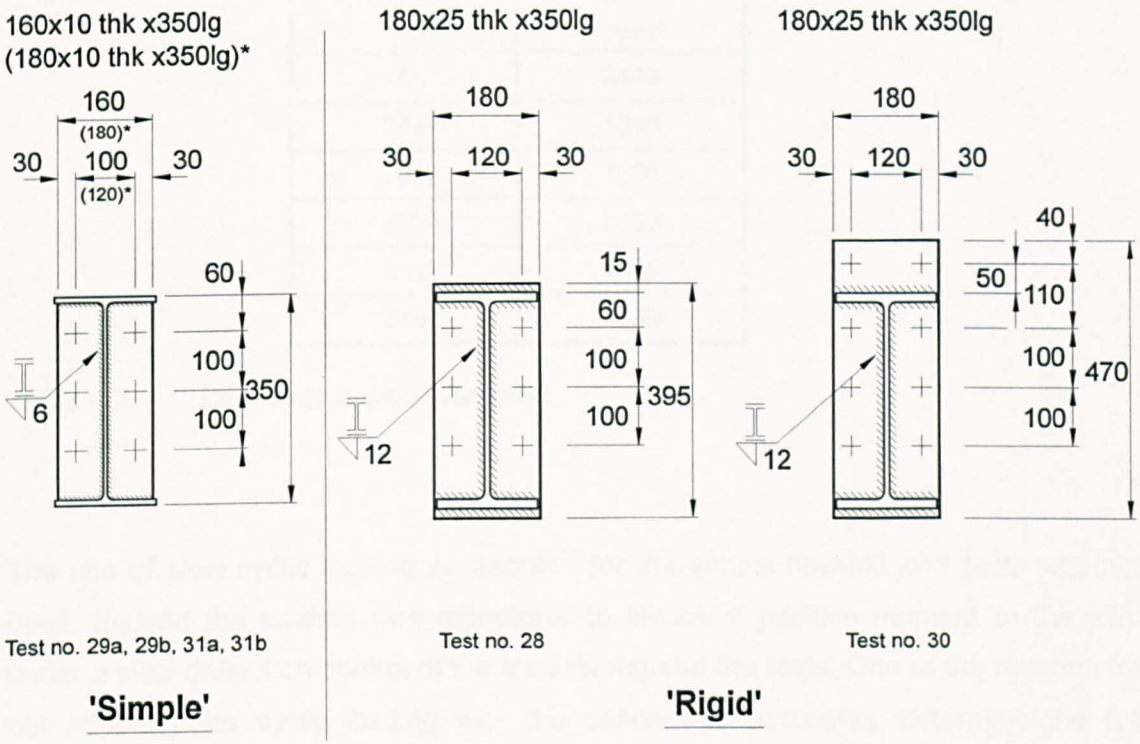

Notes:
(1) For endplate test nos 31a, and 31b the bolt cross centres are 120 mm
(2) For section sizes refer to table 4.1
(3) All holes drilled to 22 mm dia to accept M20(8.8) bolts

Figure 4.1 Endplate details adopted in test programme

Test No.	*Column Section Size*	*Steel Grade*	*Beam size*	*Endplate Type*	*Endplate Thk.*	*Bolt Cross-centres*
Simple flush endplates						
29a	Rigid- Full contact	-	356x171x45 UB	Flush	10	100
29b	Rigid-No contact	-	356x171x45 UB	Flush	10	100
31a	Rigid-Full contact	-	356x171x45 UB	Flush	10	120
31b	Rigid-No contact	-	356x171x45 UB	Flush	10	120
Rigid extended and flush endplates						
28b	Rigid-No contact	-	356x171x67 UB	Extended	25	120
30b	Rigid-No contact	-	356x171x67 UB	Flush	25	120

Note: For joint details refer to Figure 4.1

Table 4.1 Schedule of Endplate Tests

Test No.	Leverarm (mm)
28b	2440
29a	1338
29b	1338
30b	2433
31a	1340
31b	1339

Table 4.2 Leverarm position for jack

The use of slow cyclic loading as adopted for the simple flowdrill joint tests was not used. Instead the loading was monotonic to induce a positive moment to the joint under a slow deflection control of the load throughout the tests. One of the reasons for not adopting the cyclic loading was the concern to accurately determine the full relationship of the positive moment-rotation characteristic. The instrumentation of the joint consisted of an inclinometer positioned on the beam, similar to that for the flowdrill tests described in section 3.4.1, with a further inclinometer used to observe the rotation of the rigid base column. As a check on the accuracy of the inclinometers, two LVDT's were positioned outside the top and bottom beam flanges. No bolt movements nor bolt loads were monitored in these tests as relatively high bolt loads, approaching tensile capacity, were expected.

The chapter from this point onwards is split into the two sections reporting individually on the simple and rigid endplates tested.

4.2 'Simple' flush endplates

The simple flush endplates tested used the same test rig as was adopted for the simple flowdrill joint series of tests, but modified as shown in Figure 4.2, by using a rigid column base in place of the SHS columns.

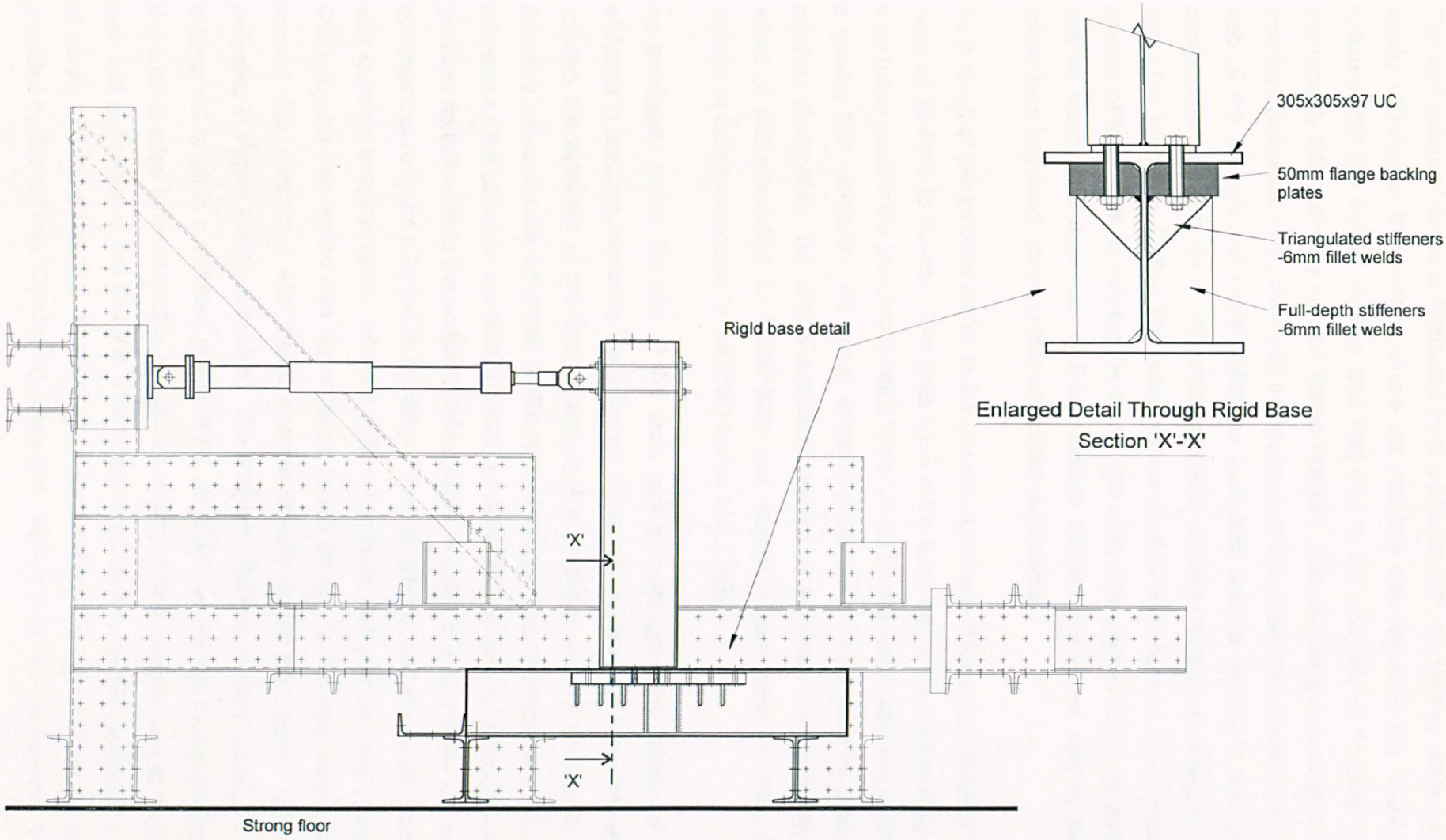

Figure 4.2 Details of test rig used for 'simple' isolated endplate tests

The rigid column base was fabricated from a 305x305x97 UC section which had been locally stiffened at the position where the endplate was bolted to the column. This ensured that the overall rotation was that due to the endplate in bending and not significantly influenced by column flange flexibility. The stiffening consisted of two 50 mm thick flange backing plates with triangulated stiffeners welded to both the plate and web of the section. Full depth stiffeners were also welded directly in line with the compression flanges. An arrangement of 22mm diameter holes was drilled to accept either the 100mm or 120mm bolt cross centres used in the endplates. This reduced the amount of fabrication by utilising the same rigid base arrangement for all six tests. The column recorded a maximum of 0.003 radians rotation due to the test rig flexibility rather than any direct consequence of column deformation.

As a result of the backing plates to the column, the flange thickness increased from a nominal 15.4mm to 65.4mm. The bolts used in the tests had to be substantially longer than those used in the previous flowdrill tests. Under tensile load it was recognised that a greater bolt elongation will occur, increasing the bolt's contribution to overall joint rotation. Fortunately, the simple endplates resulted in relatively low loads where the effect of bolt elongation for these tests was negligible (estimated at under 0.0005 radians at failure compared to the final rotation of 0.1 radians).

As previously stated the aim of the tests was to investigate the behaviour of the endplate in isolation, removing the influence of the column flexibility from the moment-rotation characteristic of the joint. However, the presence or lack of column flange flexibility influences the deformed profile of the endplate. The two extremes of restraint afforded to the endplate are that of either a totally rigid column or where the column provides no influence to the endplate deformation. In order to examine the two extreme conditions of restraint afforded to the simple flush endplates, two tests were conducted with identical endplate details where a different extreme restraint had been used. The first endplate was tested with the endplate bolted directly to the rigid base while the second was conducted with packs inserted directly under the beam's flanges, as indicated in Figure 4.3(a) and 4.3(b). The endplate which is in direct contact with the column will result in a distorted profile of Figure 4.3(c), where the restraint afforded to the outside edge induces double curvature bending. Plastic hinges form at the column web and at position of the bolt line. The endplate which was packed results in a profile of single curvature bending as shown by Figure 4.3(d) through the lack of restraint provided by the column. Conducting these two identical tests for the extreme restraint

conditions shown allows the effect of the column's stiffness influencing the overall moment-rotation response of the joint to be examined.

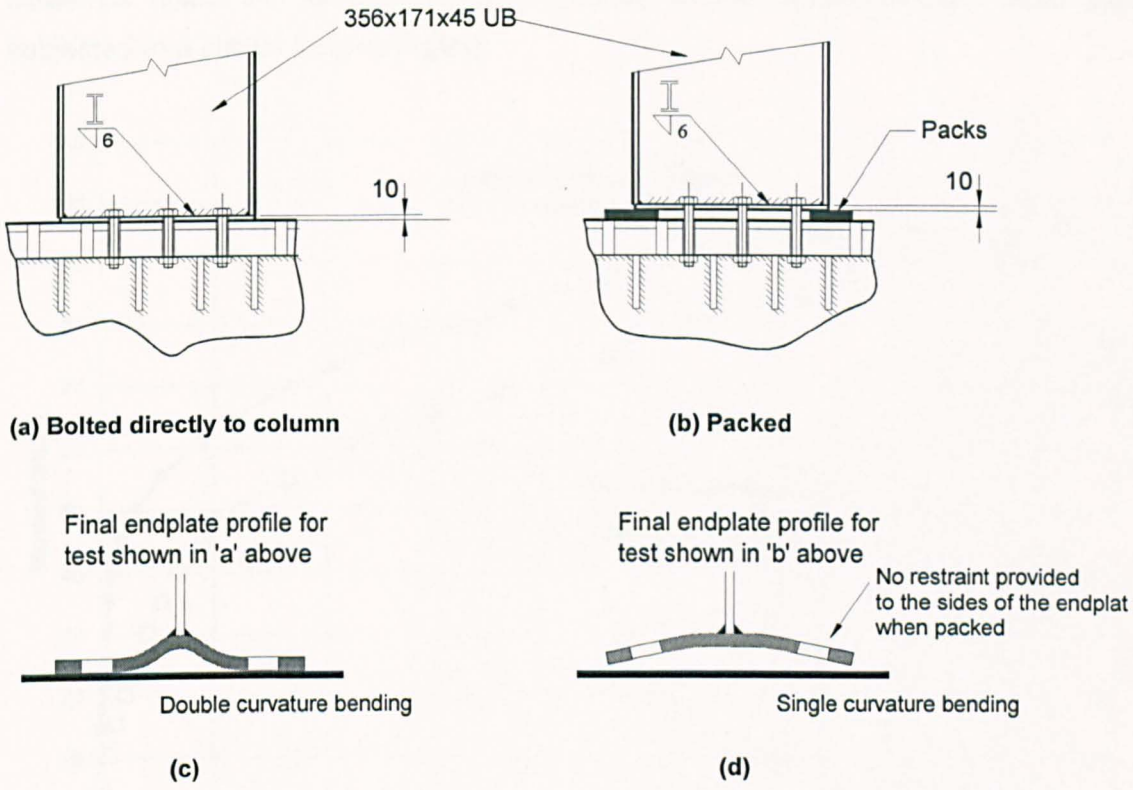

Figure 4.3 Testing arrangements adopted for Isolated endplates

4.2.1 'Simple' isolated endplate test results

The first of the endplates tested was conducted on the 10mm flush endplate attached to a 356x171x45 UB with nominal 6mm fillet welds and bolt cross centres of 120mm (test nos. 31a and 31b as identified previously in Table 4.1).

Test no. 31a was bolted directly to the rigid column face with M20(8.8) fully threaded bolts, 130mm long, with standard washers under the bolt head. The bolts were tightened to a torque of 160 N.m as in previous tests to give a consistent value and permit direct comparison. The joint was then subjected to a positive moment, where upon the maximum moment-resistance attained was 95 kN.m at 0.074 radians. Figure 4.4 shows the moment-rotation behaviour for this joint. At the early stages of the test, the joint was unloaded at a moment of 10 kN.m so as to bed the joint and reduce the risk of slippage, however in the case of this joint there was inevitably some slippage as the bolts moved into bearing in the clearance holes. This was a problem found with all

the tests with the joint geometry rotated through 90 degrees and unable to respond in a natural manner which under gravity would have allowed the bolts to bear in the clearance holes. All the subsequent joint tests for the simple endplate tests were subjected to a similar loading regime.

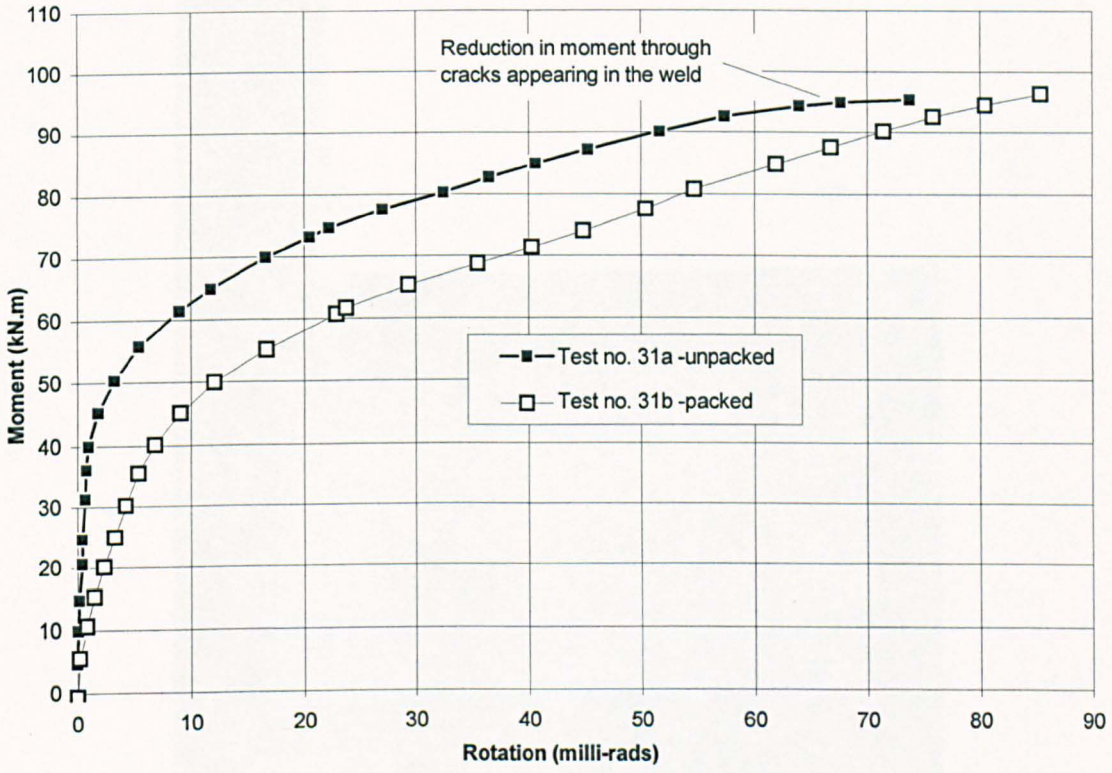

Figure 4.4 *Comparison of isolated flush endplate tests for bolt cross centres of 120mm*

The endplate exhibited excellent ductility, with the test stopped at high rotations where failure was attributed to gross deformation of the endplate, as shown in Figure 4.5. It can be seen that the endplate deformation was restricted to the area around the top row of bolts where the double curvature bending of the plate is clearly visible, which indicated that relatively large bolt prying forces were generated during the test. The top row of bolts was also plastically deformed at the head of the bolt, although the bottom two rows were found not to have suffered any damage. It was also observed after the test that cracks had formed in the heat affected zone (HAZ) of the weld close to the top row of bolts thereby causing a reduction in the joint's moment capacity at the latter stages of the test as noted in Figure 4.4. The only visible sign of yielding on the beam, apart from the endplate, was that of the top and bottom beam flanges. The compression flange had uniformly yielded adjacent to the endplate.

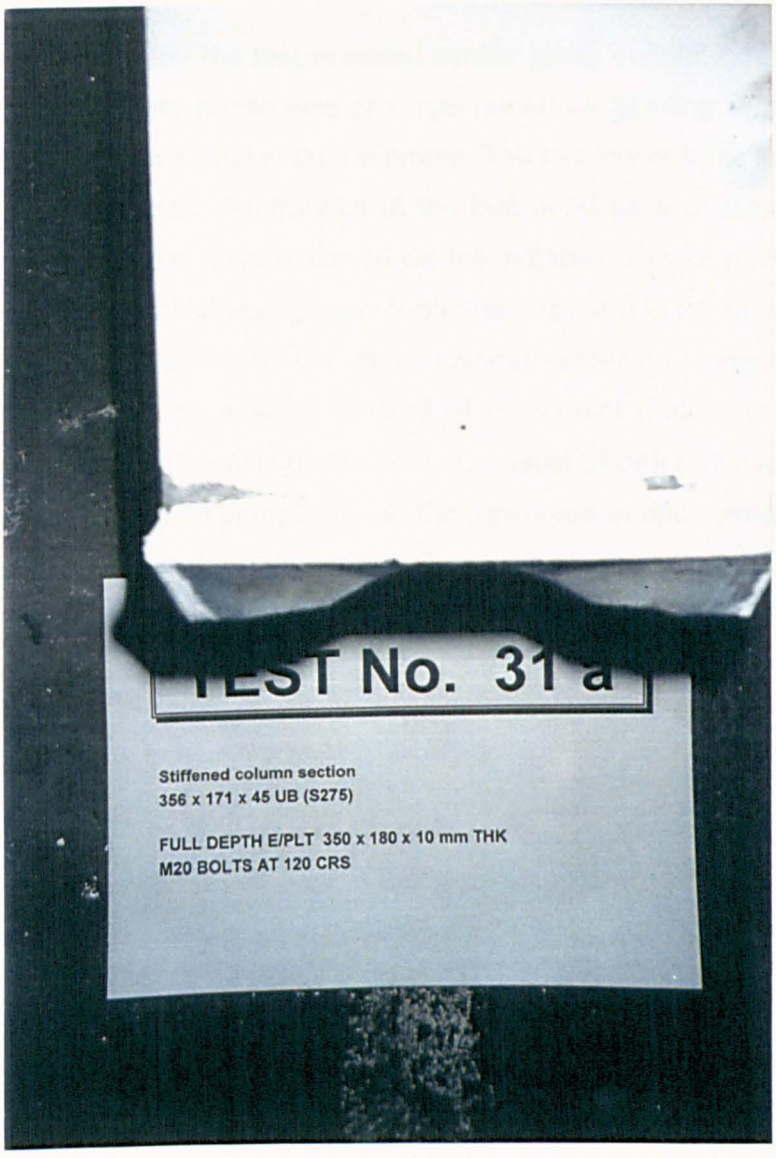

Figure 4.5 View of final deformed endplate for test no. 31a

The next endplate to be tested was no. 31b. The detail was nominally identical to the one previously tested except that it incorporated packs underneath the beam flanges as shown in figure 4.3(b). The pack thickness used was 20mm which allowed sufficient freedom of movement to the edge of the endplate to avoid any contact with the column. The packs were centred at the tips of the beam's compression flange in an attempt to simulate the conditions of the flowdrill joint, where the position of the packs represent the stiffness of the tube walls. The load was applied to the joint at the same loading rates to the previous joint. Figure 4.4 shows the full moment-rotation characteristic of the test compared directly with its equivalent unpacked endplate of test no. 31a. A final moment resistance of 96.3 kN.m at a rotation of 0.085 radians was recorded before the test was stopped through excessive rotation.

Examination of the joint after the test revealed similar gross endplate deformations as previously, but the endplate profile was of single curvature bending. Figures 4.6 and 4.7 show photographs of the final endplate profile. The top row of bolts in this test had also shown excessive plastic deformation at the bolt head as a consequence of the endplate flexibility which had also occurred on the adjacent row of bolts below. The severity of the bolt deformation was greater than that observed in the unpacked joint of test no. 31a. It was also found that the packs inserted under the compression flange had yielded slightly providing a small amount of movement under the compression flange and shifted the rotation axis of the joint. The level of deformation of the packs can be considered as small in comparison to that observed in other areas of the joint. This was especially true for the compression flange which showed signs of excessive yielding at the tips of the flanges similar to that observed in the simple flowdrill joint tests using the SHS column.

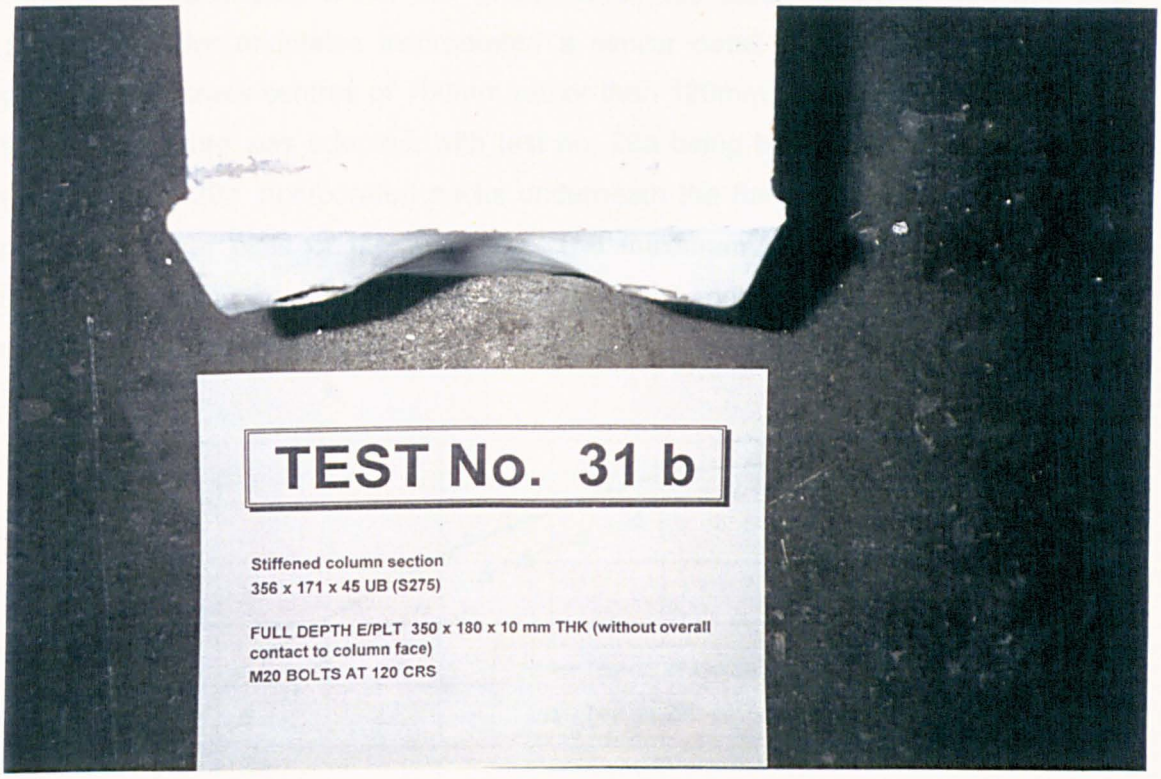

Figure 4.6 Top view of endplate test no. 31b

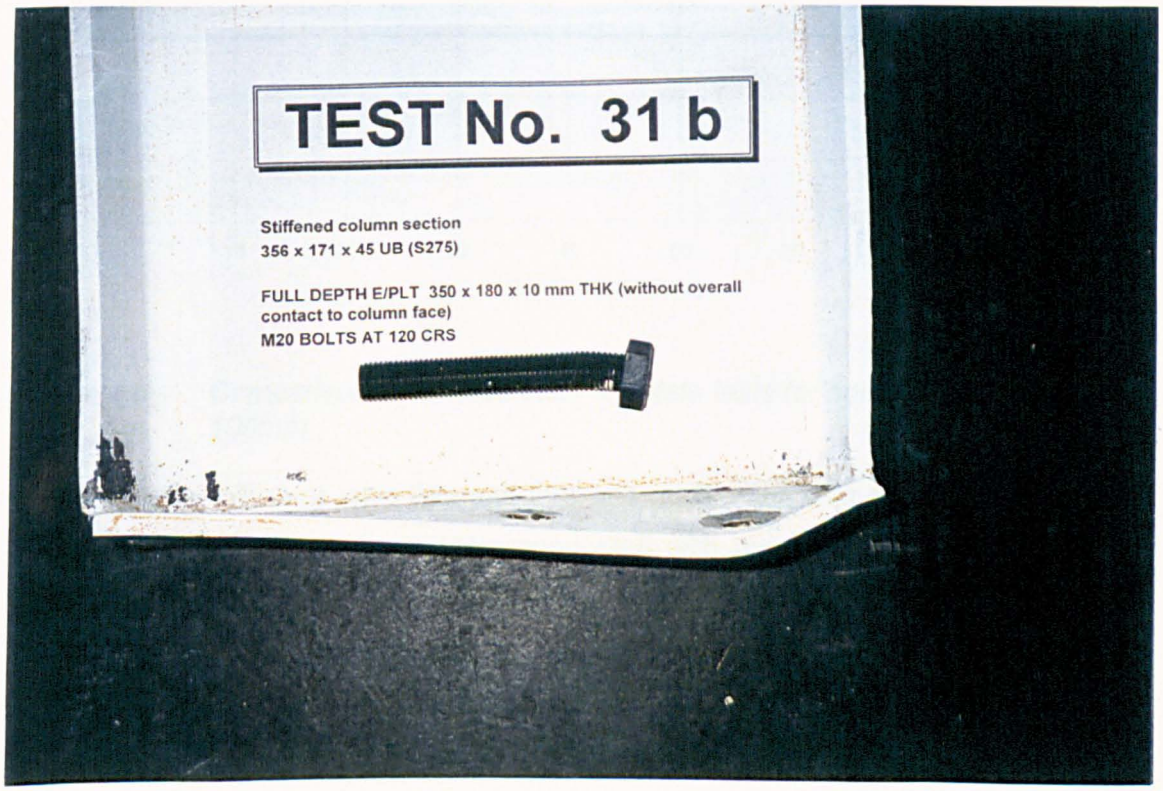

Figure 4.7 Side view of deformed endplate test no 31b

Other tests conducted within this group concerned tests numbered 29a and 29b. These particular endplates incorporated a similar detail to 31a and 31b, but now adopting bolt cross-centres of 100mm rather than 120mm previous. Exactly the same testing procedure was adopted, with test no. 29a being bolted directly to the column while test no. 29b incorporated packs underneath the flanges. Figure 4.8 shows the moment-rotation plots of the two tests. The maximum moment-resistance attained during tests 29a and 29b was 107 kN.m at 0.061 radians, and 107 kN.m at 0.076 radians respectively.

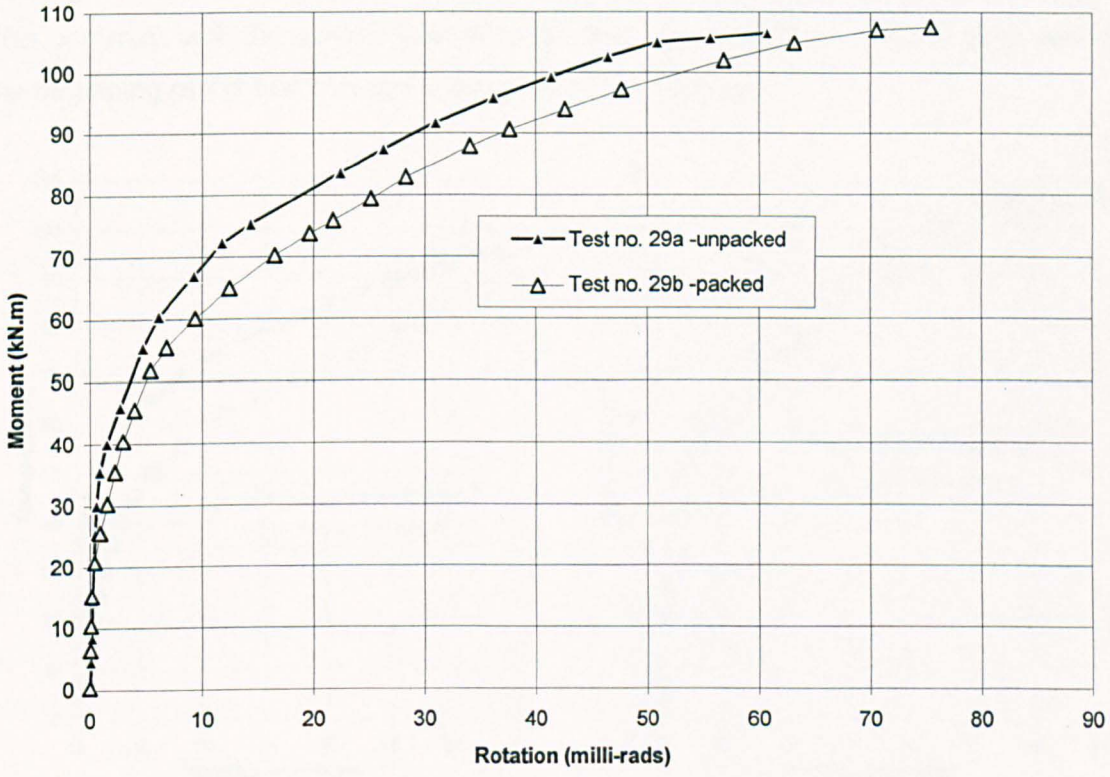

Figure 4.8 *Comparison of Isolated flush endplate tests for bolt cross centres of 100mm*

In general the failure of tests 29a and 29b was ductile and was identical to the failure of the preceding two endplate tests conducted with the 120mm bolt cross centres, although a much higher moment-resistance and stiffness was observed. Because of the attainment of a higher moment the compression flange yielded much more extensively and, at the latter stages of each test, yielding had progressed into the web of the beam. A sound was heard during the final stages of test no. 29b which was attributed to a crack developing in the weld at the tips of the flanges, resulting in a levelling off at the end of the moment-rotation curve.

4.2.2 Comparison of 'simple' endplate performance

For comparison purposes, the moment-rotation characteristics plotted previously are reproduced in Figures 4.9(a) and 4.9(b) below, which relate to the 120mm and 100mm bolt cross-centres. The two characteristics shown in each comparison relate to the endplate being either packed or unpacked underneath the beam flanges. The characteristic of the plots are essentially similar, providing ductility at large rotations ideal for simple construction. All the curves respond with initial linear stiffness, until yielding into a plateau of limited stiffness after the endplate had plastically deformed. This contrasts with the simple flowdrill tests which responded non-linearly from almost the beginning of the test due to the flexibility of the tube face.

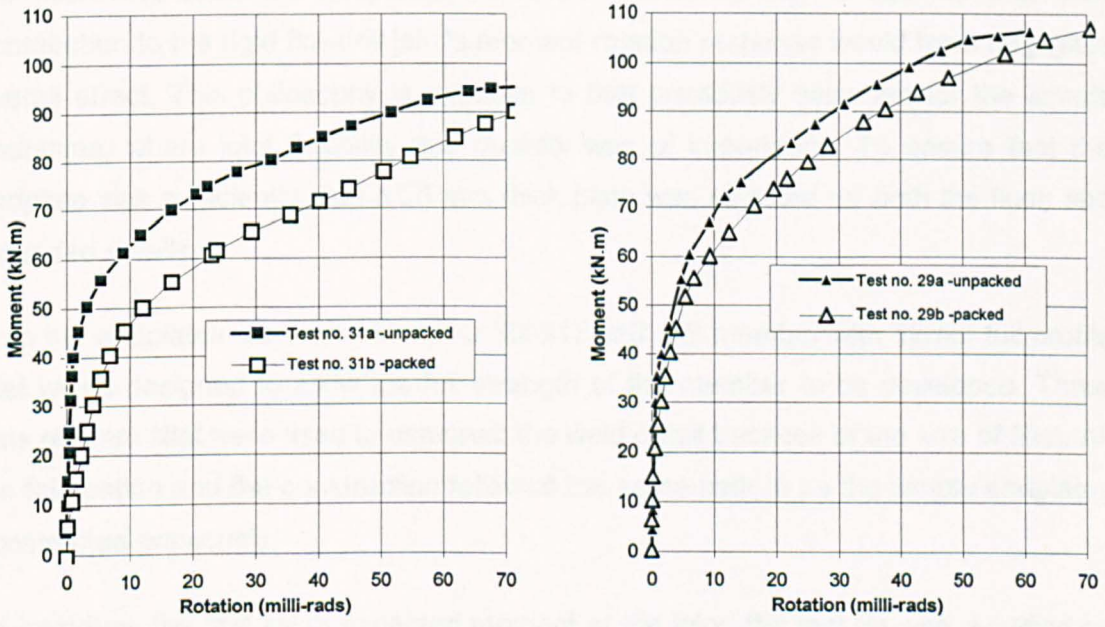

(a) 120 mm bolt cross centres *(b) 100 mm bolt cross centres*

Figure 4.9 Moment-rotation response of simple isolated endplate tests

One of the features of both Figures 4.9(a) and 4.9(b) is the difference observed in the moment-rotation characteristics between the packed and unpacked tests. It is evident that as the bolt cross-centres increase, the initial stiffness of the joint decreases. Similarly the packed joints exhibit a reduced initial stiffness as the restraint of the column base is removed, where the differences observed between the packed and unpacked endplate response for the 120mm bolt cross-centre is significantly greater in magnitude compared to that found with 100mm bolt cross-centres. It was also

observed that, as the bolt cross-centres are increased, then the moment-rotation response for the unpacked endplate deviates at an earlier stage in the joint's loading history relative to that of the packed endplate. The results show that the restraint and flexibility of the column will provide an important influence on defining the overall joint's rotation.

4.3 'Rigid' endplate tests

The 'rigid' endplate tests were conducted using flush and extended endplates, identified as test numbers 28b and 30b, noted in Table 4.1. The endplate details were nominally identical to those used in the 'rigid' flowdrill joint tests reported in the following chapter. They were conducted prior to the rigid flowdrill tests to ensure both the flush and extended endplates would be sufficiently stiff to assume that their contribution to the rigid flowdrill joint's moment-rotation response would have negligible overall effect. This philosophy is opposite to that previously assumed for the simple endplates, where joint flexibility and ductility was of importance. To ensure that the endplate was sufficiently rigid a 25 mm thick plate was selected for both the flush and extended details.

Both the endplates were attached to a 356x171x67 UB member with 12mm full profile fillet welds designed to allow the full strength of the member to be developed. Three runs of 6mm fillet were used to construct the weld detail because of the size of fillet. All the fabrication and the construction followed the same pattern as the simple endplates constructed previously.

To introduce the 300 kN.m expected moment at the joint, the test rig was modified by substantially increasing the leverarm of the jack, as shown in Figure 4.10. In adopting such a large leverarm and hence cantilevered beam length, there was a slight possibility of the beam exhibiting lateral torsional buckling. To avoid any out of plane effects, two rollers and lateral supports were positioned as shown in Figure 4.10. To reduce the overall quantity of steel required, a full strength splice was also introduced into the beam which was positioned 800 mm from the connection at sufficient distance to avoid any possible interference with the endplate or yielding of the beam. The splice was designed for the maximum moment at this position, adopting M20 HSFG bolts with load indicating washers to enable the bolts to be torqued to their proof load. Adopting the HSFG bolts, slippage at the splice was avoided that may have had an undesirable effect on the inclinometer's sensitivity to sudden movement.

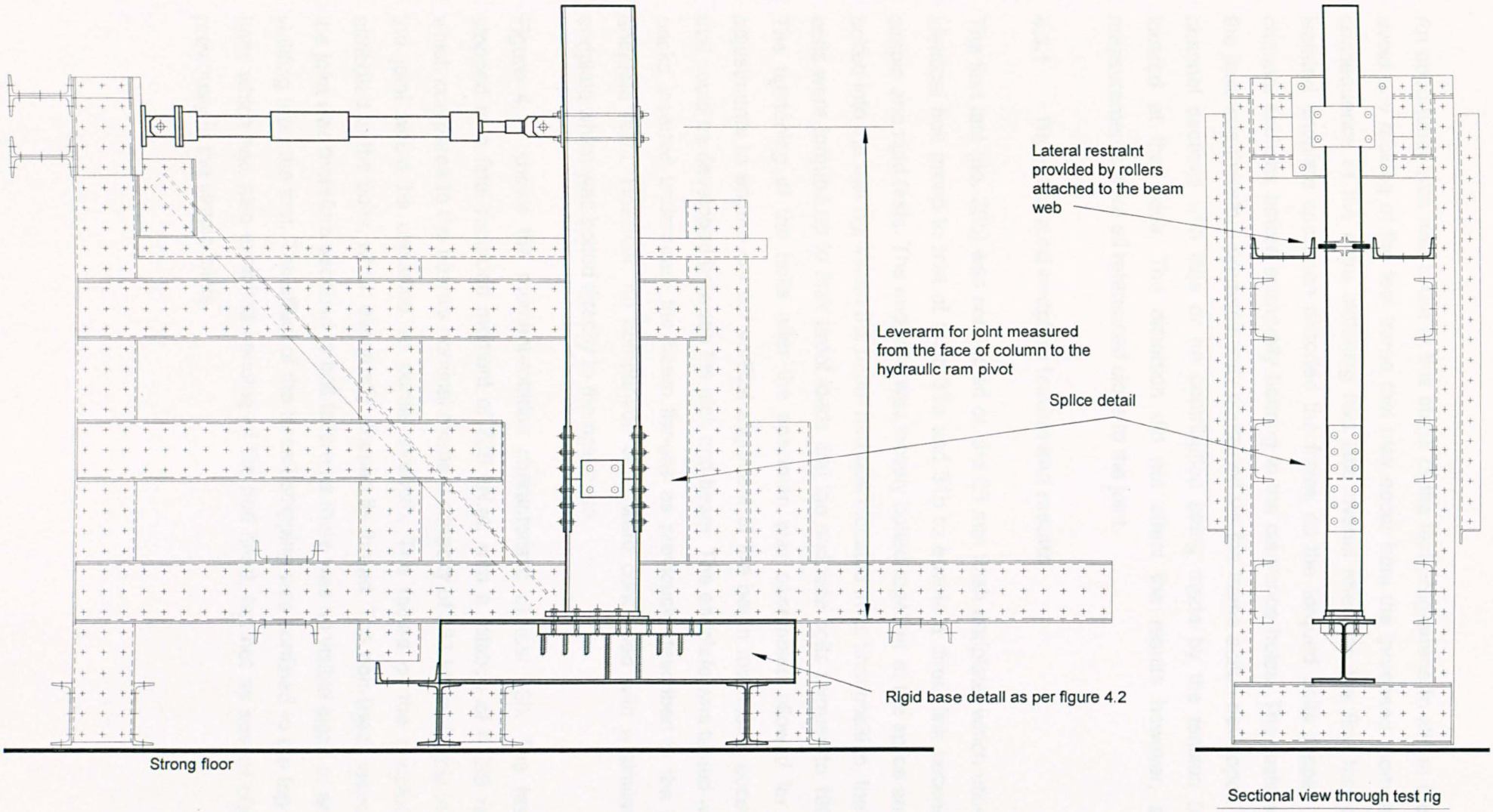

Figure 4.10 Detail of test rig used to test 'rigid' isolated endplates

An opportunity was also taken at this stage of the test programme to stiffen the rig to avoid any racking of the test frame that may occur from the increased moment. The consequence of the extra stiffening had little overall effect as the first test on the isolated endplate specimen distorted the frame as the torqued bolts slipped in the channel sections before eventually bearing in the clearance holes. The resistance of the jack was therefore predominantly contained via the frame action developed by the channel sections with little or no contribution being made by the tension bracing located at the sides. The distortion did not affect the results however, as the measurements were all referenced close to the joint.

4.3.1 Rigid isolated endplate testing and results

The first test (no. 30b) was conducted on the 25 mm flush endplate, which utilised an identical bolt group to that of tests 31a and 31b to enable a direct link between the simple and rigid tests. The endplate was loosely bolted together at the splice and then bolted into the test rig. When the beam had been located in its final position, the splice bolts were torqued up to their proof loads and the endplate bolts torqued to 160 N.m. The tightening of the bolts after the specimen was assembled allowed for minor adjustments to ensure correct vertical alignment of the beam minimising eccentricity that could be developed between the jack and beam. The endplate was tested with the packs inserted underneath the beam flanges as previously described in the simple endplate tests. However, no comparison tests were conducted with a similar flush endplate which was bolted directly to the rigid base.

Figure 4.11 shows the moment-rotation characteristic of test 30b. The test was stopped at a final recorded moment of 239 kN.m, with a rotation of 0.029 radians, which compares to the beam's nominal moment capacity of 333 kN.m. In this instance the joint would be classified as partial strength. The failure of the endplate was attributed to the bolts, which eventually stripped its thread. The non-linear response of the joint was therefore ascribed to bolt failure as there was no visible signs of endplate yielding after the test. The effect of the thread stripping was confined to the top row of bolts which had also exhibited bending of the bolt head, but not as severe observed previously in the simple joints.

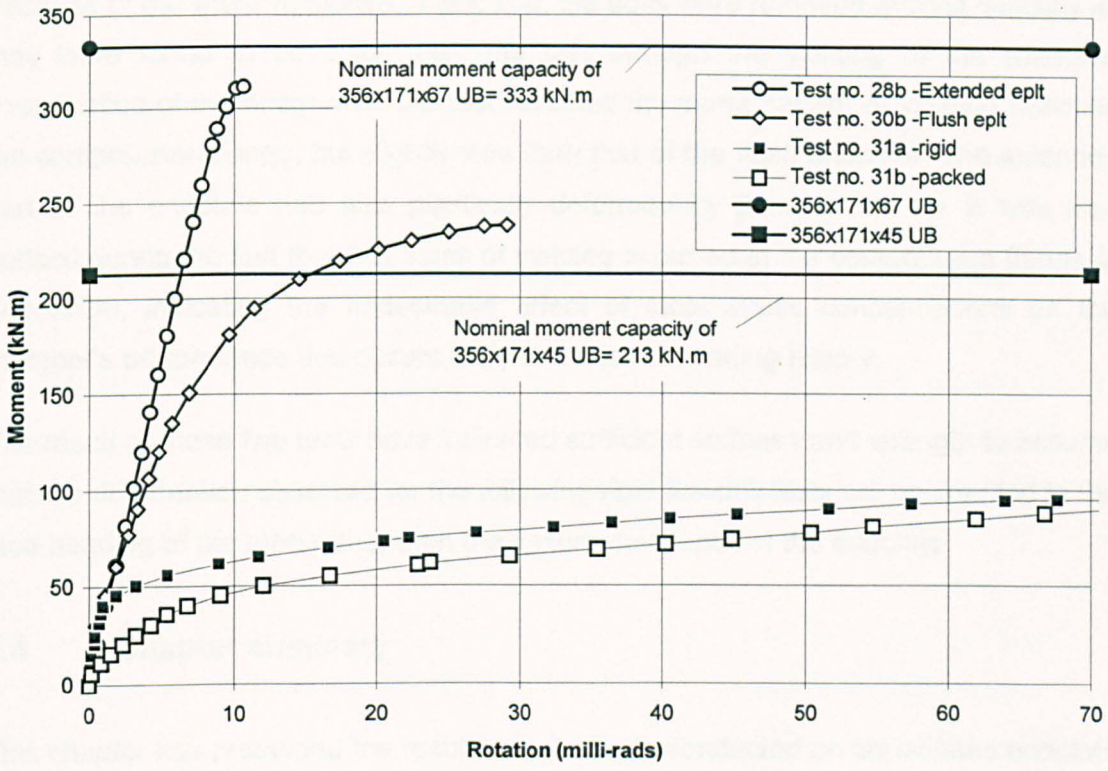

Figure 4.11 Moment-rotation response for rigid endplates with simple endplate comparison

During the test it was observed that local yielding of the compression flange of the beam occurred at about 150 kN.m, which is approximately half the beam's nominal moment capacity. The yielding of the beam at the end of the test extended along the full width of the compression flange and along the full web of the section. There was also some signs of yielding at the tension flange.

The second joint to be tested was no. 28b in the schedule, described in Table 4.2 previously. This was the extended endplate which is typical of the detail adopted for the rigid joints reported on in Chapter 5. A similar assembly procedure for the extended endplate was adopted as for the flush endplate. The results of the test are plotted on Figure 4.11 and directly compared to the flush endplate. The only difference between the two endplates is the addition of an extra row of bolts in the extended portion of the endplate. The endplate attained a maximum moment-resistance of 312 kN.m at 0.012 radians before the jack capacity was reached and the test stopped. The final moment-resistance is just below the beam's nominal moment capacity. However the linearity of the joint's response and the limit imposed by the jack rather than the joint failing, all contribute to the joint being classified to EC3 as full strength and rigid if the test had continued to joint failure.

Because of the linear response of test 28b, the bolts were removed without difficulty as they were found to be slack after the test through the yielding of the washers. Examination of the beam after the test revealed the same pattern of yielding affecting the compression flange, but slightly less than that of the flush endplate. The extended part of the endplate had also plastically deformed by 2mm at the tip. It was also noticed during the test that first signs of yielding occurred in the compression flange at 142 kN.m, indicating the undesirable effect of local stress concentrations on the member's performance that occurs early in the joint's loading history.

The result of these two tests have indicated sufficient stiffness and strength to assume that the deformation observed for the following rigid flowdrill tests will be credited to the face bending of the tube rather than the flexure developed in the endplate.

4.4 Chapter summary

This chapter has presented the results of joint tests conducted on six isolated endplate specimens nominally identical to the details found in the main programme of tests using Flowdrill tubular sections. The tests indicated significant variability of the moment-rotation response when two extreme cases of restraint was imposed onto the endplate from the column. All the simple joint tests and the flush endplates used for the 'rigid' connection were found to be partial strength and semi-rigid. Only the extended endplate exhibited enough moment capacity to be classified as full strength.

Chapter 5

Experimental tests on 'rigid' Flowdrill joints

In traditional open section joints which have been used as moment-resisting connections there has always been a tendency to consider only the moment capacity of the joint. The rotation response has usually been assumed to be rigid, i.e. deformations are so small that their effect can be neglected. The 'simple' Flowdrill joints tested previously indicated a relatively flexible response, caused mainly by the deformation of the column face. When applied to simple joints the flexibility is not a problem, but an advantage, as they are usually required to simulate the conditions of a pinned joint and flexibility is therefore beneficial. In situations where the joints are assumed to be rigid, there is an obvious need to examine the ultimate moment capacity for strength requirements but to also consider (with equal concern) the amount of rotation which the joint will undergo at a serviceability load level. For this reason a series of 'rigid' joints was developed and the tests of these is reported in this chapter.

5.1 Programme of joint tests

The programme of tests relating to the rigid series of joints is shown in Table 5.1, with details of the joint geometry shown in Figure 5.1. The rigid joints were devised and tested after the simple joints had been completed. The results of the first series of tests therefore influenced the rigid series with regard to member sizes and endplate thickness. Unfortunately because of the schedule of testing, similar batches of steel could not be used in the rigid series of joint tests to enable a direct comparison to the simple tests conducted previously. However, material tests were undertaken for all batches the results of which are given in Appendix B.

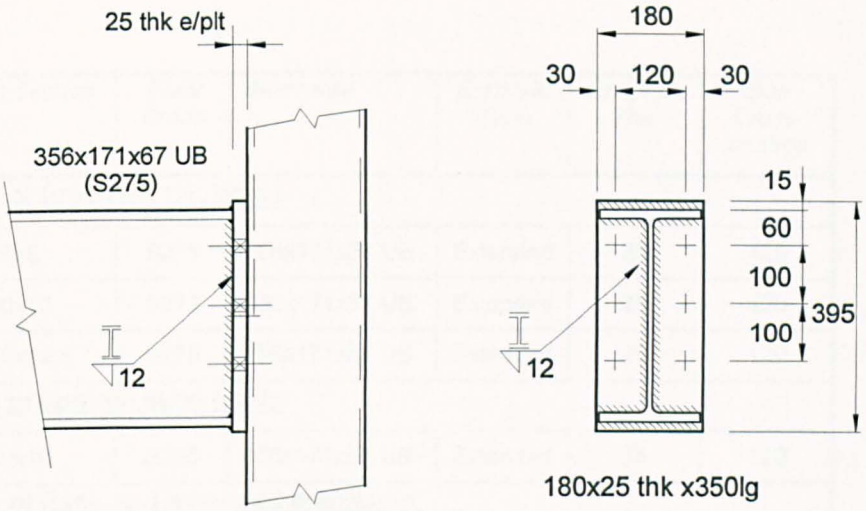

Flush Endplate Detail (FE)

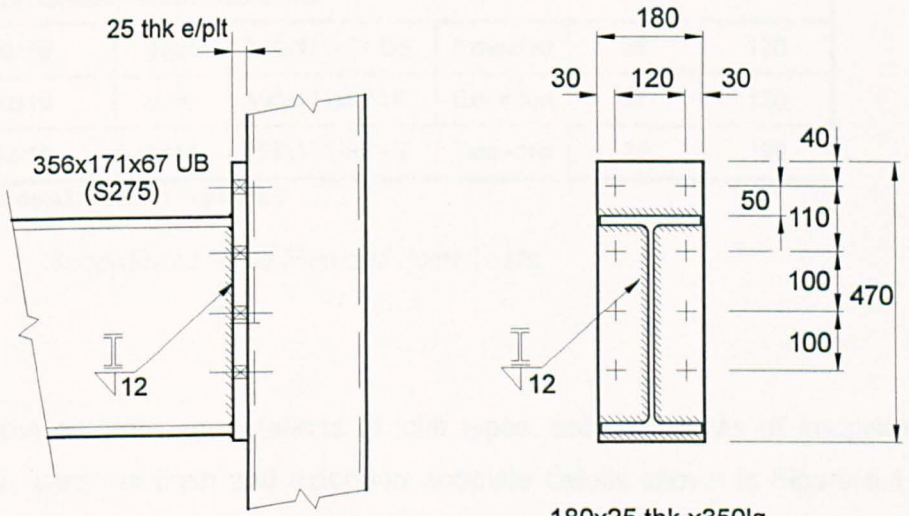

Extended Endplate Detail (EE)

Note:
(1) All holes drilled to 22 mm dia to accept M20(8.8) bolts

Figure 5.1 Details of endplates used in rigid series of Flowdrill tests

Test No.	Column Section Size	Steel Grade	Beam size	Endplate Type	Endplate Thk.	Bolt Cross-centres
Comparison of tube wall thickness						
19	200x200x8	S275	356x171x67 UB	Extended	25	120
20	200x200x10	S275	356x171x67 UB	Extended	25	120
21	200x200x12.5	S275	356x171x67 UB	Extended	25	120
Comparison of column steel grade						
23	200x200x10	S355	356x171x67 UB	Extended	25	120
Comparison of flush and extended endplates						
25	200x200x10	S275	356x171x67 UB	Flush	25	120
26	200x200x8	S275	356x171x67 UB	Flush	25	120
Comparison of Hollo-bolt Connection						
32	200x200x10	S355	356x171x67 UB	Extended	25	120
32b	200x200x10	S355	356x171x67 UB	Extended	25	120
33	200x200x10	S355	356x171x67 UB	Extended	25	120

Note: For joint details refer to Figure 5.1

Table 5.1 Schedule of Rigid Flowdrill Joint Tests

To reduce the different permutations of joint types, only two types of endplate were used. These were the flush and extended endplate details shown in Figure 5.1. Both endplates had the same 120mm bolt cross-centres positioned as close as possible to the sides of the column wall to reduce the extent of face bending and increase the joint's moment capacity. The cross centres used were the maximum allowable before clearance becomes a problem inside the SHS with adjacent flowdrill connectors at 90 degrees. The joint variation was again reduced by adopting only the 200 box column and 356 serial beam size for comparison.

The programme was devised to investigate the flexural response of the column face as this was found to be the main cause of failure in the simple joints. Both the endplate and beam section sizes were therefore selected to ensure that their contribution to the joint's overall rotation would remain relatively small in comparison to that shown by the tube face. To ensure this, both the size of the endplate and the beam was substantially greater than that adopted in practical situations. Hence, the adoption of a 25mm thick endplate welded to the top weight in the 356 serial beam size. Tests on both the flush

and extended endplates in isolation, reported on in Chapter 4, confirmed that the resistance of the endplate detail is significantly above that of the joint's recorded moment capacity using the SHS column.

The various parameters investigated in the programme are grouped together within Table 5.1 under their respective headings. These included comparison of tube wall thickness, where 8mm, 10mm and 12.5mm walled column sections have been used with the extended endplate detail. Both the flush and extended endplate details were also investigated with the intent of examining improved joint performance. The steel grade was also varied between S275 and S355. In addition to these tests, there was a direct comparison between the Flowdrill connector and an equivalent blind bolting system developed by Lindapter International plc, called the 'Hollo-bolt', which will be reported on separately in section 5.5.

5.2 Fabrication and material strength

The fabrication of the test specimens was completed within the department's own workshop. The fabrication details were identical to the isolated endplate tests noted in section 4.5. The endplates were welded to the beam with 12mm fillet welds, applied to the full profile of the section. The flanges of the beam were not reinforced with stiffeners which allowed the beam to yield and contribute to the overall rotation of the joint (albeit by a small amount).

The column specimens were delivered to the department pre-cut to the required length. The position of the flowdrill holes were marked out and centre popped on each of the columns before being delivered to Tubemasters Ltd. for Flowdrilling. The returned sections were surveyed and the flowdrill thread depth measured. The results are included in Chapter 3, Table 3.2. A full account of the survey can be found in Appendix B. Tensile tests were conducted on steel coupons cut from the column specimens as an independent check. The results for each batch of steel is shown in Table 5.2, together with British Steel's own test results for yield strength comparison.

Section size	Steel grade	Tensile coupon tests			British Steel Test Certificates	
		Yield	Young's modulus	UTS[1]	Yield	UTS[1]
		(N/mm^2)	(kN/mm^2)	(N/mm^2)	(N/mm^2)	(N/mm^2)
200x200x8.0 SHS	S275	346	206	489	367	494
200x200x10.0 SHS	S275	329	211	477	337	470
200x200x10.0 SHS	S355	427	217	560	448	561
200x200x12.5 SHS	S275	307	207	452	316	484

Notes: (1) UTS- Ultimate tensile strength
(2) All values presented are averaged longitudinal yield stress

Table 5.2 Summary of tensile coupon results and comparison to British Steel test certificates for column specimens

5.3 Joint test procedure and assembly

The joints were all tested in the cantilever arrangement as shown in Figure 5.2. The test rig had previously been used to test the isolated (nominally identical) endplates as reported in Chapter 4. Only a small modification was required to the rig to allow the columns to be bolted directly to the strong floor. As part of the simple joint tests, the test arrangement required a system of complex roller supports to allow the introduction of axial column load. The sections used in the rigid joints have substantially increased wall thickness compared to those used in the simple joints. Investigating the effect of axial load on such joints would have led to impractically high applied loads and thus this effect was not investigated. This allowed the adoption of a much simpler fixing, shown in Figure 5.2, with the column bolted between two channels. The arrangement still allowed the column to respond in flexure as the moment was applied to the joint.

The test instrumentation developed for the simple joint series was also adopted for the rigid joints. The strain gauge bolts were not used in the tests as bolt forces were expected to be relatively high for connections designed as primarily moment-resisting and would therefore damage the bolts. The inclinometers were also positioned at the same location; 125mm above the column face on the centre-line of the beam with another inclinometer located on the centre line of the column. Both the inclinometers and the transducers used to measure bolt displacements were read at five second intervals by an Orion data logger.

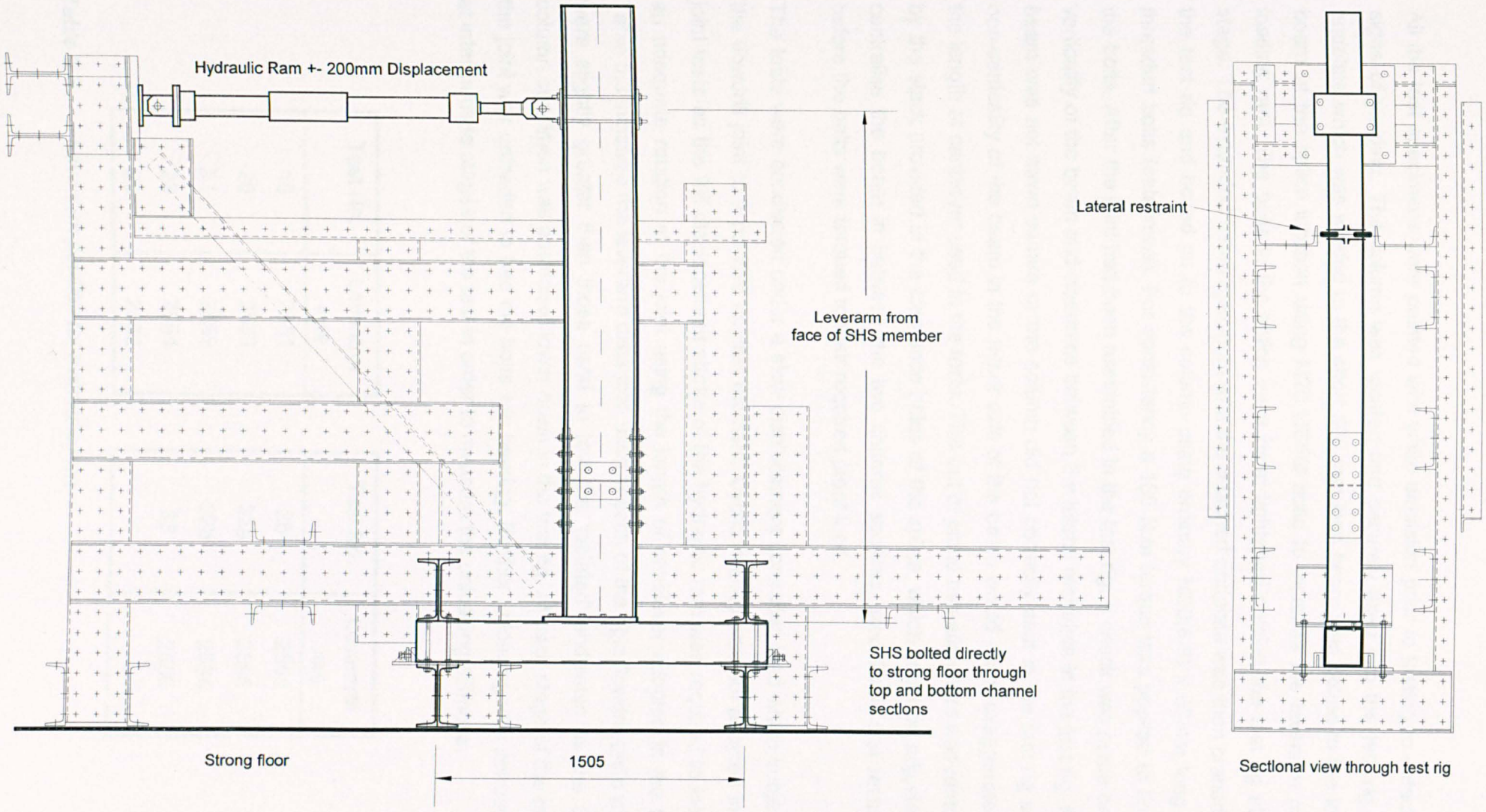

Figure 5.2 Details of test rig used for rigid flowdrill joints

All the test specimens were painted with white emulsion prior to testing to detect any signs of yielding. The column was located and securely fixed into the test rig. The endplate which was welded to the short 800 mm long beam was bolted to the longer beam at the splice location using M20 HSFG bolts to increase the leverarm of the loading ram. The bolts in the splice were hand tightened outside the test rig at this stage. The extended beam specimen with the attached endplate was then craned into the test rig and bolted on to the column using ordinary M20(8.8) x 60mm long fully threaded bolts (setscrews). For consistency a 160 N.m torque was applied to tighten the bolts. After the joint had been assembled in the test rig, a check was made on the verticality of the beam and clearance between the lateral restraints in the test rig. If the beam was not sawn square or the column did not correctly seat in the test rig some non-verticality of the beam in the minor axis of the beam would arise, exaggerated by the length of cantilever used in the tests. This out of plane mis-alignment was removed by the slack provided in the clearance holes of the splice, which could be adjusted to centralise the beam in between the two channel sections used for lateral restraint, before the bolts were torqued to their required proof load.

The tests were conducted under a slow displacement controlled load which subjected the flowdrill joint to a positive applied moment. Cyclic loading was not adopted in the joint tests as the full displacement stroke of the hydraulic ram was required to induce an adequate rotation at the joint using the length of cantilever adopted in the test. Table 5.3 indicates the leverarm distances used in each of the rigid flowdrill tests which were slightly greater than those used to test the 'isolated' endplates as the SHS column specimen was positioned lower down in the test rig. At each stage of the tests, the joint was unloaded to bed the bolts into bearing. Further unloading was conducted at intermediate stages of the test in order to measure the unloading stiffness.

Test No.	Leverarm (mm)
19	2551
20	2553
21	2553
23	2554
25	2552

Test No.	Leverarm (mm)
26	2553
32a	2555
32b	2554
33	2556

Table 5.3 Leverarm position for hydraulic ram

5.4 Discussion of rigid Flowdrill joint tests

The test results are presented under each of the identified groups previously mentioned for investigation. For ease of interpretation of the moment-rotation data, key points on the curves have been selected which best represent the original experimental results as a series of multi-linear lines. As in the case for the simple joints, the original full load hysteresis plots can be found in appendix A for all the joints tested. In cases where greater clarity is required in the main text, then the full curve shall be referred to. The joint tests will be reported in group order and not the sequence in which they were tested. Comparisons will also be made, where necessary, to both the series of tests conducted on the simple joints and the isolated endplates reported previously.

5.4.1 Comparison of extended endplates with variation of tube wall thickness

The first series of joint tests was conducted on the extended endplates where the column thickness was varied. This particular endplate detail has been widely adopted in cases where the joint's moment capacity is required to approach that of the beam. The comparison of the extended endplates was conducted over a series of three joint tests in which the 8mm, 10mm and 12.5mm walled thickness was examined for the 200x200 serial sized SHS using grade S275 material.

The first test conducted in this group was joint test no. 21, where the extended endplate was bolted to the 200x200x12.5 mm SHS. Figure 5.3 shows the endplate bolted to the column and the linear voltage distance transducers (LVDT's) located above the bolts to measure the relative bolt displacements prior to testing. In this case only the column was painted with white emulsion and the beam left unpainted.

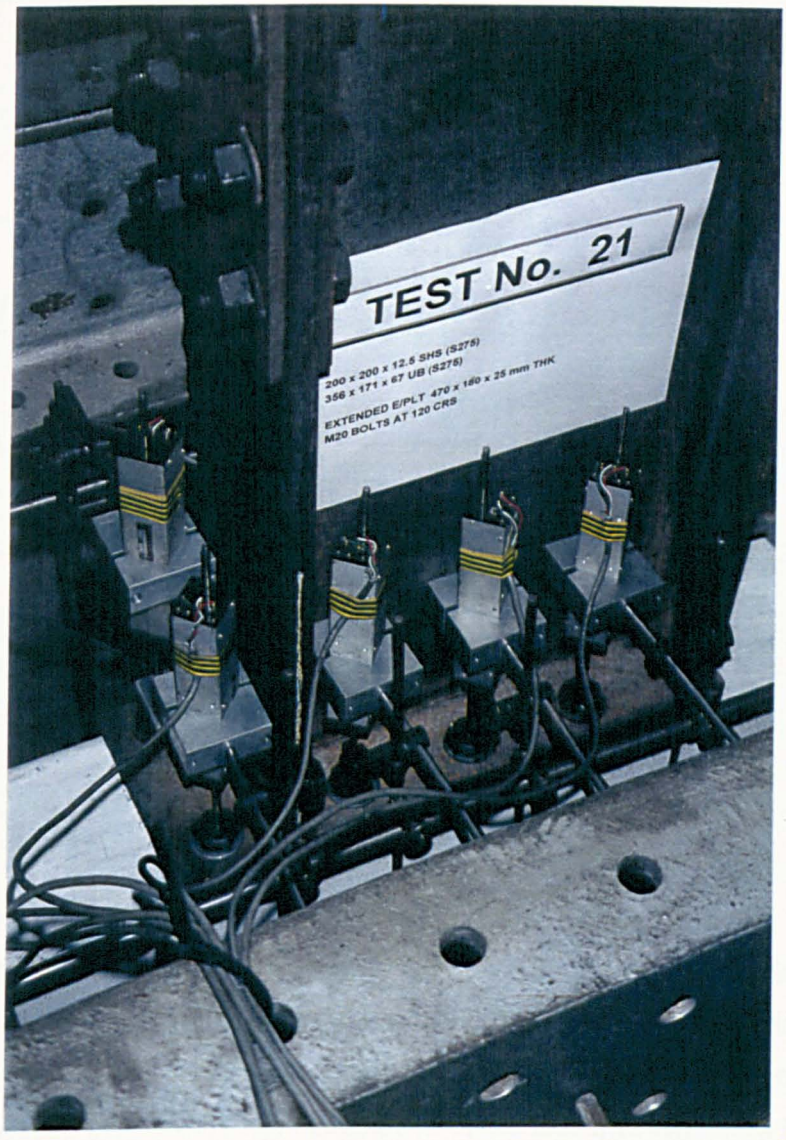

Figure 5.3 *Test no. 21 showing instrumentation to the joint prior to testing.*

A 75 kN.m moment was applied to the joint before being unloaded. At this level of moment the joint responded initially linearly. Figure 5.4 shows the full moment-rotation characteristic of the joint. The load was steadily increased to fail the joint, until the hydraulic ram registered no further increase in load, levelling off at 236 kN.m at 0.020 radians. The pump capacity was not sufficient at this stage to initiate the failure observed in the simple joints consisting of a long linear plateau after the joint had yielded, even though the joint had exhibited a non-linear response which was clearly approaching the joint's final capacity. The joint was subsequently unloaded.

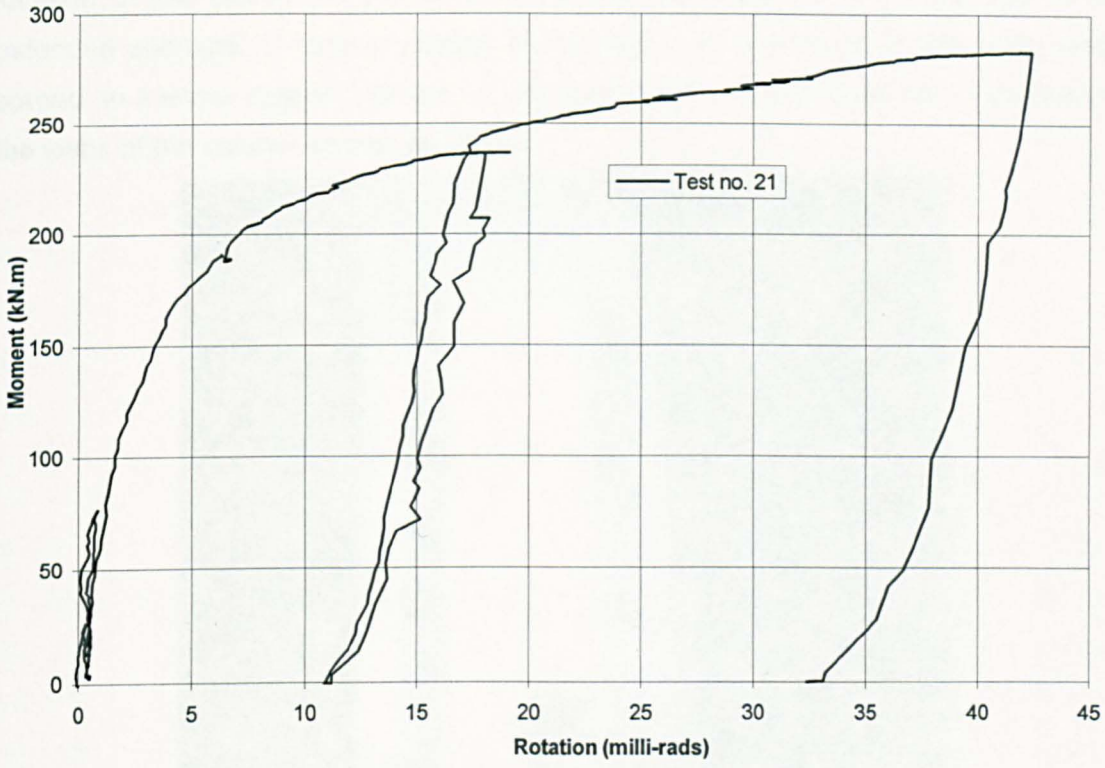

Figure 5.4 Moment-rotation characteristic for joint test no. 21

It was later found that the pump control valve had accidentally worked loose which reduced the pressure output. The test was resumed the following day, with the readings of transducers and inclinometers reset to their final position. Fortunately the ram had not been disconnected and the test was commenced from the position which it had finished the previous day. The resumption of the test was important to determine the final ductility of the joint. When reloaded, the joint followed the same loading stiffness as observed when unloading previously. The moment-resistance of the joint continued to increase until the joint was stopped at a final recorded moment-resistance of 283 kN.m and at a rotation of 0.042 radians. No bolt pull-out was observed for this test.

The joint detail had exhibited excellent ductility, with rotations in excess of the ultimate rotations that would be found in practice. The moment-rotation characteristic is clearly non-linear from an early stage of the loading history. Examination of the joint after the test revealed that the majority of rotation of the joint had occurred from the flexural action of the tube face with the unbolted endplate showing no signs of deformation. There was however some yielding of the beam's compression flange during the latter stages of the test. Figure 5.5 shows the final deformed column after the test. The

location of the bolt in the photograph indicates the position of the top row of the extended endplate. Extensive yielding of the tube face was found in this area, which spread, to a lesser degree, into the second row of bolts. The yielding also migrated into the webs of the column section by 25mm.

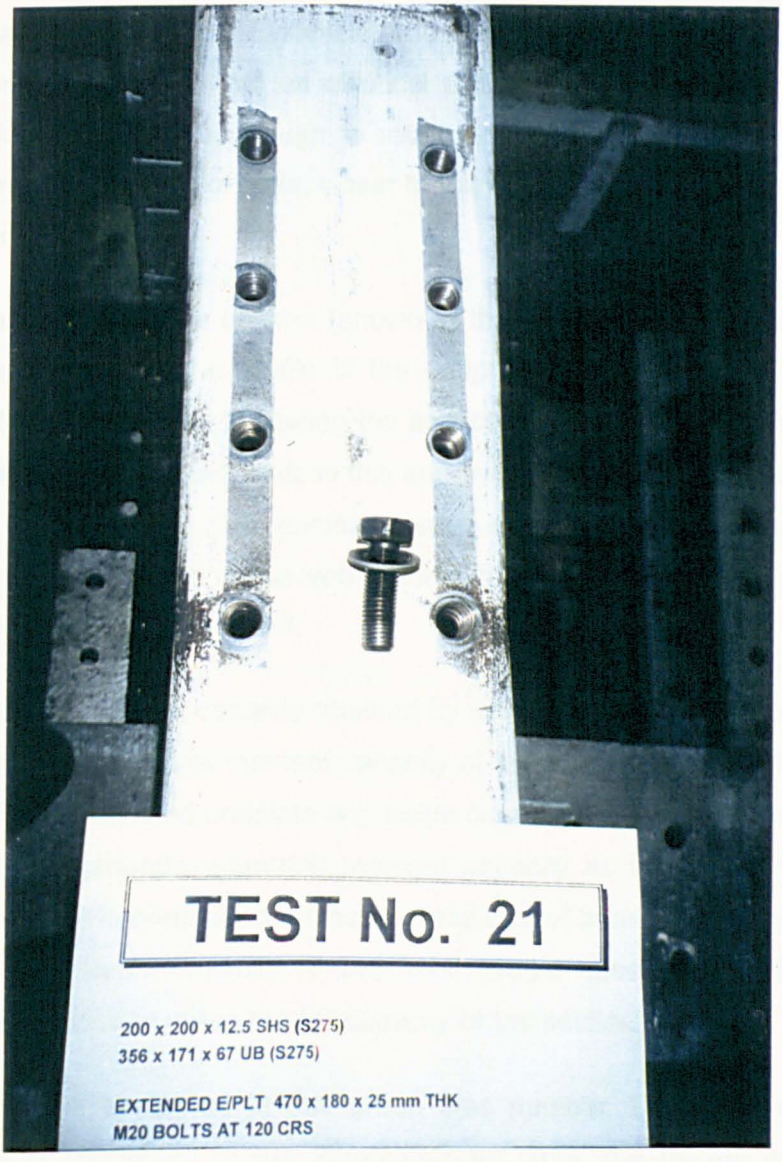

Figure 5.5 *Test no. 21- Final deformed column after the test.*

The bolt shown in figure 5.5 was removed with great difficulty from the top row of the endplate, as the flowdrill thread had deformed appreciably and was close to thread stripping before the test was stopped. The bolt is shown plastically deformed at the lower length of the bolt thread as a result of the column face being distorted. The bolt's stiffness was not able to restrain the column face when subjected to a tensile load. The washer under the bolt head had also showed signs of severe indentation. A closer inspection of the hole showed signs of greater distortion to the top of the flowdrill

thread than that of the bottom, resulting in a relatively small contact area between the two threads that, during the latter stages of the test, provided relatively small resistance to the bolt-pull out. It can also be seen that the stiffness of the endplate resulted in the bolts remaining vertical which induced a greater stress on one side of the bolt's thread than the other. Evidence of this can be seen in Figure 5.5 where the flowdrilled hole has distorted into an elliptical profile. This contrasts with the simple endplates which were flexible enough to rotate with the bolt and thus reducing bolt bending. The remaining rows of bolts, closer to the compression zone of the joint, were removed with relative ease.

The compression zone of the column (shown at the top of photograph 5.5) exhibited severe indentation around the profile of the endplate. Note the extent to which the endplate indentation travelled, indicating the axis of rotation for this joint pivoting. The webs of the column buckled outwards in this area with yielding being observed down to opposite face of the column. It is unclear if such extensive yielding would affect the response of a joint connected to the web of the column as no tests were conducted to investigate this 3D joint arrangement.

The 283 kN.m final moment capacity attained by the joint classifies the connection as partial strength as the nominal moment capacity of the beam was 333 kN.m. It should be realised that the extended endplate and beam combination is an extreme test of the column's ability to generate adequate moment capacity as the top serial weight of beam was adopted. Theoretically the smaller serial size of beam could have been used where the nominal beam capacity of 213 kN.m would have allowed the extended endplate and bolt group to utilise the full capacity of the section.

The second joint to be tested in this group was number 19, where an extended endplate detail is connected to the 200x200x8mm SHS, the thinner section to be adopted in the 'rigid' series of tests. A similar loading pattern was used for this joint detail as was employed previously. A moment of 35 kN.m was first applied to the joint before being unloaded and then reloaded to failure. The full moment-rotation response is shown in Figure 5.6.

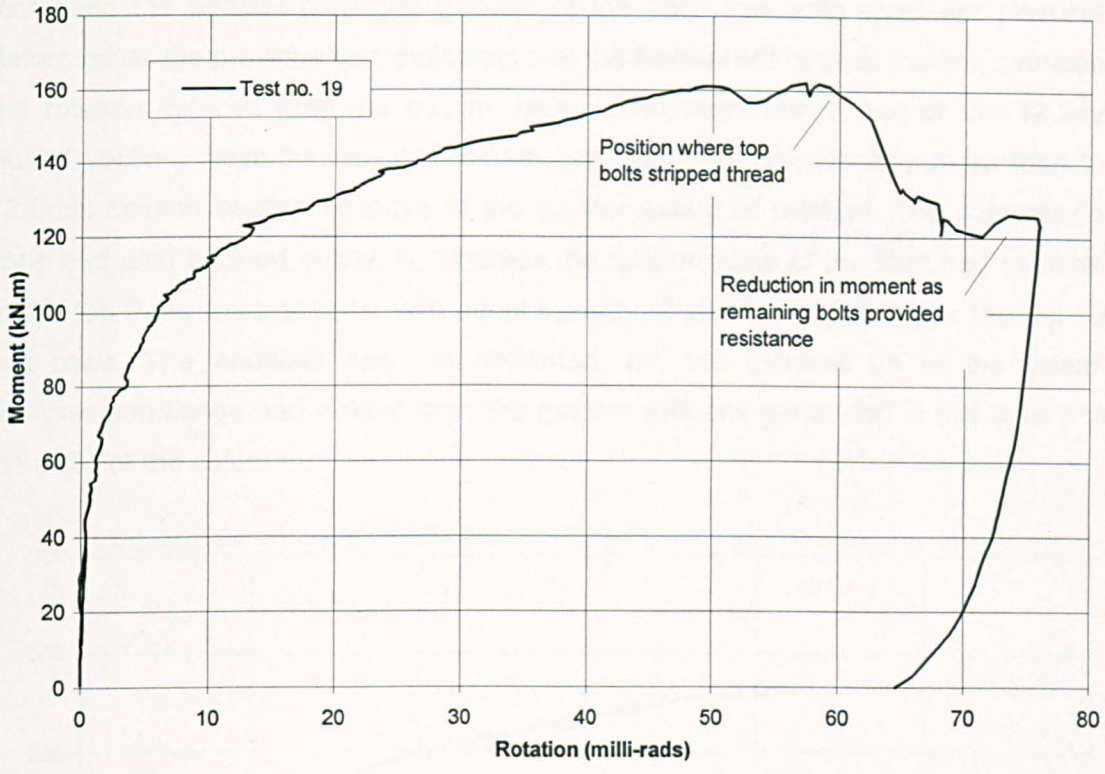

Figure 5.6 Moment-rotation characteristic for extended endplate of joint test no. 19

This particular test was different from the others because at a joint rotation of 0.057 radians the top bolts stripped the flowdrill thread and the bolts pulled out of the SHS face. This subsequently corresponded to a sudden drop in moment as shown in Figure 5.6, until stabilising at a lower level. The maximum moment attained by the joint before the bolts stripped was 162 kN.m. After the bolts had failed the lower level of moment was achieved through the remaining bolts still being effective. Essentially at this stage the extended endplate was simulating a flush endplate. At 0.075 radians the test was stopped and the joint unloaded.

The moment-rotation curve for the joint exhibited a ductile failure for the practical range of rotation, i.e. a rotation which would be theoretically less than that observed under serviceability loads before the bolt pulled out. The rotation of this joint was significantly greater than that observed previously in test no. 21. It is quite probable that such a failure would have occurred for test no. 21 if sufficient rotation had been applied. The curve also followed a linear stiffness between the rotations of 0.020 and 0.050 radians after the joint had fully yielded.

The endplate was unbolted from the column to examine the face. Some difficulty was encountered in removing the bolts, which when unbolting from the column may have

increased the already damaged threads of the bolt. The bolts were not plastically deformed as the previous test, indicating that the flexural stiffness of the bolt overcame the rotation induced from the column face deformation, unlike that of the 12.5mm walled section. Nevertheless, the column had deformed considerably more than the 12.5mm column section because of the greater extent of rotation. The compression zone had also buckled outwards, whereas the tension zone of the joint had extended to the top three rows of bolts, with equal severity of yielding observed for the top two bolt rows. The endplate had not deformed, but the extreme tip of the beam's compression flange had yielded from the greater stiffness generated in this area from the walls of the column.

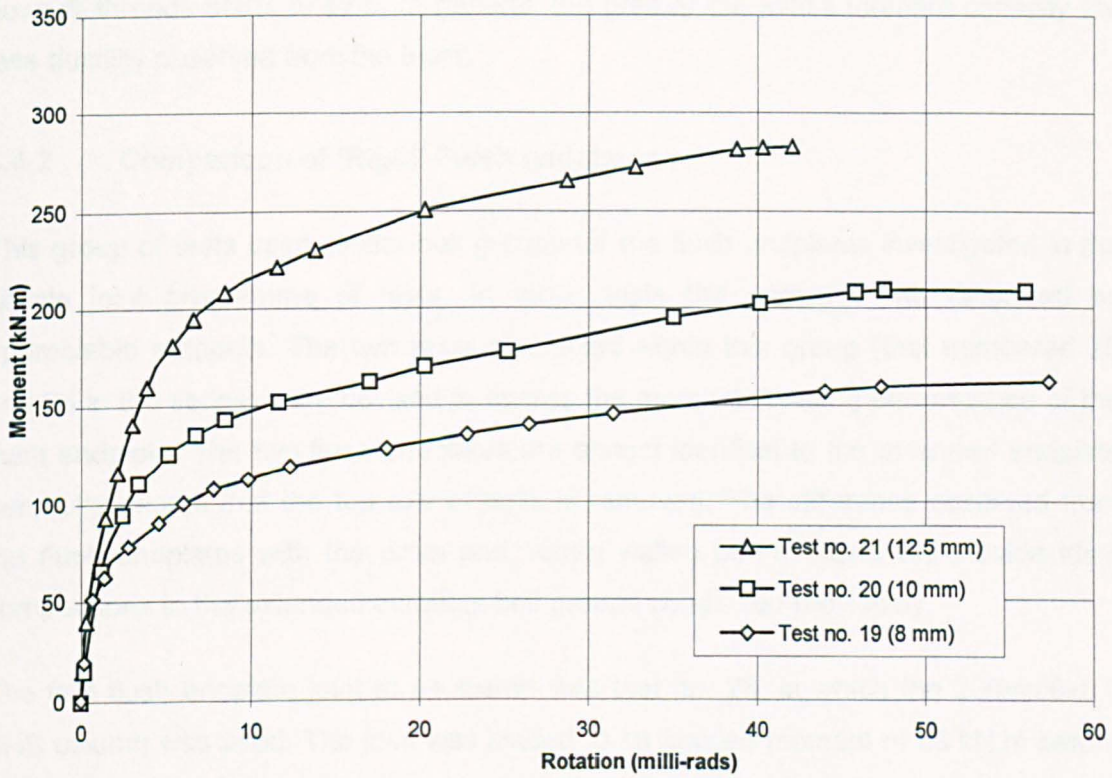

Figure 5.7 *Comparison of moment-rotation response for extended endplates with wall thickness of tubular columns varying between 8mm, 10mm and 12.5mm*

The next test in the series was test no. 20 conducted with the 200x200x10mm SHS column section. The joint failure was similar to that seen in the last test, in which the bolt stripped its thread. The final moment-resistance attained by the joint was 208 kN.m at 0.056 radian rotation. Figure 5.7 above, plots the moment-rotation envelope of test no. 20 together with the moment-rotation responses of the two previous tests 21 and 19. Examination of the column specimen after the test revealed similar patterns of

face deformations as in the previous two joint tests. Similarly, the extent of buckling to the compression zone of the 10mm walled column was a direct interpolation between that exhibited by the 8mm and 12.5 mm column sections.

Clearly the influence of the tube wall was as expected in that the increased moment-resistance of the flowdrill joint is dependant on the increase in the thickness of column wall. Each individual joint response shown in Figure 5.7 exhibits a similar initial stiffness before the relationship progresses into an early non-linear response. The stiffnesses at 0.010 radians just after first yield, are surprisingly consistent, after which the joints exhibit reduced stiffness followed by a long plateau before reducing to zero stiffness at the end of each test indicating imminent joint failure as the top row of flowdrill threads starts to strip. In general, the greater the joint's moment capacity the less ductility observed from the tests.

5.4.2 Comparison of 'Rigid' Flush endplates

This group of tests used similar bolt groups for the flush endplates investigated in the simple joint programme of tests. In those tests the endplate had deformed by appreciable amounts. The two tests conducted within this group (test numbered 25 and 26 in the series) were devised to assess the moment-resisting performance of the flush endplate. The two flush endplates are almost identical to the extended endplate geometry except that the top row of bolts is removed. The difference observed from the flush endplates with the 8mm and 10mm walled box sections will provide ideal comparisons to the extended endplate bolt groups conducted previously.

The first flush endplate joint to be tested was test no. 26, in which the 200x200x8.0 SHS column was used. The joint was loaded to an applied moment of 25 kN.m before being unloaded to almost zero moment. The load was then reapplied to the joint, until the test was stopped due to excessive rotation rather than any sudden failure attributed to bolt pull out. The maximum moment-resistance developed by the joint was 104 kN.m at a rotation of 0.062 radians. Again good ductility and post yield stiffness was observed. Figure 5.8 shows the moment-rotation characteristic for this joint together with a direct comparison to the extended endplate of test no. 19 which adopted the same column section. The difference of incorporating an extra bolt row is clearly shown with the increased strength and stiffness attainable with the extended endplate of test no. 19.

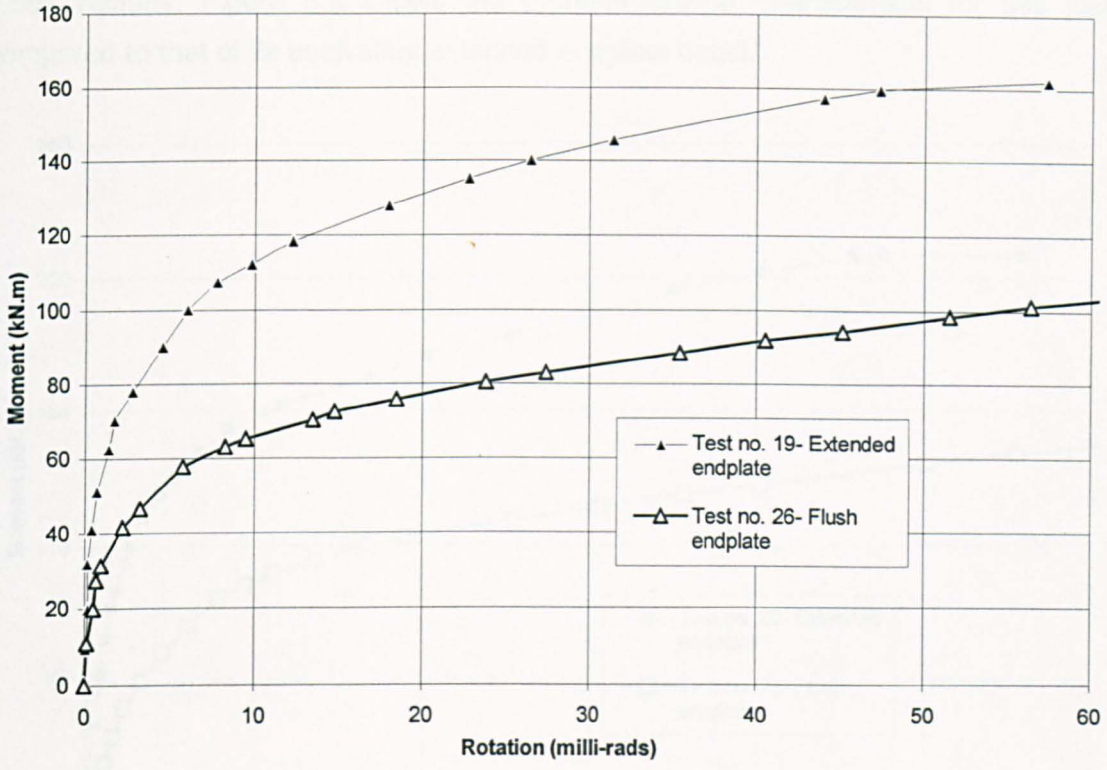

Figure 5.8 *Comparison of response of flush and extended endplates for the 200x200x8 SHS column*

The endplate unbolted from the column section without any undue difficulties, even though the face of the column had deformed significantly. No damage was visible to either the endplate or the beam, indicating that the rotation observed in the joint was attributed to that of the column section. The compression zone of the column was deformed directly under the compression flange of the beam. The walls were buckled locally in this area, extending a third of the way down the depth of the SHS. In the area of the tension zone the severity of the deformation of the top row of bolts also extended into the walls of the column by 25mm. The second row exhibited slightly less yielding with the third row relatively deformation free as this line represented the final rotation axis of the joint.

The last flush endplate to be tested was test no. 25 which was bolted to the 200x200x10 SHS column specimen. As the flush endplate of test no. 26 was undamaged it was subsequently re-used for this test. The loading sequence for the joint test was identical to the previous test by loading the joint initially to 40 kN.m and then unloading. The moment was then reapplied to the joint until being stopped through excessive rotation. The maximum moment attained was 138 kN.m at a rotation

0.062 radians. Figure 5.9 shows the moment-rotation characteristic for this joint compared to that of its equivalent extended endplate detail.

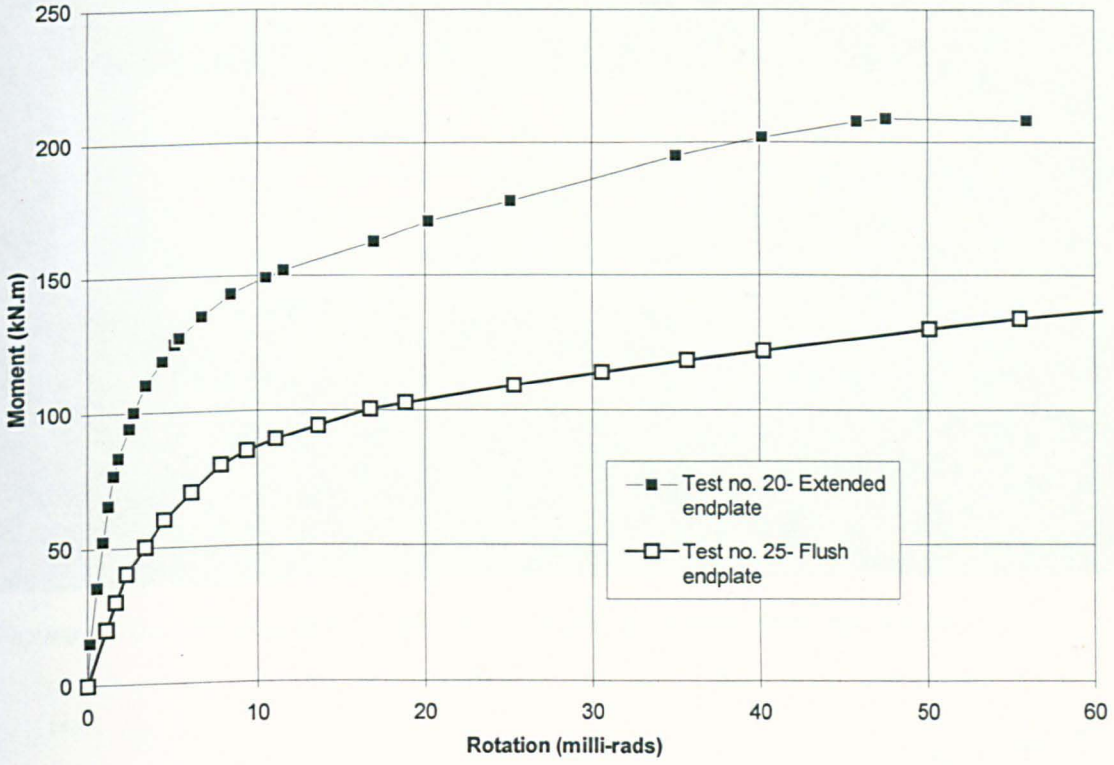

Figure 5.9 *Comparison of response of flush and extended endplates for the 200x200x10 SHS column*

The deformation exhibited by the 200x200x10 SHS column was similar to that of 200x200x8 SHS except that the yielding was more severe. Figure 5.10 shows a photograph of the column after the test. The extent of deformation on the face is clearly shown together with the extent of the yielding into the walls of the column which has been highlighted by a marker pen on the paint. Interestingly the whole of column face which was in contact with the endplate rotated as a rigid body due to the stiffness of the 25mm endplate. Finally as a direct comparison, Figure 5.11 shows the moment-rotation curves of the two flush endplates plotted together.

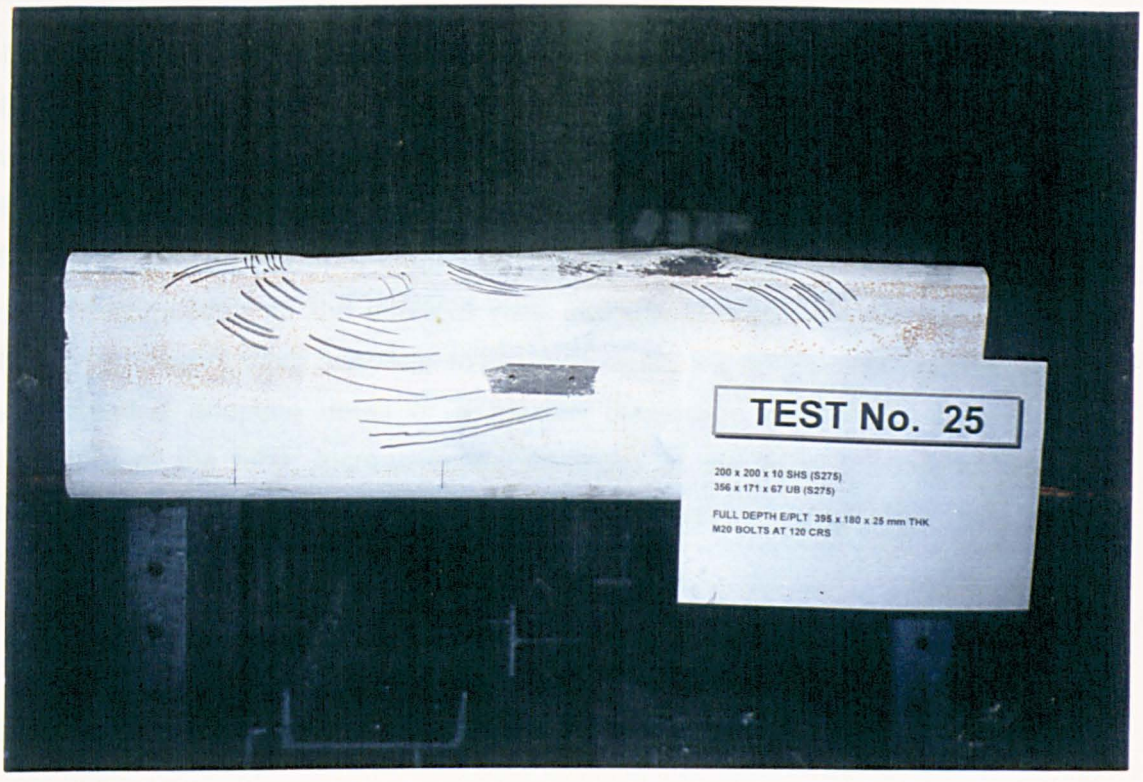

Figure 5.10 Photograph of deformed column specimen after test no. 25

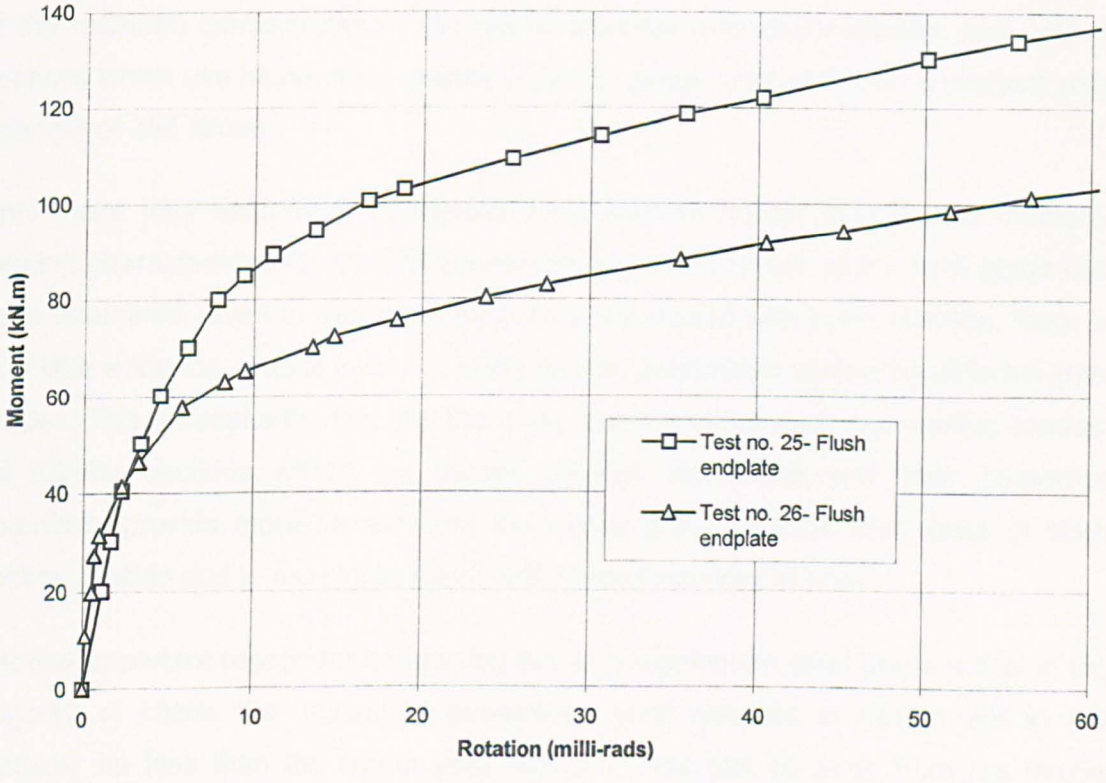

Figure 5.11 Comparison of moment rotation response for 'rigid' flush endplates

Looking back at the comparison made between the flush and the extended endplates, the increase of moment capacity over the flush endplates for the 10mm and 8mm columns, at say 0.020 radians, was approximately 63% and 70% respectively. The increase available at this rotation for the flush endplates when the tubular wall thickness is increased from 8mm to 10mm shown in Figure 5.11 is only 42% (which also takes account of the different yield strength between the column sections). It therefore appears more beneficial to increase locally the leverarm of the bolts by either an extended endplate detail or a haunch connection rather than increasing the thickness of the tube. Increasing the thickness of the tube to allow for additional strength and stiffness at the joint should be a last resort, for problems that are only local in nature.

5.4.3 Effect of column steel grade for extended endplate joints

Most of the flowdrill tests to date have been conducted with using S275 steel grade (design grade 43), where the nominal specified yield strength is 275 N/mm^2. This part of the research concentrates on the use of identical extended endplates and column sections which use higher steel grades of S355 (design grade 50) with a nominal yield strength of 355 N/mm^2.

Until these joint tests were completed there was no known data on the moment-rotation characteristics for flowdrill connectors where the effect of the steel grade had been examined. Even in traditional joint tests, conducted with open sections, there is very little evidence of tests involving identical joint geometries comparing different steel grades. This is despite the fact that this comparison is of the most important to conduct for tubular sections where the stocky columns associated with their properties potentially provide more benefit from the higher grade of steel than those of open section profiles due to the higher minor axis second moment of area.

Another important reason for conducting this investigation on steel grade is that in the majority of cases the 'minimum' guaranteed yield adopted in design will almost certainly be less than the actual yield strength. This can be seen from the tensile coupon test results where in one particular instance the yield stress for design grade 43 could almost be reclassified as design grade 50. There is also a strong probability that higher grades of steel will be used either by accident or by availability. For the majority of these cases it is expected the increased strength will provide an added

amount of safety which is usually beneficial but this may be accompanied by reduced rotation capacity. However, the testing of the two nominally identical joints provides the necessary data to assess any likely increased stiffness which may in some instances be developed.

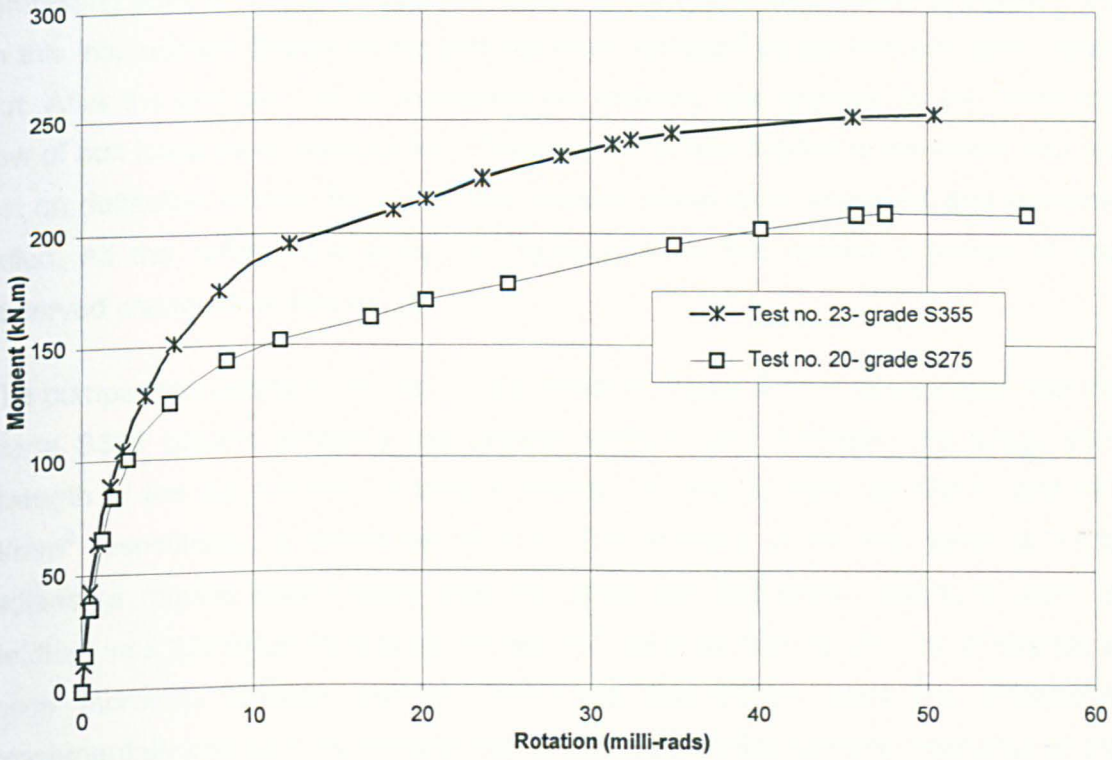

Figure 5.12 *Comparison of extended endplate moment-rotation characteristics with variation of column grade*

The two tests for comparison were numbered 20 and 23 in the schedule of Table 5.1. Joint test no. 20 involving the 200x200x10mm SHS grade S275 column has been reported previously in section 5.4.1 above, to which reference should be made. Joint test no. 23 was conducted with a nominally identical extended endplate detail but bolted to a grade S355 SHS column. At the beginning of the test a moment of 60 kN.m was applied to the joint before being unloaded. Moment was reapplied to the joint up to 200 kN.m before unloading to 125 kN.m to determine the unloading stiffness. The moment was steadily increased until a sound was heard at 0.040 radians which corresponded to a blip on the moment-rotation characteristic. This was attributed to the top bolt's pulling out and a subsequently reduced post yield stiffness. The load was further increased until the bolts were completely pulled out of the flowdrill holes, where upon a sudden drop in moment occurred, similar to the plot of test no.20. Figure 5.12 shows the moment-rotation envelope for test no. 23 together with its equivalent test no.

20 utilising a grade S275 column. The maximum moment attained by the joint was 253kN.m at a rotation of 0.050 radians.

The extent of both the bolt pull-out and the column yielding is shown in Figures 5.13 and 5.14 which are photographs of joint test no. 23 taken after the tests. The interesting point to note is the bolt pull-out at the top row of bolts shown in Figure 5.13. In this instance the thread on the bolt has been removed as the bolt has been pulled out. After the bolt had lost all resistance the moment was reduced as the remaining row of bolt loads were redistributed. Obviously if the load applied to the beam was not set on deflection control the joint in this position would have 'unzipped' and suddenly failed. All the deformation shown in Figure 5.14 on the column is similar to that observed previously in test no. 20.

The comparison between the two curves shown in Figure 5.12 is as expected with the grade S355 column behaving with greater stiffness and strength. The actual yield strength of the two columns of tests numbered 20 and 23 was 329 N/mm^2 and 427 N/mm^2 respectively, a difference of 30%. The moment of the two joints at 0.015 radians (a rotation level directly after the joints had first shown extensive signs of yielding) was 200 kN.m for test no. 23 and 157 kN.m for test no. 20. The difference in these moments between the two tests was thus 27%. These two differences experimentally compare reasonably well to indicate that the moment-resistance of the joint can be related by the ratio of yield stress. A series of curves can therefore be predicted with reasonable accuracy by adopting various ratios of yield strength. This reasoning can also explain the difference observed in the post yield stiffness between 0.015 and 0.030 radians (as indicated in Figure 5.12) where the S355 column grade exhibited a slightly higher stiffness than that observed for the S275 grade of steel. A ratio of 37% was also calculated for the different post yield (membrane) stiffnesses of the joints.

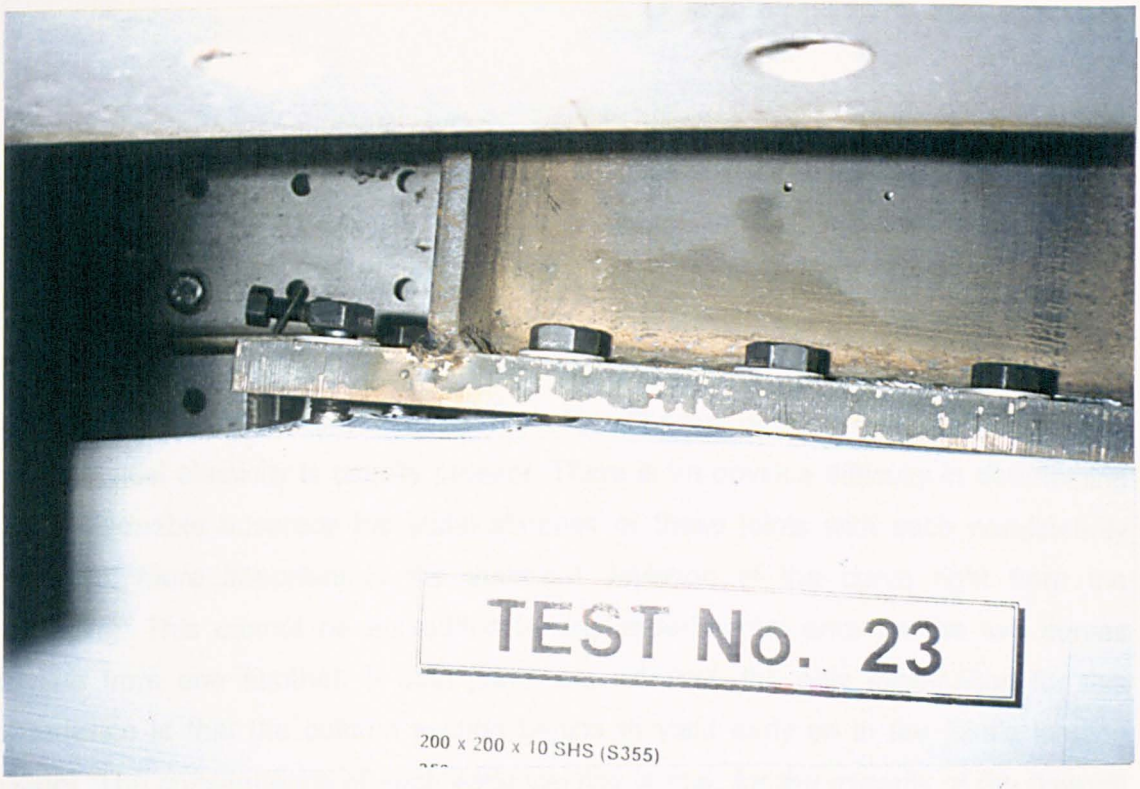

Figure 5.13 Joint test no. 23 after failure

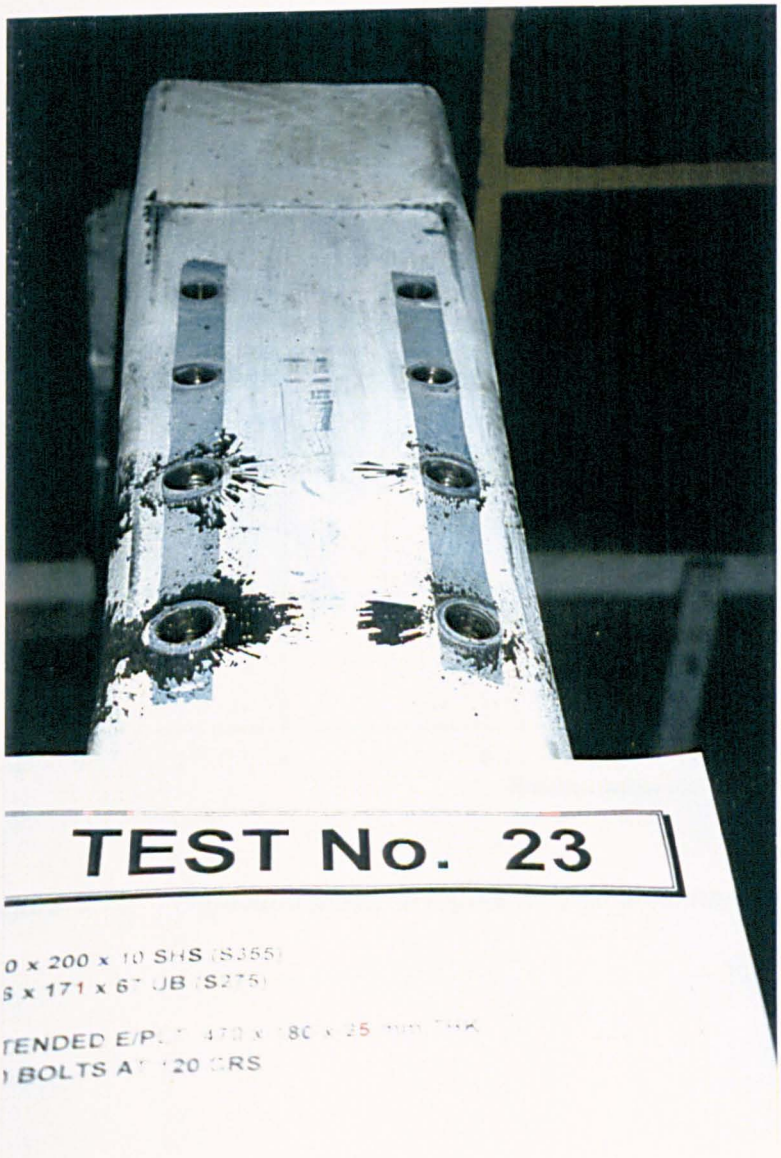

Figure 5.14

Joint test no. 23 column deformation shown after endplate unbolted

Comparison of the two moment-rotation characteristics also shows that the lower grade of steel used in joint test no. 20 deviates from the higher grade of steel of test no. 23 early on in the loading history. To show this more clearly Figure 5.12 has been replotted in Figure 5.15 to a more suitable scale to show the initial portion of the joint's response between 0 and 0.020 radians. The two curves are highly non-linear, with apparently no initial linear stiffness exhibited, unlike that of open sections where some form of initial elasticity is usually present. There is an obvious difficulty in determining with reasonable accuracy the initial stiffness of these joints with such non-linearity exhibited. More important is the apparent deviation of the curve right from the beginning. This cannot be accredited to any experimental error as the two curves deviate from one another. If both joints are identical, the only explanation for this occurrence is that the column section begins to yield early on in the joint's loading history. The consequence of such early yielding is that, for the majority of the flowdrill joints, it is quite probable that some local plasticity will be present under typical serviceability loading.

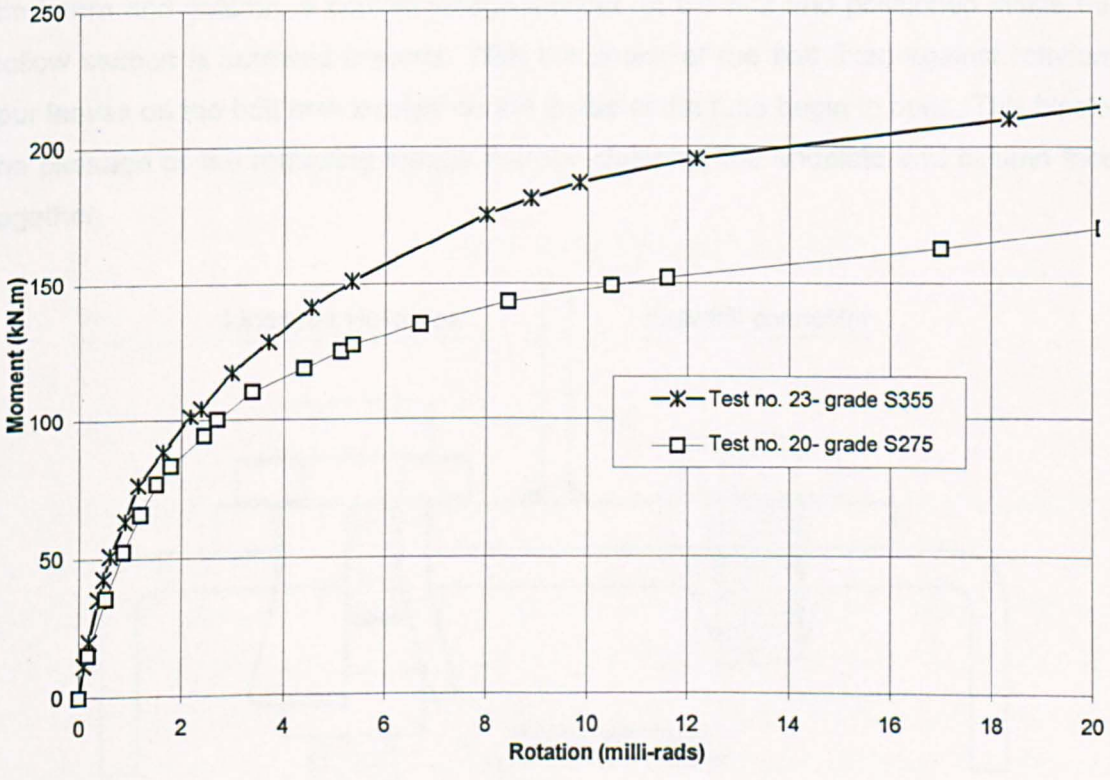

Figure 5.15 Replotted graph of Figure 5.12 to an enhanced rotational scale

5.5 Hollo-bolt joints

This section describes the joint tests conducted using a new blind bolting product from Lindapter International called Hollo-bolt. Originally the joint test programme had only considered the Flowdrill system. It was apparent that as a comparison, the testing of joints using the new bolts may be of interest in expanding the research. As a consequence two extra joint tests numbered 32 and 33 were planned for which nominally identical flowdrill test results were available for direct comparison of the joint's performance.

Conceptually the two bolts are completely different, as shown in Figure 5.16 below, which are illustrated in sectional view as they would finally appear in practice. The Hollo-bolt works on the principle of being able to expand on the inside of the SHS to clamp both the endplate and column together. The advantage of this system is that the column is only required to be drilled normally albeit with a larger diameter hole and does not need any special preparation. After inserting the bolt through the endplate of the beam and column, a conical wedge located on the bolt and positioned inside the hollow section is screwed inwards. With the shank of the bolt fixed against rotation, four leaves on the bolt now located on the inside of the tube begin to open. This blocks the passage of the retracting wedge thereby clamping the endplate and column face together.

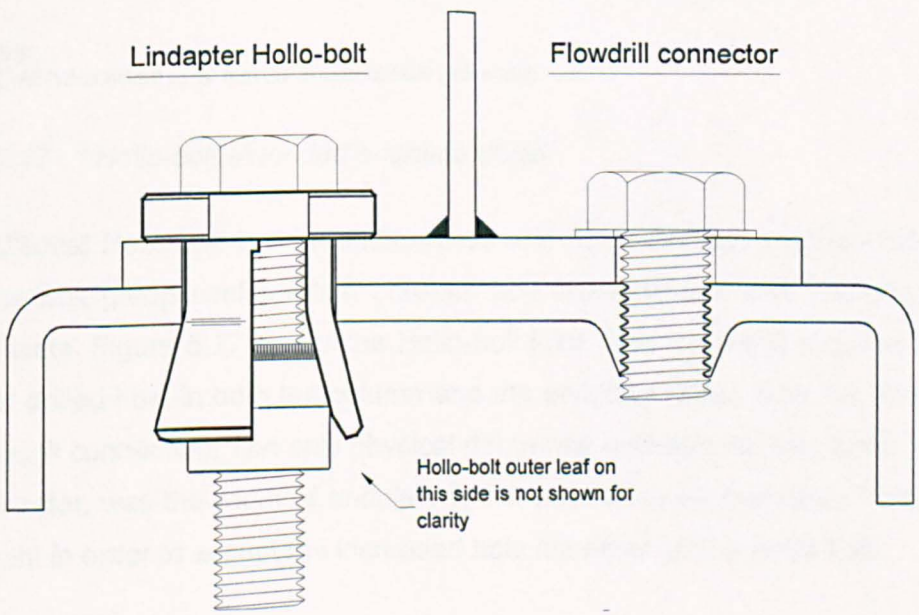

Figure 5.16 Details of Hollo-bolt and Flowdrill connectors

5.5.1 Joint details and programme of tests

For comparison, tests 23 and 24 of the flowdrill programme were used as the bench marks for the Hollo-bolt tests. The two joints that were tested had nominally identical endplate details that were welded to a 356x171x67 UB (design grade S275) and bolted to a 200x200x10 SHS (design grade 50) column. The difference between the flowdrill tests was that the column section of test 24 was filled with concrete. These two joint details were selected because of their high stiffness and moment capacity and provided an excellent comparison for the Hollo-bolt's performance

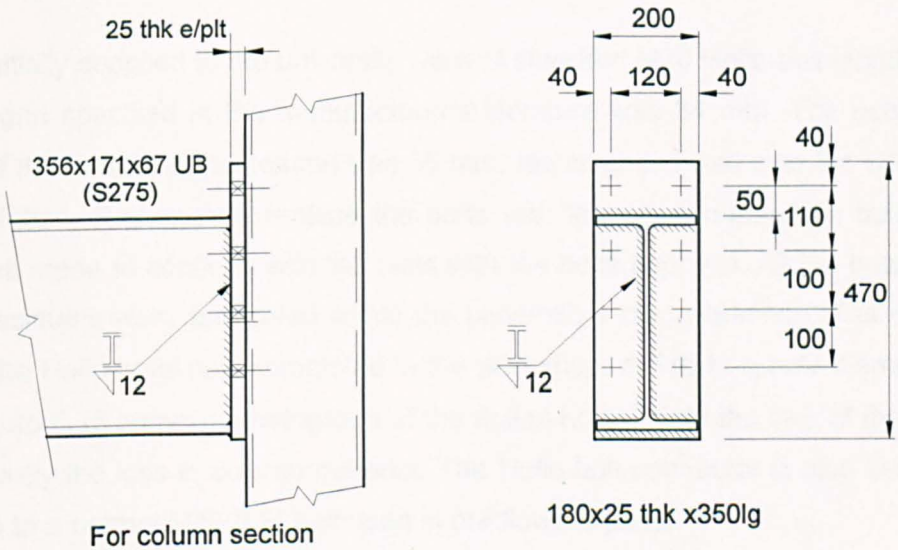

Extended Endplate Detail (EE)

Note:
(1) All holes drilled to 33 mm dia to accept M20 Hollo-bolts

Figure 5.17 Hollo-bolt extended endplate detail

The additional Hollo-bolt tests (numbered 32 and 33 in the test programme) adopted the same bolt group configuration (120mm bolt cross-centres and 100 pitch) as the flowdrill tests. Figure 5.17 shows the Hollo-bolt joint. The Hollo-bolt requires a 33 mm diameter drilled hole in both the column and the endplate rather than the 22 mm used with flowdrill connection. The only physical difference between the two joints, excluding the connector, was the width of endplate which needed to be increased from 180 mm to 200 mm in order to accept the increased hole diameter for the Hollo-bolt.

5.5.2 Fabrication and assembly of Hollo-bolt joints

The steel used for the SHS columns (design grade 50) was cut from the same length of tube used for the flowdrill tests. The yield strength was 427 N/mm^2 obtained from the coupon tests taken from the section. The only variability in batch steel for the two tests was when the standard flame cut endplate of width 180 mm was substituted for the 200 mm flat. The relatively thick 25 mm endplate used in the tests resulted in small deflections which were unlikely to significantly affect the overall moment-rotation curves produced.

The bolts initially supplied to the university were of standard M20 Hollo-bolt length. The amount of grip specified in the manufacturer's literature was 34 mm. The actual ply thickness of the endplate and column was 35 mm, resulting in 1 mm over the specified recommendation. Rather than replace the bolts with longer, non-standard bolts, the decision was made to continue with the tests with the bolts supplied. All the beams for the test specimens were fabricated within the university's own workshop. The normal drilling for the Hollo-bolts was completed in the workshop, drilled to a hole diameter of 33 mm. Figure 5.18 shows a photograph of the drilled holes. Note the size of the holes and importantly the loss in column material. The Hollo-bolt connector is also shown in comparison to a normal M20(8.8) bolt used in the flowdrill joints.

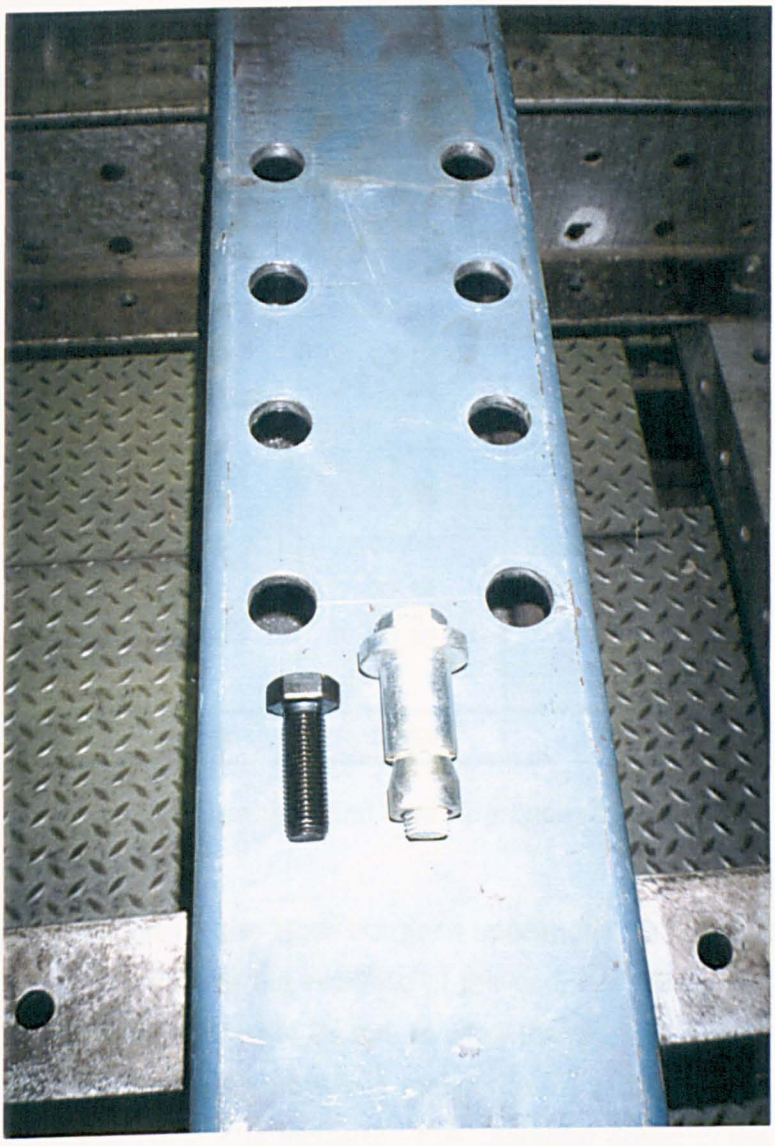

Figure 5.18 Photograph of drilled column before joint test and assembly

The fabrication of the Hollo-bolt specimens incurred a problem as the bolts could not be inserted due to a mis-alignment of the holes in the endplate and column. In this case there was no tolerance in the joint detail partly because of the manufacturer's recommendation of close tolerance holes which when combined with the use of a large group of bolts, had the effect of exaggerating the relatively small errors in marking out of the sections. A survey of the drilled holes and bolt sizes are shown in table 5.4 where the average endplate and column diameter holes measured 33.02 mm and 33.07 mm respectively. The average bolt diameter was 32.48 mm which allowed a hole clearance of 0.5 mm. This problem should not have occurred as the endplate could have been drilled with a larger diameter hole to allow extra clearance to the bolt

without causing any detriment to performance. A rewriting of Lindapter's installation instructions is suggested.

	Bolt diameter	column hole diameter.	endplate hole diameter
	32.66	32.98	33.11
	32.49	33.12	32.77
	32.48	32.77	33.14
	32.52	32.98	33.00
	32.35	33.05	32.95
	32.41	33.04	33.17
	32.43	33.14	33.14
	32.50	33.10	33.30
Average	**32.48**	**33.02**	**33.07**

Table 5.4 Survey of bolt diameters and hole clearance (all values in mm)

At this stage of fabrication for the Hollo-bolt joint specimens, the endplate had been welded to the beam which made the redrilling of the endplate an impractical solution. The column was therefore redrilled to 34 mm to allow the extra clearance to insert the bolts. The diameter of the hole was within Lindapters recommendation of 33mm + 1.0mm and -0.2mm tolerance. The increased hole diameter drilled in the column was now more onerous to the bolt's performance.

The M20 bolts used in the Flowdrill joints were torqued to 160 N.m whereas the Hollo-bolts were torqued to the recommended 300 N.m. The tightening of the bolts to 300N.m required a substantial effort using a moderate sized ratchet torque wrench. The process required the use of two people; one was required to torque the bolt and the other to prevent the shank of the bolt from turning. It was also noticed that on one bolt there was a slight gap between the head of the bolt and the endplate after it had been torqued to the required value. It appeared that as the bolt was tightened the inside edge of the drilled column hole may 'bite' into the expanding leaves rather than clamping the endplate and column together. The use of load indicating washers may be an alternative solution to the torque wrench.

After tightening the bolts, the column of test specimen 33 was filled with concrete to the same specification as used in test no. 24 for the equivalent flowdrill joint. The aggregate size was determined by the practical requirement of the concrete to be pumped into the column and the need to flow between the Hollo-bolts. The average of three cube tests taken on the day of the test revealed an actual compressive strength of 50.7 N/mm^2.

In comparing the two systems, the length of the Hollo-bolt is such that to successfully connect two incoming beams at 90 degrees to a tubular column with M20 bolts would require the pitch of the bolts to be staggered to avoid any clashes of the bolts. This problem would only occur for SHS members that are relatively small on plan compared to the diameter of the bolts used.

5.5.3 Comparison of test results

The first of the Hollo-bolt tests (numbered 32 in Table 5.1 schedule) proved to be unsuccessful with premature bolt-pull out failure. As noted earlier the standard bolt lengths had been used to connect plates with a combined thickness 1 mm in excess of the maximum value recommended by the manufacturer. The bolt shank was not long enough to open sufficiently to generate the mechanical clamping action. This resulted in the bolts pulling straight out of the column when the moment was applied to the joint. Figure 5.19 shows the moment-rotation curve of test no. 32 compared against its equivalent flowdrill joint test no. 23. The maximum moment capacity attained by the joint was 83 kN.m at 0.020 radians. The bolt pull-out commenced at the start of the test being characterised by the very low stiffness of the joint compared to the flowdrill test. It is suggested that the moment attained from this test can be attributed to friction generated as the bolt pulled through the connected plates. Figure 5.20 shows a photograph taken inside the column tube after the test. This illustrates the ease with which the bolts pulled out of the column and the lack of expansion of the bolt leaves.

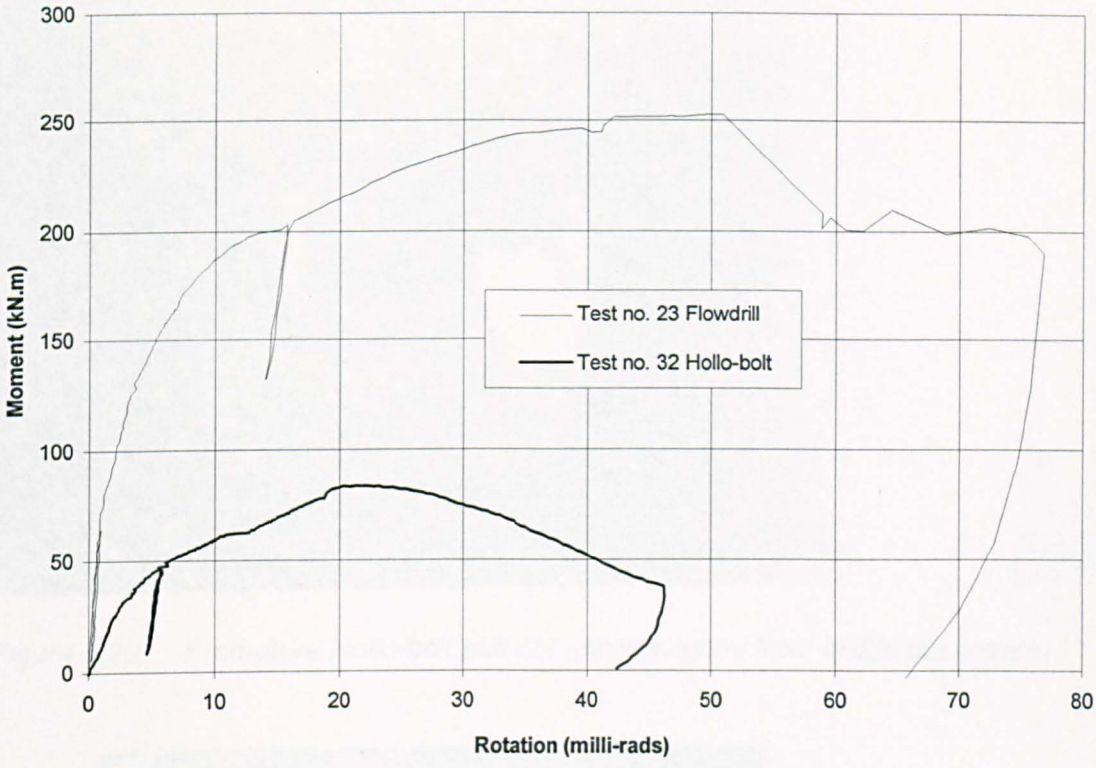

Figure 5.19 *Moment-rotation curve for Hollo-bolt Joint test no. 32 compared to equivalent flowdrill joint*

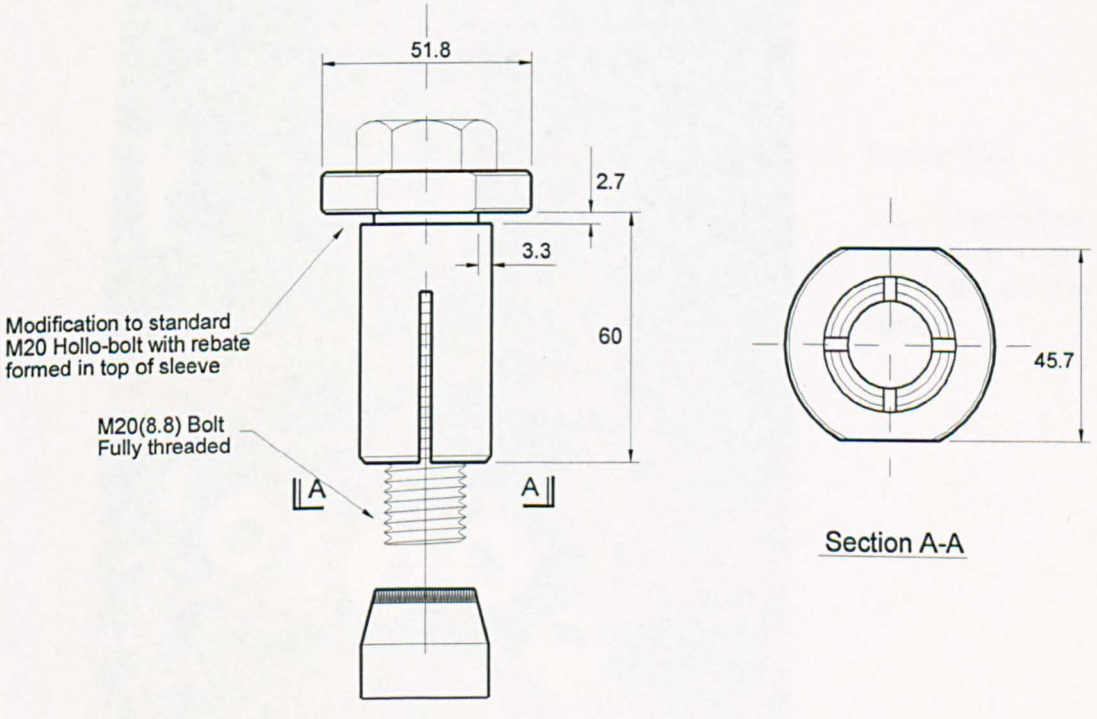

Figure 5.21 *Details of Modified Hollo-bolt used in joint test 32b*

Figure 5.20 Premature Hollo-bolt pull out photographed from inside the column

Figure 5.22

View of modified Hollo-bolts from inside the column section

Examination of the column after the test revealed no signs of visible damage. The diameter of the holes had been measured and found to be within the 34 mm previously drilled. It was decided to repeat the test with the same beam, column and joint components, but to use modified non-standard Hollo-bolts with longer shanks. Bolts were supplied with a shank length 15 mm longer than the standard length previously used. They were also modified with a slight rebate under the rim as shown in Figure 5.21. This was a direct result of a larger series of tests on Hollo-bolts conducted by British Steel at their Swinden Laboratories which found that the initial stiffness of Hollo-bolt joints did not compare favourably with the Flowdrill system. The added feature is intended to improve the clamping force of the bolt and hence the initial stiffness.

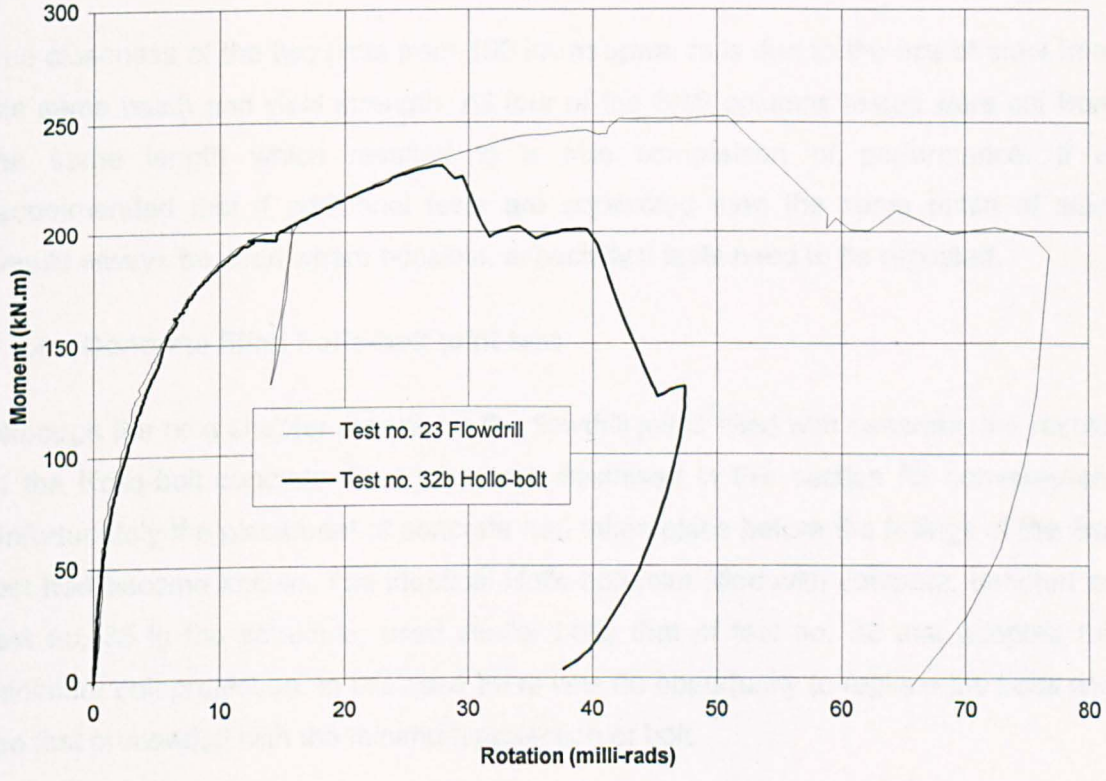

Figure 5.23 Comparison of Hollo-bolt and Flowdrill joint response

The joint test number was reclassified as test no. 32b and proceeded with the original section sizes but now adopting the longer bolt lengths. Figure 5.22 shows the view of the bolts from inside the tubular column prior to testing. In this case the leaves are now fully expanded when compared to that of the previous test shown in Figure 5.20. The moment-rotation relationship for the Hollo-bolt joint test is shown in Figure 5.23 with the response of the flowdrill joint test no. 23 for direct comparison. The results show good agreement between the two, with the Hollo-bolt following the flowdrill plot up to

0.028 radians until failing at a maximum moment of 230 kN.m. The differences in the initial portion of the plot up to failure of test 32b is well within normal experimental tolerances.

Although significant yielding and deformation of the tube face was observed, failure of the joint was caused by the expanded Hollo-bolt 'leaves' on the inside of the tube failing in tension. The failure of the bolt in tension was accelerated by the sharp edge of the drilled hole in the SHS face cutting into the leaves of the expanded bolt inside the tube, reducing the effective area of the bolt in tension. Any reduction in the diameter of the outer bolt would reduce the tensile capacity in cases where the wall of the tube is relatively thick and overall failure can not be attributed to the SHS face bending which avoids the bolt being cut in this manner.

The closeness of the two plots from 150 kN.m upwards is due to the use of steel from the same batch and yield strength. All four of the SHS columns tested were cut from the same length which resulted in a true comparison of performance. It is recommended that if additional tests are conducted then the same batch of steel should always be used where possible, especially if tests need to be repeated.

5.5.4 Concrete filled hollo-bolt joint test

Although the next chapter reports on the flowdrill joints filled with concrete, the results of the Hollo-bolt concrete filled joints are discussed in this section for convenience. Unfortunately the placement of concrete had taken place before the failings of the first test had become known. The identical Hollo-bolt joint filled with concrete, denoted as test no. 33 in the schedule, used similar bolts that of test no. 32 that adopted the minimum bolt projection. In this case there was no opportunity to replace the bolts and the test proceeded with the minimum projection of bolt.

At first, the joint of test no. 33 responded well, providing initially a high stiffness as shown in the moment-rotation plot of Figure 5.24. At 0.020 radians a reoccurrence of the bolt-pullout seen in test no. 32. was observed. There was little evidence of the column yielding.

In this test the beneficial aspects of the concrete fill allowed sufficient confinement of the bolts for the moment capacity of the joint to be recorded as 197 kN.m. before deteriorating. The moment-rotation characteristic of this joint did not follow the

equivalent flowdrill comparison of test no. 24 as seen by the two plots in Figure 5.24. The interaction between concrete and steel was not the same.

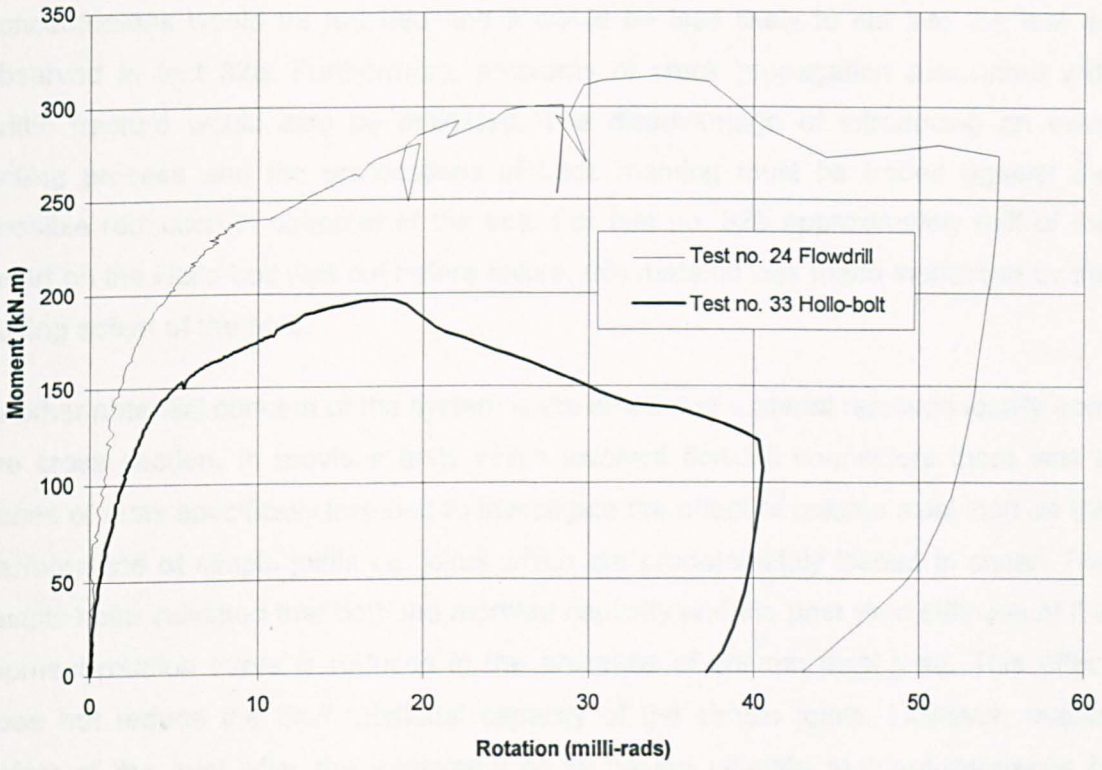

Figure 5.24 *Comparison of Moment-rotation curves for Hollo-bolt and flowdrill connectors with concrete filled columns*

5.5.5 Observations for the use of Hollo-bolt connectors

The modified Lindapter M20 Hollo-bolts of test 32b performed as equivalent to the M20 Flowdrill bolts during the initial stages but exhibited a reduced ductility at failure.

One of the concerns found from the tests has been the apparent pull-out of the bolts at relatively low tensile bolt loads when the bolt clamps together a ply thickness at the upper end of the manufacturer's recommendations. As the two tests which failed from this were over the recommended maximum limit specified, albeit by only one millimetre, no firm conclusions can be drawn as both tests 32 and 33 are made invalid. It is suggested that further investigation into the sensitivity of bolt projection and amount of grip be carried out urgently. The modified bolts which were 15 mm longer had performed adequately.

The failure mechanism of the bolt, initiated by the inside edge of the drilled hole cutting into the leaf of the shank as the bolt is loaded in tension, could be improved by back reaming the column holes. If a chamfer was placed at this position stress concentrations would be reduced and it would be less likely to cut into the leaf as observed in test 32b. Furthermore, problems of crack propagation associated with brittle fracture would also be mitigated. The disadvantage of introducing an extra drilling process and the practicalities of back reaming must be traded against the possible reduction in diameter of the bolt. For test no. 32b approximately half of the insert on the Hollo-bolt was cut before failure, this material was made ineffective by the cutting action of the hole.

Another potential concern of the system is the amount of material removed locally from the cross section. In previous tests which involved flowdrill connectors there was a series of tests specifically included to investigate the effect of column axial load on the performance of simple joints i.e. joints which are predominately loaded in shear. The results have indicated that both the moment capacity and the post yield stiffness of the moment-rotation curve is reduced in the presence of column axial load. This effect does not reduce the final rotational capacity of the simple joints. However, overall safety of the joint after the attainment of its design ultimate moment-resistance is lowered as the joint is more sensitive to sudden failure with relatively small increases of applied moment.

If Hollo-bolt joint details are constructed on all sides of a 200x200x10 SHS column and these joints use M20 bolts, then 33 percent of the cross-section is removed. The stress normally induced in tubular members is considerably greater than its open section equivalent because of its structural efficiency. The effect which will have on axial load capacity of such joints requires further investigation.

The final observation from the tests and recommendation is that the Hollo-bolt connectors should not be used in '*moment*'-resisting joints where the SHS has been filled with concrete until adequate test data can substantiate their rotational capacity. This does not restrict their use as shear connectors. The reason for this is that the moment-rotation curves for the flowdrill tests showed a significant reduction in rotational capacity when concrete filled columns are used (reported on in Chapter 6). A similar reduction would therefore be expected for the Hollo-bolt, which has already been previously shown to produce less rotational capacity than the Flowdrill joint when the column is unfilled.

5.6 Chapter summary

This chapter has reported on a series of joint tests to investigate the moment capacity of flowdrill joints using flush and extended endplate details. The joints have been shown to exhibit highly non-linear moment-rotation responses from almost the beginning of the test. All the joints were classified as semi-rigid and partial strength, although the partial strength classification could have been improved by using the smaller serial size of beam. All the joints failed by either excessive column face distortion or bolt pull-out. Column failure occurred as a direct result of adopting endplate thickness in excess of that which initiated endplate failure. The rotation exhibited by the joints at failure were found to be beyond the practical limits required.

Also observed in the test series has been the effect of steel grade on the connection performance. In this case, two identical joint details with different steel grades resulted in two distinct moment-rotation characteristics that deviated early in the joint's loading history. The early deviation indicated the presence of yielding in the connection before the attainment of serviceability loads.

Finally, the Hollo-bolt connector has been compared to the flowdrill system via tests on nominally identical joints. Serious limitations were found with the manufactures bolt projection specification, where the upper limit specified in the trade literature resulted in the bolt pulling out without clamping the endplate to the column. Comparisons of performance with flowdrill using longer bolts indicated close similarities with the flowdrill moment-rotation characteristic, although significantly less rotation ductility was observed with the Hollo-bolt connector.

Chapter 6

Flowdrill joints- Concrete filled

This chapter of the work reports on the behaviour of all the flowdrill joint tests with the columns filled with concrete. The reason for conducting this series of joint tests was to provide an insight into how the concrete may enhance the properties of the joint.

The use of concrete filled tubular columns has major advantages in two specific areas which are increased load capacity and improved fire resistance of the column. The additional load capacity is primarily a direct result of increased compressive resistance of the concrete core of the cross section, rather than any additional strength from a reduced column slenderness achieved by the enhanced second moment of area. The fire resistance of the column is improved by the concrete acting as a heat sink to dissipate the heat away from the outer steel which is known to have reduced strength and stiffness at elevated temperatures. These two features enable the column to be designed with a relatively small cross sectional area when compared to equivalent traditional open section columns.

These advantages all relate to the 'column' performance and are well documented [52] with practical examples cited directly relating to buildings. However, the performance of the joint has not been investigated so thoroughly, with no known data existing on the moment-rotation characteristic of joints with flowdrill connectors. This particular portion of the programme was initiated to investigate the effect of this aspect on the joint's performance.

6.1 Programme of joint tests

The joint tests conducted with concrete filled columns is shown in Table 6.1. Essentially the programme has been split into the two previous sections of 'simple' and 'rigid' flowdrill joints reported in chapters 3 and 5 respectively. The joint tests in this series are therefore identical to their unfilled counterparts, except for the column being concrete filled. A direct comparison between the unfilled and filled tests can be conducted. The unfilled joints used as comparisons are noted in the last column of

Table 6.1 for reference. Details for each of the joint geometries can be found from Figure 3.1 (Chapter 3, pg. 3-3) and Figure 5.1 (Chapter 5, pg. 5-2).

Test No.	*Column Section Size*	*Steel Grade*	*Beam size*	*Endplate Type*	*Endplate Thk.*	*Bolt Cross-centres*	*Unfilled comparison joint test*
Comparison of concrete filled columns with simple flush endplates							
14	200x200x8	S275	457x152x52 UB	Flush	10	100	2
15	200x200x8	S275	356x171x45 UB	Flush	10	100	4
16	200x200x6.3	S275	356x171x45 UB	Flush	10	100	7
17	200x200x8	S275	254x146x31 UB	Flush	10	100	10
Comparison of concrete filled columns for rigid joint details							
22	200x200x10	S275	356x171x67 UB	Extended	25	120	20
24	200x200x10	S355	356x171x67 UB	Extended	25	120	23

Note: (1) For joint details refer to Figure 3.1 and 5.1

Table 6.1 Flowdrill joint tests- Concrete filled and unfilled comparisons

All the tests shown in Table 6.1 were conducted at the same time as their unfilled counterparts and using the same testing arrangement. The grouping and reporting of the joint tests is therefore one of convenience. Unless stated differently, the testing procedure adopted for the previous unfilled joints was used for the concrete filled joints.

As shown in Table 6.1 the joints are split into the categories of simple and rigid. The tests conducted under the simple group of joints, numbered 14, 15, 16 and 17 in the series, used only the flush endplates. No tests were carried out on the flexible partial depth endplates. The use of the flush endplate detail was to examine the increased moment capacity and stiffness of simple joints which results from concrete filling. Test nos. 14, 15 and 17 relate to serial beam depths of 457, 356 and 254 respectively, while the effect of altering the tube thickness from that of 8mm to 6.3mm is examined in test no. 16. For the rigid series of tests, only the extended endplate detail was investigated. Two joints were examined in this group, where the only difference was the grade of steel used.

6.1.1 Material properties

All the steel used for the concrete filled joints was selected from the same batch adopted for the unfilled joints. The yield strength for the SHS columns and dimensional survey can be found in Appendix B.

The concrete used for the 'simple' joint tests was obtained from a commercial source. The mix specified was for C40 grade concrete with a low aggregate size that would be normally suitable if used on site with a concrete pump. A strength of 40 N/mm^2 was expected after 28 days. The final compressive strength and flexural strength provided by the 100mm concrete cube samples is shown in Table 6.2.

The concrete used for the two rigid tests was mixed within the department's laboratory instead of using a commercial source due to the small quantity required. The specification for the concrete was similar to that of the simple joints with a mix that would be pumped into the tube, which required a 10mm aggregate size and a compressive design strength of 40 N/mm^2 after 28 days. The average compressive strength of three cube samples selected from each joint and conducted on the day of the test is shown in Table 6.2. The concrete mixed within the department attained higher values to the compressive strengths obtained from a commercial source.

Test No.	Compressive strength (N/mm^2)	Tensile strength (N/mm^2)
14	43.4	3.6
15	43.4	3.6
16	43.4	3.6
17	43.4	3.6
22	50.8	-
24	50.2	-

Table 6.2 Concrete cube and tensile strengths

6.1.2 Construction, fabrication and testing of concrete filled joints

All the fabrication of the steel for both the simple and rigid endplates were identical to the procedure used for the unfilled joints. The joints adopted the same test arrangements as described for the unfilled joints. The leverarm positions of the hydraulic ram for the concrete filled joints are shown in Table 6.3, where the distance to the ram was measured from the connection face. The loading to the joint through the ram was applied in one direction only. Cyclic loading was not therefore used for these tests. The reason for this was the opinion that the use of cyclic loading may mask or induce a different failure mechanism in the joint because of the special properties of concrete cracking.

Joint test no.	Leverarm (mm)
14	1320
15	1006
16	1005
17	1008
22	2557
24	2555

Table 6.3 Leverarm positions for concrete filled joints

The test procedure for the joints also played a part in the way the tubes were concrete filled, requiring different practices for the simple and rigid tests. Traditionally the construction of a building would result in steel erection prior to concrete filling of the tubes. To fill the tube with concrete the mix would normally be pumped in from the top via the use of a concrete pump and tremie pipe, or at the bottom of the column through special valves fabricated into the base of the tube (a technique favoured on the continent). The advantage of allowing the concrete to be pumped into the column from the bottom allows the full height of the column to be completed in one operation, with excellent compaction of the mix. To provide a realistic joint test the endplate must be bolted to the column before the concrete is poured.

The problem with bolting the endplate to the column for the simple joints was the requirement to incorporate strain gauged bolts into the test that needed to be tightened

in the laboratory and then reused in other tests. There was also a problem with a restriction on the specimen size for safe handling into the rig. These two problems required the specimens to be bolted together after the concrete had hardened. To alleviate these problems ordinary bolts were inserted into the flowdrill holes before concreting and then removed after the concrete had set. This allowed the beam specimen to be bolted to the column prior to testing. The bolts used when concreting were longer than the ones adopted for the test which avoided any obstruction when the strain gauged bolts were fully tightened. The bolts were removed from the column with little difficulty, although the flowdrill threads were retapped, mainly to remove the slurry which seeped through before the concrete had fully set. The flowdrill hole is not water tight as reported in tests conducted on water ingress at Swinden laboratories [33]. Problems of leakage may be more severe in practice with excessive seepage due to a greater hydrostatic head during concreting the full height of the building. Because the bolts were removed, they were obviously not embedded and in this respect were not representative of normal practice.

The concrete was also stopped short of both ends of the column to ensure that the axial nip used in the testing of the joints would be applied only to the steel and not to the concrete. This was only a requirement for the simple joints were an axial load was used to restrain the column in position as part of the testing arrangement (cf. Figure 3.2). Stopping the concrete short avoided any unnecessary bedding in and movement during the tests.

For the rigid joints, the endplate was bolted to the column prior to concreting. This was possible for these joints because of the splice detail located into the loading beam, which reduced the specimen size, and the use of normal grade (8.8) bolts in the connection. The concrete was placed into the columns in two pours. The level of the concrete was taken past the top row of bolts by approximately the depth of column section, to simulate the full height of the column being filled. The concrete was compacted fully accelerating the amount of leakage from the flowdrill holes, as previously observed in the simple joints. The water and cement from the concrete had leaked from the flowdrill holes, which for the rigid joints was found to be more severe as the endplate did not provide a reasonable seal. This problem can only be considered more an aesthetic point of view rather than from any structural concern, as the cement which was lost through the lack of water tightness was only a small amount, although increased static head may cause a far greater problem in practice.

In general all the simple and rigid joints were tested after 28 days to allow the concrete to attain its full design compressive strength.

6.2 Comparison of concrete filled simple joints to unfilled joints

Each of the four tests adopted similar patterns of failure. Figure 6.1 below shows the moment-rotation response for the tests nos. 14 , 15 and 17 where flush endplates for the 457, 356 and 254 serial size beams have been bolted to the concrete filled 200x200x8 SHS column. The amount of endplate deformation and yielding observed by the plates increased from minimal bending on the 254 UB to noticeable endplate bending for the 457 UB (test no. 14). All endplates showed signs of single curvature bending. The compression flange of the beam also showed signs of distress by yielding uniformly over the entire flange rather than locally at the extreme tips of the flange in the case of unfilled joints. The difference in yield pattern being influenced by the relatively stiff column compression zone of the filled section.

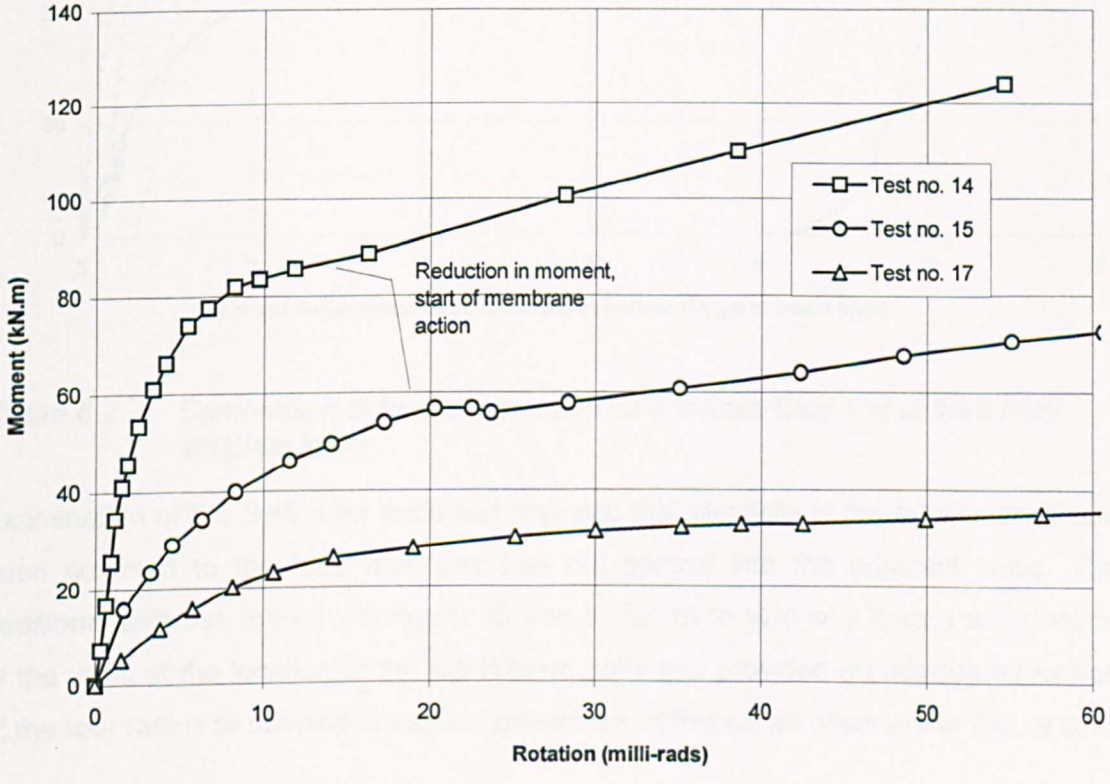

Figure 6.1 *Comparison of moment-rotation characteristics for concrete filled joints of 254, 356, and 457 serial beam sizes*

When filled with concrete, the webs of the SHS were unable to buckle in the region of the compression zone, which shifted the axis of the joint's rotation towards the compressive flange of the beam, immediately altering the moment-rotation response by increasing the initial stiffness. The increased stiffness attained in the compression zone is shown graphically in Figure 6.2, where the relative deflection of the compression flange of the beam is plotted against the moment in the joint for test number 16. As a comparison the plot of the equivalent unfilled joint, test no. 13, is also shown in Figure 6.2.

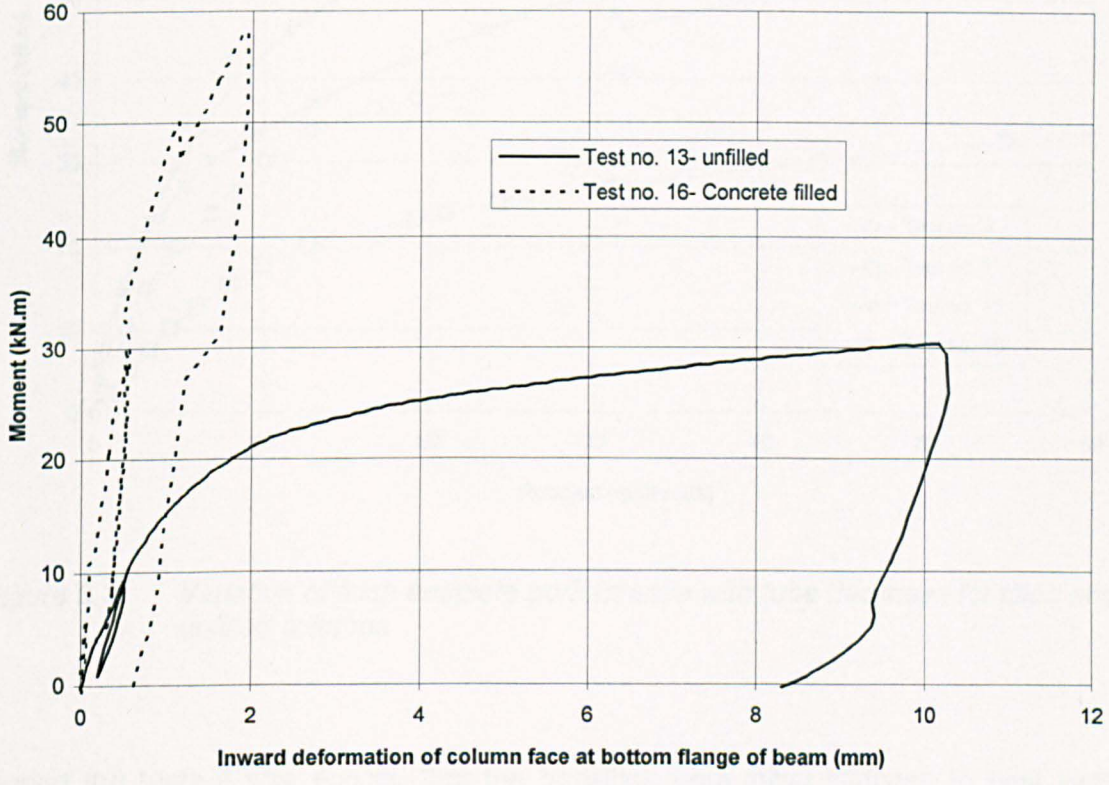

Figure 6.2 *Comparison of tube deformation for concrete filled and unfilled Flush endplate joints*

Examination of the SHS after each test revealed that plasticity in the tension zone had been confined to the tube face and had not spread into the adjacent webs. The additional stiffness from the concrete fill was sufficient to stop any inward deformation of the walls at the location of the top tension bolts and provided an adequate reaction at the root radius to develop increased membrane stiffness, as observed in Figure 6.1.

This type of failure was also apparent for test number 16, where the standard 200x200x8 SHS column used in the joint tests was replaced with a smaller 200x200x6.3 SHS column. This joint compares directly with test no. 15 which utilises

the same 356 serial size beam and flush endplates. Figure 6.3 shows the relationship between these two tests and their equivalent counterparts. The increased stiffness and moment from the concrete filled sections rises above their non-filled equivalents.

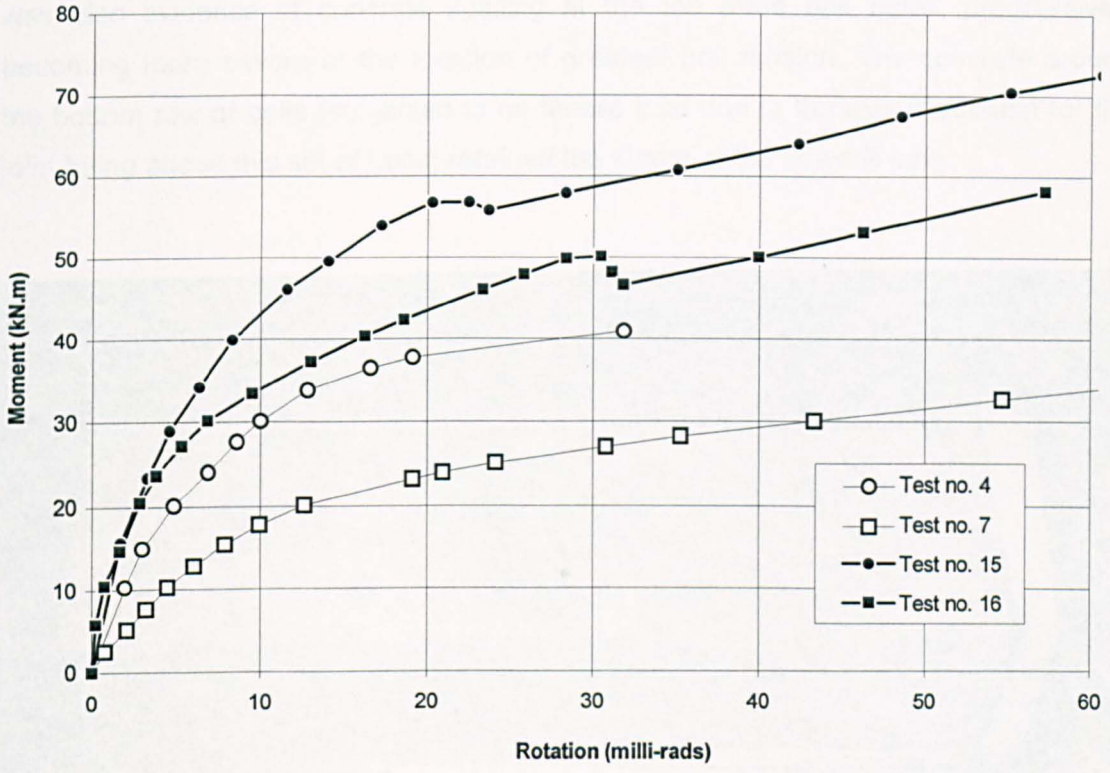

Figure 6.3 *Variation of flush endplate performance with tube thickness for filled and unfilled columns*

During the tests it was noticed that the transition from initial stiffness to post yield stiffness i.e. the portion of the moment-rotation characteristic at high rotations which tends to be linear, was shown not to be as smooth as that of the unfilled joints. This can be seen in Figure 6.3, where an apparent negative stiffness occurs between 0.020 and 0.030 radians. In some cases the post yield stiffness of the joint is referred to as the joint's membrane stiffness. Although, membrane action can be prominent at high rotations, the action of strain hardening can also influence the characteristic of the joint and as such the reader should be aware that the two effects are active in determining the joint's response. The post yield stiffness after these rotations was observed to be linear after the apparent drop in moment. This effect was observed in nearly all of the simple flush endplate tests.

The apparent loss of moment may be due to the concrete cracking in the compression zone of the column directly in line with the beam flange. The column of test 14 was cut away from the concrete at the location of the joint to reveal a shear crack directly in line with the position of the beams compression flange, as shown in figure 6.4. There was also evidence of concrete spalling at the top three bolt holes, progressively becoming more severe at the location of greatest bolt tension. The concrete around the bottom row of bolts (subjected to no tensile load due to the axis of rotation for the joint being above this set of bolts) retained the shape of the flowdrill lobe.

Figure 6.4 *Steel tube cut away to reveal concrete spoiling and cracking for test number 14*

6.2.1 Failure mechanism of concrete filled joints

It would be incorrect to suggest that the bond between the bolt and the concrete caused the spalling of the concrete and associated loss in stiffness observed in Figure 6.3, because the bolts for this particular test were removed after the concrete had started to set and the tensile strength of the concrete (tested at 3.6 N/mm^2) was not sufficient to generate the amount of bond for the corresponding moment applied. It is also recognised that because the concrete shrinks during setting, the bond between the concrete and steel is less than that of concrete which encases steel columns. Therefore spalling is assumed to be the result of bolt rotation as the face of the SHS deforms under load. Under normal flexural action of simply supported beams, end rotations would be present and a certain amount of moment would be transferred into the column from the fixity of the joint. With concrete filling, more moment would be attracted to the column due to the increased joint stiffness. The use of either a fin plate or tee section joint, where no projections are made into the SHS, allows the concrete to be left intact as the beam rotates. However, in the case of the flowdrill joint the subsequent rotation and concrete spalling mentioned previously would cause some damage to the core of concrete. With the joints subjected to a high moment to shear ratio, there was little opportunity to examine the effect which the spalling of the concrete would have on the shear load transfer from the beam to the column and then into the concrete core. Further investigations are therefore recommended.

The direct effect of the concrete fill on the moment-rotation response of the joints as seen by Figure 6.1 and 6.3 is to increase the initial stiffness and moment capacity. This can be seen again from Figure 6.5 where the plots of tests 14, 2, and 1 are shown. These relate to a joint combination which incorporates the 457 UB and 200x200x8 SHS column, where either a partial depth or flush endplate has been used. The flush endplates shown are either concrete filled or unfilled. The results show a marked difference in joint characteristic simply by filling the SHS column with concrete. Table 6.4, also highlights the differences between concrete and unfilled joint. Both the initial stiffness and the membrane stiffness increase substantially, resulting in substantial end fixity and moment to the column.

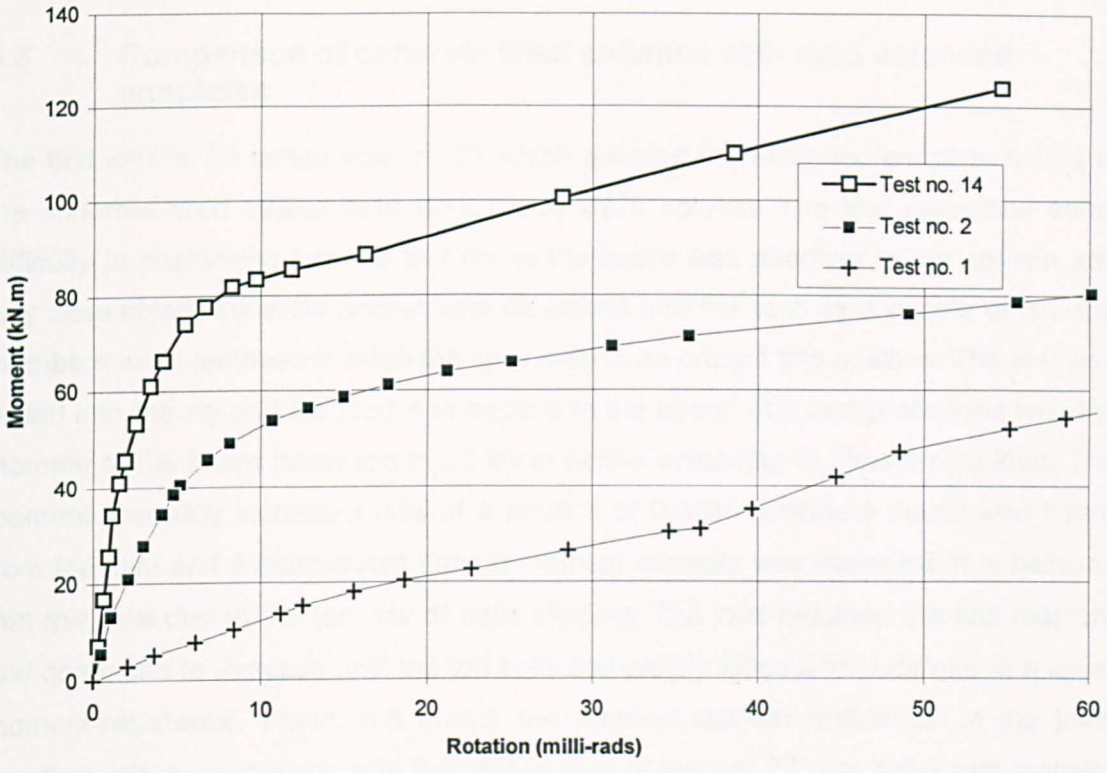

Figure 6.5 *Variation of joint performance for 457 UB serial size beam for flush and partial depth endplates*

Test No.	Max. Moment (kN.m)	Max. Rotation (radians)	Initial Stiffness (kN.m/rads)	* % increase	Membrane Stiffness (kN.m/rads)	* % increase	Moment at 10 milli-rad rotation (kN.m)	** % increase
10	26	0.069	2140		121		13	
17	36	0.065	3810	**78**	145	**20**	22	**69**
4	41	0.032	5880		-		30	
15	73	0.061	18600	**216**	457	**-**	43	**43**
2	82	0.064	10000		390		53	
14	124	0.055	33300	**233**	891	**128**	84	**58**
7	34	0.061	2500		224		18	
16	58	0.057	16000	**540**	453	**102**	34	**89**

* Percentage increase in stiffness over equivalent non concrete filled specimen
** Percentage increase in moment over equivalent non concrete filled specimen.

Table 6.4 *Joint stiffness*

6.3 Comparison of concrete filled columns with rigid extended endplates

The first joint to be tested was no. 22 which adopted the extended endplate bolted to the concrete filled 200x200x10 SHS grade S275 column. The test presented some difficulty in positioning into the test rig as the beam was attached to the column and fully assembled. To allow access and clearance into the test rig a couple of bracing members were removed to allow the specimen to be craned into position. The test was bolted into the rig and the load was applied to the beam. The test proceeded with the moment to the beam increased to 25 kN.m before unloading to almost zero load. The moment gradually increased until at a rotation of 0.0035 radians a sound was heard from the joint and a subsequent drop in moment capacity was observed. It is believed that this was due to the top row of bolts slipping. The joint regained the lost moment and continued to increase until the top bolts completely failed and stabilised at a lower moment-resistance. Figure 6.6 shows the moment-rotation resistance of the joint, together with a comparison with the unfilled joint of test no. 20. The maximum moment attained during the test was 288 kN.m at a rotation of 0.043 radians.

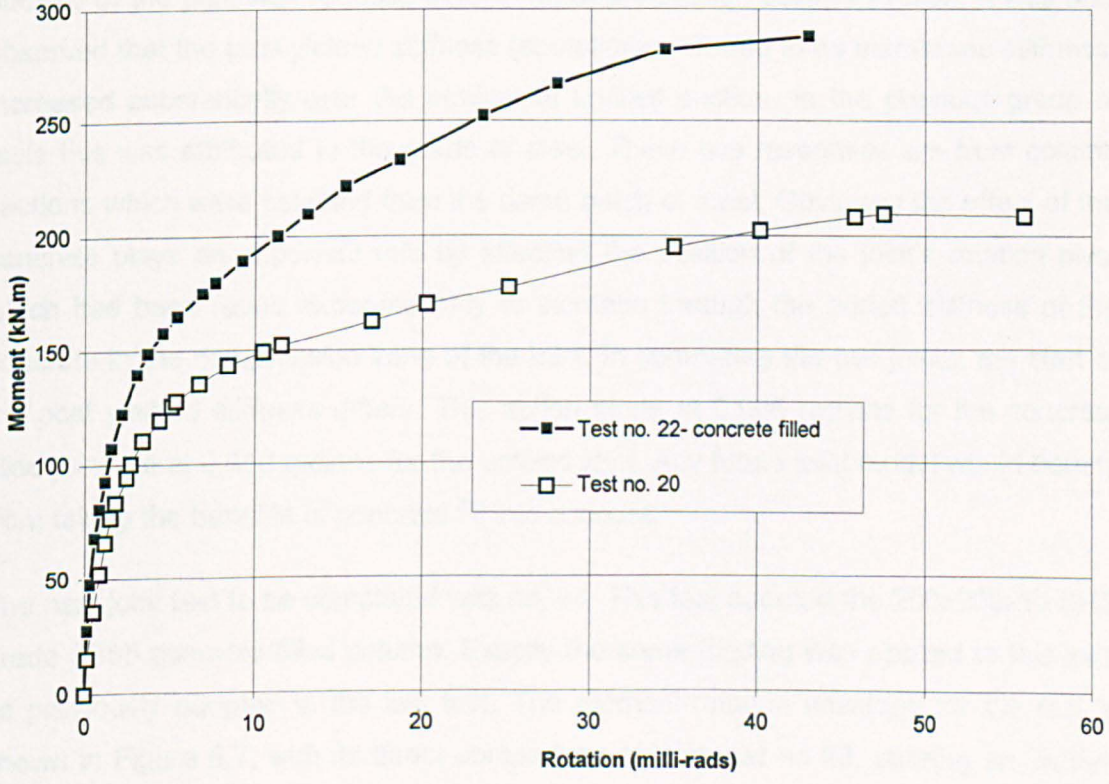

Figure 6.6 *Moment-rotation characteristic for joint test no. 22 compared to unfilled joint of test no. 20*

Examination of the beam after it had been unbolted from the column revealed that the endplate had suffered no visible damage. The beam had yielded in the compression flange and extended into parts of the web. The extent of the yielding was across the full width of the flange, which had been initiated at the centre spreading outwards to the extreme tips. The sign of yielding which was encountered early on in the test was similar to that using the isolated endplate details described in Chapter 4. Inspection of the column revealed extensive face deformation in the top three rows of bolt holes. There was little evidence that there was any deformation in the compression zone of the joint. As with the simple concrete filled joints, yielding had been confined to the connection face with no visible signs of damage to the webs. The concrete providing sufficient stiffness at the corners of the SHS column to stop any inward movement of the webs. The lack of movement therefore increased the potential of the column face to develop membrane forces during the latter stages of the joint test thereby increasing the moment capacity of the joint and the post yield stiffness.

The joint response shown in Figure 6.6 illustrates the increased initial stiffness and post yield stiffness of the joint. The moment capacity of the joint had increased significantly from the contribution of the concrete. With the increased strength the ductility of the joint was reduced below that of the unfilled column section. It was also observed that the post yielded stiffness (sometimes referred to as membrane stiffness) increased substantially over the equivalent unfilled section. In the previous group of tests this was attributed to the grade of steel. These two responses are from column sections which were selected from the same batch of steel. Obviously the effect of the concrete plays an important role by affecting the position of the joint's rotation pivot which has been found experimentally to increase through the added stiffness of the concrete in the compression zone of the joint. In comparing the two joints, the start of the post yielded stiffness differs. This action starts at 0.006 radians for the concrete filled joint but at 0.010 radians for the unfilled joint. Any future joint model would benefit from taking the benefits of concrete fill into account.

The next joint test to be completed was no. 24. This test adopted the 200x200x10 SHS grade S355 concrete filled column. Exactly the same loading was applied to this joint as previously adopted in the last test. The moment-rotation envelope for the test is shown in Figure 6.7, with its direct comparison of joint test no 23, utilising an unfilled column member. The joint attained a final moment of 316 kN.m at a rotation of 0.034 radians before the top bolts pulled out and reduced the moment on the joint. The initial stiffness and moment capacity of the flowdrill joint exceeded its values of all other

previous tests. The nominal moment capacity of the 356x171x67 UB beam was 333kN.m which indicates the performance of the partial strength connection. The behaviour and failure of the joint emulated the previous test except that the initial stiffness and moment capacity was significantly higher.

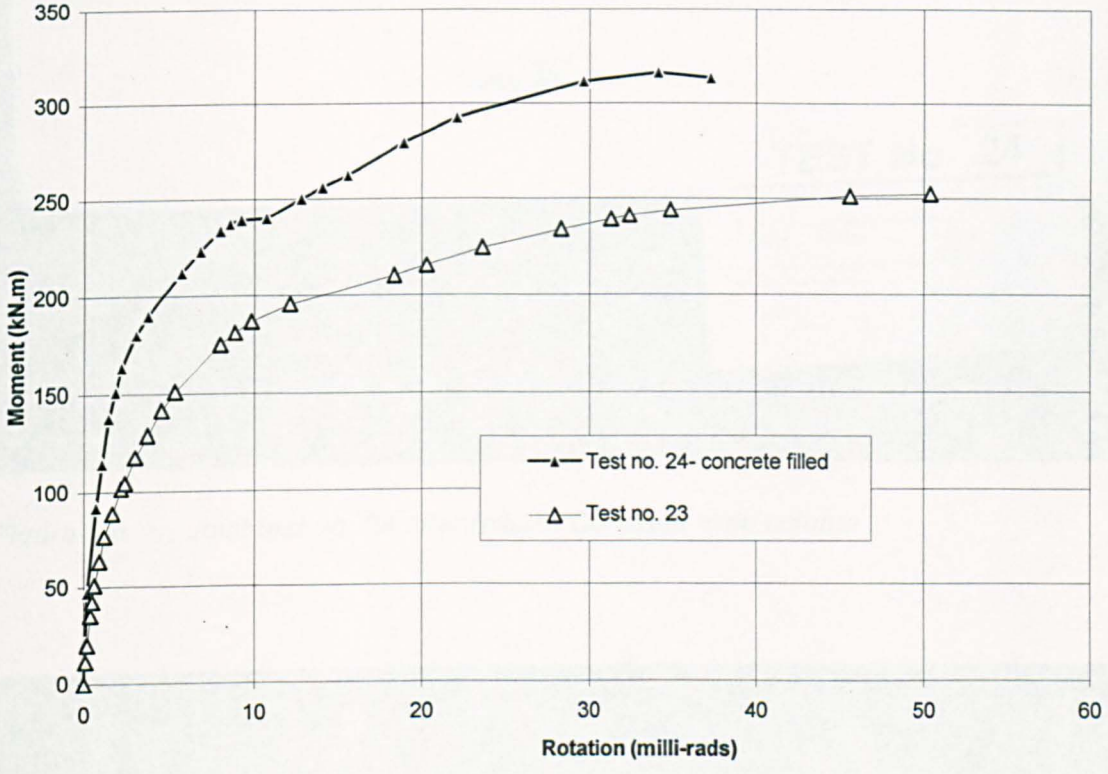

Figure 6.7 *Moment-rotation characteristic for joint test no. 24 and comparison to unfilled joint test no. 23*

Examination of the endplate revealed some slight distortion to the extended portion of the plate. The beam was severely yielded in both the compression flange and the web. Inspection of the column face revealed a similar deformation to the concrete filled joint tested previously. Figures 6.8 and 6.9 show photographs of the column sections for joint tests no. 24 and 23 respectively. Clearly the extent to which the compression zone contributes to joint flexibility is evident. The beneficial effect of the concrete reduces the deformation and increases the capacity of the joint. The effect of the concrete will in some instances be equivalent to increasing the thickness of the tubular column by one serial size.

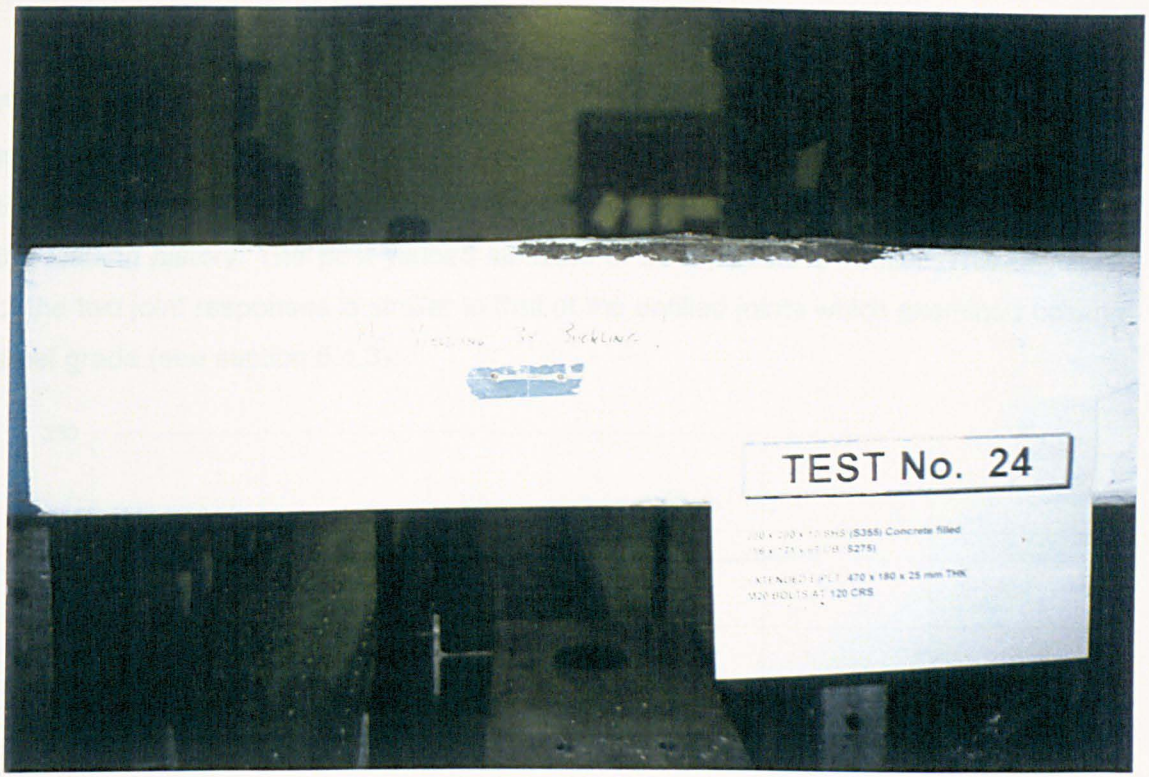

Figure 6.8 *Joint test no. 24 after failure- Concrete filled column*

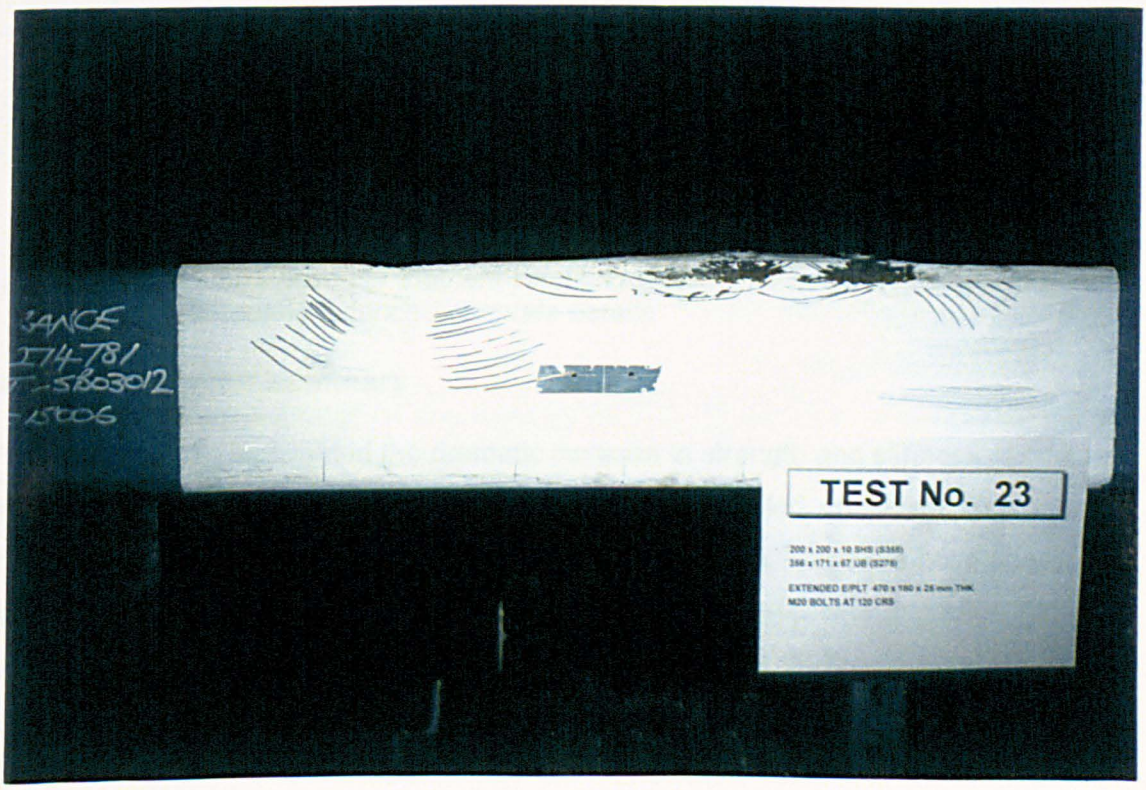

Figure 6.9 *Joint test no. 23 after failure- Unfilled column section*

Finally, to emphasise the effect of steel grade, a comparison of the two concrete filled joints is shown in Figure 6.10. In this instance the lower grade of steel (S275) of joint test no. 22 deviates from the higher grade of steel (S355) of joint test no. 24 early in the loading history. The post yielded stiffness of both joints are similar. This deviation of the two joint responses is similar to that of the unfilled joints which examined column steel grade (see section 5.4.3).

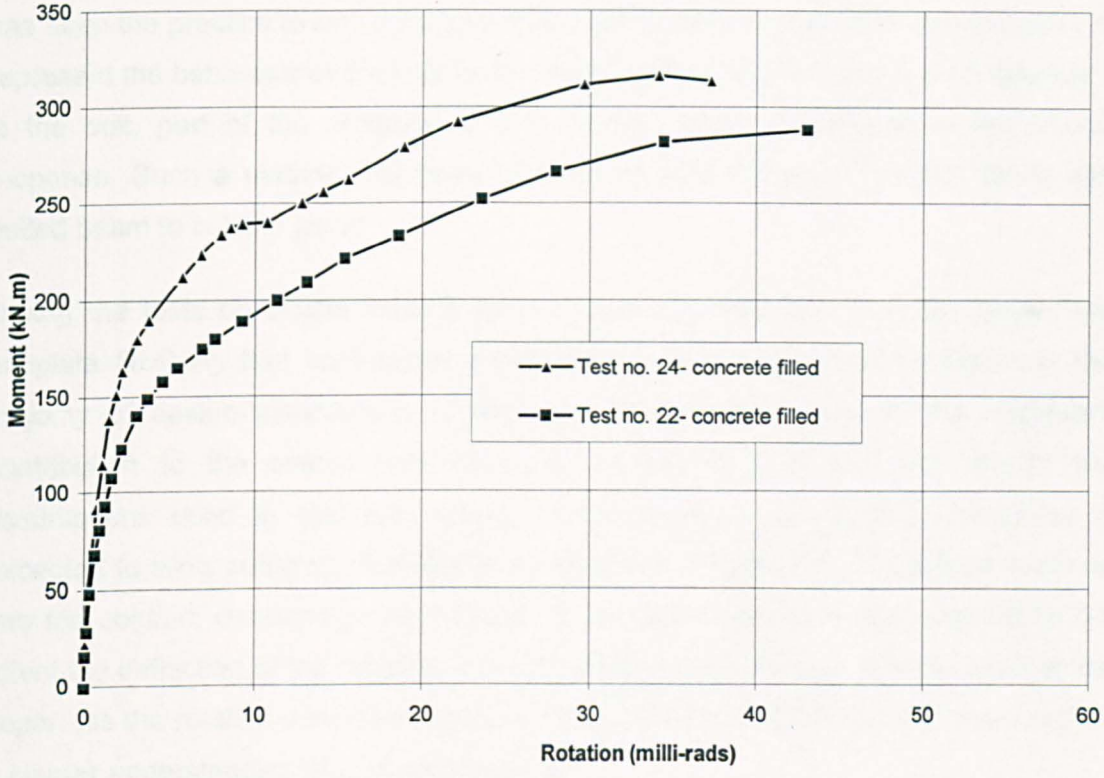

Figure 6.10 Comparison of moment-rotation response for concrete filled columns adopting extended endplate details

6.4 Chapter summary

This chapter has highlighted the dramatic increase in strength and stiffness of concrete filled flowdrill joints when compared directly to their unfilled equivalent, for both the 'simple' flush endplates and the 'rigid' extended endplates. The tests have shown that the compression zone resistance of the column is substantially increased thereby allowing the axis of rotation of the joint to be located towards the compression flange of the beams compared to unfilled columns. The shift in rotation has a direct influence to the joint's stiffness. As a consequence of the increased capacity, the ductility of the rigid joints is reduced, with bolt pull-out occurring when the column face has undergone gross deformation. Based on EC3 guidance, all joints would be classified as semi-rigid partial strength.

Chapter 7

Endplate flexibility and 'component' method of analysis

The load paths which occur within joints are usually highly complex. Because of this, it has been the practice to simplify a joint into a model which consists of 'components', to represent the behaviour of the joint under load. Each component of the joint, whether it is the bolt, part of the endplate or the column flange, contributes to the overall response. Such a method has been adopted by EC3 Annex J [47], which deals with bolted beam to column joints.

During the tests on simple flowdrill joints it was observed that, in a few cases, the endplate flexibility had contributed significantly to the joint's overall rotation. In the majority of design situations it is important to be able to assess the endplate's contribution to the overall joint flexibility, as the fixity of the joint affects the assumptions used in member design. For instance, a pin jointed connection is expected to allow sufficient flexibility in the endplate to avoid inducing a large moment into the column; conversely, the amount of fixity in an assumed rigid connection will affect the deflection of the member and the overall frame stiffness. A joint model which separates the rotation developed by the endplate from that of the column may result in a clearer understanding of joint performance.

An analytical solution based on the component method to determine overall joint flexibility is described within EC3 Annex J. The principles of the method allow for the possible extension to joints which do not conform to typical joint details. To extend the component method used in EC3 to flowdrill joints, a series of separate isolated component tests would be required. Unfortunately, this was not possible due to the restraints of the test programme, and as such a different approach was necessary to assess the contribution of the endplate's flexibility during the flowdrill joint tests. A method was considered of determining the behaviour of simple flowdrill joints by the addition of two separate isolated characteristics which represent both the endplate and column face. If successful, the 'endplate characteristic' could be calculated analytically from EC3 and combined to the author's own moment-rotation model for the 'column face' which is reported in Chapter 8, which has been developed on the basis of a semi-

empirically treatment because of the lack of information on the component response of the complete flowdrill joint.

This chapter therefore has two aims. The first is to compare the isolated simple flush endplates reported in Chapter 4 with the methods used in EC3 Annex J. The second is to examine the feasibility of combining both the endplate and column face moment-rotation characteristics tested in isolation to determine if the joint characteristic is representative for a geometrically similar flowdrill joint.

7.1 EC3 joint model compared with isolated endplate response

Within this section the isolated endplate moment-rotation characteristic of test nos. 31a and 31b (reported in Chapter 4) are compared to the predicted moment-rotation response of the analytical joint model from EC3 Annex J [47]. This part of the Eurocode determines both the ultimate moment capacity and rotational stiffness for bolted endplates. The two tests compared are identical, although different restraint conditions were used to the edge of the endplate, resulting in test no. 31a being bolted directly to the column section whereas test no. 31b was packed away from the base allowing no restraint to the endplate edges.

For the two isolated endplates used in the comparison the 'ultimate moment capacity' was taken to be the test moment recorded at a rotation of 0.025 radians rather than being determined by an analytical value from EC3, as no coupon tests were available to determine the yield stress for the endplate material. A brief overview of the method adopted in EC3 for determining the joints rotational stiffness is provided in the following section.

7.1.1 Overview of EC3 design principles for rotational stiffness

The basic model used by EC3 part 1.1 revised Annex J to determine joint rotational stiffness is similar in principle to that of the component based method for the ultimate moment-resistance. According to EC3, the rotational stiffness S_j of a joint, for a given moment $M_{j,Sd}$, may be obtained with sufficient accuracy from:

$$S_j = \frac{E.z^2}{\mu \sum \frac{1}{k_i}} \qquad \text{.....(7.1)}$$

where

k_i is the stiffness coefficient representing component i

z is the joint's leverarm

μ is the stiffness ratio $S_{j,ini}/S_j$

$S_{j,ini}$ is the value of S_j when the moment $M_{j,Sd}$ equals zero, i.e. the initial stiffness of the joint

The stiffness ratio μ is determined from:

$$\mu = \left[\frac{1{,}5.M_{j,Sd}}{M_{j,Rd}}\right]^{\psi} \qquad \text{but } \mu \geq 1 \qquad \text{.....(7.2)}$$

where ψ = 2,7 (from Figure J.9).

The stiffness ratio above is simply a curve fitting relationship with the parameter ψ of 2.7. The parameter operates when the moment of the joint attains 2/3 the ultimate moment of resistance. Up to this point the curve exhibits a linear initial stiffness.

As the isolated endplates were tested against a rigid column the stiffness coefficients k_i need only to be concerned with the endplate and bolt elongation. The column flange does not therefore contribute to the joints overall flexibility. The two coefficients for

both the endplate and bolt elongation are denoted as k_5 and k_7 and are provided below for reference:

$$k_5 = \frac{0{,}85.\ell_{eff}.t_p^{\,3}}{m^3} \qquad \text{.....(7.3)}$$

where:

ℓ_{eff} is the smallest of the effective lengths given for this bolt row (individually or as part of a bolt group) in Figure J.8

m is defined in J.3.5.8, which relates to the distance between the bolt and the web

$$k_7 = 1.6A_s/L_b \qquad \text{.....(7.4)}$$

where

A_s is the tensile stress area of the bolt

L_b is the elongation length of the bolt

A full account of the model is provided in EC3 revised Annex J to which reference should be made.

7.1.2 Comparison of analytical and experimental moment-rotation response

Figure 7.1 shows the actual moment-rotation response for the 10mm isolated flush endplate of test's 31a and 31b compared to the predicted moment-rotation characteristics derived from EC3. The calculated responses assume the model incorporates two rows of bolts to be effective. The main difference between the predicted unpacked and packed joint response is dependent upon the final moment capacity (determined experimentally from a corresponding joint rotation of 0.025 radians).

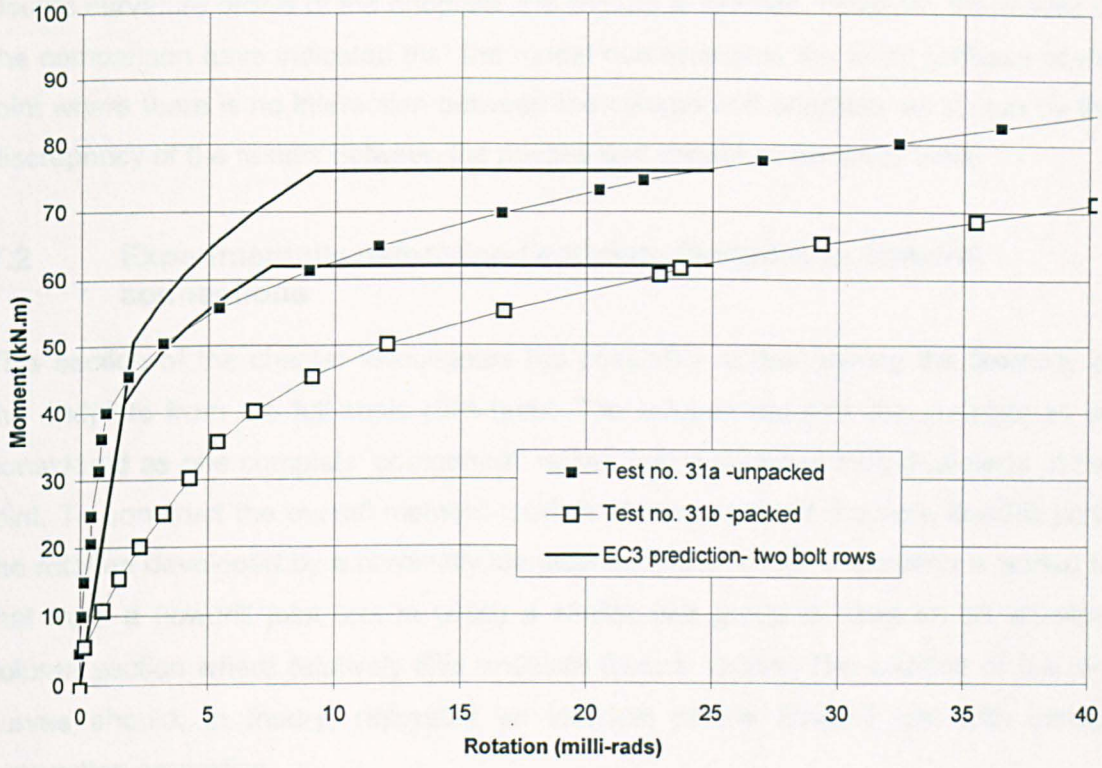

Figure 7.1 Comparison of predicted moment-rotation to experimental results

The predicted moment-rotation characteristics shown in Figure 7.1 are essentially bi-linear models which have been chamfered at two-thirds of the ultimate moment capacity. The model takes no account of any increase in strength after the ultimate moment is reached, which was observed for all the simple isolated joint tests.

In general, the moment-rotation predictions of Figure 7.1 appear to be more in agreement with the flush endplate bolted directly to the rigid base rather than the packed arrangement. The model predicts an initial stiffness of 24800 kN.m/radian compared to an actual value for test 31a of 51500 kN.m/radian. The predicted joint model therefore underestimates the initial stiffness of the joint by a factor of about 2.1. The cut off position at two thirds the ultimate moment capacity coincides with the actual deviation from non-linearity of the joint, although, this is determined by the original selection of the ultimate moment of resistance as that corresponding to an arbitrary 0.025 radians. As for the prediction for the packed endplate, which has an initial stiffness of 8740 kN.m/radian, the model overestimates the initial stiffness by a factor of 2.8.

For normal cases of open section bolted connections, EC3 Annex J model appears to be adequate in predicting the joint's response for rotational behaviour where the

double curvature profile of the endplate and column is induced. However, the results of the comparison have indicated that the model overestimates the initial stiffness of the joint where there is no interaction between the column and endplate, as shown by the discrepancy of the results between the packed and unpacked endplate tests.

7.2 Experimentally determined endplate flexibility in flowdrill connections

This section of the chapter investigates the possibility of determining the flexibility of the endplate from the full scale joint tests. The solution requires the endplate to be considered as one complete 'component' rather than a series of individual parts of the joint. To construct the overall moment-rotation characteristic of a simple flowdrill joint, the rotation developed by a nominally identical endplate tested in isolation is added to that from a flowdrill joint test in which a similar bolt group is used on an identical column section where relatively little endplate flexure occurs. The addition of the two curves should, in theory, represent an identical simple flowdrill test with similar connection properties.

To examine the feasibility of this method, three moment-rotation characteristics with similar bolt group details were required from the joint test programme. Joint test no. 6 provided a simple flowdrill flush endplate connection detail ideal for comparison in which similar bolt groups were adopted in other tests to allow both the endplate and column face components of the joint to be determined separately. The endplate moment-rotation component was from test no.31 (Chapter 4), and the column face contribution provided by test no. 26 (Chapter 5). A summary of all the joint parameters are presented in Table 7.1.

Joint test no.	Column size	yield strength (N/mm^2)	Beam size	Bolt cross centres (mm)	Endplate thickness (mm)
6	200x200x8 SHS	318	356x171x45 UB	120	10
26	200x200x8 SHS	346	356x171x67 UB	120	25
31	Rigid column	N/A	356x171x45 UB	120	10

Table 7.1 Joints used in comparison

All three joints are related to the flush endplate using the 120mm bolt cross centre connected to the 200x200x8 SHS column. This endplate was selected because it exhibited the greatest signs of bending and, as such, its contribution to overall joint rotation is clearly visible. Of the two isolated flush endplates tested with the 120mm bolt cross centres, the packed moment-rotation response was used as this test showed signs of single curvature bending which resembled the final endplate deformation to that of the actual 'simple' flowdrilled joint of test no. 6. The rigid joint test no. 26 adopted a similar bolt group to that of the previous two but incorporated a 25mm thick endplate. Details of both these endplates can be found in Figure 4.1. The three moment-rotation characteristics of the joints mentioned are plotted in Figure 7.2.

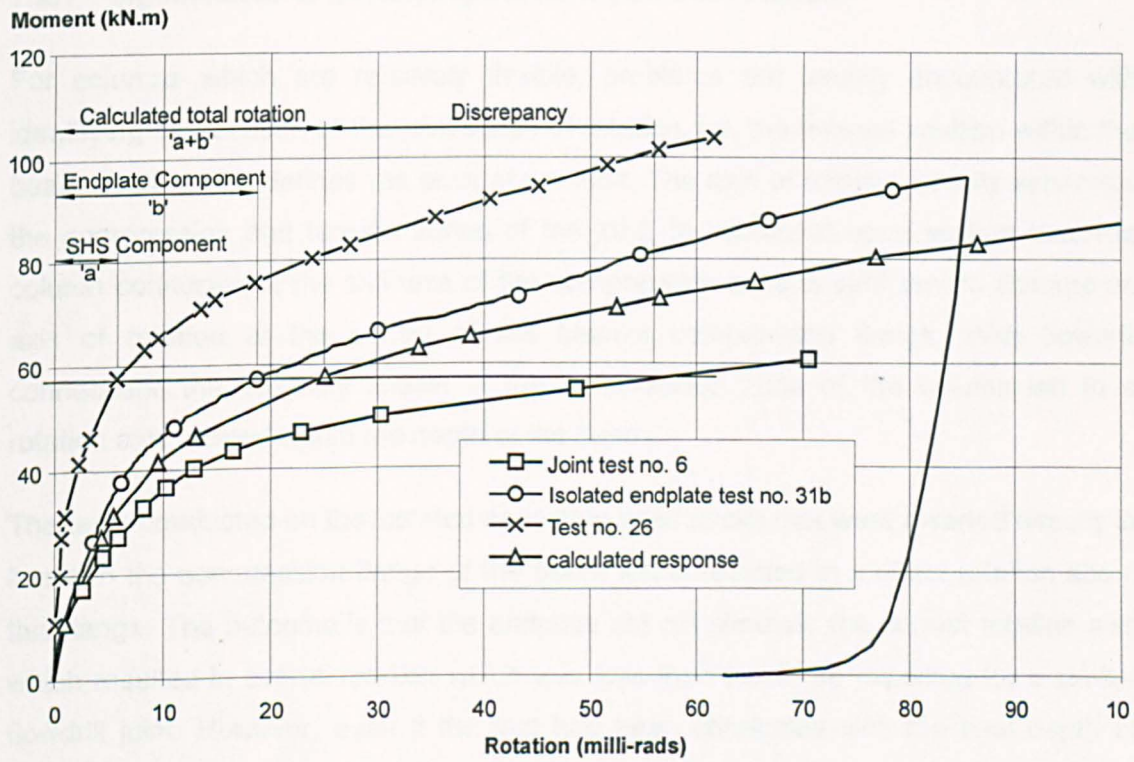

Figure 7.2 *Comparison of the theoretical calculated moment-rotation response constructed from the joint tests in isolation to actual flowdrill test number 6*

The upper curve shown on Figure 7.2 is the moment-rotation curve obtained in a flowdrill test with the over thick (25 mm) endplate, which is assumed to represent the contribution of SHS deformation to overall joint rotation. The addition of rotation of this curve at any level of moment to those of the isolated endplate test no. 31b represents the theoretical calculated response of the two component parts of the joint; the SHS flexural response and the endplate. It is immediately apparent that this curve does not correspond with the actual result of test no. 6, resulting in a significant error at large

rotations. Part of this discrepancy is due to the difference in endplate depth of test no. 26 which was 395 mm rather than 350 mm (refer to Figure 4.1). This has the effect of increasing the lever arm to the uppermost bolts by 30 mm (approximately a 10% increase). A further discrepancy was also found in the yield strength of the two SHS columns, which because of the delay in testing between the simple and rigid flowdrill joints resulted in the column SHS being procured from a different batch of steel (9% increase). Whilst these differences are significant they do not account for the discrepancy shown between the two moment-rotation curves in Figure 7.2. A more likely explanation is the influence of the joint's axis of rotation and the relative stiffness between the endplate and column face.

7.2.1 Significance of identifying the joint's axis of rotation

For columns which are relatively flexible, problems are usually encountered with identifying the location of the joint's axis of rotation, i.e. the internal position within the beam depth which defines the pivot of the joint. The axis of rotation usually separates the compression and tension zones of the joint. In traditional open section beam to column connections, the stiffness of the compression zone is sufficient to assume an axis of rotation at the centre of the beam's compression flange. With flowdrill connections the flexibility shown in the compression zone of the column led to a rotation axis located within the depth of the beam.

The tests conducted on the isolated endplates used packs that were inserted directly in line with the compression flange of the beam which resulted in a direct rotation about this flange. The outcome is that the endplate did not simulate the correct rotation axis which resulted in overall rotation which was less than would be expected for a similar flowdrill joint. However, even if the test had been conducted with the final depth of rotation axis observed for the flowdrill joint, this would not have provided the correct solution as the rotation axis has been observed to migrate from the top of the beam, travelling down the member as the bolt loads are redistributed (see Figure. 3.18).

7.2.2 Relative stiffness of endplate and column

Another reason identified for the discrepancy of the calculated moment-rotation curve in Figure 7.2 can be attributed to the interaction known to exist between the endplate and column. As testing of the isolated endplates proceeded it was observed that the restraint offered by the column significantly affected the moment-rotation response. It was assumed that by packing the endplate from the rigid base of the column the two extreme conditions of joint tests observed in the flowdrill joint could be created. These two conditions can be graphically illustrated in Figure 7.3(a) and (c) below by considering the relative stiffness between the endplate and column in typical situations found in the flowdrill joints.

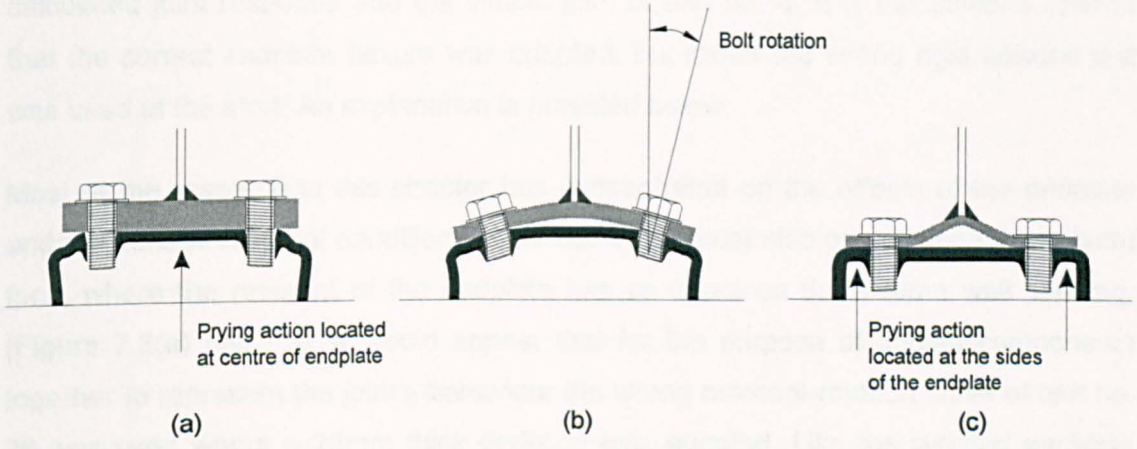

Figure 7.3 Relative stiffness between endplate and column face

Figure 7.3 shows the various endplate profiles which would result from different combinations of endplate thickness, column thickness and bolt cross-centres, when the bolts are subjected to tensile loading. Figure 7.3(a) illustrates the case of the rigid endplate and the effect on the column, typically observed in test no. 26, whereas Figure 7.3(c) highlights the situation of a relatively flexible endplate connected to a stiff column section in which the endplate deforms into double curvature bending. Both of these cases are extremes but may occur in practice. However, the majority of simple flowdrill joints resembled the end profile indicated in Figure 7.3(b), which is typical of test no. 6. In this instance an equal amount of flexural action was observed in both the endplate and column.

As a direct result of the endplate and column face stiffness shown in Figure 7.3 prying forces act at different positions. The bolts are subjected to an increased bolt load as a consequence of the joint geometry. Although no prying action was observed in the

tests, it is believed that in relatively stiff column sections prying action will act at the edges of the endplate, as indicated in Figure 7.3(c), producing double curvature bending in the endplate. This is similar to a traditional open section beam and column joint detail. Similarly, in the detail where a rigid endplate is shown, the prying action is located at the centre resulting in the 'column' face deforming into a profile resembling double curvature bending.

The adoption of the packed isolated endplate provided the greatest flexibility in the connection. In reality there would be some degree of restraint provided by the column section, similar to that shown in Figure 7.3(c), which would be beneficial to the moment-rotation curve. A moment-rotation curve for the column face which is stiffer than the one adopted would consequently increase the discrepancy between the calculated joint response and the simple joint of test no. 6. It is the author's opinion that the correct endplate flexure was adopted, but rather the wrong rigid flowdrill test was used at the start. An explanation is provided below.

Most of the research in this chapter has concentrated on the effects of the endplate and the various restraint conditions. A similar effect must also prevail upon the column face, where the restraint of the endplate has an effect on the column wall bending, (Figure 7.3(a) and (c)). It would appear that for the purpose of adding components together to represent the joint's behaviour the wrong moment-rotation curve of test no. 26 was used where a 25mm thick endplate was adopted. Like the isolated endplate tests of Chapter 4, a further joint test should have been conducted on an identical flowdrill joint where the rigid endplate is packed from the face of the column section, thereby allowing no restraint to the column face of the SHS and allowing bolt rotation to occur. The two flowdrill joint tests conducted with the rigid endplates would be added to their counterpart isolated endplate tests to provide the two extreme cases that would construct the boundaries to the simple joint test of no. 6. With reference to the differences found in the isolated endplate tests, the boundaries of the calculated flowdrill joints would most likely vary over a wide range.

The significance of this result is that there is evidently a complex interaction between the flexural action of the endplate, bolt stiffness and tube wall, resulting in the error observed in Figure 7.2. which cannot be overlooked.

7.3 Chapter summary

Comparisons were conducted with EC3 Annex J on the moment-rotation response of isolated endplate tests. A close agreement with EC3 Annex J was found for the endplates bolted directly to the rigid base over those which were packed. Unfortunately, due to insufficient time and programming constraints, the joint model provided by EC3 revised Annex J could not be applied to the complete flowdrill joints as additional tests were required to determine appropriate component stiffness coefficients for the SHS column. Further work in this area using either the component approach or appropriate analytical treatments, will undoubtedly lead to a uniform method of joint design.

A discrepancy was also found when a simple flowdrill joint test was compared to a calculated moment-rotation response determined from the addition of the endplate tested in isolation and the response from the column face using a rigid endplate. An error between the actual and calculated joint response was found. The reason for this error was the interaction that exists between the relative stiffness of the column face and the endplate. As a consequence the effect of the joint's axis of rotation was misinterpreted when isolated tests are conducted. Any future joint model which accounts for the endplate stiffness should allow for these effects.

Chapter 8

Joint model and design

In the previous chapters a programme of flowdrill joint tests was described which determined the moment-rotation characteristics for typical welded endplate details connected to SHS column members. This chapter reports on a joint model developed to predict the moment-rotation characteristic of such joints where the column provides the majority of the joint's rotation capability. For the purpose of the model, the endplate is assumed to be 'rigid'. This restriction does not necessarily mean unacceptable levels of inaccuracy, as the simple joint tests have shown that the flexibility of the column wall will, in most cases, govern the overall response of the joint. Using the moment-rotation characteristics from these joint tests a model has therefore been developed to estimate the full non-linear rotational characteristic of the joint.

Although the flowdrill joint tests have been used to provide the necessary validation for the model, guidance provided in this chapter is written so it may also be applied to both the Hollo-bolt joints and the Ultra-twist bolt developed by Huck International. The emphasis is therefore on the joint design rather than the fastener system, although an assessment of the performance of the flowdrill thread as the face is deformed has been included later in this chapter for completeness. The following sections of this chapter therefore describe a step by step procedure of how the model was developed, indicating where improvements can be made with regard to greater accuracy. Background information is also presented where appropriate.

8.1 Joint test data used in the models validation

The flowdrill joint tests provided the majority of the reference material required for comparison during development of the model. To supplement the Sheffield joint tests, six moment-rotation characteristics were also used from a joint test programme conducted by British Steel at their Swinden Laboratory. The tests, initiated to investigate the behaviour of the flowdrill connector in moment-resisting connections and conducted before the author's, provided valuable additional data.

A group of eight of the tests conducted at Sheffield provided a true response of the column's performance (discounting the repeat joint tests with the Hollo-bolts). A further seven flush endplate joints that were originally used to investigate the simple connections were also included in the comparison as these tests showed no visible signs of significant endplate deformation, and had properties similar to the moment-resisting joints. The remaining joint tests (excluding the flexible endplates) provided additional evidence in determining the joint's final mode of failure which was found to be highly complicated.

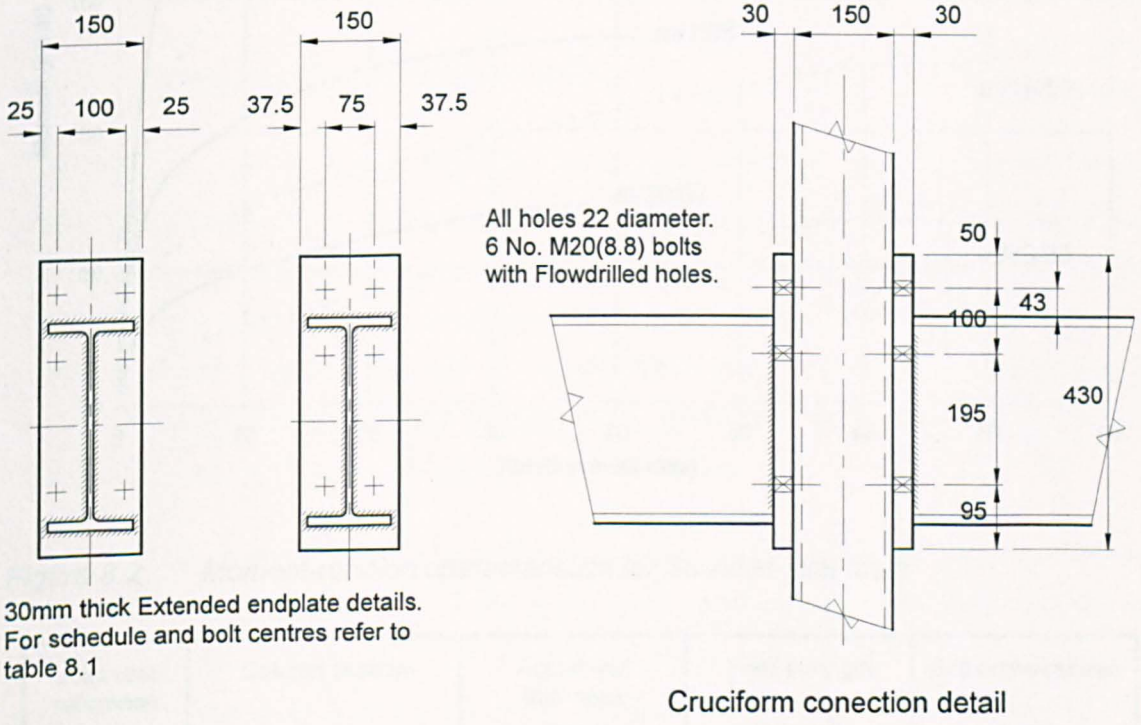

Figure 8.1 Details of Flowdrill joint tests conducted by British Steel

The Swinden Laboratory joint tests were different in both geometry and test procedure. All the tests were conducted on extended endplate details as shown in Figure 8.1. The endplates were 30mm thick and the full width of the column, which avoided any problems of flexibility of the face in the compression zone thereby increasing the capacity of the joint. The size and shape of the endplate reflected the programme's aim to test the performance of the connectors and not the joint. The beam section was also reinforced to avoid any yielding and permit its reuse with other joint details. The endplate, as noticed in Figure 8.1, was also extended beyond the bottom flange of the beam, increasing the leverarm to the bolts and the joint's own resistance to applied moment. This is at variance with traditional design practice where the bolt leverarm for calculating the moment capacity would normally be assumed at the centre of the

compression flange. All the joint tests were conducted in the cruciform test arrangement

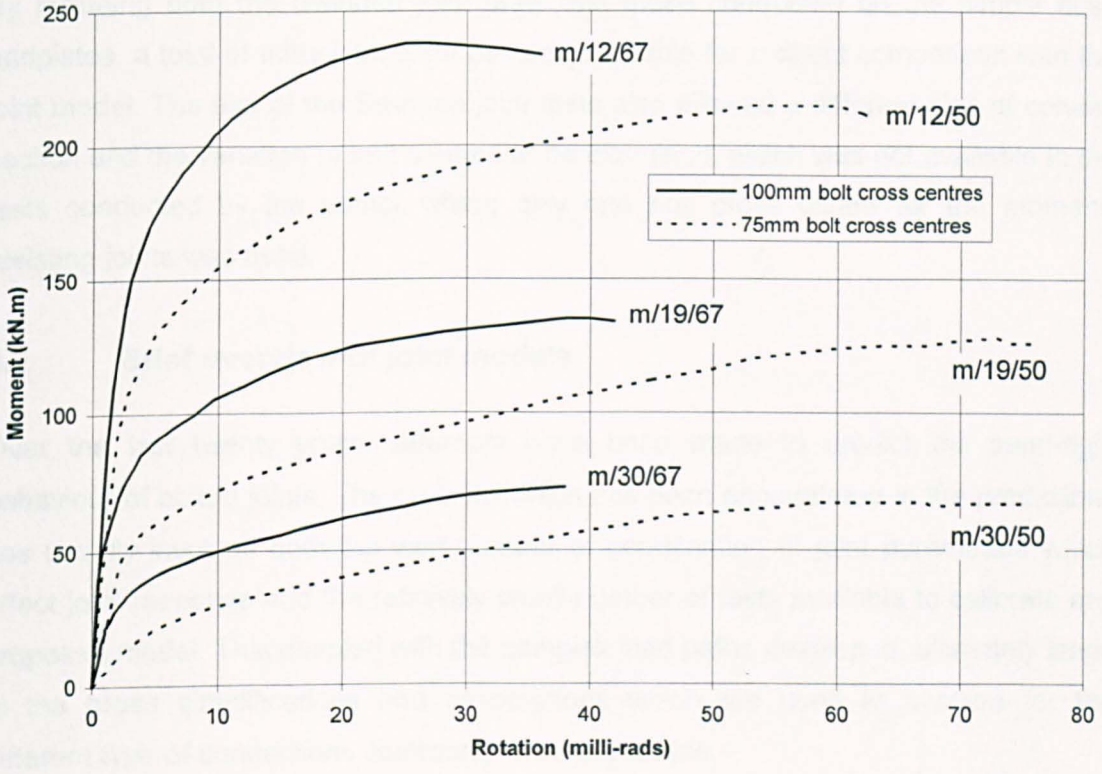

Figure 8.2 Moment-rotation characteristics for Swinden joint tests

Joint test reference	Column section	Actual wall thickness (mm)	Yield strength (N/mm^2)	Bolt cross centres (mm)
m/12/67	150x150x12.5 SHS	11.9	280	100
m/12/50	150x150x12.5 SHS	11.9	280	75
m/19/67	150x150x8.0 SHS	7.7	272	100
m/19/50	150x150x8.0 SHS	7.7	272	75
m/30/67	150x150x5.0 SHS	4.75	303	100
m/30/50	150x150x5.0 SHS	4.75	303	75

Table 8.1 Joint properties of Swinden Joint tests

The moment-rotation characteristics for the Swinden test programme are reproduced in Figure 8.2 (reproduced from reference 36), while Table 8.1 provides the necessary yield strength and various parameters investigated by the tests. Only the 150x150 serial size of column was used with three thickness combinations. The other parameter

which was varied was the bolt cross centres which were either 75mm or 100mm as indicated.

By including both the Swinden joint tests and those conducted on the simple flush endplates, a total of thirty joint tests become available for a direct comparison with the joint model. The use of the Swinden joint tests also allowed a different size of column section and the variation of bolt centres to be examined, which was not available in the tests conducted by the author where only one bolt cross centre for the moment-resisting joints was used.

8.2 Brief overview of joint models

Over the last twenty years, attempts have been made to predict the semi-rigid behaviour of bolted joints. The problem which has been encountered in the predictions has usually involved both the vast number of combination of joint parameters which affect joint response and the relatively small number of tests available to calibrate any proposed model. This coupled with the complex load paths developed, ultimately leads to the gross simplifications and assumptions which are used to account for the different type of connections commonly used in practice.

There are two general approaches taken to model a joint's overall behaviour. The first is to represent the behaviour of the joint by a combination of discrete analytical components that simulate the main properties of the joint. A joint can therefore be assumed to consist of a series of spring and beam elements [54] which represent the response of the joint. The properties which are assigned to each component are determined from isolated tests and calibrated by actual joint test data. A more sophisticated variation of this type of approach is Finite Element (FE) modelling of the complete joint where the geometry is completely defined [55]. The benefit of using FE modelling is that parametric studies may be conducted on joint variations without the need for results from expensive tests. The disadvantage of the FE models is the complexity which it can introduce into the problem.

The second solution to joint modelling is the use of curve fitting techniques. In this instance an analytical expression is used to best represent the characteristic of the joint test behaviour. These types of model can either represent the data, or provide some predictive mechanism based on the joint's geometry and properties.

One of the simplest mathematical expressions is a linear [56] or bi-linear [57-60] representation of the moment-rotation curve. Such relationships are incapable of following the true non-linear behaviour of the actual curve, as seen in Chapter 7, when modelling the isolated endplates to the simplified bi-linear expression of EC3. The joint models which use this approach usually concentrate on determining the ultimate moment capacity of the joint. The ultimate strength of the joint may be derived from a yield line model with reasonable accuracy, although the amount of rotation developed is not so readily calculated. The bi-linear model is more suited to the traditional open section joints where the initial stiffness is observed for a large proportion of the joint's loading. Such an expression for the flowdrill joints would be inappropriate due to its early deviation from the initial stiffness favouring the use of a non-linear representation.

To model the non-linear characteristic of the joint a polynomial function has been used by Sommer [61] that statistically represented a number of joint tests conducted on header plate details. The function was determined from a series of experimental joint tests in which a number of parameters was altered one at a time. The effect of each parameter on the joint's behaviour was incorporated into the polynomial. The final equation developed is reproduced below as equations (8.1) and (8.2) for reference.

$$\phi = 5.1x10^{-5}(KM) + 6.2x10^{-10}(KM)^3 + 2.4x10^{-13}(KM)^5 \quad \text{.....(8.1)}$$

where

$$K = t^{-1.6}g^{1.6}d^{-2.3}w^{0.5} \quad \text{.....(8.2)}$$

(where t, g,d and w represent geometrical parameters of the joint)

One of the better solutions to accurately curve fit any experimental data set but without any prediction capability is that used by Jones et al [62], where the B-spline curve fitting technique allowed a smooth and accurate fit to experimental data from a single test. At the same time, Ang and Morris [63] replaced the polynomial function of Sommer with a function originally developed by Ramberg and Osgood [64] , which is shown reproduced in Figure 8.3 with the notation developed in this chapter. The advantage of this curve is that only three parameters are required; the initial stiffness (K_i), the moment capacity ($M_{j,Rd}$) and a parameter which defines the shape of the curve (Ψ). A similar relationship was also developed by Kishi and Chen [65].

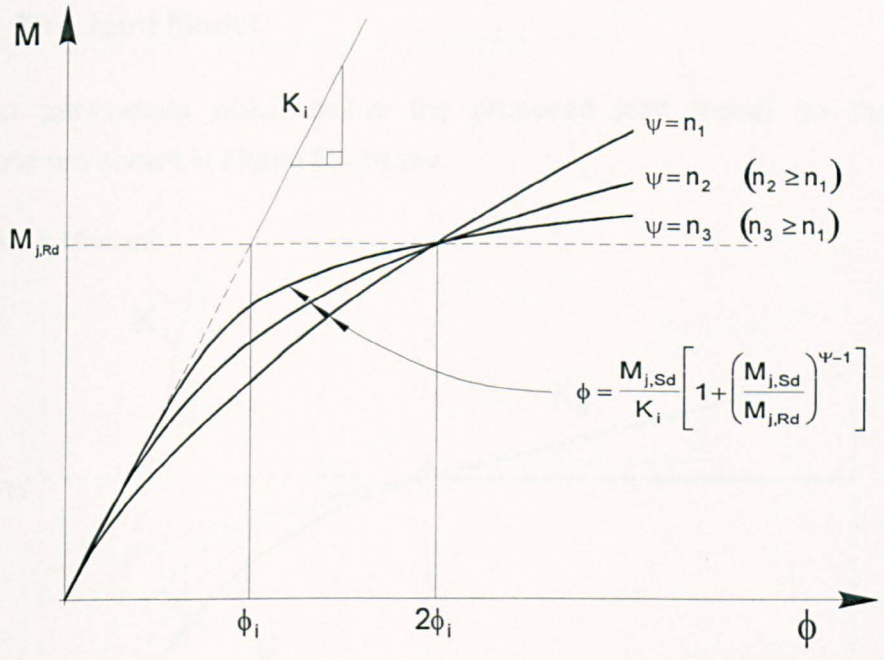

Figure 8.3 Ramberg-Osgood function

Joint models have been developed which accurately fit the characteristic of experimental data. The problem encountered in the majority of the preceding models is the ability to *predict* confidently the joint's response; a curve fit such as the one described by the polynomial function of eq.(8.1) developed by Sommer is accurate only to the limits of the test data. With the limited amount of tests, the extrapolation of the prediction equation to connection sizes outside the original test programme will undoubtedly raise serious doubts about its accuracy. The solution may not to search for greater accuracy of the curve fitting, but rather to encapsulate the actual moment-rotation characteristic between two less sophisticated curves that define upper and lower bounds to the test data. This would also recognise and reflect the obvious inaccuracies in experimentally derived results. It is this kind of approach which has been taken in the development of the model, determining a lower bound solution to the joint's response.

8.3 The Joint Model

The main parameters which define the proposed joint model for the flowdrill connections are shown in Figure 8.4 below.

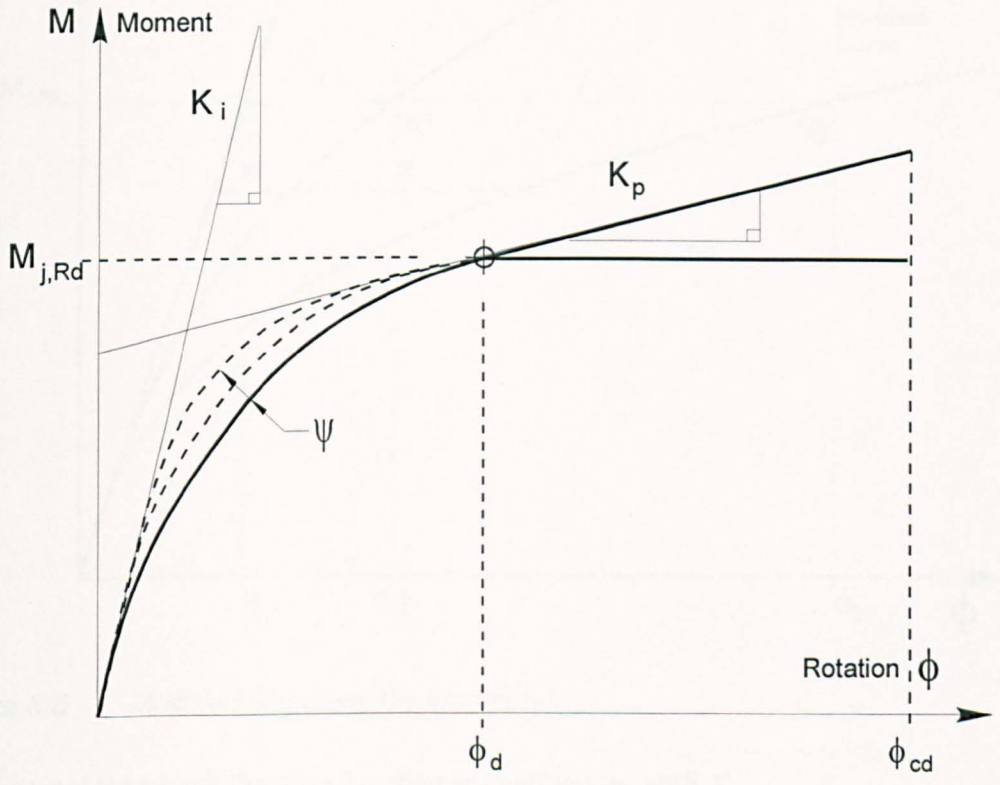

Figure 8.4 Moment-rotation parameters

The parameters used in Figure 8.4 are as follows;

$M_{j,Rd}$	design ultimate moment capacity of the joint
K_i	initial stiffness of the joint
K_p	The post yield stiffness of the joint after the joint has shown signs of excessive deformation
ϕ_d	rotation developed at the design ultimate moment of resistance
ϕ_{cd}	rotation capacity
ψ	shape parameter of the curve

The curve shape is represented by the Ramberg-Osgood function, previously shown in Figure 8.3. In its original form the curve was unable to represent the early non-linear moment-rotation characteristic of the joint tests, requiring point **A'** ($M_{j,Rd}$, $2.\phi_i$) of the

curve to be 'stretched' to point **'B'** ($M_{j,Rd}$, ϕ_d) as indicated in Figure 8.5. This approach now introduces a fourth parameter into the model

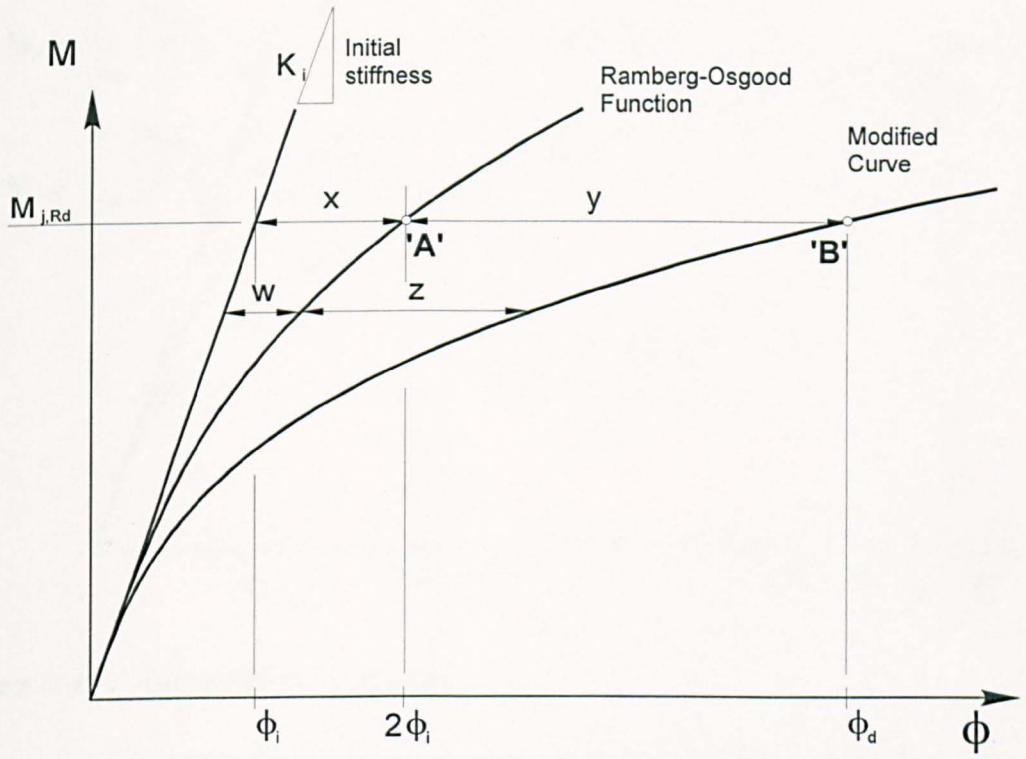

Figure 8.5 Modified Ramberg-Osgood curve

The original Ramberg-Osgood function is rewritten as eq(8.3),

$$\phi_{r-o} = \frac{M_{j,Sd}}{K_i}\left[1+\left(\frac{M_{j,Sd}}{M_{j,Rd}}\right)^{\psi-1}\right] \qquad \text{.....(8.3)}$$

in which

$M_{j,Sd}$, moment of joint

ϕ_{r-o}, rotation at moment $M_{j,Sd}$

The transformation of eq(8.3) into the modified curve requires a simple ratio from the initial stiffness of the joint shown by Figure 8.5 above as;

$$\frac{x}{y} = \frac{w}{z} \qquad \text{.....(8.4)}$$

The values of parameters of x, y, w, and z, are indicated in Figure 8.6.

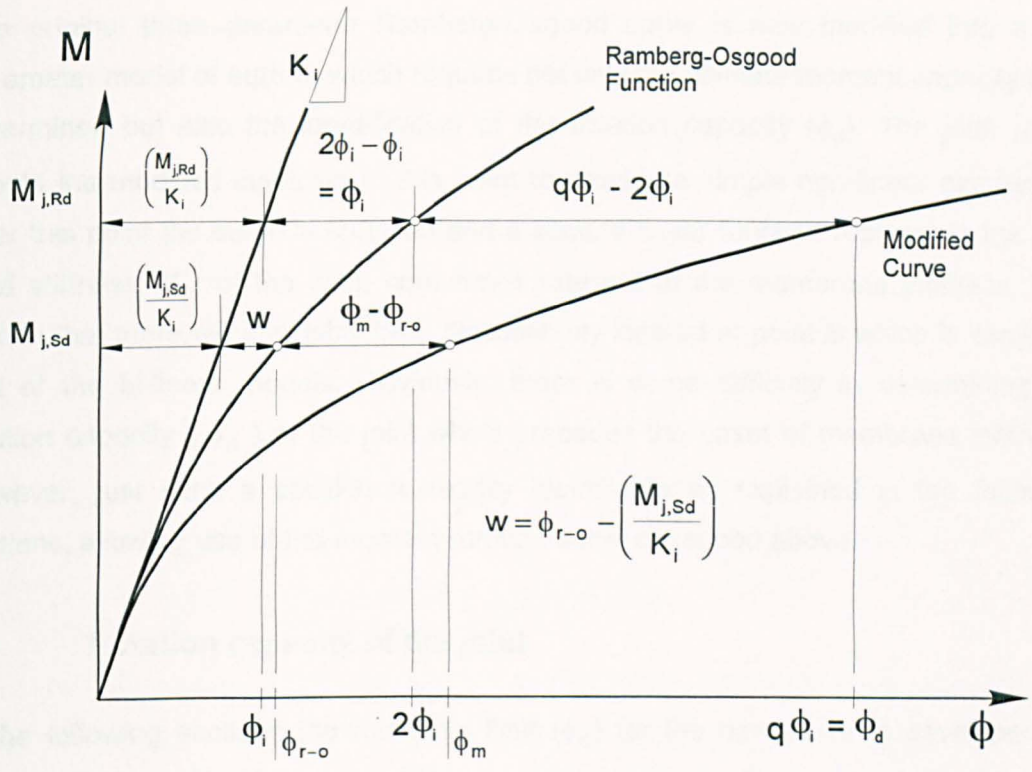

Figure 8.6 Curve fitting parameters

with; ϕ_{r-o}, representing the rotation developed for the Ramberg-Osgood curve at a moment of $M_{j,Sd}$

ϕ_m representing the rotation developed for the modified curve at a moment of $M_{j,Sd}$

Using eq(8.4), and substituting the relative parameters noted in Figure 8.6, an expression can be found as follows;

$$\frac{\phi_i}{q\phi_i - 2\phi_i} = \frac{\phi_{r-o} - \left(\frac{M_{j,Sd}}{K_i}\right)}{\phi_m - \phi_{r-o}} \qquad \text{..... (8.5)}$$

which simplifies to;

$$\phi_m = \left(\phi_{r-o} - \frac{M_{j,Sd}}{K_i}\right)(q-2) + \phi_{r-o} \qquad \text{..... (8.6a)}$$

where;

$$q = \frac{\phi_d . K_i}{M_{j,Rd}} \qquad \text{..... (8.6b)}$$

The original three parameter Ramberg-Osgood curve is now modified into a four parameter model of eq(8.6) which requires not only the ultimate moment capacity to be determined but also the identification of the rotation capacity (ϕ_d). The joint model adopts the modified curve up to this point to provide a simple non-linear expression. After this point the curve is curtailed and a second linear function represents the post yield stiffness (K_p) of the joint, sometimes referred to the membrane stiffness. This means that there will inevitably be a discontinuity located at point B which is similar to that of the bi-linear models. Obviously, there is some difficulty in determining the rotation capacity (ϕ_d) of the joint which precedes the onset of membrane stiffness. However, just such a position is readily identifiable as explained in the following sections, allowing use of the moment-rotation curve described above.

8.4 Rotation capacity of the joint

In the following sections the rotational limit (ϕ_d) for the new curve is developed, to identify the transition from the joint's non-linear response to the start of membrane stiffness. The majority of joint tests conducted have clearly shown considerable ductility and flexibility during the tests. In most cases there was no easily defined point where the joint had obviously failed; the tests were curtailed due to excessive joint rotation frequently accompanied by gross deformation of the column wall.

The overall rotation of the joint depends upon the location of the joint's axis of rotation and the amount of bolt displacement from the columns face flexibility. The next few sections discuss the method and procedures for determining both the rotation axis of the joint and the limits imposed on face deformation which determine the rotation capacity of the joint and, more importantly, the fourth parameter of the joint model.

8.4.1 Identifying the axis of rotation

The response and movement of the point of rotation of the joint is tied to its overall failure. Movement of the joint's rotation axis or 'pivot' is highly non-linear depending on the plasticity occurring in the column face. The degree of movement observed in a typical joint detail can be seen in Figure 8.7. In this relationship the position of the axis of rotation (noted as distance 'y') is plotted against the joint moment; the endplate detail is also illustrated opposite at the same scale as the graph.

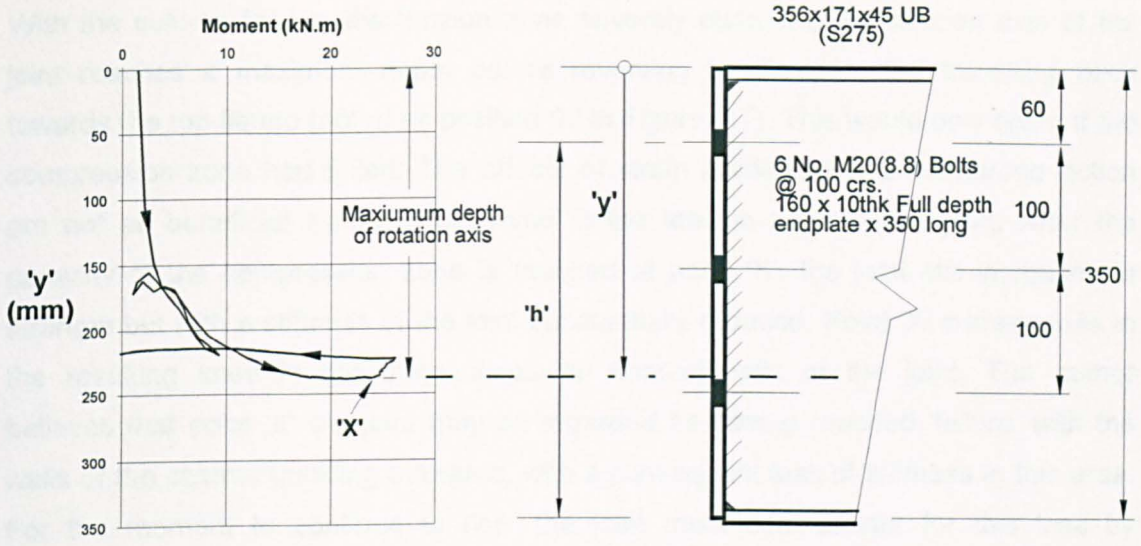

Figure 8.7 Typical movement of the axis of rotation.

When moment is first applied, the joint rotates about an axis which is within the top half of the beam depth. Usually this position is determined by the relative elastic stiffnesses of the compression zone and the tension zone of the joint. Had the beam been welded directly to the column's face, both the stiffness of the compression and tension zones of the joint would be equal and in this case the rotational axis would be approximately at the mid-depth of the beam.

With flowdrill joints the differences of endplate width and bolt cross centres complicates the joint's response by developing different stiffness in these regions. At first the transducers indicate a rotation axis for the joint which is doubtful. The accuracy of the transducers at such low rotations of the joint may be questionable due to the small deflections recorded. Accuracy in the data is improved as the rotations increase towards the end of the joint test.

As moment is gradually applied to the joint, the column face at the top two bolt rows begins to yield. The next row of bolts then begin to increase in load until eventually these yield. The consequence is that the axis of rotation migrates down the beam depth as the process continues. During this stage the load carried by the top bolts is progressively increased as the face of the column deforms and thus permits greater forces to be sustained by virtue of membrane action. The continual migration of the axis position relies on the compression zone providing enough strength and stiffness to accommodate the bolt forces and provide an adequate reaction. The resistance of the compression zone is obviously aided by the width of the endplate reducing the column face from bending in this area.

With the column face in the tension zone severely distorted, the rotation axis of the joint reaches a maximum depth before reversing in direction and travelling back towards the top flange (noted as position 'X' in Figure 8.7). This would only occur if the compression zone had failed. The effects of strain hardening and membrane action are not as beneficial as those observed in the tension zone of the joint. After the capacity of the compression zone is reached at point 'X', the joint still increases in strength but with a stiffness of the joint substantially reduced. Point 'X' corresponds to the resulting knee in the moment-rotation characteristic of the joint. The author believes that point 'X' the joint may be regarded as having reached 'failure' with the walls of the column buckling outwards, with a consequent loss of stiffness in this area. For the moment to continue to rise, the joint must compensate for this loss by increasing the effective depth of the compression zone, hence the reversal in the travel of the joint's axis of rotation. The compression zone therefore has a controlling influence on the joint performance. During testing there were no LVDT's positioned to monitor the outward deformation of the side walls and it cannot be confirmed that the resulting reversal of the travel of the rotational axis corresponded to the column wall buckling.

By calculating the maximum rotation axis for each of the joints, broad guidance can be given concerning the extent to which the axis of rotation travels within the depth of beam section. Table 8.2 presents the results from all the available transducers which could be relied upon, for both the unfilled and concrete filled column sections. The dimension 'h' is the distance from the top bolt row to the edge of the endplate, with 'd' indicating the depth of travel. In this way the dimension 'h' is related to the bolt group which governs the joint performance.

As observed in Table 8.2 the axis of rotation differs between the concrete filled and unfilled joints. This would be as expected as the compression zone in the concrete filled section were unyielding and these specimens did not show any signs of the reversal of movement of the joint's axis of rotation. The results indicate that an average depth to rotation was 0.69 and 0.87 for the unfilled and concrete filled sections which can be rounded to **0.7** and **0.9** respectively. It must be realised that the rotation axis depends on a number of parameters but this simplification may be applicable to design. Errors may well be incurred for unfilled column sections where the endplate width is significantly less than that of the column face, reducing the compression zones stiffness and resulting in an earlier failure before the 0.7 limit depth is reached. There may even be cases were bolt pull out occurs prior to the attainment of the final depth of

rotational axis assumed for design. Notwithstanding these difficulties, an adequate rotation axis location has been defined which provides an indication to the extent to which the compression and tension zones extend. However, a separate check should be performed for bolt pull out and further investigations required with endplates of variable width to determine the endplate width to column face width ratio for which the simplification is appropriate.

Test No.	h (mm)	d (mm)	Ratio d / h	Type of endplate
Unfilled SHS joints				
2	390	264	0.67	FE
4	290	213	0.73	FE
5	290	210	0.72	FE
6	290	246	0.85	FE
7	290	196	0.68	FE
11	290	189	0.65	FE
12	290	178	0.61	FE
13	290	176	0.61	FE
18	290	203	0.70	FE
19	430	296	0.69	EE
20	430	293	0.68	EE
21	430	295	0.69	EE
23	430	306	0.71	EE
25	320	226	0.71	FE
26	320	233	0.73	FE
32b	430	273	0.63	EE
		Average	**0.69**	
Concrete filled SHS joints				
14	390	357	0.92	FE
15	290	262	0.90	FE
16	290	257	0.89	FE
17	190	167	0.88	FE
22	430	352	0.82	EE
24	430	336	0.78	EE
		Average	**0.87**	

Note: FE- Flush endplate. EE- Extended endplate

Table 8.2 Measured axis of rotation for flowdrill joint tests

8.4.2 Appropriate limits for column face deformation

The second part of the problem in defining rotation limits corresponds to the amount of column face deformation developed at the bolt location. Historically, face deformation limits were imposed at serviceability load levels to avoid excessive wall deformations for joints known to be flexible. A generally accepted criterion is that used by the IIW [66] for truss chord members where the branch member load is limited to that which causes a face deformation corresponding to 1% of the SHS width, regardless of connection type or geometry.

A limit which is based on the SHS width would appear to be unsuitable for use with a bolted endplate connection. This can be explained more clearly by reference to a moment-resisting joint supporting a cantilevered beam. This situation is far more onerous than that encountered in truss connections, as the beam relies on the column face for both stiffness and strength. In this case, any deformation of the column wall would inevitably cause a disproportionate deflection to the tip of the cantilevered beam. The importance of estimating the limits on the column wall deflection cannot be overstated.

Although the face deformation limit was originally proposed for the 'working' load case, the use of deformation limits imposed on column faces has previously been used to determine the ultimate failure of a joint. Such a method has been employed by Yeomans [36], where the serviceability load corresponding to the 1% limit is multiplied by partial safety factors from appropriate codes of practice to find the ultimate capacity of the flowdrill joint.

Other limits imposed on the deformation of the column face have been proposed in areas concentrating on investigating the semi-rigid nature of tubular joints, with either welded open section to tubular column details or joints fabricated from tubes only. Szlendak & Ligocki [12] determined an ultimate failure load for a series of open section beams welded to square hollow sections that corresponded to the maximum rate of change on the moment-rotation characteristic. Another approach defined by Yura et al. [67], was based on the practical deformation limit of ultimate capacity on tubular joints when the strain on the member along its entire length is four times that of the yield strain. The work of Lu et al. [68] has also contributed in this field by conducting both a parametric finite element study and an experimental programme on open section beams welded to hollow section columns. The deformation proposed by Lu

was similar to that of the one percent rule, but a three percent deformation limit of the column face at ultimate limit state was adopted.

The use of methods which are based on the width of the column causes problems for joint details that incorporate different bolt cross-centres as shown in Figure 8.8. Bolts which are detailed close to the wall have been observed to produce a joint detail which has high initial stiffness and moment capacity, but low rotational capacity; the low rotational capacity being a direct result of the lack of deformation of the column face. The opposite occurs where the bolts are positioned nearer the centre of the column face, thereby creating a more flexible connection. A point which may be used to determine the joints ultimate rotation is the rotation which defines the start of the joint's post yield stiffness (K_p). It is obvious that there will be two different identifiable points that define the rotation limit of the joint when the bolt centres are different. A fixed amount of column face deformation based on a percentage value of column width would seem to be inappropriate.

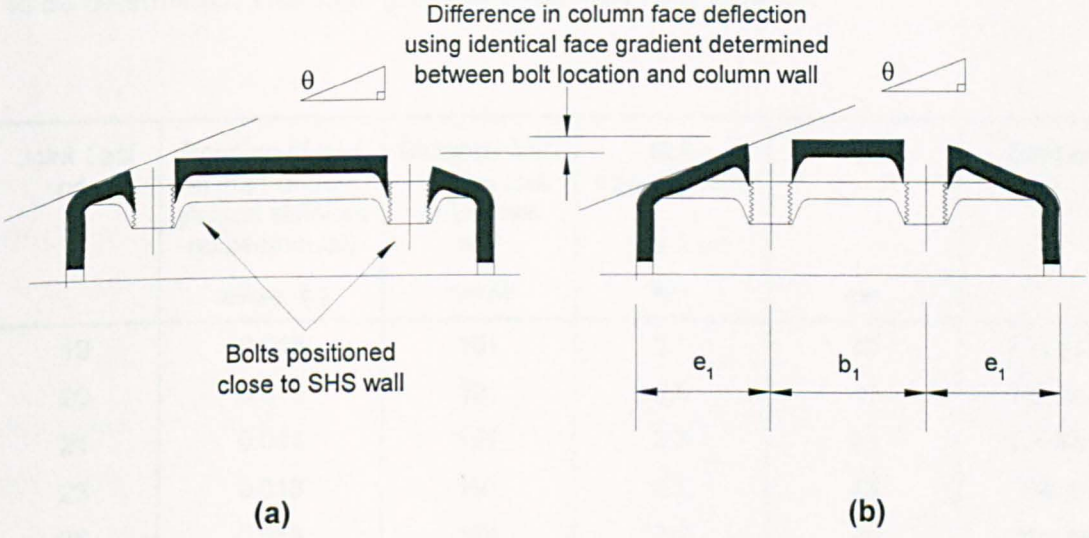

Figure 8.8 Proposed deformation limits of column face

Instead of relying on a fixed level of face deformation, a more flexible approach is required which can allow for different rotation levels based on bolt cross centres. A method is therefore proposed by the author in which the hinge rotation (or gradient) of the column face may best determine the deformation limit of the joint at 'ultimate' limit state (or more correctly, at a rotation of ϕ_d). Hence, the gradient of the column face determined by the column width and the bolt cross-centres. The advantage of constructing the deformation limit around this criteria allows the extent of plasticity

present for the different bolt centres to be at similar levels with hinge rotations in the face being equal.

8.4.3 Determination of ϕ_d and ϕ_{cd} parameters for joint rotation

In the previous section, a method was outlined which limited the SHS face deformation at the ultimate limit state to a gradient developed at the edge of the section. By using a specific gradient and combining it with the axis of rotation of the joint determined in section 8.4.1, thereby allows the rotational capacity (ϕ_d) to be found. Unfortunately, the method explicitly requires a value to be assigned to the edge gradient to represent the deformation limit of the column at which post yielded stiffness (K_p) forms a prominent part of the joint's capacity. The problem was tackled by reversing the process and examining the experiment results to identify and assess the joint's rotation at which the post yield stiffness of the joint starts. Using the identified rotation and the distance from the rotational axis to the bolt location, thereby allows the bolt deflection to be determined. The edge gradient could then be calculated.

Joint Test no.	Rotation of joint at start of post yielded stiffness (experimental) radians (ϕ)	Distance from rotation axis to 2nd bolt row mm (v)	Bolt displacement ($=\phi$ x v) mm	'e_1' mm	Gradient
19	0.016	191	3.1	40	1 in 12.9
20	0.013	191	2.6	40	1 in 15.4
21	0.014	191	2.7	40	1 in 14.8
23	0.013	191	2.5	40	1 in 16
25	0.018	124	2.2	40	1 in 18
26	0.019	124	2.4	40	1 in 16.7
M/30/67	0.0095	173	1.6	25	1 in 15.6
M/30/50	0.015	173	2.6	37.5	1 in 14.4
M/19/67	0.009	173	1.6	25	1 in 15.6
M/19/50	0.016	173	2.8	37.5	1 in 13.4
M/12/67	0.0095	173	1.6	25	1 in 15.6
M/12/50	0.0145	173	2.5	37.5	1 in 15
				Average	**1 in 15**

Table 8.3 Determination of column face gradient at rotation ϕ_d.

Using the method described, the bolt displacements are presented in Table 8.3. The distance used in the calculation was measured from the axis of rotation to the 2nd bolt row, rather than the top bolt row. The reason for this is that when the point is identified on the moment-rotation characteristic of the joint, the assumption is that the yield line model has fully developed and this is only valid when the column face has yielded. If the distance to the top row of bolts had been used then the 2nd row of bolts would not have yielded sufficiently to experience either the membrane or strain hardening effects. This corresponds to only the top two bolts developing a yield line model. Ideally, better results would have been obtained from a series of tests involving a bolt group of only two in the tension zone.

Nevertheless, the results shown in Table 8.3 are consistent giving an average gradient of **1 in 15**, with little scatter before the effects of membrane and strain hardening become dominant that develops into the joints post yield stiffness. It is interesting to note that greater consistency is achieved in the Swinden joint tests than those carried out by the author. This is no way a reflection on the test procedure but more a result of the endplate detail as only two rows of bolts were incorporated in the tension zone compared to the three rows of bolts used by the author. The third row of bolts contributed to the moment-rotation characteristic at relatively high joint rotation which made the identification of the start of the post yield stiffness more difficult as these bolts would not have yielded, even though the joint had sustained a substantial overall rotation.

A similar procedure was also adopted to determine the final rotation capacity of the joint (ϕ_{cd}), identified in the joint tests where the thread stripped in the Flowdrill hole. Table 8.4 presents the results of all the tests that encountered this type of joint failure. The gradient at the edge of the column indicates a value between 1 in 1.8 and 1 in 3.0. Because this is such a dangerous type of failure it is recommended the lowest gradient of **1 in 3** be adopted as the limit when determining the final rotation capacity of the joint. Note that in these calculations the bolt displacement, and hence the face deformation, was based on the distance between the 'top' bolt and the joint's rotation axis, assuming the endplate to be 'rigid'.

Test no.	Experimental rotation at bolt pull out radians (ϕ)	Distance from rotation axis to top bolt mm (w)	Bolt displacement ($=\phi$ x w) mm	'e_1' mm	Gradient
19	0.058	301	17.5	40	1 in 2.3
20	0.056	301	16.9	40	1 in 2.4
22	0.043	387	16.6	40	1 in 2.4
23	0.050	301	15.1	40	1 in 2.6
24	0.035	387	13.5	40	1 in 3.0
M/30/67	0.037	273	10.1	25	1 in 2.5
M/30/50	0.064	273	17.5	37.5	1 in 2.1
M/19/67	0.039	273	10.6	25	1 in 2.4
M/19/50	0.076	273	20.7	37.5	1 in 1.8
M/12/67	0.030	273	8.2	25	1 in 3.0
M/12/50	0.053	273	14.5	37.5	1 in 2.6

Table 8.4 Determination of final column face gradient for bolt pull out

Using the above gradients and the assumed axis of rotation for the joint allows both the design rotation (ϕ_d) and the rotation capacity (ϕ_{cd}) of the joint to determined. Table 8.5 presents the rotation limits calculated from the proposed method. The experimental moment for each of the joint tests corresponding to the defined rotation is also noted in Table 8.5. The moment identified for each of the joints will be used later in the chapter and is compared directly against the analytical values derived from the joint model.

Joint test no.	Predicted bolt displacement at yield (1 to 15) (mm)	Calculated rotation limit ϕ_d (milli-radians)	Experimental moment capacity $M_{j,expt}$ (kN.m)	Rotation capacity of joint ϕ_{cd} (milli-radians)	Max. moment attained by joint test (kN.m)
2	3.3	19.3	62.4	61	82
4	3.3	32.4	40.9	82	41
5	4.0	38.8	44	99	56
6	2.7	25.9	48.4	66	61
7	3.3	32.4	27.4	82	34
8	3.3	32.4	109.3	82	123
10	3.3	25.1	20.3	125	26
11	3.3	32.4	26.3	82	34
12	3.3	32.4	24.3	82	26
13	3.3	32.4	25	82	30
14	3.1	12.2	86.4	44	124
15	3.1	19.0	56.9	58	73
16	3.1	19.4	43.9	60	58
17	3.1	17.9	28.4	89	36
18	3.3	32.4	44	82	50
19	2.7	14.0	123.7	44	162
20	2.7	14.0	156	44	208
21	2.7	14.0	230.7	44	283
22	2.3	8.4	184.1	30	288
23	2.7	14.0	200.8	44	253
24	2.3	8.4	236	30	316
25	2.7	21.5	105.5	60	138
26	2.7	21.5	78.3	60	104
m/30/67	1.7	9.6	49	31	73
m/30/50	2.5	14.5	34.5	46	67
m/19/67	1.7	9.6	106	31	135
m/19/50	2.5	14.5	81	46	127
m/12/67	1.7	9.6	204	31	235
m/12/50	2.5	14.5	167	46	215

Table 8.5 Experimental joint test moment capacity for future comparisons

8.5 Ultimate design moment capacity of the joint ($M_{j,Rd}$)

The prediction of the ultimate moment capacity of the joint is one of the main parameters used in the development of all joint models and more importantly in connection design. The capacity of a joint is determined from the bolt force distribution shown in Figure 8.9(a). The bolt forces are multiplied by their appropriate leverarm distance, measured from the centre of compression (F_c), the magnitude of compression applied being equal and opposite to the summation of all the bolt forces generated in the joint ($F_{t,n}$).

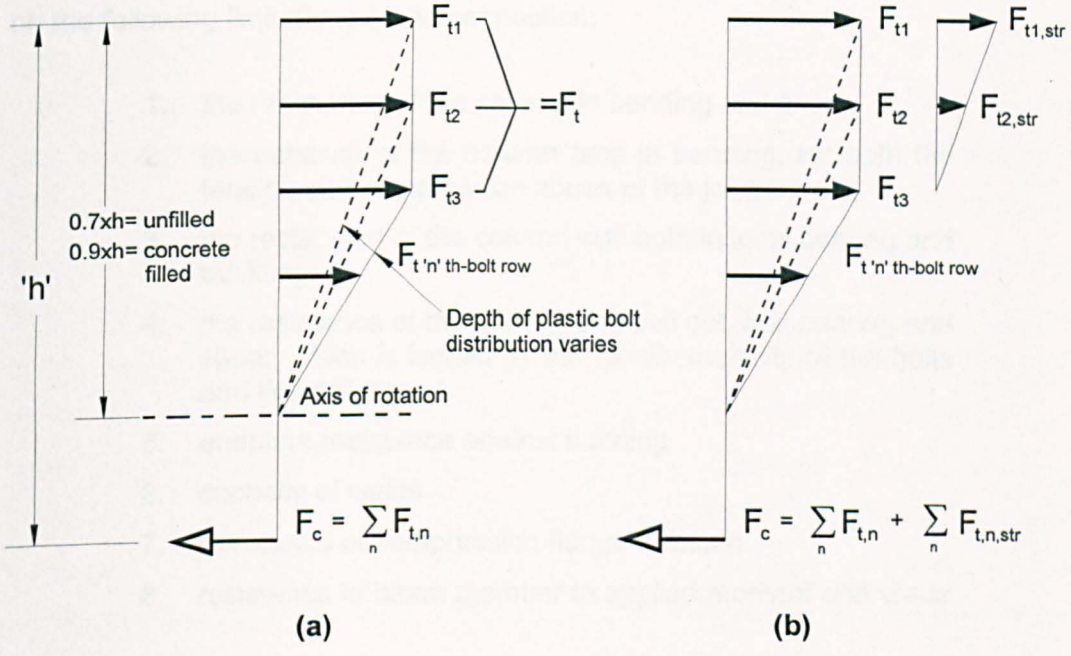

Figure 8.9 Bolt distribution used to determine ultimate moment capacity

Figure 8.9(a) assumes a plastic distribution of bolt forces which results in equal bolt loads, similar to those used in traditional open section major axis joint design method. A linear variation of bolt force distribution follows from the end of the plastic distribution down to the axis of rotation, separating the tension and compression zones of the joint. The figure has been drawn to illustrate the case of up to three rows of bolts adopting a plastic distribution of load (the total force of this distribution indicated as F_t in the following capacity equations). It is worth noting that the plastic distribution can be less than or greater than the three bolt rows shown, so long as the bolt pull out criteria of a 1 to 3 edge gradient on the column face is not violated at the top row of bolts. This type of situation may well exist for endplate details that have a bolt location at mid-depth of the section. If the endplate is relatively deep and contains significantly more

bolts located in the tension zone, then the joint benefits from a plastic distribution of bolt forces. For the joint tests used to compare the model prediction, a maximum plastic distribution of only two bolt rows was assumed in all cases.

The second bolt force distribution shown in Figure 8.9(b) is similar to that of the first bolt force distribution but has been modified to allow for both the effects of strain hardening and membrane action indicated by the additional linear variation of bolt forces superimposed on to the top bolt row ($F_{tn,str}$). The use of this bolt distribution will be explained in more detail later in the chapter.

The calculation of the maximum bolt forces developed in the joint will therefore depend on the following limitations of the connection;

1. the resistance of the column in bending and shear.
2. the capacity of the column face in bending, for both the tension and compression zones of the joint.
3. the resistance of the column wall both in local bearing and buckling
4. the resistance of the bolts to bolt pull out, bolt bearing and shear, which is limited by the tensile capacity of the bolts and flowdrill thread
5. endplate resistance against bending
6. capacity of welds
7. resistance of compression flange of beam
8. resistance of beam member to applied moment and shear

To simplify the analysis, all checks which would be required to the endplate and beam (items numbered 5 to 8) are assumed to be of adequate strength and ductility for the main failure criteria to be that determined by either the column section or bolts. This assumption is valid for all tests conducted as all the actual test failures were found to be attributed to these two main areas of joint behaviour. Each of the remaining items described above will be examined in the following sections of this chapter to enable the moment capacity of the joint to be calculated.

8.5.1 Brief review of yield line models and assumptions of plastic design

The majority of strength predictions on joints have been derived from the use of limit analysis which is more commonly referred to as yield line models. The theory according to Prager [69] states that an upper bound solution exists when;

1. the system obeys the criteria of plastic flow and the boundary conditions of movement
2. the condition of incompressibility is satisfied
3. the work done by external loads must equal the internal work dissipated by the yield lines of the model.

Use of yield line models for connections has been mainly restricted to joints comprising tubular sections and the development of open section beam to column connections where yield line patterns develop in the column and endplate flanges. Design guidance has usually been provided by both the IIW and CIDECT for the tubular joints and EC3[47] for the open section joints. The yield line models used have normally adopted a pattern of straight yield lines. These models have also been used in situations where open section beams have either been welded directly to the face of an SHS or to the minor axis of an open section column [70]. Experimental verification of this type of analysis has led to the connection being simplified to a series of branch plates welded to the column section; the assumption being that the branch plate would represent the properties of the beam flange. The patterns proposed from this work included the circular fan pattern of Figure 8.10(a) and the conventional straight yield line pattern of Figure 8.10(b).

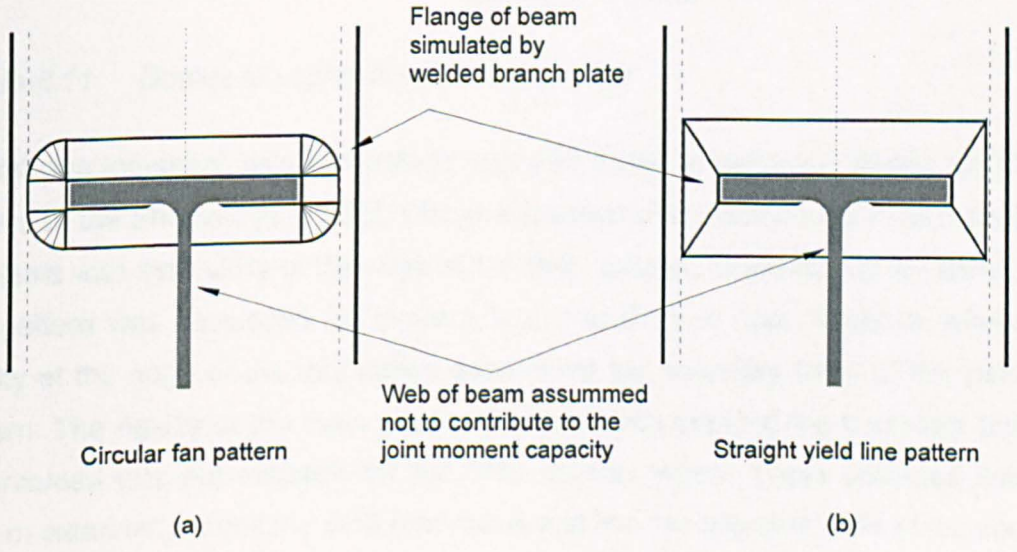

Figure 8.10 Typical yield line patterns

Similar straight yield line models have been adapted to the case of bolted endplate connection tests conducted by Kato [23] bolted to SHS columns, and Kim's [71] one sided bolted flush endplates to the minor axis open section columns. In these cases the centre of the hole provided the intersection for the yield lines, with the inside root radius of the column providing the outer boundary. Recent research in this area conducted by Gomes et al. [72] on bolted connections to minor axis columns developed the yield line model further by using a log spiral fan pattern similar to that illustrated in Figure 8.11. In this case each bolt holes have been represented by an equivalent rectangle, identical to the approach used with the welded flange detail above. The model has also been selected by Vandegans [73] to determine the limit load for endplates connected to concrete filled SHS columns through the use of welded threaded studs. Initial calculations with experimental results provided reasonable accuracy using this model.

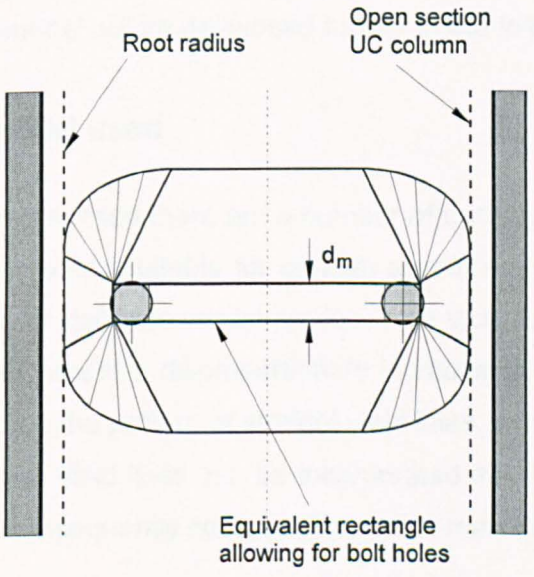

Figure 8.11 Gomes log-spiral fan yield line pattern

At first, the log-spiral yield line pattern was also found to resemble closely the failure pattern of the Sheffield joint tests. Closer inspection of the developed pattern revealed problems with the rigidity of the edge of the SHS column. Originally the log-spiral yield line pattern was developed for minor axis connections of open sections, where the rigidity at the edge of the root radius determined the boundary limits of the yield line pattern. The rigidity of the open section flanges which enabled the boundary limits to be enforced was not available for the SHS column, where it was observed that the pattern extended around the SHS root radius and into the adjacent walls of the section. This immediately introduces the possibility of a significant error into the use of the

model. There are also some doubts raised by Wood[74], that log spiral fans are not valid for the square yield criterion used in the model, unless a more appropriate criterion was developed. Due to the complex nature of the equation produced from the model it would also be difficult to implement a reduction to the yield line hinge capacity due to the presence of axial load. The same objection can also be applied to circular fans. The use of log-spiral or circular fans is therefore considered to be inappropriate for design and effort is concentrated on the simpler straight yield line model.

So far, all the yield line patterns have related to local mechanisms incorporating either one bolt row or a welded flange. All of the Sheffield joint tests have incorporated multiple bolt rows in which traditional joint design usually assumes that the top two bolt rows provide equal bolt loads. To account for the extra row of bolts, Yeomans [36] has extended the existing model used for the truss joint to cover the adjacent bolt rows by assuming that the top four bolts pull out as a rigid body, similar to that of the SHS branch of a truss. This model will be developed further in the following sections.

8.6 Yield line model used

In each yield line model proposed there are a number of underlying assumptions which make the use of these models suitable for only an approximate solution to the joint's capacity. Each variation of yield line model produces an increase in accuracy over the previous model, but may create a disproportionate increase in complexity. The model used is therefore based on the pattern of straight yield lines, where the presence of the column's axial load on the yield lines can be incorporated into the design. The results of using this model are subsequently compared to actual test results.

Figure 8.12 shows the yield line pattern assumed in both the tension and compression zones of the column face to determine the joint's capacity. The two yield patterns in this instance are shown separately, with the compression yield line being defined by the axis of rotation of the joint determined previously from section 8.4.1.

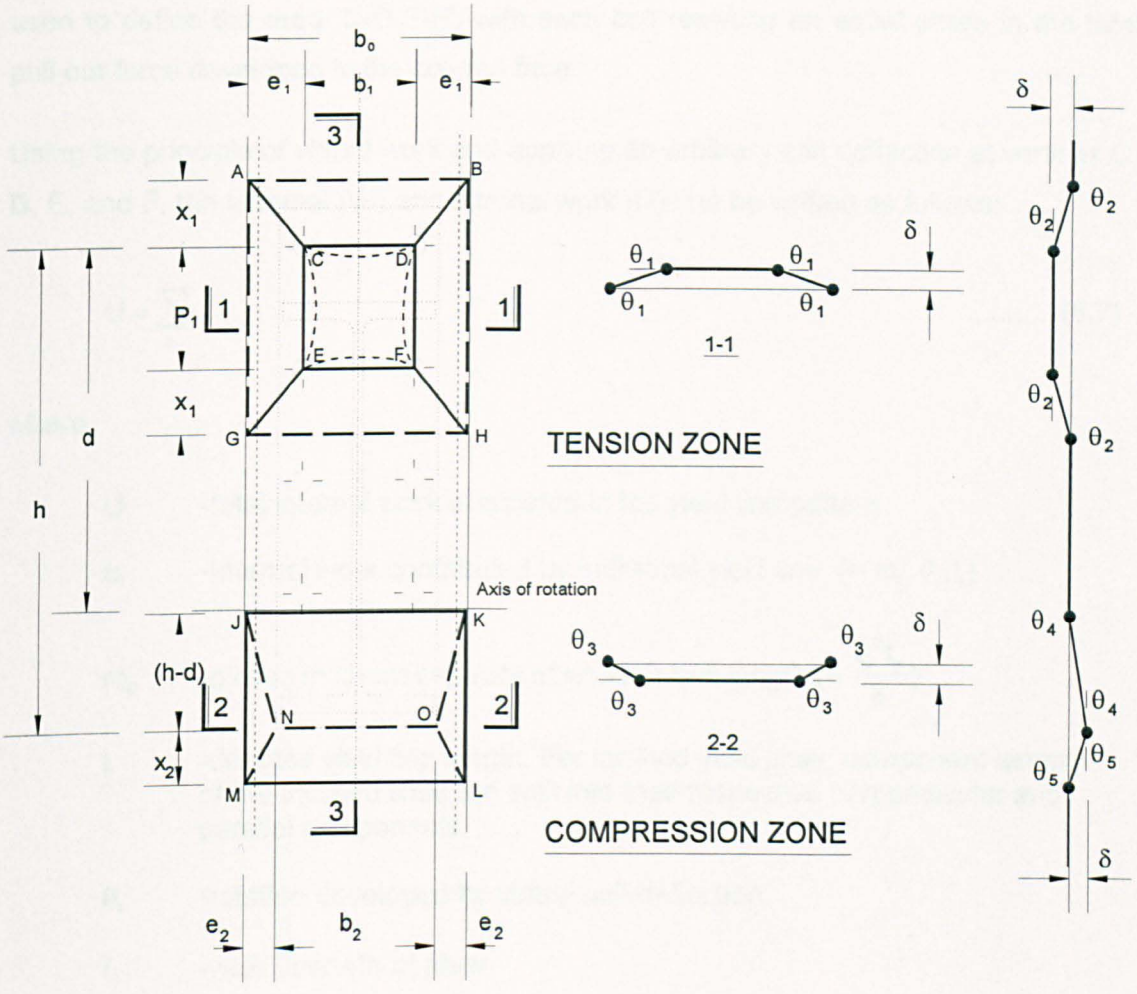

Figure 8.12 Yield line model assumed to develop in column face

8.6.1 Resistance of column tension zone

For the tension zone of the unfilled SHS columns the yield lines emanate from the centre of the bolt hole and extend over the full breadth of the column rather than the start of the corner radius of the SHS. The reason for the full width of the section being used is the flexibility shown in the tests at the edge of the column (along the length of 'A' to 'G') which provides inadequate stiffness to justify the assumption of a rigid support. It was also found that the yield lines 'CD', 'DF', 'FE', and 'EC' were concave (shown dotted in Figure 8.12 above) through the lack of stiffness generated at the bolt. This differs from the normal all round welded tubular branch connection which defines and supports the formation of straight yield lines. The configuration of the straight yield line pattern will remain similar to the pattern shown regardless of the number of bolts

used to define the area 'C-D-E-F', with each bolt resisting an equal share in the total pull out force developed in the column face.

Using the principle of virtual work and applying an arbitrary unit deflection at vertices C, D, E, and F, the external (W) and internal work (U) can be written as follows;

$$U = \sum_{i} u_i \qquad \text{.....(8.7)}$$

where

U -total internal work dissipated in the yield line pattern

u_i -Internal work contributed by individual yield line $(= m_p.\theta_i.l_i)$

m_p -plastic moment capacity of wall per unit length $(= \frac{t_0^2 f_y}{4})$

l_i -denotes yield line length. For inclined yield lines, component length of the inclined lines are split into their respective perpendicular and parallel components.

θ_i -rotation developed by virtual unit deflection

f_y -yield strength of steel

The external work developed at the bolt group location

$$W = F_t.\delta \qquad \text{.....(8.8)}$$

where

W -total external work developed by the bolt load moving an arbitrary unit deflection

F_t -total force produced by bolts from yield line pattern and bolt group assuming plastic distribution of loading

δ -arbitrary unit deflection at bolt position

For the internal work of the yield line model there are two hinge moment capacities that depend on the orientation of the yield line. The moment capacity for the component of yield lines parallel to the longitudinal axis ($m_{p\text{-}par}$) is unaffected by the presence of the axial stress and the full plastic moment capacity of the column wall (m_p) is used. A

reduced moment capacity ($m_{p\text{-}per}$) is required in the model analysis for the component yield lines that are perpendicular to the column axis when the column is subjected to longitudinal stress from either axial load or flexural action. From Coates et al [75] the reduced moment capacity in the presence of axial load and bending is given by;

$$m_{p-per} = (1-n^2).m_p \qquad \text{.....(8.9)}$$

where

$$n = \frac{f}{f_y} = \frac{N}{A.f_y} + \frac{M}{S.f_y} \qquad \text{.....(8.10)}$$

in which

f	-stress developed in column face through applied loading
N	-axial load applied to the column at ultimate limit state
A	-sectional area of column
M	-moment applied to column at the joint
S	-plastic sectional modulus of tubular column

The virtual rotations for the model as shown in Figure 8.12 are as follows;

$$\theta_1 = \frac{\delta}{e_1}, \qquad \theta_2 = \frac{\delta}{x_1}$$

The internal work (energy) of the parallel yield lines (including the components for the inclined yield lines) can be expressed as

$$U_{par} = 2\left[2.m_{p-par}.\theta_1.l_{ac} + m_{p-par}.\theta_1.l_{ag} + m_{p-par}.\theta_1.l_{ce}\right]$$

$$= \frac{4.m_{p-par}.\delta}{e_1}\left[2.x_1 + P_1\right] \qquad \text{..... (8.11)}$$

Similarly the perpendicular component of internal work is given by

$$U_{per} = \frac{2.m_{p-per}.\delta}{x_1}\left[2.e_1 + b_0 + b_1\right] \qquad \text{.....(8.12)}$$

The total work developed by the yield lines being the addition of (8.11) and (8.12). To maximise 'x_1', when $\frac{\partial(U_{par}+U_{per})}{\partial x}=0$.

$$\frac{\partial(U_{par}+U_{per})}{\partial x}=\delta\left[\frac{8.m_{p-par}}{e_1}-\frac{4.m_{p-per}.e_1}{x_1^{\,2}}-\frac{2.m_{p-per}.b_0}{x_1^{\,2}}-\frac{2.m_{p-per}.b_1}{x_1^{\,2}}\right]=0$$

Noting that, $2.e_1+b_1=b_0$, the solution when 'x_1' is a minimum value

$$x_1=\frac{1}{2}\sqrt{\frac{m_{p-per}}{m_{p-par}}(e_1.2.b_0)} \qquad \text{..... (8.13)}$$

Equation (8.13) above is a similar expression to the original work of Johanson's 'affinity' theorem which treats the orthotropic properties of a slab by reducing the lengths of the yield lines. In the above expression the orthotropic nature is explicitly incorporated by a reduction of moment capacity. The expression for 'x_1' can now be back substituted into eq (8.11) and (8.12), noting that with total internal work equals external work, δ can be eliminated to determine the bolt load for the tensile yield line model as;

$$F_t=4.m_p\left[\frac{2.x+P_1}{e_1}+\frac{(1-n^2)b_0}{x_1}\right] \qquad \text{.....(8.14)}$$

The above equation is almost identical to those of the IIW [66] and CIDECT [76] expressions, dealing with tubular branch member connected to an SHS chord. The difference is in the treatment of axial load in which the expression is now incorporated more directly, whereas both IIW and CIDECT adopt a global reduction function derived from experimental data and dependent upon the geometry of the joint.

8.6.2 Resistance of column compression zone

There are numerous ways in which the compression zone of a joint may fail. The mode of failure which occurs is primarily dependant upon the relative widths of the endplate and column. Plates which are at least as wide as the column tend to cause failure of the sidewalls whereas narrow endplates will tend to push in the front face of the tube. Both of these failure modes were evident in the test programme.

Previous research into the behaviour of the compression zone has involved either experimental tests conducted on branch plates or full scale tests on truss joint details[77]. The most recent contribution has been through the work of Lu & Wardenier [14] who examined, both experimentally and numerically, the effect of axially loaded branch plates welded to the SHS. This research has covered both uniplanar and multiplanar connections. Using the results of a parametric study based on numerical models, a series of equations were formulated using regression analysis to predict the capacity. The results provided reasonable correlation to the experimental tests when the flexural action of the face determined the joint's capacity. However, the accuracy was reduced and erratic when the width of the branch plate approached that of the column's width ($\beta \geq 0.85$).

To accommodate the situations where the endplate width approaches that of the column, a simple interactive approach is used to cover cases between the column face failing in flexure and the column web crippling. This assumes that the endplate and beam are adequate to develop the full capacity of the SHS column. According to the procedures adopted by CIDECT [76], a joint which has a β ratio value less than 0.85, allows the yield line analysis to be acceptable for design. When the width of the branch chord (or in this case the endplate) is equal to the width of the column (β =1), then the capacity is based on the failure of either buckling or bearing of the web. At β values in-between these limits a linear interpolation of the capacity of the column in the compression zone should be assumed. The following development of the model is now split into these two criteria.

Capacity of face when $\beta \leq 0.85$ (narrow endplates)

Using the same analytical procedure for deriving the tension zone model of section 8.6.1, but adopting the compression zone model shown in Figure 8.13, an expression can be written where the width of the endplate in the compression zone results in $\beta \leq 0.85$ as eq(8.15). No allowance has been made for the interaction between the compression and tension yield line models.

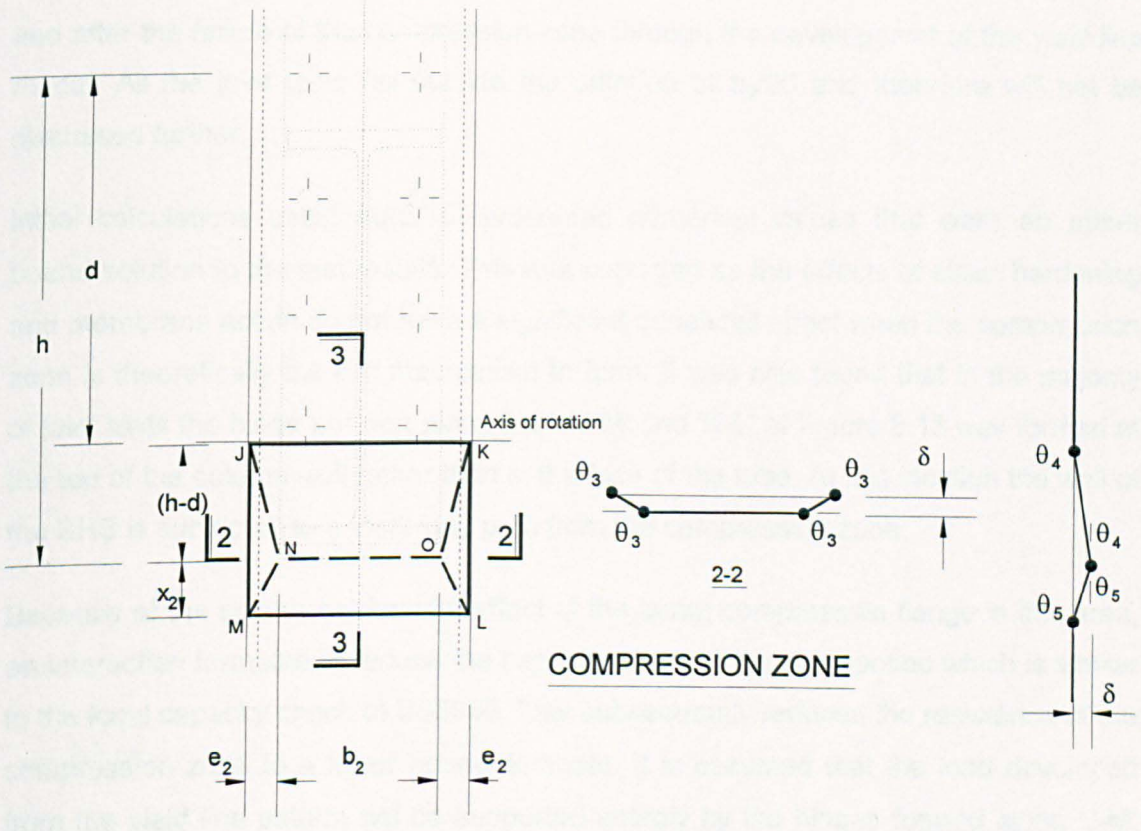

Figure 8.13 Compression zone yield line model for joint

$$F_c = m_p\left[\frac{4}{e_2}(h-d+x_2)+(1-n^2)2.b_0\left(\frac{1}{x_2}+\frac{1}{h-d}\right)\right] \qquad \text{.....(8.15)}$$

where

$$x_2 = \frac{1}{2}\sqrt{\frac{m_{p-per}}{m_{p-par}}(e_2.2.b_0)} \qquad \text{.....(8.16)}$$

In the pattern proposed in Figure 8.13 the yield line 'NJ' is extended to the rotation axis of the joint, unlike the tension zone model. This is expected because of the physical interference from the endplate which influences the yield line pattern to develop to point 'J'. The expression does not account for any effect of punching shear[70] which, as stated by Gomes et al. [72], can be neglected for cases where the tube thickness is greater than $b_0/20$. In these instances the flexural action will dominate failure. In the majority of tests conducted there were some visible signs of the endplate indenting into the face of the column, although this probably occurred after the face had deformed, and after the failure of the compression zone through the development of the yield line model. All the joint tests fall outside the criterion of $b_0/20$ and therefore will not be discussed further.

Initial calculations using eq(8.15) presented numerical values that were an upper bound solution to the test results. This was expected as the effects of strain hardening and membrane action do not have a significant beneficial effect when the compression zone is theoretically the last mechanism to form. It was also found that in the majority of joint tests the hinge position along lines 'J-M' and 'K-L' of Figure 8.13 was formed at the top of the column wall rather than in the face of the tube. At this location the wall of the SHS is subjected to a local load path from the compression zone.

Because of the severe detrimental effect of the beam compression flange in this area, an interaction formulae to reduce the capacity of the hinge is proposed which is similar to the local capacity check of BS5950. This subsequently reduces the resistance of the compression zone to a lower bound estimate. It is assumed that the load developed from the yield line pattern will be supported entirely by the hinges formed along 'J-M' and 'K-L'. A reduction of hinge capacity will only affect these two hinge lines of the model. The assumption of allocating all the load to the outside hinge lines is a simplification of the real distribution of load. The simplified interaction formula can be written as follows:

$$\frac{F_c}{A_e.f_y} + \frac{m_r}{m_{el}} \leq 1.0 \qquad \text{.....(8.17)}$$

where

A_e, -effective area of hinge length (distance J to L of column wall)

m_{el}, -elastic moment capacity of hinge (conservative assumption)

m_r, -reduced moment capacity available for yield line analysis

Rearranging eq(8.17),

$$m_r = \left(\frac{f_y.t_0^2}{6}\right)\left(1-\frac{F_c}{2.A_e.f_y}\right) \qquad \text{.....(8.18)}$$

Similarly expression (8.18) for the reduced moment capacity for hinges 'JM' and 'KL', can be substituted into eq(8.15) giving:

$$F_c = m_r\left[\frac{2(h-d+x_2)}{e_2}\right]+m_p\left[\frac{2(h-d+x_2)}{e_2}+(1-n^2)2.b_0\left(\frac{1}{x_2}+\frac{1}{h-d}\right)\right] \qquad \text{.....(8.19)}$$

One of the disadvantages of the final expression is the iterative approach required for its solution. This treatment of reduced moment capacity to the hinges of the SHS wall is not dissimilar to that proposed by Szlendak [12] . Here a complex expression was developed to incorporate the effect of membrane forces in the model, which involved a global mechanism of an open section beam welded to an SHS column. A similar treatment of the compression zone could have been used to include the effect of membrane stress, but the complexity of the geometry would have resulted in serious errors. The advantage of the method proposed above is that it is simpler than Szlendak's method, even if the interactive equation is less convenient, its implementation will result in a safer, lower bound solution as used later on in the final predictions of joint capacity.

Capacity of face when $\beta = 1$ (wide endplates)

In cases where $\beta = 1$ i.e. the endplate is the same width as the column, the capacity of the compression zone is based on the bearing and buckling capacity of the SHS wall. To calculate the bearing capacity, traditional analysis has usually assumed the distribution of stress to be represented by a plastic effective width approach. An assumption is made that the compression flange supplies all the compressive force of the connection. The force is then transferred via a 1 to 1 dispersion through the endplate to the face of the SHS. A further 1 to 2.5 dispersion through the thickness of the tube wall represents the effective bearing length. This is represented in Figure 8.14(a) and is typical of the method used in BS5950 [78].

A different method was required to accommodate the Swinden joint tests. The difficulty encountered in these tests was that the endplate extended past the compression flange of the beam. The 30mm thick endplate also had high flexural rigidity, which

effectively nullified the assumption regarding the centre of the compression zone. Had the stiff bearing length been calculated using a procedure similar to that in BS5950, the effect of the load dispersion through the 30mm endplate would have produced on plan a bearing length extending into the tension zone of the joint. A more appropriate bearing length was obviously required for these tests.

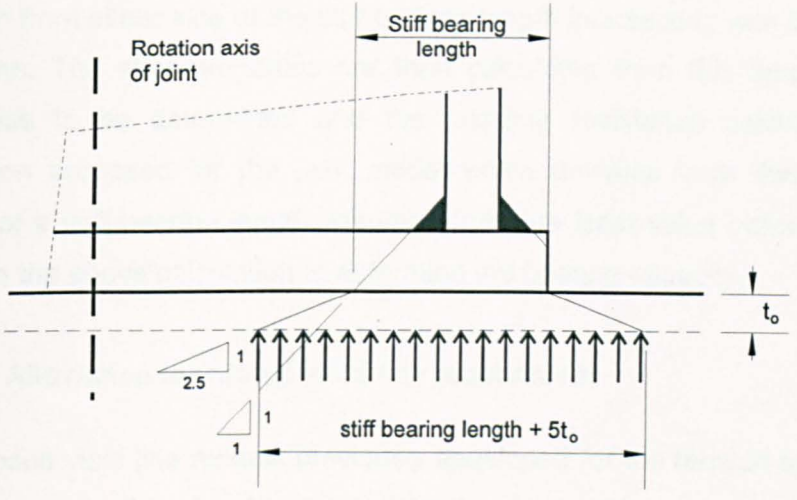

(a)- Normal bearing length used

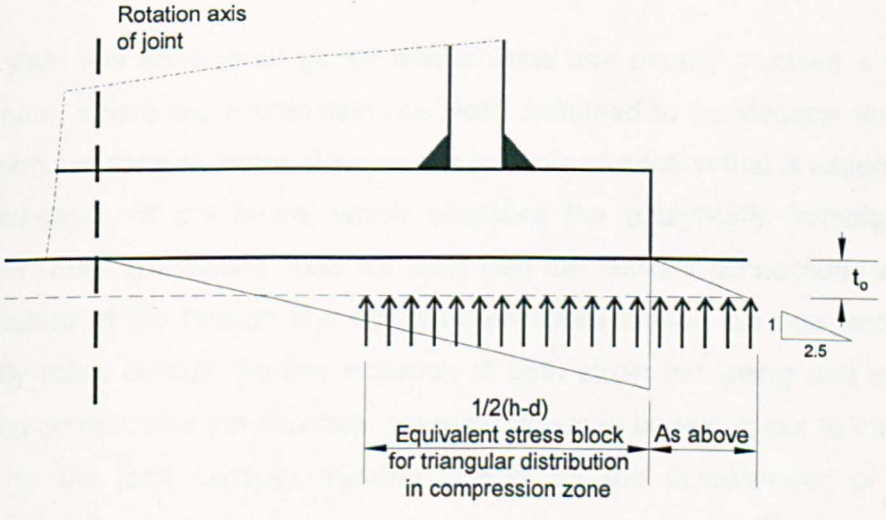

(b)- Modified bearing length

Figure 8.14 Stiff bearing lengths adopted for joint tests

As a conservative estimate of the bearing length for the full width endplates and the Swinden flowdrill joints, it is proposed that the values indicated in Figure 8.14(b) be adopted. Here a triangular distribution of load is assumed under the compression zone, extending to the rotational axis of the joint. In addition to this bearing length, the 1 to 2.5 dispersion through the tube thickness is also added at the edge of the

endplate. It is proposed that the smallest effective length of the two methods shown in Figure 8.14(a or b) is used to calculate the final bearing capacity of the section.

The buckling resistance of the SHS wall is calculated by current design practice using BS5950 cl. 4.5.2.1 [78] and capacity tables [79, 80], whereby an effective width of the column wall is assumed to act as a strut. The width of the strut is calculated from a 45 degree dispersion from either side of the stiff bearing length intersecting with the centre line of the column. The strut properties are then calculated from this length allowing the slenderness to be determined and the buckling resistance calculated. The only modification proposed for the joint model which deviates from this method is the adoption of a stiff bearing length assumed from the least value obtained from Figure 8.14, as in the above calculation to determine the bearing capacity.

8.6.3 Allowance for global yield line mechanism

The proposed yield line models previously developed for the tension and compression zones are assumed to develop independently of one another. In some situations the two mechanisms will combine to form a global mechanism that will reduce the predicted joint capacity.

Previous yield line analysis of global mechanisms has usually involved a welded I-section beam, where the mechanism has been assumed to be identical for both the compression and tension zones. This results in a axis of rotation that is assumed to act at the mid-depth of the beam, which simplifies the analytically formulation of a mechanism. Such a situation does not exist with the flowdrill connections where the unequal nature of the tension and compression zones makes the analytical solution significantly more difficult. Further inclusion of both strain hardening and membrane effects also complicates the situation. However, it would be wrong not to make some reduction to the joint capacity allowing directly for the development of a global mechanism forming in the joint.

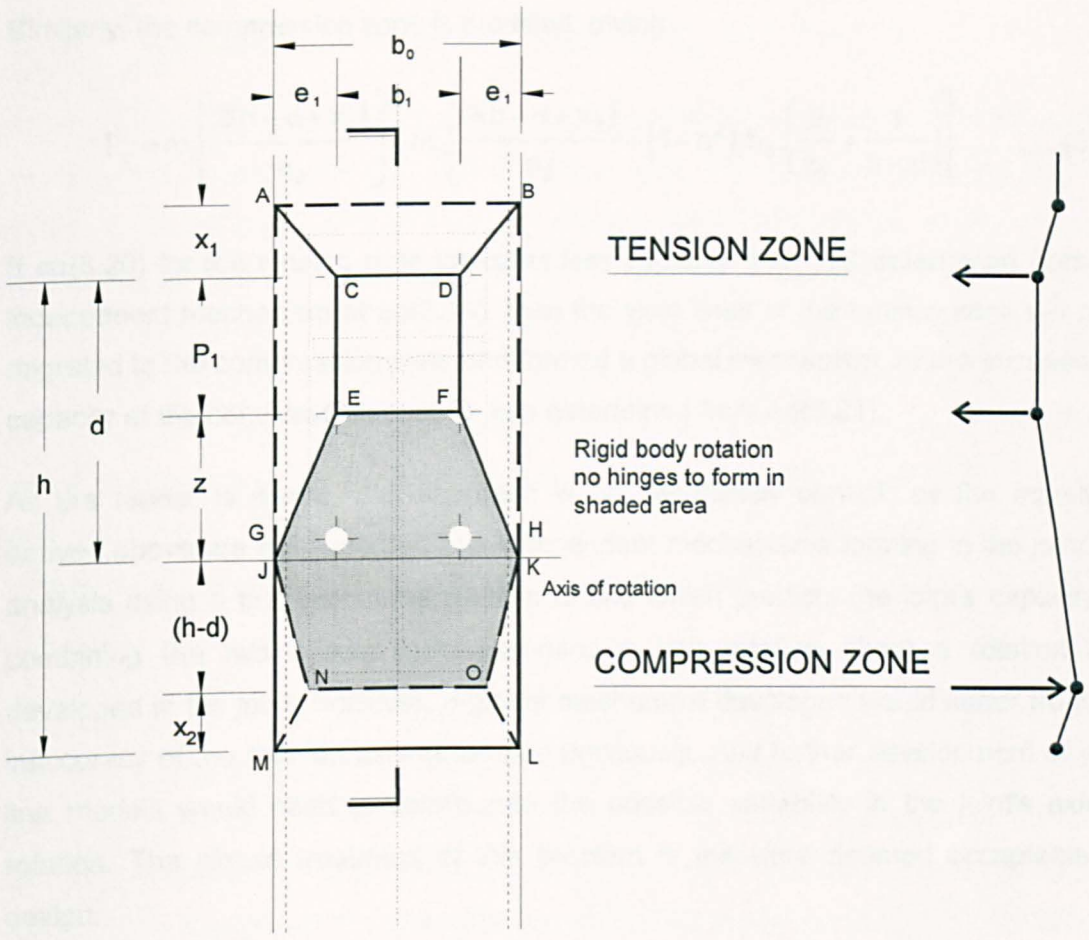

Figure 8.15 Modification to yield line model to account for global mechanism

As a simplification, the yield line pattern developed in the column face for both the tension and compression zones are assumed in the modified pattern of Figure 8.15. In this pattern the yield lines 'J-K' and 'G-H' merge together which allows the shaded portion of the face to rotate as one rigid body. In this way, the hinge lines 'J-K' and 'G-H' do not contribute to the capacity of both the compression and tension zones. Using a similar analytical procedure which developed the previous capacity of the tension and compression zones of eq(8.14) and eq(8.15), the resulting expressions for the global mechanism can be rewritten as;

$$F_t = m_p\left[\frac{4.(x_1+P_1+z)}{e_1}+(1-n^2).b_0.\left(\frac{2}{x_1}+\frac{1}{z}\right)\right] \qquad \text{.....(8.20)}$$

Similarly, the compression zone is modified, giving

$$F_c = m_r\left[\frac{2(h-d+x_2)}{e_2}\right] + m_p\left[\frac{2(h-d+x_2)}{e_2} + (1-n^2).b_0.\left(\frac{2}{x_2}+\frac{1}{h-d}\right)\right] \quad \text{.....(8.21)}$$

If eq(8.20) for the tension zone indicates less capacity than that determined from the independent mechanism of eq(8.14), then the yield lines of the tension zone will have migrated to the compression zone and formed a global mechanism. In this instance the capacity of the compression zone is also determined from eq(8.21).

As the reader is aware, this approach is not technically correct, as the equations derived above are still based on two independent mechanisms forming in the joint. An analysis using a true global mechanism is one which predicts the joint's capacity by combining the two effects from assuming a unit rotation about a rotation axis developed in the joint. However, a global mechanism developed would suffer from the inaccuracy of the rotation axis developed previously. Any further development of yield line models would need to incorporate the possible variability in the joint's axis of rotation. The simple treatment of this problem is therefore deemed acceptable for design.

8.6.4 Modification to include for concrete fill

The addition of concrete fill to the tube has two distinct advantages- it increases both the moment capacity and the stiffness of the joint. The increased joint strength is a direct result of the improved capacity of the compression zone arising from the increased bearing and buckling capacity of the column. In terms of joint capacity, substantial benefits are achieved when equal load is applied from both sides of the tube. Such a situation would exist for a cruciform joint arrangement subjected to equal moments. The capacity of the compression zone is calculated from the bearing capacity of the concrete. With cantilevered joint tests a different failure mode controls, with the out of balance moment generated inducing shear into the column and reducing the capacity of the compression zone compared with that of the cruciform test.

Although the main increase in capacity can be credited to the compression zone, the concrete fill was also noticed to affect the tension zone of the joint. The concrete in this area was able to stiffen the SHS corners to allow the yield lines to develop in the face of the section thereby reducing the amount of flexure. To account for this, the effective width (b_0) in the yield line expressions is modified to b_0-t_0. This modification increases the capacity of the tension zone and gives closer agreement with test results.

There will, however, be some discrepancy in the results as the effect of membrane action in the joint (an unknown and undefined quantity in the analysis) would be considerably increased due to the restraint developed at the corners of the column. It is also quite probable that a cruciform joint will be significantly stiffer than those tested in a cantilever arrangement as the effect of shear in the concrete is reduced.

8.6.5 Comparison of analytical results with actual tests

Using the proposed yield line models described previously, the predicted tension and compression zone capacities are presented in Table 8.6. The tension zone value (F_{t1}) represents the total bolt load in one row. The final values for the compression zone of the joints (F_c) were produced from the various calculations that depend on the ratio of endplate width to column (β_2). The numerous variations in the values for the compression zone indicates the diversity of the joints tested. None of the concrete filled column sections are limited by the compression zone and as such no value is given in the table. It is assumed that the concrete filled joint will provide adequate resistance in this area and not contribute to the failure of the joint; tension zone failure will govern. The table also indicates the use of both global and local mechanisms.

In the majority of the joints, only the top four bolts are assumed to develop into the yield line pattern. However, in the two joints with only a 254UB (test nos. 10 and 17), where only one bolt row is in tension, the value of P_1 in expressions (8.14) and (8.19-8.21) is zero, resulting in a yield line pattern which consists of only one row. In general, the extent to which the yield line pattern develops depends on the face deformation limits imposed in section 8.4.2, where the top and bottom displacement of the bolts are within the gradients determined by the rigid rotation of the endplate.

The predicted ultimate moment capacity for each of the joint tests is shown in Table 8.7. The table has been constructed from the capacities of the compression and tension zones of Table 8.6 and using the bolt distribution shown previously in Figure 8.9(a). Table columns (1 to 4), provide the bolt force and leverarm of the bolts used to determine the capacity of the joint; the leverarm dimension being the value in parenthesis. Column (7) provides the predicted moment capacity ($M_{j,Rd}$) which is compared with the experimental value ($M_{j,expt}$) taken from Table 8.5. The ratio of the two is provided in column (9).

Joint test no.	Calculation of compression zone resistance (F_c)					F_c	F_{t1}
	$\beta_2 \leq 0.85$	$\beta_2 = 0.85$	$\beta_2 = 1.0$		$\beta_2 = 0.9$		
	(kN)	(kN)	Bearing (kN)	Buckling (kN)	(kN)	(kN)	(kN)
2	*194*			301		**194**	**80**
4	*165**			298		**165**	**79**
5	*168**			302		**168**	**70**
6		212*	339	322	249	**249**	**94**
7	*108**			191		**108**	**50**
8	*377**			674		**377**	**187**
10	*168*			302		**168**	**123**
11	*102**			191		**102**	**48**
12	*96*			191		**96**	**43**
13	*103*			191		**103**	**47**
14	*Concrete filled*						**82**
15	*Concrete filled*						**87**
16	*Concrete filled*						**53**
17	*Concrete filled*						**122**
18	*165**			303		**165**	**79**
19		259	482	404	*307*	**307**	**99**
20		363	596	525	*417*	**417**	**141**
21		501	751	676	*559*	**559**	**196**
22	*Concrete filled*						**150**
23		472	774	673	*539*	**539**	**184**
24	*Concrete filled*						**196**
25		332	493	500	*386*	**386**	**146**
26		227	383	372	*275*	**275**	**98**
m/30/67			203	*139*		**139**	**37**
m/30/50			203	*139*		**139**	**28**
m/19/67			326	*265*		**265**	**88**
m/19/50			326	*265*		**265**	**67**
m/12/67			588	*491*		**491**	**217**
m/12/50			588	*491*		**491**	**165**

Note: *, denotes the use of global yield line mechanism

β_2 = ratio of endplate width to column width

Table 8.6 Design resistance of compression and tension zones of joint

Joint test no.	1st bolt row*	2nd bolt row*	3rd bolt row*	4th bolt row*	Total bolt force	F_c	Moment $M_{j,Rd}$	Joint Test Moment $M_{j,expt}$	Ratio $\frac{M_{j,Rd}}{M_{j,expt}}$
	(1)	(2)	(3)	(4)	(5)	(6)	(7)	(8)	(9)
	kN (m)	kN (m)	kN (m)	kN (m)	(kN)	(kN)	(kN.m)	(kN.m)	
2	80 (0.390)	80 (0.290)	34 (0.190)		194	**194**	61	62.4	0.98
4	79 (0.290)	79 (0.190)			158	**165**	38	40.9	0.92
5	70 (0.290)	70 (0.190)			140	**168**	34	44	0.76
6	94 (0.290)	94 (0.190)			189	**249**	45	48.4	0.94
7	50 (0.290)	50 (0.190)			101	**108**	24	27.4	0.88
8	187 (0.290)	187 (0.190)			373	**377**	90	109.3	0.82
10	123 (0.190)				123	**168**	23	20.3	1.15
11	48 (0.290)	48 (0.190)			97	**102**	23	26.3	0.88
12	43 (0.290)	43 (0.190)			86	**96**	21	24.3	0.85
13	47 (0.290)	47 (0.190)			93	**103**	22	25	0.90
14	82 (0.390)	82 (0.290)	49 (0.190)	17	229		66	86.4	0.77
15	87 (0.290)	87 (0.190)	33 (0.090)		208		45	56.9	0.79
16	53 (0.290)	53 (0.190)	20 (0.090)		127		27	43.9	0.62
17	122 (0.190)				122		23	28.4	0.82
18	79 (0.290)	79 (0.190)			157	**165**	38	44	0.86
19	99 (0.430)	99 (0.320)	47 (0.220)		246	**307**	85	123.7	0.69
20	141 (0.430)	141 (0.320)	67 (0.220)		350	**417**	121	156	0.77
21	196 (0.430)	196 (0.320)	93 (0.220)		485	**559**	168	230.7	0.73
22	150 (0.430)	150 (0.320)	96 (0.220)	42	438		139	184.1	0.75
23	184 (0.430)	184 (0.320)	88 (0.220)		455	**539**	157	200.8	0.78
24	196 (0.430)	196 (0.320)	125 (0.220)	54	570		181	236	0.77
25	146 (0.320)	146 (0.220)	28 (0.120)		320	**386**	82	105.5	0.78
26	98 (0.320)	98 (0.220)	19 (0.120)		214	**275**	55	78.3	0.70
							0		
m/30/67	37 (0.390)	37 (0.290)			75	**139**	25	49	0.52
m/30/50	28 (0.390)	28 (0.290)			57	**139**	19	34.5	0.56
m/19/67	88 (0.390	88 (0.290)			176	**265**	60	106	0.57
m/19/50	67 (0.390)	67 (0.290)			134	**265**	46	81	0.56
m/12/67	217 (0.390)	217 (0.290)			433	**491**	147	204	0.72
m/12/50	165 (0.390)	165 (0.290)			330	**491**	112	167	0.67

Note -* values in brackets denote leverarm distances to bolts. Bolt loads un-bracketed

Table 8.7 Predicted moment-resistance capacities for joints

The leverarm associated with the bolt force used in Table 8.7 was determined by taking the fulcrum as the bottom 'edge' of the endplate rather than the more traditional assumption of the centre of the beam's compression flange. One of the reasons for assuming the fulcrum at this position was a direct result of observation in the joint tests in which it was noticed that the edge of the endplate coincided with the central hinge line position of the compression yield line model. The use of this position in the joint model also allowed the Swinden joint tests to be compared more correctly with those of the author. In their tests the relatively stiff endplate which extended beyond the compression flange resulted in the centre of compression acting below the flange. Use of the traditional centre of compression flange in the calculation of the joint's capacity for both test programmes was therefore inappropriate.

The results of Table 8.7 indicate predicted moment capacities all below the actual moment capacity, except for test no. 10, which predicts a slightly higher moment capacity. One of the reasons for the discrepancy in test no. 10 is the error in the assumed position of the rotation axis. The value used was an average obtained from experimental data, for joints predominately containing multiple bolt rows. The offending joint is one which incorporates the 254 UB and has only one bolt row in the tension zone. It is therefore expected that the compression and tension stiffnesses of the joint (which determine the rotation axis) are nearly equal and would result in a rotation axis closer to the mid-depth of the beam rather than the 0.7x'h' value assumed. If a higher rotation axis had been used then the rotation limit used to select the moment from the test data for comparison would be increased, allowing the result to be more favourable.

With the simple joints, where the endplate width is less than the column width, the capacity based on limiting the force in the compression zone appears to estimate the joint capacity reasonably close to that of the actual test values. Where the compression zone is not the failure criterion, then the model predicts a lower moment capacity, ranging from 0.5 to 0.8 of the actual value. The predictions are on the safe side and there is obviously more capacity in the joint which is influenced by the effects of strain hardening and membrane stiffness contributing to the joint's capacity. A modification to the model is therefore required to account for these effects and is discussed in the following sections.

8.6.6 Inclusion of Strain Hardening and Membrane action into the model

It is the usual practice to ignore the benefits of strain hardening and membrane action in routine design, knowing that the benefits often offset the limitations and simplifications assumed in plastic design. In this way, the upper bound limit of plastic design provides a safe solution which is practical and simple. This assumption is true when dealing with plastic frame design, where the rotations developed are relatively small and the sequence of hinge formation can usually develop within a small loading interval. This is not the case in a joint, in which rotations are significantly greater and plasticity can occur at an early stage in the joint's loading and therefore the influence of strain hardening and membrane effects is proportionally greater. Including both effects in the model would thus allow for a better curve fit to the actual response of the joint.

The problem encountered when dealing with these effects is that the interaction between the two occur at different stages of joint loading. Although membrane action is present from the beginning of joint loading, it is only after sufficient deformation of the face has occurred that it becomes pronounced. The effect of strain hardening influences joint response only after the column's face has yielded. The situation is also complicated by the geometry of the joint, where the top bolts may have deformed sufficiently for membrane action to develop, but the bolt row below, exhibiting less deformation, is benefitting from only strain hardening. The conclusion is that it is impossible to accurately separate the two effects from one another.

The simplest solution found to the problem is to use one single increase in joint capacity to allow for both of these effects. This can be accomplished by incorporating a yield line pattern that is superimposed onto the previously developed yield line pattern to provide an additional bolt force of ($F_{t1,str}$). Figure 8.16 shows the proposed pattern developed for the top bolt row.

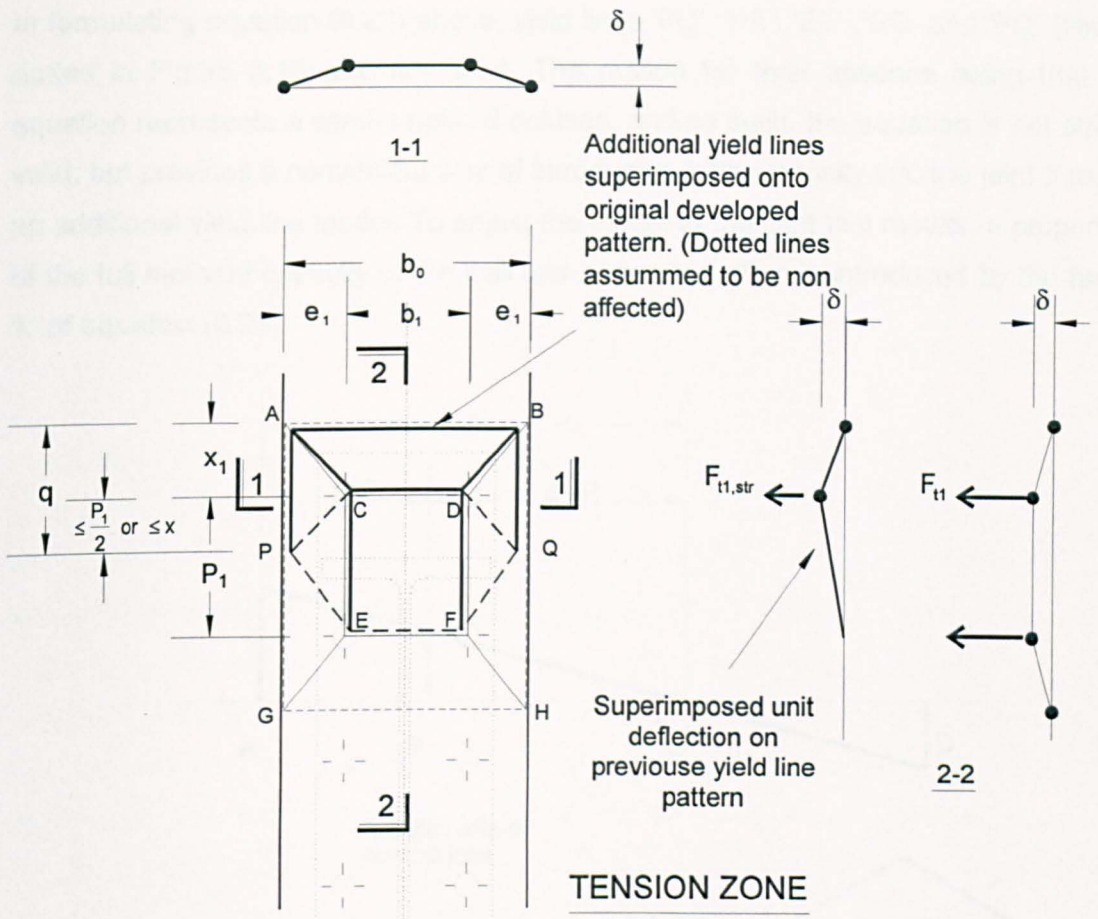

Figure 8.16 Geometry of yield line pattern used for strain hardening

The unit deflection (δ) is applied to the top bolt row location. It is assumed that the unit deflection of the previous model developed is not included in the analysis and does not contribute or interfere with the development of this new model. Using the analytical procedure developed previously, a relationship for the yield line pattern can be written as follows;

$$F_{t1,str} = m_{str}\left[\frac{2}{e_1}\left(q + P_1 + x_1\right) + \left(1 - n^2\right)\left(\frac{2.b_o}{x_1} + \frac{b_1}{P_1}\right)\right] \quad \text{.....(8.22)}$$

where

$m_{str} = k.m_p$, proportion of the moment capacity of the wall in flexure..... (8.23)

In formulating equation (8.22) above, yield lines 'PC', 'PE' ,'EF' ,'DQ' and 'FQ' (shown dotted in Figure 8.16) are not used. The reason for their absence being that the equation represents a semi-empirical solution, and as such, the equation is not strictly valid, but provides a convenient way of introducing extra capacity into the joint through an additional yield line model. To adjust the model to the joint test results, a proportion of the full moment capacity of the wall has been used. This is introduced by the factor 'k' of equation (8.23).

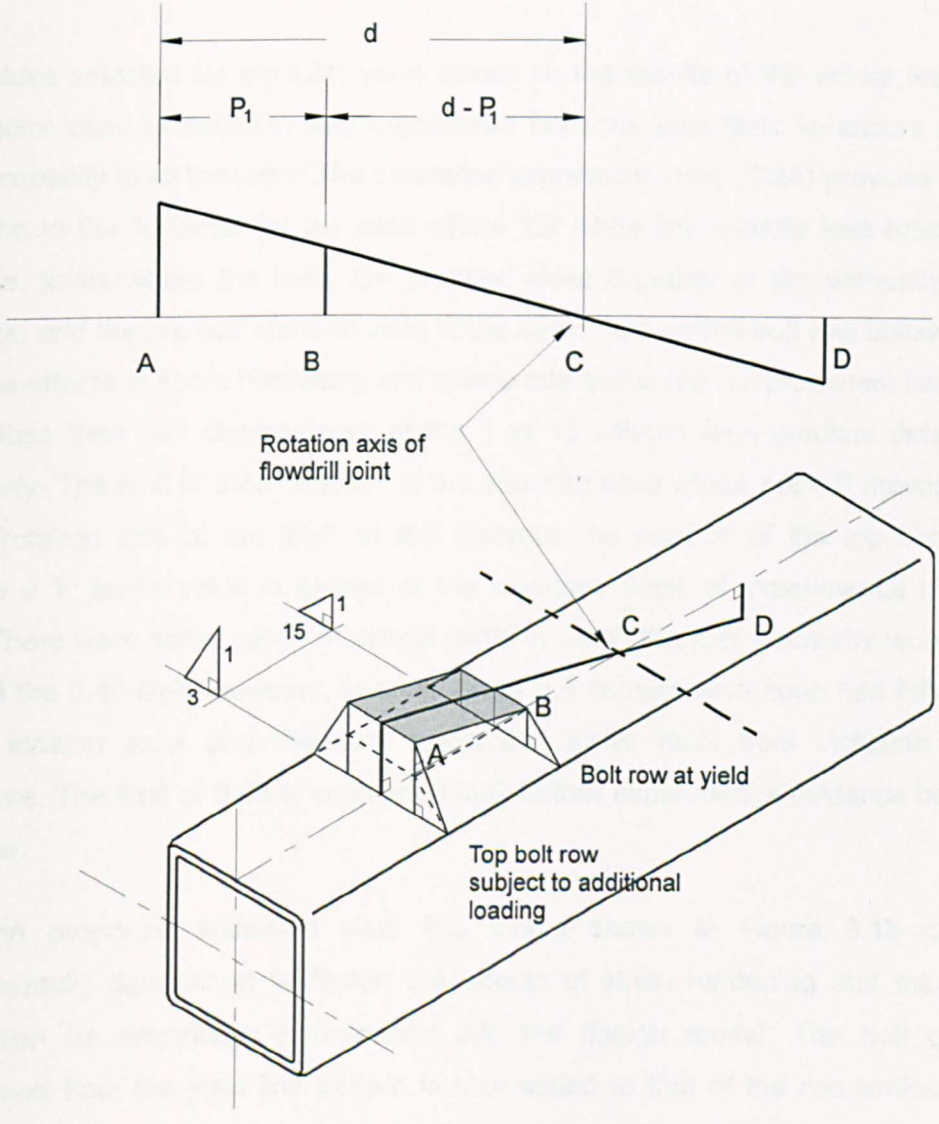

Figure 8.17 Joint rotation for strain and membrane effects

The value 'k' has been related to the amount of rotation developed in the yield line. The rotation developed in the yield line hinge is determined from the corner of the SHS at the location of the top row of bolts, as indicated schematically in Figure 8.17 as point A. Point B, denotes the displacement of the bolt on the original yield line pattern, at the

assumed bolt displacement using the edge gradient of 1 to 15. If the geometry of the joint alters with the lower bolt B moving closer to the top bolt then the rotation of the hinge line is less severe and would benefit less from strain hardening and membrane action in the model. Therefore to account for these different connection details, the 'k' value used has the following relationship;

$$k = 0.78\left[\left(\frac{d}{d-P_1}\right)-1\right] \quad \leq 0.45 \qquad \text{.....(8.24)}$$

The values selected for eq(8.24) were based on the results of the actual tests. The 0.78 factor used in eq(8.24) was determined from the joint tests to ensure a lower bound capacity to all the tests. The bracketed expression in eq. (8.24) provides a linear reduction to the 'k' factor for the case where the hinge line exhibits less rotation; for example, joints where the bolts are grouped close together at the extremity of the endplate, and the top bolt starts to yield at the same time as the bolt row below. In this case the effects of strain hardening and membrane action are not prominent before the bolts attain their bolt displacement at the 1 to 15 column face gradient determined previously. The limit of 0.45 imposed is the opposite case where point B moves closer to the rotation axis of the joint. In this instance the rotation of the top bolt would develop a 'k' factor value in excess of the boundary limits of experimental test data used. There were some cases of simple joints in which the joint geometry would have violated the 0.45 limit. However, in such cases the compression zone had failed prior to the tension zone and therefore invalidated these tests from inclusion in this procedure. The limit of 0.45 is suggested until further experimental evidence becomes available.

With the proposed additional yield line model shown in Figure 8.16 and the experimentally determined 'k' factor, the effects of strain hardening and membrane action can be empirically incorporated into the design model. The bolt capacity determined from the yield line pattern is now added to that of the conventional yield line pattern of the tension zone developed previously. The yield line pattern shown in Figure 8.16 should not, however, be allowed to extended past the first bolt row. The yield line pattern only represents the local capacity of the top bolt with a linear distribution of bolt load as indicated previously in Figure 8.9(b). It is envisaged that the inclusion of these effects should be an option and at the discretion of the designer. One of the major advantages of the method is a design procedure that can effectively determine the limits to which the tension zone yield line model extends. This is

accomplished using the subsequent limits of column face gradients imposed in Figure 8.17.

8.6.7 Discussion of final predicted joint moment capacity

Table 8.8 presents the predicted values of the joint's moment-resistance, using the bolt distribution shown in Figure 8.8(b) and including the effects of membrane and strain hardening. The format for the table is similar to that of Table 8.7, except for column (2) which shows the additional bolt load provided by the above yield line pattern. The bolt forces in this column have in some cases been reduced by the values denoted by the parenthesis [ ], which were limited by the resistance of the compression zone of the joint, shown shaded in columns (6) and (7). The summation of all the bolt loads will not exceed the previously derived compression zone resistance. The ratio of the estimated capacity of the joint to actual capacity is indicated in column (10). This has been shown graphically in Figure 8.18, where both columns (8) and (9) have been plotted to show the degree of scatter in the results.

The comparison of experimental to predicted ultimate moment capacity shows the closeness of the results when the effect of the strain hardening and membrane is allowed for in the analysis. The majority of the cases predict safe lower bound solutions to actual test data, although this was accounted for when determining the value of the 'k' factor to ensure a lower bound fit. The compression zone yield model has also shown an excellent agreement to the joint tests when this was the main mode of failure for the joint. It must be stated that the predicted joint capacities are compared against values taken as the assumed failure of the joint. All of the predictions were below the 'maximum' moment attained during the tests.

Joint test no.	1st bolt row	Additional Bolt Force to first row	2nd bolt row	3rd bolt row	4th bolt row	Total bolt force	F_c	Moment $M_{j,Rd}$	Joint test moment $M_{j,expt}$	Ratio
	(1)	(2)	(3)	(4)	(5)	(6) (kN)	(7) (kN)	(8) (kN.m)	(9) (kN.m)	(10)
2	80 (0.390)	43-[43]=0	80 (0.290)	34 (0.190)		194	194	61.0	62.4	0.98
4	79 (0.290)	44-[36]=8	79 (0.190)			165	165	40.1	40.9	0.98
5	70 (0.290)	39-[11]=28	70 (0.190)			168	168	41.7	44	0.95
6	94 (0.290)	53	94 (0.190)			241	249	60.4	48.4	1.25
7	50 (0.290)	28-[21]=7	50 (0.190)			108	108	26.1	27.4	0.95
8	187 (0.290)	103-[99]=4	187 (0.190)			377	377	90.7	109.3	0.83
10	123 (0.190)					123	168	23.4	20.3	1.15
11	48 (0.290)	26-[21]=5	48 (0.190)			102	102	24.8	26.3	0.94
12	43 (0.290)	23-[13]=10	43 (0.190)			96	96	23.6	24.3	0.97
13	47 (0.290)	25-[15]=10	47 (0.190)			103	103	25.3	25	1.01
14	82 (0.390)	30	82 (0.290)	49 (0.190)	17	260		78.3	86.4	0.91
15	87 (0.290)	48	87 (0.190)	33 (0.090)		255		58.6	56.9	1.03
16	53 (0.290)	29	53 (0.190)	20 (0.090)		155		35.7	43.9	0.81
17	122 (0.190)					122		23.2	28.4	0.82
18	79 (0.290)	44-[36]=8	79 (0.190)			165	165	40.0	44	0.91
19	99 (0.430)	54	99 (0.320)	47 (0.220)		299	307	107.9	123.7	0.87
20	141 (0.430)	78-[10]=68	141 (0.320)	67 (0.220)		417	417	150.1	156	0.96
21	196 (0.430)	106-[32]=74	196 (0.320)	93 (0.220)		559	559	199.3	230.7	0.86
22	150 (0.430)	56	150 (0.320)	96 (0.220)	42	494		162.8	184.1	0.88
23	184 (0.430)	99-[16]=83	184 (0.320)	88 (0.220)		539	539	192.7	200.8	0.96
24	196 (0.430)	72	196 (0.320)	125 (0.220)	54	643		211.9	236	0.90
25	146 (0.320)	80-[14]=66	146 (0.220)	28 (0.120)		386	386	103.2	105.5	0.98
26	98 (0.320)	53	98 (0.220)	19 (0.120)		268	275	72.1	78.3	0.92
m/30/67	37 (0.390)	21	37 (0.290)			95	139	33.3	49	0.68
m/30/50	28 (0.390)	16	28 (0.290)			72	139	25.3	34.5	0.73
m/19/67	88 (0.390	48	88 (0.290)			224	265	78.5	106	0.74
m/19/50	67 (0.390)	37	67 (0.290)			171	265	59.8	81	0.74
m/12/67	217 (0.390)	117-[60]=57	217 (0.290)			491	491	169.7	204	0.83
m/12/50	165 (0.390)	89	165 (0.290)			419	491	147.0	167	0.88

Table 8.8 Final predicted moment capacity of joints compared to test data

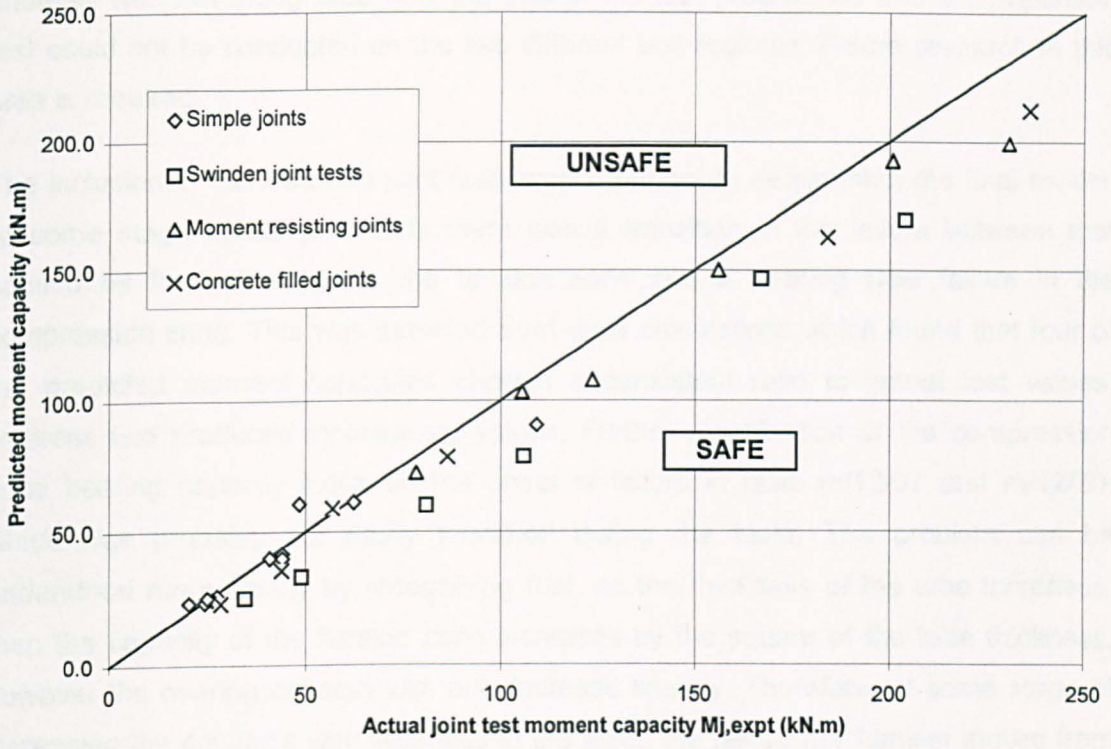

Figure 8.18 Scatter of predicted results

The only poor result of the series of tests was joint test no. 6, which indicated a failure ratio of 1.25. The reason for the overestimation of moment capacity was because of the flexibility of the endplate. In this particular test the flush endplate had contributed significantly to the overall rotation of the joint. The comparative moment was determined from a rotation of the joint assuming the bolt had displaced a gradient of 1 to 15, and the endplate was rigid. Obviously because of the endplate flexure the assumed rotation was wrong, resulting in a moment lower than one would have expected. This can be seen from the results of an identical bolt group from test no.26 where a rigid endplate was used. In this case the ratio was 0.92, significantly improved relative to that of test no. 6. This highlights the fact that no account of the endplates flexure is allowed for in this model, making it unsuitable for use with joints assumed to be pinned.

From a comparison of the two different test programmes between the joints tested at Sheffield by the author and those of British Steel Swinden Laboratories, it appears that the cantilever test results are in closer agreement with the estimated moment capacity. The cruciform test results are consistently lower. One explanation is experimental error, but a more likely reason is that the cantilever tests induce a more severe

condition of stress and yield into the web panel. Unfortunately the influence of this anomaly was not recognised until the end of the test programme and a comparison test could not be conducted on the two different test regimes. Future research in this area is required.

The inclusion of the Swinden joint tests was important in determining the final model. At some stage of the joint tests there was a transition in the failure between that caused by flexural action in the tension zone and a bearing type failure in the compression zone. This was detected from early calculations which found that four of the predicted moment capacities showed a consistent ratio to actual test values, whereas two produced inconsistent values. Further examination of the compression zone bearing capacity indicated the onset of failure in tests m/12/67 and m/12/50, which was probably not easily identified during the tests. The problem can be understood more clearly by recognising that, as the thickness of the tube increases, then the capacity of the tension zone increases by the square of the tube thickness; however the bearing capacity can only increase linearly. Therefore, at some stage of increasing the column's wall thickness in the tests, the failure mechanism moves from bending to bearing.

The results indicate that when the endplate is the full width of the column and the tube thickness is towards the lower end of the standard serial size range, then a tension zone failure will govern the joint's design. When the wall size increases or the endplate reduces in width, then the compression zone will govern the joint's mode of failure. What is interesting from the results is the fine balance which exists between the two modes of failure, affected by only slight changes in the joint's geometry. The benefit of concrete filling clearly has potential to increase the capacity of the joint.

8.7 Initial stiffness (K_i)

The initial stiffness of the joint is defined as that occurring at the beginning of the joint's loading history, where the response is elastic. If the joint produces a relatively high stiffness there are usually difficulties in determining an accurate value. In instances where no initial linearity is observed in the joint's response (as seen in the flowdrill tests), the joint's unloading stiffness has sometimes been used as it provides a more consistent value.

A typical approach used in predicting the initial stiffness of the joints is based on the component method previously mentioned in Chapter 7. In this approach the face of the column is treated as a series of individual components with different stiffness. The response of these components reflect the connection's overall behaviour. Unfortunately, this method was found to be impractical for flowdrill joints as;

1. the rotation axis of the joint was not accurately defined.
2. a complex pattern of stress and strain in the face of the column wall arises
3. it is difficult to determine the load path accurately and develop adequate component representation in the compression zone of the joint.
4. various factors are required to allow for concrete fill, multi-connection and wall slenderness.

Of the list above, the most important error was the inability to accurately determine the elastic rotational axis of the joint. As seen previously in Figure 8.7 the axis of rotation for the joint started near to the top of the beam section. This location could not be found experimentally with any confidence. The ability to determine the joints rotational axis for the initial stiffness is more important than that of the axis of rotation in the plastic condition, as the stiffness of both the tension and compression zones directly determines the value. Inaccuracy in modelling the stiffness of the compression and tension zones of the joint would obviously cause severe errors. In previous methods which adopt the component method, this problem is avoided by assuming an adequately stiff bearing at the compression flange which is assumed to define the rotational axis for the joint. No such stiff bearing is available for the unfilled flowdrilled joints, where the compression zone is rather flexible. Because of these problems a different approach was used in the model.

An alternative approach to predict the initial stiffness of a joint is to define an equation that best fits the experimental data of the joint tests, with the geometrical and material parameters used in the expression. This type of approach has been used recently by Szlendak [81], to determine both the full moment-rotation characteristics of joints using open section beams welded to tubular columns. A multiple regression analysis on a series of 72 joint tests was conducted by Szlendak to produce the following equation that predicts the initial stiffness;

$$K_i = 4.11.E.t_0^3 \frac{\beta.\eta.\lambda_0}{\left(1-\frac{\beta}{2}\right)^2} \qquad \text{.....(8.25)}$$

The purpose of reproducing equation (8.25), is to show for the readers own reference, the complexity which curve fitting produces. The problem is that the accuracy of the equation is only as good as the test data and the limits imposed by the joint parameters. Undoubtedly, the equation will predict with accuracy the known joints tested, as the symmetrical tension and compression zone geometry of the joints produced a known mid depth elastic neutral axis. Although closer examination of Szlendak results still indicated scatter in the predictions, especially towards the top range of a joint's stiffness in which 100 to 200 percent errors are to be found. This level of inaccuracy was also found in Chapter 7, with comparisons of the isolated endplates to that of EC3 model to determine the initial stiffness. It would seem sensible, with the problems of adequate experimental accuracy of the data, that any future expression developed should be relatively simple but improve on this level of accuracy.

In developing an empirical expression for the initial stiffness it is proposed that the following factors which have been known to influence the joints performance should be incorporated into a predictive equation;

1. moment capacity of the joint, (based on the column's face, and not limited by weld or bolt failure), $M_{j,Rd}$
2. depth of connection, 'h'
3. tension zone bolt cross centres to column width ratio, $\beta_1 = \frac{b_1}{b_0}$
4. compression zone endplate to column width ratio, $\beta_2 = \frac{b_2}{b_0}$
5. yield strength, f_y

Included within the predictive equation is the previously derived moment capacity. The use of this parameter allows a logical way of accounting for the geometrical properties of the joint. However, by allowing the moment capacity to be used explicitly in the predictive equation, it is possible that two identical joints with different grades of steel with different ultimate capacities would have different initial stiffnesses. However, if the two joints that are geometrically identical they would have identical initial stiffnesses as elastic principles usually define this portion of the moment-rotation characteristic. To compensate for this, the steel grade is incorporated into the model.

The process of incorporating part of the ultimate capacity design procedure has also been used in EC3. Yield lines that were determined for the ultimate capacity are used explicitly in the component method to find the initial stiffness. This process has been simplified in the authors own model by adopting the full moment capacity of the joint. The use of this previously derived moment capacity does not provide a solution on its own, as the position of the rotation axis of the joint influences the initial stiffness. Further parameters are therefore required to allow for this situation and these are geometrical properties based on the tension and compression zones of the joint. A modified expression for β_2, now called $f(\beta_2)$, and based on these parameters is proposed as follows;

$$f(\beta_2) = \frac{M_{j,Rd}}{K_1} \cdot \frac{275}{f_y} \cdot \frac{1}{h} \cdot \beta_1 \qquad \text{.....(8.26)}$$

It is assumed that a variable function is required to the compression zone parameter (β_2). To determine the numerical constant for this function, Figure 8.19 plots the right hand side of equation (8.26) against (β_2). A straight linear fit of the data is shown superimposed to determine appropriate values of $f(\beta_2)$, for $\beta_2 \geq 0.80$. For β_2 less than this value there is a lack of data, but it is clear that β_2 will not approach zero and it is likely that some cut-off value is required. In the absence of experimental evidence this has arbitrarily been made at the value of 0.86, although it is recognised that this is non-conservative and will require subsequent adjustment.

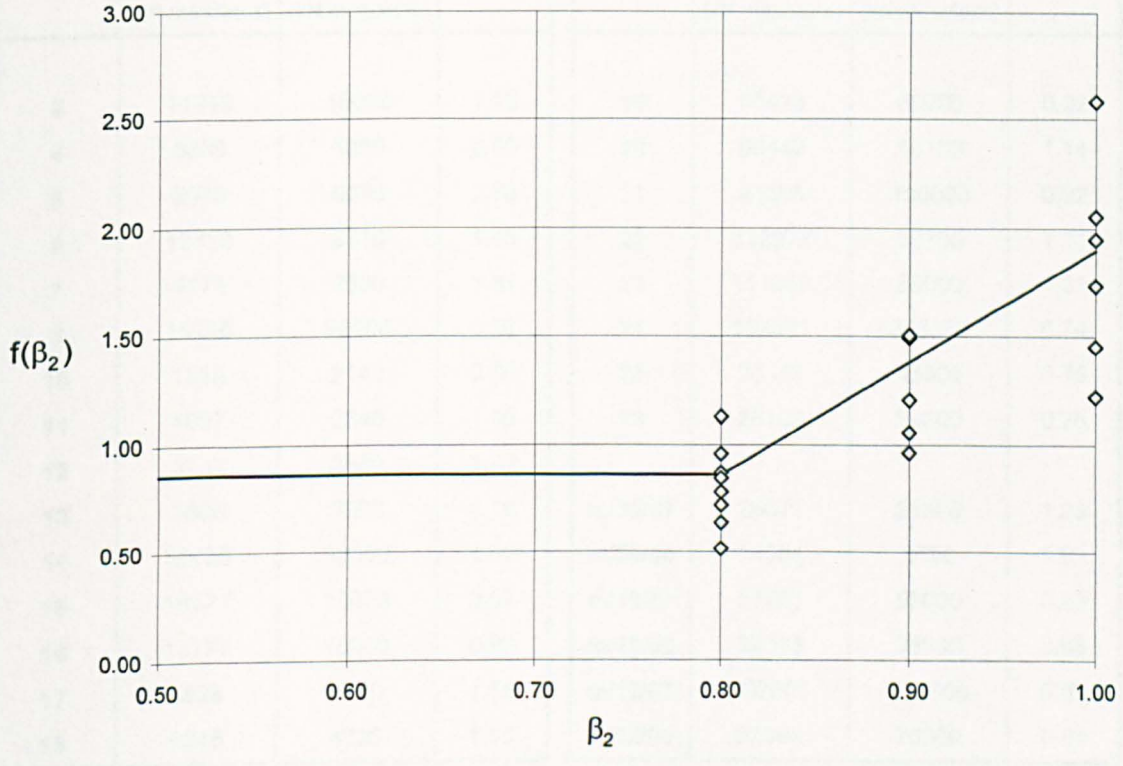

Figure 8.19 Determination of function for compression zone parameter

Rearranging eq (8.26) for K_i produces;

$$K_i = \frac{f(\beta_2).M_{j,Rd}.f_y.h.\beta_1}{275} \qquad \text{.....(8.27)}$$

where

$$f(\beta_2) = 5.2.\beta_2 - 3.3 \quad \text{for cases in which} \quad 0.8 \leq \beta_2 \leq 1.0 \qquad \text{.....(8.28)}$$

$$f(\beta_2) = 0.86 \quad \text{when } \beta_2 \leq 0.8 \qquad \text{.....(8.29)}$$

Using eq (8.27), Table 8.9 below compares the predicted initial stiffness with actual results from the joint tests. As expected, having used a curve fitting exercise, the results are in close agreement considering the difficulties of assessing the actual initial stiffness of the joint previously mentioned with both the range and diversity of the test data. It is believed that this simple expression proposed above will provide as good as, if not better accuracy, than the use of the component method.

Joint test no.	Predicted K_i (kN.m/radians)	Experimental K_i (kN.m/radians)	Ratio
2	11910	10000	1.19
4	5805	5880	0.99
5	5076	6670	0.76
6	13439	9410	1.43
7	4175	2500	1.67
8	15216	20000	0.76
10	1918	2140	0.90
11	4007	3640	1.10
12	3702	3640	1.02
13	3809	3200	1.19
14	36435	33300	1.09
15	18127	18600	0.97
16	14777	16000	0.92
17	5928	3810	1.56
18	6245	4630	1.35

Joint test no.	Predicted K_i (kN.m/radians)	Experimental K_i (kN.m/radians)	Ratio
19	55413	60000	0.92
20	66449	58100	1.14
21	91696	100000	0.92
22	112072	85700	1.31
23	111009	85000	1.31
24	182371	248000	0.74
25	33442	43800	0.76
26	26103	34300	0.76
m/30/67	26671	21600	1.23
m/30/50	14084	8750	1.61
m/19/67	51793	53000	0.98
m/19/50	29683	35000	0.85
m/12/67	102608	125000	0.82
m/12/50	62998	75000	0.84

Table 8.9 Initial stiffness of joints

8.8 Membrane stiffness-(K_p)

The proposed model takes no account of the increased strength of the joint through membrane stiffness. This follows the findings of section 3.7.6, where it was observed that serviceability loading applied to the column reduces the membrane stiffness of the joint. As a conservative assumption membrane stiffness has been neglected.

8.9 Curve fitting parameter-(ψ)

This section of work uses the modified Ramberg-Osgood eq(8.6), developed earlier in the chapter, to define the full moment-rotation curve for the joints. To determine the parameter (ψ) the actual test data was used rather than the predicted values. The value selected to best represent the test data was $\psi = 4.5$ which gives a lower bound curve fit to the joint test data. Typical moment-rotation curve fits for joint tests 12 and 20 are shown in Figure 8.20.

The modified Ramberg-Osgood equation compares well to the experimental data, with the use of the additional parameter (ϕ_d) clearly enhancing the accuracy of the curve fit shown in Figure 8.20. At this value of rotation, the post yield stiffness (K_p) is assumed to be zero as shown. Originally the equation was only intended to define the initial portion of the curve, up to the start of the post yield stiffness. However, it was found that the curve is able to fit the experimental moment-rotation data during the latter stages of the joints loading cycle remarkably well.

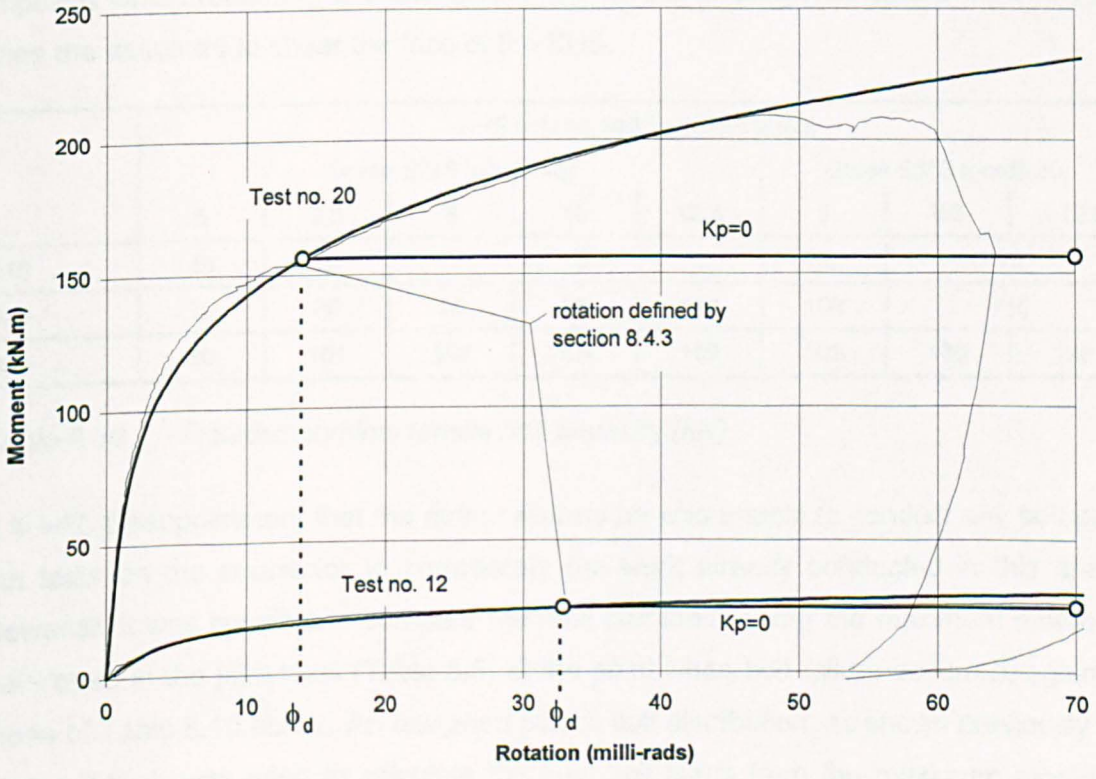

Figure 8.20 Typical curve fit to experimental joint test data

8.10 Flowdrill tension and shear bolt capacity

The final check on the capacity of the joint relates to the performance of the flowdrill connector. This is probably the most important of all the checks required to avoid any sudden and catastrophic failure of the joint. This type of failure was observed in the testing of the moment-resisting joints (Chapter 5), as the top row of bolts suggested thread stripping.

The tensile bolt capacities of flowdrill connectors have been determined from isolated tests conducted by British Steel's Swinden Laboratories on various thicknesses of tubular sections. Table 8.10 below reproduces the tensile bolt capacities from reference 49, based on those tests. The guidance provided for shear and bearing capacities of the bolt are similar to that of traditional design, where the bearing capacity of the column wall is determined from the thickness of the tube and the nominal bolt diameter. Interestingly no account of the flowdrill lobe is used to increase the bearing capacity of the bolt which, for bolts predominately in shear, can be onerous for column tubes of relatively small tube wall thickness. A second check has also been imposed which relates to a shear type failure of the column wall, where the two bolt lines are assumed to shear the face of the SHS.

	RHS column wall thickness t_0 mm							
	Grade S275 (grade 43)					Grade S355 (grade 50)		
	5	6.3	8	10	12.5	5	6.3	8-12.5
M16	46	60	70			59	70	
M20	70	85	95	97	110	102	110	
M24	80	101	122	134	159	103	130	159

Table 8.10 Flowdrill nominal tensile bolt capacity (kN)

It is with disappointment that the author reports he was unable to conduct any bolt pull out tests on the connector to corroborate the work already conducted in this area. However, it was possible to compare the final bolt loads using the maximum moment developed in the joint tests (Table 8.5) at the point when bolt failure occurred, against those of Table 8.10 above. An assumed plastic bolt distribution, as shown previously in Figure 8.9(a), was used to calculate the final bolt loads from the maximum moment attained in the joint test from Table 8.5. Using this bolt distribution provides the lowest bolt load for the maximum moment and therefore provides a conservative estimate of the bolt capacity from the joint tests.

Joint test no.	Max. Moment from Table 8.5. (kN.m)	Wall thickness (mm)	Column grade	Bolt capacity from Table 8.10 (kN)	Estimated bolt load (kN)	Ratio
2	82	8.0	S275	95	*54*	*0.57*
4	41	8.0	S275	95	*43*	*0.45*
5	56	8.0	S275	95	*58*	*0.61*
6	61	8.0	S275	95	*64*	*0.67*
7	34	6.3	S275	85	*35*	*0.41*
8	123	12.5	S275	110	**128**	**1.16**
10	26	8.0	S275	95	*68*	*0.72*
11	34	6.3	S275	85	*35*	*0.41*
12	26	6.3	S275	85	*27*	*0.32*
13	30	6.3	S275	85	*31*	*0.36*
14	124	8.0	S275	95	*78*	*0.82*
15	73	8.0	S275	95	*76*	*0.80*
16	58	6.3	S275	85	*60*	*0.71*
17	36	8.0	S275	95	**95**	**1.00**
18	50	8.0	S275	95	*52*	*0.55*
19	162	8.0	S275	95	**95**	**1.00**
20	208	10.0	S275	97	**122**	**1.26**
21	283	12.5	S275	110	**166**	**1.51**
22	288	10.0	S275	97	**162**	**1.67**
23	253	10.0	S355	110	**148**	**1.35**
24	316	10.0	S355	110	**177**	**1.61**
25	138	10.0	S275	97	**128**	**1.32**
26	104	8.0	S275	95	**96**	**1.01**
m/30/67	73	5.0	S275	70	*54*	*0.77*
m/30/50	67	5.0	S275	70	*49*	*0.70*
m/19/67	135	8.0	S275	95	**99**	**1.04**
m/19/50	127	8.0	S275	95	**93**	**0.98**
m/12/67	235	12.5	S275	110	**173**	**1.57**
m/12/50	215	12.5	S275	110	**158**	**1.44**

Table 8.11 *Summary of bolt forces theoretically calculated in test from maximum moments*

The findings of the analysis are presented in Table 8.11. The results which are shaded in the table denote the bolts which actually pulled out of the flowdrill hole during their test. The ratio in the end column is a percentage of the tested flowdrill bolt capacity. Any ratio below unity indicates that the bolt force did not attain its specified ultimate capacity as stated from Table 8.10. As observed in Table 8.11 the results of the majority of simple joints, numbered 2 to 18, did not attain this load. This is not a serious problem as the joint tests were stopped due to excessive rotation and not through any indication of bolt failure. In general, all of the Sheffield moment-resisting joint tests managed to pass their tabulated bolt capacities, with ratios exceeding unity. The bolts which were close to a ratio of one were found to correspond to the 8mm column wall thickness. Subsequent increase in wall thickness above 8mm resulted in the bolt exceeding their nominal capacities. Interestingly, the results for the Swinden tests showed a similar pattern, with the 8 mm column wall showing ratios of bolt force to specified bolt capacities close to unity; although two of the tests, m/30/67 and m/30/50, concerning the 5.0 mm walled column raise some concern. It appears that, at this thickness of column, the bolt capacity recommended by Table 8.10 is on the unsafe side, with ratios less than unity.

One of the reasons for the apparent unsafe values may be in how the original tests were conducted on the flowdrill connector to determine the bolt's capacity. In the tests, conducted by Swinden Laboratories, only the threaded lobe was attached to the bolt and pulled apart as if part of a nut and bolt combination. There was no interaction of face deformation incorporated in the tests. A more appropriate and realistically determined value would have been to induce and maintain a known column face deformation (such as an edge gradient as adopted in section 8.4.3) and followed by testing the bolt to failure. In this way the top part of the thread would have deformed away from the bolt thread reducing the capacity of the bolt and producing a more realistic value. The tensile bolt capacities determined for column sections less than 8.0 mm should therefore be treated with extreme caution, and further investigations conducted immediately.

8.11 Accuracy of the model.

Throughout the development of the model, the philosophy has always been to concentrate on the lower bound solution for determining the joint's moment-rotation curve. Both the curve fitting and moment capacity were selected to achieve this. In the majority of design situations the least favourable or lower bound limit is usually the major parameter required. There are however a few cases in which an upper bound solution is more appropriate e.g. the maximum moment which may be transmitted through the connection. The proximity of these limits may be taken as a measure of the accuracy of the modelling process.

It is proposed that for an upper bound limit, the ultimate moment capacity ($M_{j,Rd}$) derived in the previous sections are factored by the values shown in Table 8.12. The factors applied to the ultimate moment of the connection depend on the location in which the joint is situated i.e. a cruciform or cantilevered geometry corresponding to an interior or edge column connection respectively. The values determined have been found experimentally, to ensure that the predicted capacity calculated by the model when factored would exceed the actual joint test values. The two factors presented in the table reflect the level of uncertainty in the model between the two arrangements and on the tests conducted on the cantilever joints at Sheffield and the cruciform tests carried out at Swinden Laboratories (see section 8.6.7).

Moment-rotation characteristic	Connection type	Factor to be applied to $M_{j,Rd}$
Lower bound limit	Cruciform	1.0
	Cantilever	1.0
Upper bound limit	Cruciform	1.5
	Cantilever	1.25

Table 8.12 Factors for upper and lower bound moment-rotation envelope

Adopting these values and using the calculated properties determined in this chapter the full joint envelope for tests 12, 20 and 21 (relating to the extended and flush endplate details) can be shown in Figure 8.21. Joint test no. 21 is included within the group to show the least favourable case in which the model has been applied. Both the upper and lower limits of each curve fit are shown to provide the design envelope of

the joint; the lower bound curve being derived from the direct application of the expressions developed in this chapter and the upper bound being the factored lower bound curve using the values in Table 8.12. It can be clearly seen that the design envelope has the potential to determine the moment-rotation characteristic of the joint with reasonable accuracy, as long as the moment capacity of the joint is predicted accurately.

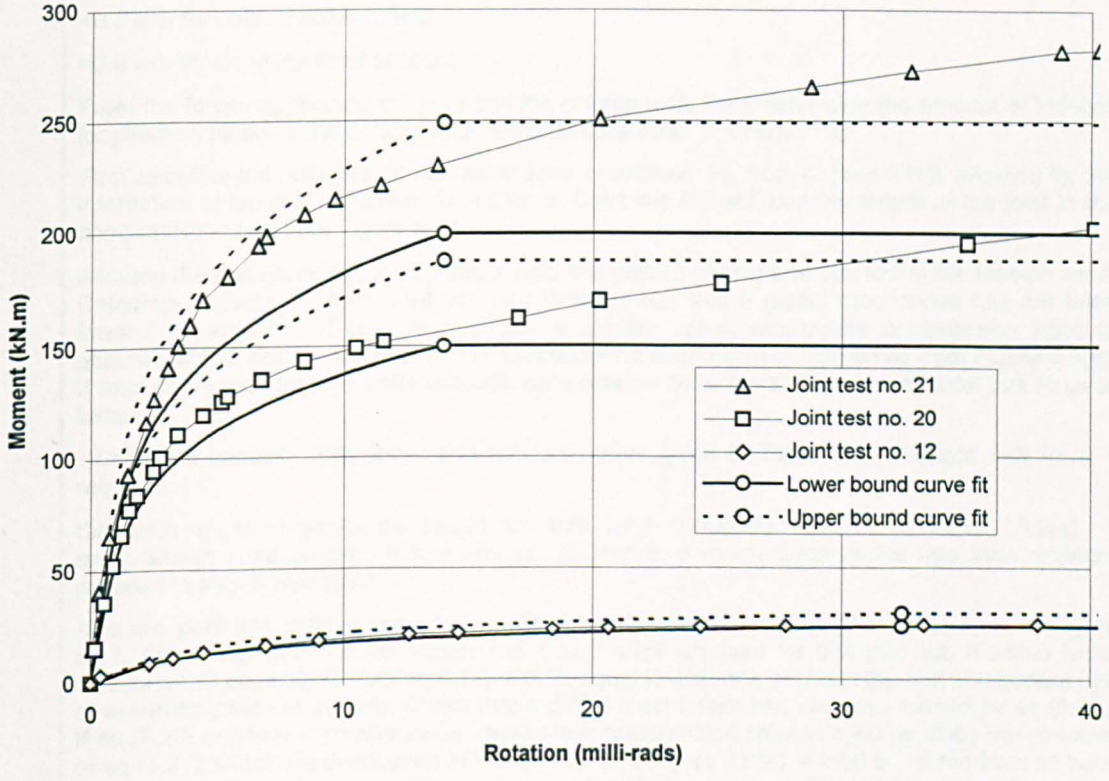

Figure 8.21 Moment-rotation envelopes for joint tests no. 12, 20 and 21

8.12 Summary of joint design procedure

Using the guidance of this chapter, Table 8.13 provides a final summary to the design procedure for determining the moment capacity and joint characteristic of flowdrill connections,. The table is intended to serve as a step by step procedure to determine the capacity of the SHS column when flush and extended endplates are bolted onto the face. For design guidance it is assumed that the endplate is designed as sufficiently rigid not to contribute significantly to the overall rotation in comparison to that of the column's performance.

Step	Instructions
1.	Determine external moment and shear on joint. Check both column and beam section have adequate capacity to sustain load
2.	If the joint requires both high stiffness and moment, locate the bolts as close as possible to the wall of the section. Allow the endplate width to approach the full width of the column.
3.	Determine bolt group parameter 'h'.
4.	Calculate rotational axis depth 'd' of the joint (section 8.4.1), =0.7 x h- for unfilled column SHS =0.9 x h- for concrete filled sections
5.	From the forces applied on the joint and the column axial load, determine the amount of induced longitudinal stress in the column face noted as parameter 'n' of eq(8.10)
6.	First calculate the column's compression zone resistance, F_c, from section 8.6.2, allowing for the interaction of longitudinal stress from step 5. Calculate the stiff bearing length of the joint in the compression zone from Figure 8.14.
7.	Assume the bolt group to develop into a yield line pattern of only one bolt row in the tension zone. Calculate capacity F_t, from eq(8.14), use P_1=0. Check that a global mechanism has not been formed by eq(8.20). If eq(8.20) provides a smaller value, recalculate compression zone to assume global mechanism of eq(8.21). Calculate the distribution of bolt forces from Figure 8.9(a). If total bolt forces from all bolts exceeds compression zone resistance, reduce total bolt force to balance. Check bolt capacity with shear and tension values given in Table 8.10. Reduce bolt force if required. Calculate moment-resistance based on bolt load distribution shown in Figure 8.9(a). If compression zone governs failure proceed to step 9. If moment-resistance less than required proceed to step 8 else END
8.	Assume yield line pattern spreads to next bolt, with 1 to 15 edge gradient as shown in Figure 8.17. Check top bolts do not violate the 1 to 3 edge gradient for bolt pull out. If within limits calculate bolt capacity F_t from eq(8.14). Set P_1 equal to distance between top bolt and bottom bolt of assumed yield line pattern. Check that a global mechanism has not been formed by eq (8.20). If eq (8.20) provides a smaller value, recalculate compression zone to assume global mechanism of eq (8.21). Calculate distribution of bolt forces from Figure 8.9(a). If total bolt force from all bolts exceeds compression zone resistance, reduce total bolt force to balance. At the discretion of the designer, use additional bolt load capacity $F_{t1,str}$ from eq(8.22). Check bolt capacity with shear and tension values given in Table 8.10. Reduce bolt force if required. Calculate moment-resistance based on bolt distribution shown in Figure 8.9(b). If compression zone governs failure proceed to step 9. If moment-resistance less than required repeat step 8 with next row else END.
9.	If moment-resistance of joint is limited by the compression resistance of the joint, either increase the width of the endplate or depth of the bolt group. An alternative is concrete filling of the tube. If the moment capacity is governed by the column face yielding, either increase the depth of the bolt group or increase the tube thickness. Restart from step 7
10.	If the full moment-rotation characteristic of the joint is required , proceed to step 11 else END
11.	Determine the moment-resistance, $M_{j,Rd}$, of the joint, including the additional bolt forces from eq(8.22). Do not limit the moment-resistance to the bolt capacity, only the tube wall. Ensure that all the bolts which are capable of providing a plastic distribution are used in the connection, however, the top and bottom bolts should still be within the limits defined by the two gradients of Figure 8.17. Check that the compression resistance is adequate, if not readjust bolt distribution to equal compression zone resistance and shear capacity of column.

Table 8.13 Summary of joint model and design for flowdrill joints

Step	Instructions
12.	Calculate ϕ_d, from section 8.4 , using the distance of the rotation axis and the displacement of bolt determined from limiting the gradient of the bottom bolt forming the plastic yield line.
13.	Calculate ϕ_{cd} from section 8.4, using the distance of the rotation axis and the displacement of bolt determined from limiting the gradient to the top bolt row.
14.	Calculate initial stiffness, K_i , from section 8.7 and eq(8.27)
15.	Determine full lower bound moment-rotation characteristic from eq(8.6), using the values calculated in steps 11 to 14.
16.	Determine full upper bound solution by multiplying the moment-resistance calculate in step 11 by the appropriate factor in Table 8.12. Re-calculate upper bound curve with increased moment-resistance and initial stiffness.
END	Design endplate to either EC3 or similar approved method with the bolt distribution and bolt forces developed above

Table 8.13 cont'd Summary of joint model and design for flowdrill joints

8.12 Chapter summary

A summary of the findings of this chapter are as follows;

1. The joint test data of the programme has been used to develop a joint model to predict the full moment-rotation characteristics of a flowdrill joint. A reasonable level of accuracy over the complete range of welded endplate connections tested has been shown to exist. The model was also applied to a series of joint tests conducted from other sources. The different test conditions of these joints and the stress in the column influences joint capacity. This effect has been allowed for in the model by reducing the capacity of the yield line hinges which cross the direction of axial stress.

2. A new deformation limit based on the edge gradient of the column face has been proposed to replace the value obtained from the one percent column width. The new method relies on yield line hinge rotation which appears to provide a more flexible approach in determining the rotational limit of the joint. By identifying a specific rotation limit to the data the modified Ramberg-Osgood curve used in the joint model fits the initial non-linear experimental data reasonably well. The results obtained using the method are promising.

3. Great effort has been concentrated on defining the failure of the compression zone of the joint, where methods have successfully been used to predict the capacity. Failure in this region has been shown to be the most important and detrimental to the joint. A method has been devised, similar to a local capacity check for sections, which

reduces the capacity of the yield hinge line at the SHS corner wall. The difficulty of this method is that an iterative solution is required, although closeness of the results is improved.

4. A method has tentatively been proposed to account for strain hardening and membrane action in the model. The ability to incorporate this into the joint's moment-resistance is left to the discretion of the designer.

5. A predictive equation for the initial stiffness of the joint has been established to a reasonable accuracy. The joint model enabled a lower bound solution to the moment-rotation curve to be obtained. To account for inaccuracies in the prediction an upper bound solution has also been proposed.

6. The bolt capacity of the Flowdrill joints under an assumed plastic distribution has been compared to the bolt capacities produced from an independent source. For column wall thickness less than 8mm the tensile bolt pull out values were significantly less than the values stated. It is recommended that any moment connection design should be limited to column thickness greater than 8mm, until further more realistic tensile bolt pull out tests can be conducted.

The model developed in this chapter does have limitations; the most notable being its inability to deal with endplate flexure, where only the response of the column determines the moment-rotation characteristics. This is not such a major problem as the endplate thickness can be increased without undue extra cost to produce a stiffer joint. Subsequent reference to EC3 to determine endplate flexure is suggested, with the bolt force distribution determined from the model.

There are also areas where improvements can be made, especially in the determination of the axis of rotation for the plastic condition. This position was found experimentally from a small selection of results. The rotation position depended on the stiffness of both the compression or tension zones of the joint which, in turn, affects the rotation limit at which the level of moment was selected. A more accurate prediction of this position, which incorporates a more realistic 'global' mechanism, may further increase the accuracy of the joint model.

As a final and important note to this chapter, some restrictions must also be applied to use of the design model. With all joint models developed from experimental work, the model can only be completely valid for the joint geometry tested. In the case of the author's work, where the model is based on a semi-empirical approach and is essentially curve-fitted to experimental data, extrapolation outside the boundaries imposed from the full scale joint tests conducted should be attempted with extreme caution. Table 8.14 below sets out the boundaries within which the tests were conducted.

Characteristic	Limitation
Tension zone bolt cross centres	$0.4 \geq \beta_1 \geq 0.67$
Compression zone endplate width	$0.8 \geq \beta_2 \geq 1.0$
Slenderness range of column wall (face- b_0 and web- h_0)	$31.7 \geq \frac{h_0}{t_0} \geq 12$
	$31.7 \geq \frac{b_0}{t_0} \geq 12$
Joint geometry and overall size	$2.53 \geq \frac{h}{h_0} \geq 0.95$
	M20(8.8) bolts with flowdrill connector
	Maximum column steel grade S355 used

Table 8.14 Restrictions imposed on joint model

Chapter 9

Parametric study of sub-frame behaviour

This chapter investigates the capacity of SHS columns using sub-frames incorporating the moment-rotation characteristics of the actual flowdrill joint tests. Use of the sub-frames enables the restraint conditions experienced in the overall global frame response to be simulated and provides a greatly simplified analysis. This study is only concerned with braced frame construction associated with nominally simply supported beam members and 'simple' flowdrill connections that exhibit a semi-rigid moment-rotation characteristic.

The following sections of the chapter begin with a brief history of column stability and discusses the behaviour of real columns and their design. Further comments address the use of numerical methods in calculating column capacity with a brief overview of the SERVAR program used in the parametric study.

9.1 Brief history of column behaviour and development

In 1759, Leonard Euler established the well known elastic critical buckling load (P_{cr}) for a pin ended, linearly elastic and perfectly straight strut. It was found that strut compressive load capacity was influenced by column length and inertia (2nd moment of area) and was given by the following relationship:-

$$P_{cr} = \frac{\pi^2 EI}{L^2} \qquad \text{.....(9.1)}$$

This elastic critical buckling load, sometimes referred to as the Euler load (P_E) can be rearranged and presented in terms of the column stress, σ_{cr}, by rewriting equation (9.1) in terms of column slenderness (L/r) as

$$\sigma_{cr} = \frac{\pi^2 E}{(L/r)^2} \qquad \text{.....(9.2)}$$

In both of these equations, the load determined considers elastic response to buckling and does not include the onset of yielding. An upper limit for the column is defined by

the squash load (P_{sq}) when the cross section has completely yielded. These two relationships (P_{sq}) and (P_{cr}) can be considered as defining the outer envelope of the column's compressive resistance to load as a function of the overall column slenderness. Figure 9.1(a) shows both the Euler and squash loads.

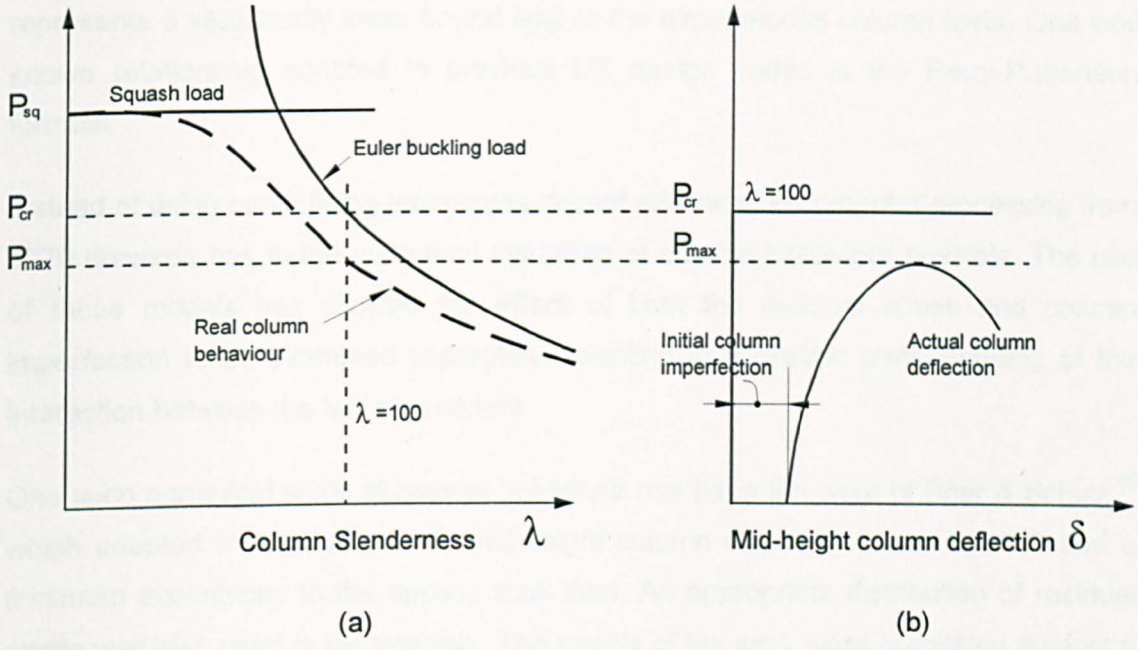

Figure 9.1 Isolated column behaviour

Column failure loads generally conform to these two relationships at low or high slenderness. Columns in the intermediate slenderness range, which covers the majority of real practical columns, usually fail through an interaction of flexural buckling and yielding. This results in a substantial deviation from the theoretical bounds of column behaviour. A plot of real load vs. deflection for such a column is shown in Figure 9.1(b) which represents one of the points on the plot shown in Figure 9.1(a).

9.1.1 Behaviour of real columns

The behaviour of real columns also depends on the initial lack of straightness and residual stresses present in a column. After an open section column is rolled at the steel mill and then allowed to cool, significant stresses are developed within the member through non-uniform thermal contractions. These contractions develop the residual stresses in the cross-section and also result in the member bowing along the full length of the column. When the column is subjected to a compressive load an additional moment is generated at mid height as a direct result of the lack of straightness. The cross section can also begin to yield prematurely from the

unfavourable distribution of residual stresses. Both effects contribute to the inelastic failure of real columns.

In practical codified design it would be usual to account for both of these occurrences by assuming one single initial geometric imperfection which semi-empirically represents a statistically lower bound limit to the experimental column tests. One well known relationship adopted in previous UK design codes is the Perry-Robertson formula.

Instead of using curve fitting techniques, recent advances in computer processing from 1970 onwards has made numerical modelling of column behaviour possible. The use of these models has allowed the effect of both the residual stress and column imperfection to be examined separately, resulting in a greater understanding of the interaction between the two parameters.

One such numerical study of column behaviour has been the work of Beer & Schulz [82] which adopted models with initial mid-height column displacement of $L_o/1000$ and a minimum eccentricity to the applied axial load. An appropriate distribution of residual stress was also used in the analysis. The results of the work were correlated against a background of large full-scale column tests which were the basis of the European column curves. The use of multiple column curves were developed as it was found that capacities were dependent on the type of section and the axis of buckling. The treatment of column stability in this way allows for both the detrimental effects of residual stresses that are more influential in thick flanged sections and also for the effect of buckling axis on column capacity. The European curves have subsequently been adopted for both EC3 and BS5950 design codes, where in the case of the latter an initial imperfection factor η is used with a modified Perry-Robertson formula to closely fit to the European strut curves.

9.1.2 Sub-frame behaviour and column restraint

The behaviour of a column in a sub-frame provides a more complex problem with both the beam stiffness and connection characteristics influencing the column's capacity. This problem was considered by Jones [83], who examined column capacities by using numerical models which incorporated idealised connection stiffness. Subsequent full scale experimental tests on sub-frames comprising of open sections for both 2D and 3D geometries were conducted by Davison [39] and Gibbons [40], respectively, to verify computer programs developed from that of the original Jones program.

The main results of their investigations showed the beneficial effects of 'simple' connections that possess relatively small degrees of restraint which significantly improve column performance. This increase was found to favour the moderately slender column ranges associated with the minor axis buckling of open sections rather than those of low slenderness. Most of the increase in column performance indicated in these previous investigations was shown to be through the beneficial effect of moment shedding at the column head. Moment shedding is a phenomenon which occurs at or near the column collapse load and usually increases column capacity. As the column starts to buckle, the subsequent rotation at the column head will result in one connection loading while the other unloads. The unloading stiffness of the connection enhances column buckling resistance.

The restraint observed by Gibbons [40] from the full scale sub-frame tests, and the results of a separate parametric study, concluded that the beneficial restraint generated by the connection for simple joint details of open sections, will in the majority of cases, outweigh the detrimental effect imposed by the moment transferred. This was indicated by a series of parametric studies where the capacity of a pin ended column computed numerically was divided by the value obtained from a corresponding sub-frame analysis where semi-rigid connections were used. This ratio, has been referred to as the alpha pin factor (α_{pin});

$$\alpha_{pin} = \frac{P_{sr}}{P_{pin}} = \frac{\text{capacity of column in semi-rigid sub frame}}{\text{capacity of isolated pin ended column}} \qquad \text{.....(9.3)}$$

A ratio below unity would indicate that the connection is detrimental to column performance, whereas values greater than unity indicate the restraint of the connection outweighs the detrimental effect of moment transfer. This philosophy of design has been adopted by Gibbons in a 'simplified approach' to column design. Here, the nominal 100mm eccentricity of the connection, used in traditional UK column design, is abandoned when using an effective length ratio of unity, thus dramatically simplifying the design procedure. Additional benefits from use of modest reductions in effective length have also been demonstrated. Further parametric studies by Carr [84] have indicated substantial benefits for the method with open sections, although alpha pin values slightly less than unity were found to occur for some edge columns.

9.2 The parametric study

The author's own parametric study is based on that developed by Gibbons, where use of the alpha pin factor (α_{pin}) provides an indication of the relative merits of each sub-frame configuration. The study was split into two parts. Part 1 of the investigation relates to flowdrill connection details of partial depth endplates, commonly referred to as flexible, whereas Part 2 of the study investigates sub frames which comprise flush endplates. Apart from the difference in connection response, all other details between Part 1 and Part 2 of the study are identical. All the joint characteristics used in this study are selected from actual joint tests. The study was conducted using the SERVAR computer program for the sub-frame analysis. A brief review of the program is presented in the following section.

9.2.1 The SERVAR computer program

SERVAR is a finite element computer program which was developed by Poggi and Zandonini at the Politechnic of Milan and was originally used to analyse two dimensional full scale frames tested by Davison [39]. The program is a 2nd order elastic-plastic frame analysis which accounts for the response of the semi-rigid joint, the spread of yield through the cross-section and the change of geometry in the members and the frame [85]. The program was formulated to consider two dimensional frames using open section members bent in the strong direction. The two dimensional analysis is not a disadvantage as the use of closed formed columns causes in-plane failure i.e. the minor axis failure of open sections (out of plane, three dimensional response) does not occur. The problem of only being able to incorporate open sections is overcome by doubling the web of an equivalent 'I' section to represent the twin walls of the SHS. The distribution of web material in this instance does not affect the overall result or the final column capacity.

The SERVAR program does not incorporate the residual stress pattern of a cross section. Fortunately the residual stresses developed in hot rolled SHS members are small compared to the large stresses which develop within open sections (typically in the order of 0.5fy). The reason for this is that the uniform thickness of the tube and the profile allows more even cooling than open sections. The only residual stress present for weldable hot formed SHS is that caused by the localised welding process during manufacture. When the tube is re-heated and reshaped into its final profile, all the

stress caused by the welding is subsequently reduced to a low level. This is not however the case for cold formed SHS members where the induction welding and cold formed bending of the section induce relatively large residual stresses. The outcome of the different manufacturing processes is that the hot formed sections are designed to the higher strut curve than their cold formed counterparts. All the joint specimens were hot formed SHS members and neglecting residual stresses did not cause any difficulties.

In previous studies [38, 40] which have investigated column capacity, the computer programs have benefited by validation against a background of full scale sub-assemblage tests. Such a validation is not attainable in the current study where only the joint test data are available. An alternative approach was required in which an appropriate initial column imperfection was selected where the capacity of the column predicted by the analysis was compared to that of an equivalent column designed to BS5950 (which is a validated lower bound solution to column test results). The following section describes the selection of the imperfection.

9.2.1.1 Selection of an appropriate initial bow imperfection

In the majority of numerical studies on column behaviour the value used for the initial bow imperfection has been column height over 1000 (L_o/1000). Surveys on actual structures exhibited a maximum mid-height displacement of L_o/1000 and a mean value of L_o/1500 [86]. Subsequent surveys of rectangular sections [87] have revealed smaller imperfections than open sections with values of L_o/3000 to L_o/6500, although the method of manufacture plays an important part in controlling these imperfections and such levels of column straightness cannot always be relied upon. Because of the lack of residual stresses within the SHS section the compressive design of non slender structural hollow sections results in the selection of buckling curve 'a'. As a consequence, Figure 9.2 shows the compressive resistance of the 200x200x8 SHS member designed to BS5950. This is directly compared against the results of a numerical analysis using SERVAR for the same section properties but adopting mid-height displacements of L_o/1000 and L_o/3000, values which represent both the open and closed formed sections.

Figure 9.2 clearly shows the significant difference in column capacities which can be obtained through the selection of the geometric imperfection, especially in the

intermediate column slenderness range of 40 to 120. In this area the maximum difference in column capacity between $L_c/3000$ and $L_c/1000$ is 13%. The difference between $L_c/3000$ and BS5950 is even greater at 23%.

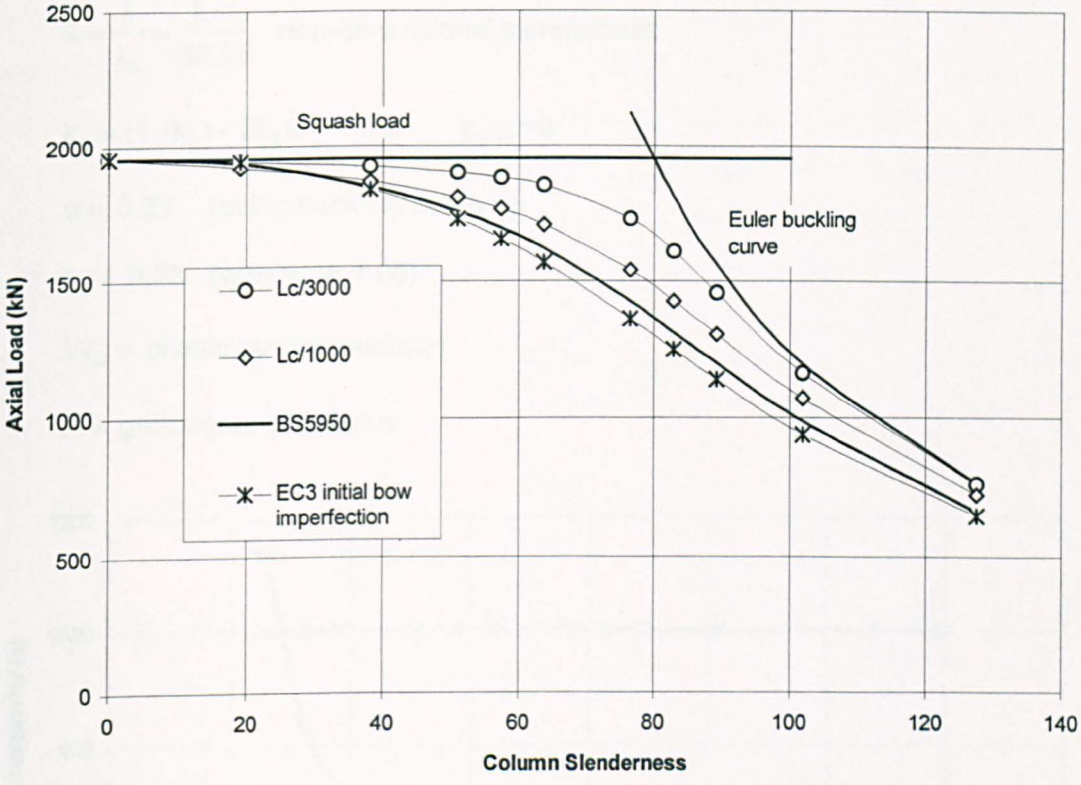

Figure 9.2 *Variation of column capacity dependent on initial column bow imperfection*

Also plotted on Figure 9.2 is the column capacity for the same section but adopting the EC3 equivalent initial bow imperfection ($e_{o,d}$). The equivalent bow imperfection is used within Eurocode 3 to enable 2nd order elasto-plastic analysis programs to be explicitly used in design. Instead of specifying a single constant value based on the column height (L_c), EC3 uses a different approach by varying the initial mid height displacement based on the columns non-dimensional slenderness, buckling curve and sectional properties. The relevant expression which relates to the SHS member is reproduced as follows.

$$e_{o,d} = \alpha(\bar{\lambda} - 0{,}2)k_\gamma W_{pl} / A \qquad \text{(EC3 Figure 5.5.1)} \qquad \text{.....(9.4)}$$

where

$\bar{\lambda} = \dfrac{\lambda}{\lambda_1} = \dfrac{L/i}{93{,}9\varepsilon}$ non-dimensional slenderness

$k_\gamma = (1 - k_\delta) + 2k_\delta \bar{\lambda}$ but $k_\gamma \geq 1{,}0$

$\alpha = 0{,}21$ (using buckling curve a)

$k_\delta = 0{,}23$ (with $\gamma_{M1} = 1{,}05$)

W_{pl} = plastic section modulus

A = gross area of column

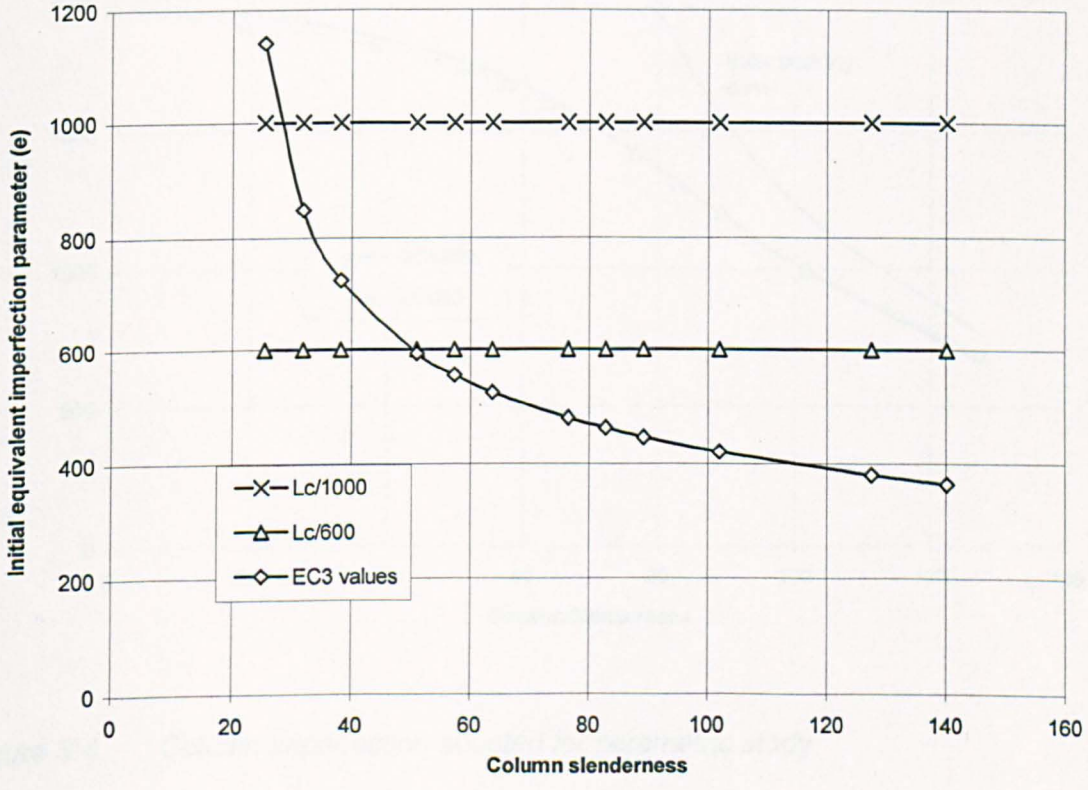

Figure 9.3 *EC3 equivalent initial bow imperfection variation with column slenderness*

Figure 9.3 shows an example of eq(9.4) with the variation of initial bow imperfection against slenderness for the 200x200x8 SHS column. The subsequent column capacity is shown in Figure 9.2 and provides a slightly lower value than that of BS5950. The lower column capacity obtained using EC3 reflects the use of higher partial material safety factor for steel. The apparent advantage of BS5950 is then curtailed by adopting

higher partial load factors, which brings the capacities given by the two codes closer together. The use of EC3 variable column imperfection in this way allows column capacity to be calculated directly from numerical methods of analysis.

The use of a variable imperfection, however good the correlation, causes an increase in complexity. In the view of the author, the added accuracy does not warrant this complexity and it is for this reason that a single value of $L_c/600$ is adopted in the study. This value has been derived from a trial and error assessment as providing a reasonable fit to the BS5950 compressive buckling curve. The two plots are shown in Figure 9.4, where the difference between the two curves is less than 2%

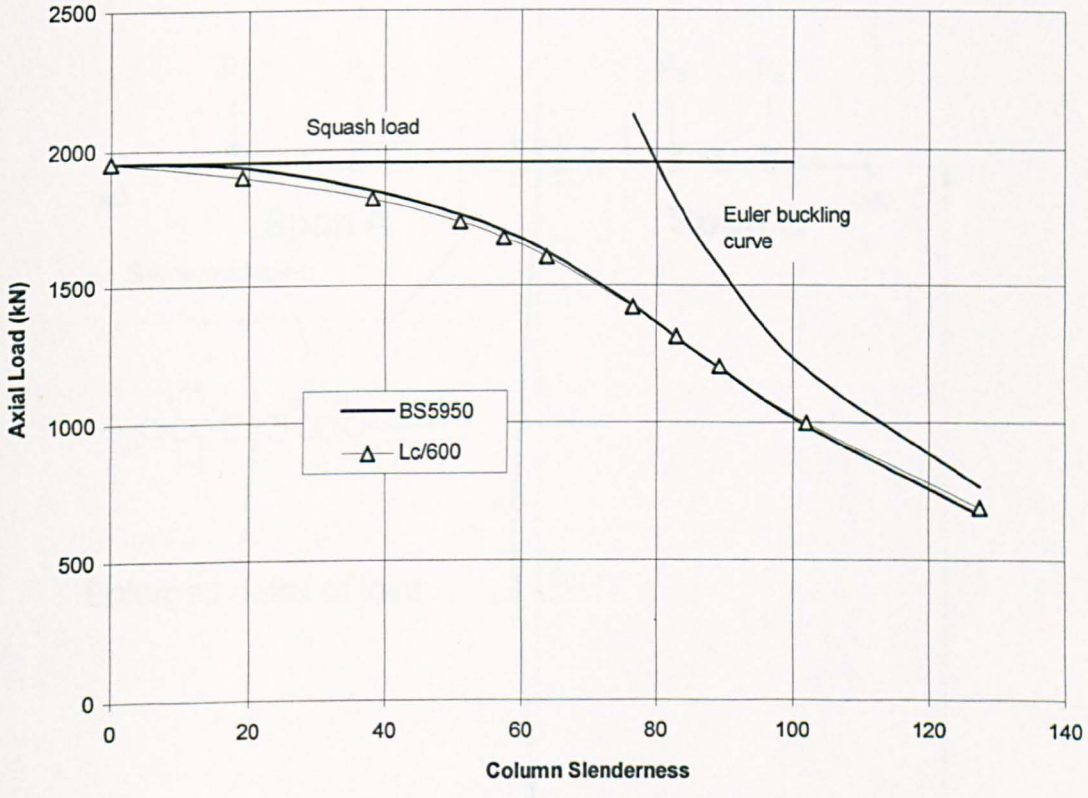

Figure 9.4 Column imperfection adopted for parametric study

9.2.2 Sub-frame parameters

The sub-frame geometry used in the study has been based around a lower ground floor storey column, with beams connected either side at first floor level. Figure 9.5 shows the nodal positions of an internal column configuration which represents the numerical model adopted in the SERVAR computer program. Both beams connected to the column use semi-rigid elements that act at 100mm from the face. A rigid link

between these elements and the centre line of the column represents the finite column depth. In the sub-frame analysis both the edge and internal columns have been allowed for in the study. The edge column representing the more severe case of disturbing moment to be applied to the column. The column has been stopped at first floor level. The presence of column continuity would have represented a more favourable condition.

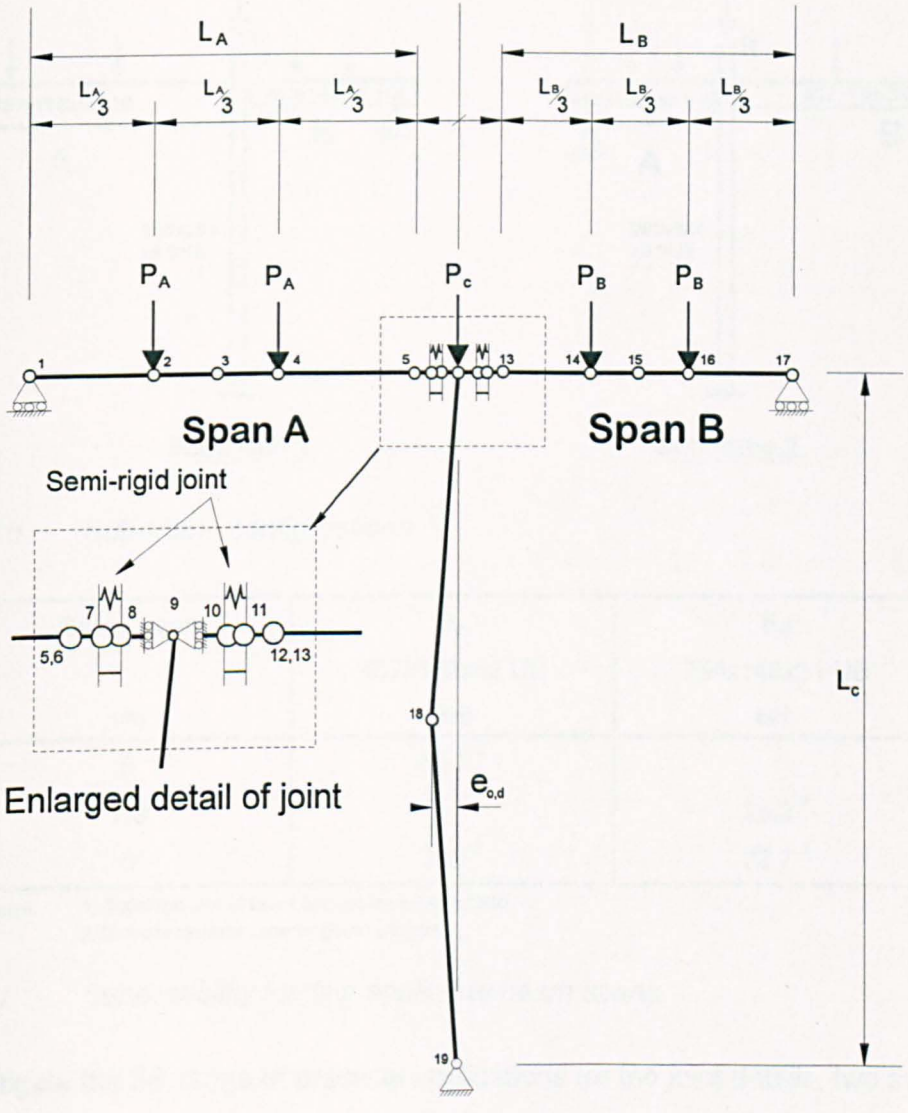

Figure 9.5 Sub-frame geometry and nodal positions

Section sizes for the study were identical to those of the joint tests. To reduce the number of sub-frame combinations, only the 200x200x 8 SHS column was analysed with two beam sizes of 457x152x52 UB and 254x146x31 UB. Both the partial depth and flush endplates have been used for each beam which represented the greatest variation in connection stiffness attained in the joint tests under the category of 'simple' connections. The column yield strength of 318 N/mm^2 and a Young's modulus of 205

kN/mm^2 were obtained from actual tensile coupon tests from the joint specimens. A yield strength for both beam members was based on a nominal 275 N/mm^2, as the beam was not expected to yield with the level of serviceability loading applied.

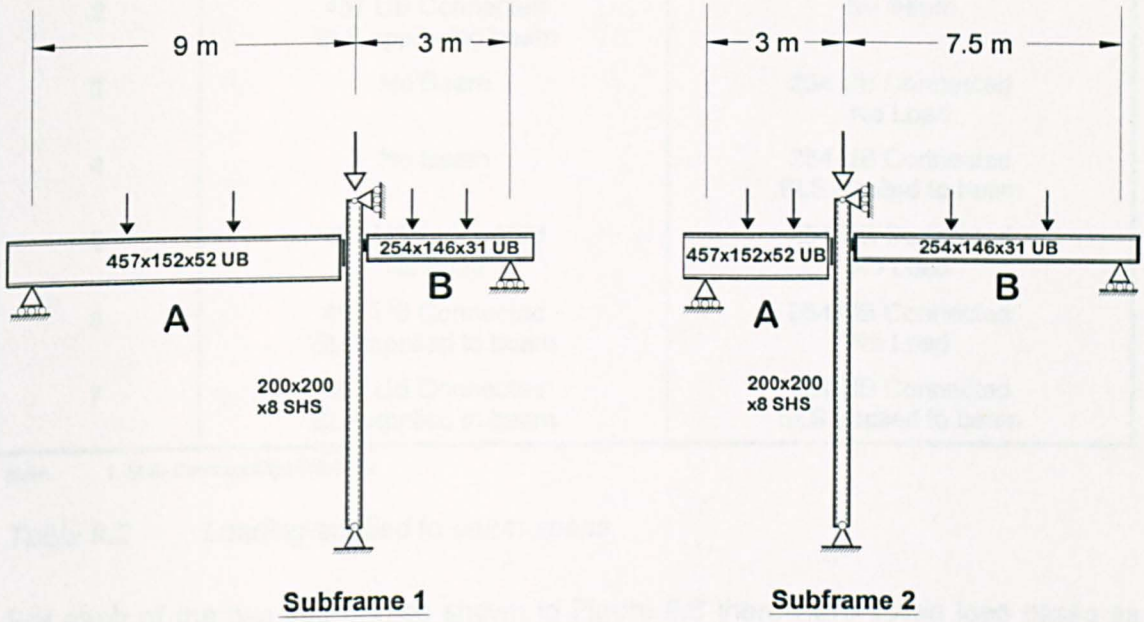

Figure 9.6 Sub-frame configurations

Beam span (m)	P_A 457x152x52 UB (kN)	P_B 254x146x31 UB (kN)
9	66.7 [2]	
7.5		25.2 [1]
3	200 [2]	72.7 [2]

Notes: 1. Deflection limit of beam governs load, (span/360)
2. Ultimate moment capacity governs loading.

Table 9.1 Serviceability loading applied to beam spans.

To investigate the full range of practical applications for the joint details, two sub-frame configurations were used as shown in Figure 9.6. All of the beam members were loaded by two point loads applied at third points along the member. The magnitudes of the point loads were determined from either the ultimate moment capacity of the beam or the maximum deflection limit at serviceability limit state, assuming the beams were simply supported. Table 9.1 indicates the point loads applied. In all the sub-frame analyses conducted, the serviceability load was applied in graduated increments. When the beam had attained its full serviceability load, then the column axial load was applied incrementally until ultimate failure of the SHS column.

Load case number	Span 'A'	Span 'B'
1	457 UB Connected No Load	No Beam
2	457 UB Connected SLS applied to beam	No Beam
3	No Beam	254 UB Connected No Load
4	No Beam	254 UB Connected SLS applied to beam
5	457 UB Connected No Load	254 UB Connected No Load
6	457 UB Connected SLS applied to beam	254 UB Connected No Load
7	457 UB Connected SLS applied to beam	254 UB Connected SLS applied to beam

Note: 1. SLS- Serviceability Limit State.

Table 9.2 Loading applied to beam spans.

For each of the two sub-frames shown in Figure 9.6 there were seven load cases as indicated in Table 9.2. The first four load cases represent edge sub-frame configurations where one of the beam spans shown in Figure 9.6 was omitted. The loading state of the beams were either fully loaded or unloaded as seen from the load cases noted in Table 9.2. The internal column configuration was considered with load cases 5 to 7.

As well as the two sub-frames and seven load cases mentioned, the study also included two column lengths of 4m and 6.5m. The two storey heights represented the two typical cases. The column's capacity for the pin ended situation for both the 4m and 6.5 m column length (P_{pin}) with mid-height displacement of $L_c/600$, are indicated in Table 9.3. These values were used for calculating the alpha pin ratios of eq(9.3).

Column length (L_c) (m)	P_{pin} (kN)
4.0	1728
6.5	1300

Table 9.3 Capacity for pin ended column

9.3 PART 1: Flexible connections

The first part of the investigation, using the sub-frame and loading cases described in section 9.2.1 related to partial depth endplates i.e. flexible connections. These sub-frames incorporated the moment-rotation characteristics of joint test nos. 1 and 9. Figure 9.7 below shows both the joint details and the multi-linear representation required for SERVAR superimposed onto the actual curves.

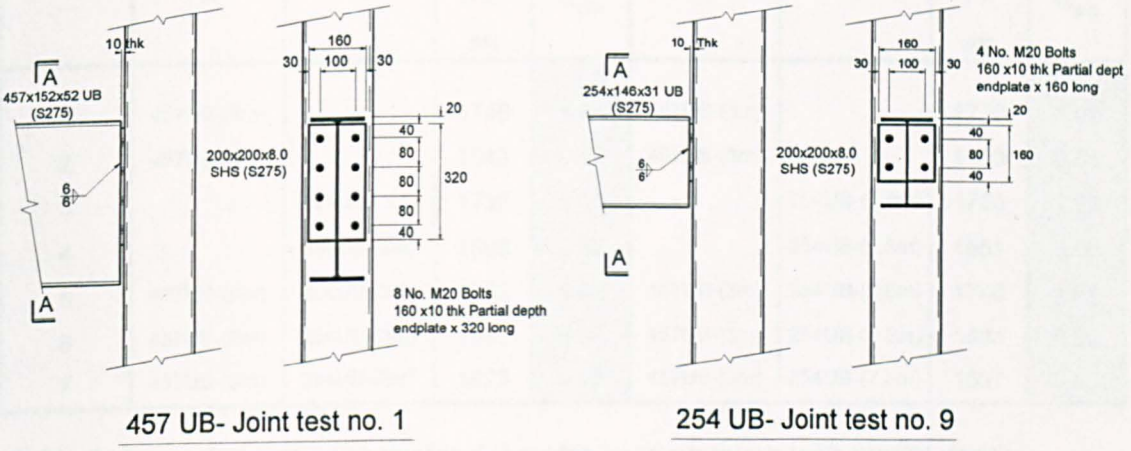

457 UB- Joint test no. 1

254 UB- Joint test no. 9

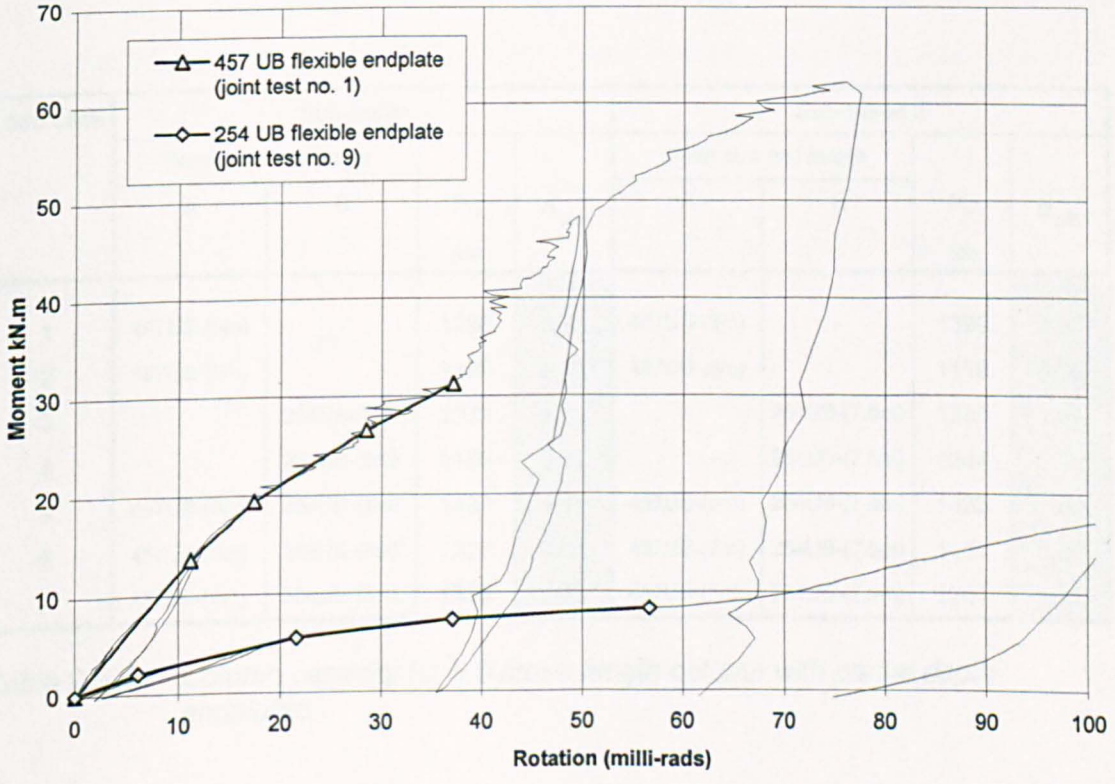

Figure 9.7 Details of moment-rotation characteristics for flexible endplates

Table 9.4 presents the column capacities P_{sr} of the sub frame analysis for the 4m column length member. The capacity of each column has been divided by the respective pin ended capacity resulting in the alpha pin factor (α_{pin}). Table 9.5 presents a similar set of sub-frame configurations, but now adopting the 6.5m long column.

Load case	Sub-frame 1				Sub-frame 2			
	Beam size and length				Beam size and length			
	A	B	P_{sr} (kN)	α_{pin}	A	B	P_{sr} (kN)	α_{pin}
1	457UB-(9m)	-	1749	**1.01**	457UB-(3m)	-	1739	**1.01**
2	457UB-(9m)		1543	0.89	457UB-(3m)		1463	0.85
3		254UB-(3m)	1732	**1.00**		254UB-(7.5m)	1735	**1.00**
4		254UB-(3m)	1593	0.92		254UB-(7.5m)	1651	0.96
5	457UB-(9m)	254UB-(3m)	1762	**1.02**	457UB-(3m)	254UB-(7.5m)	1748	**1.01**
6	457UB-(9m)	254UB-(3m)	1561	0.90	457UB-(3m)	254UB-(7.5m)	1484	0.86
7	457UB-(9m)	254UB-(3m)	1673	0.97	457UB-(3m)	254UB-(7.5m)	1537	0.89

Table 9.4 *Column capacity for 4.0 metre length column with partial depth endplates*

Load case	Sub-frame 1				Sub-frame 2			
	Beam size and length				Beam size and length			
	A	B	P_{sr} (kN)	α_{pin}	A	B	P_{sr} (kN)	α_{pin}
1	457UB-(9m)	-	1286	**0.99**	457UB-(3m)	-	1399	**1.08**
2	457UB-(9m)		1199	0.92	457UB-(3m)		1119	0.86
3		254UB-(3m)	1332	**1.03**		254UB-(7.5m)	1333	**1.03**
4		254UB-(3m)	1186	0.91		254UB-(7.5m)	1244	0.96
5	457UB-(9m)	254UB-(3m)	1437	**1.11**	457UB-(3m)	254UB-(7.5m)	1422	**1.09**
6	457UB-(9m)	254UB-(3m)	1227	0.94	457UB-(3m)	254UB-(7.5m)	1151	0.89
7	457UB-(9m)	254UB-(3m)	1336	1.03	457UB-(3m)	254UB-(7.5m)	1201	0.92

Table 9.5 *Column capacity for 6.5 metre length column with partial depth endplates*

9.3.1 Discussion of results

As seen from Table 9.4, the sub-frames where no load was applied to the beams (load cases 1,3,5) resulted in alpha pin values approaching unity. In these cases the joint had very little effect in restraining the column. In instances where the column increased in length to 6.5 m the same load cases shown in Table 9.5 result in slightly higher alpha pin values. The values were also shown to increase with subsequent increases in beam stiffness.

In the sub-frames which introduced a serviceability load to the beam (load cases 2, 4, 6 and 7), the resulting alpha pin values were less than unity, indicating that the restraint of the joint did not outweigh the detrimental effect of the connections disturbing moment. A minimum alpha pin value of 0.85 was recorded. Interestingly, the lower the alpha pin value was seen to correspond to ever increasing severity from the out of balance moment induced at the column head. This was observed directly from load case 6, in which the internal column with only one beam loaded resulted in alpha pin ratios lower than unity. In cases where both the beam spans were loaded (load case 7) an alpha pin value greater than unity was apparent. In general, a similar observed pattern of values to the unloaded beam cases were shown for the loaded beam cases, where increasing the column slenderness and beam stiffness again resulted in ever increasing alpha-pin values.

From the analysis of the sub-frames, it is apparent that the partial depth endplate has a detrimental effect on column performance in instances where substantial out of balance moments are present. It was shown that the restraint afforded by the connection and beam stiffness, indicated by the low alpha pin values, correspond to effective length factors approaching that of the system length.

9.4 PART 2: Flush endplate connections

Part 2 of the study investigates the effect of the flush endplates in the sub-frames. The sub-frame configurations used were identical to those of the previous analyse, except for using the moment-rotation characteristics of joint test nos. 2 and 10 in the analysis. Figure 9.8 shows the two joint details and their multi-linear representation used in the program superimposed onto their respective curves.

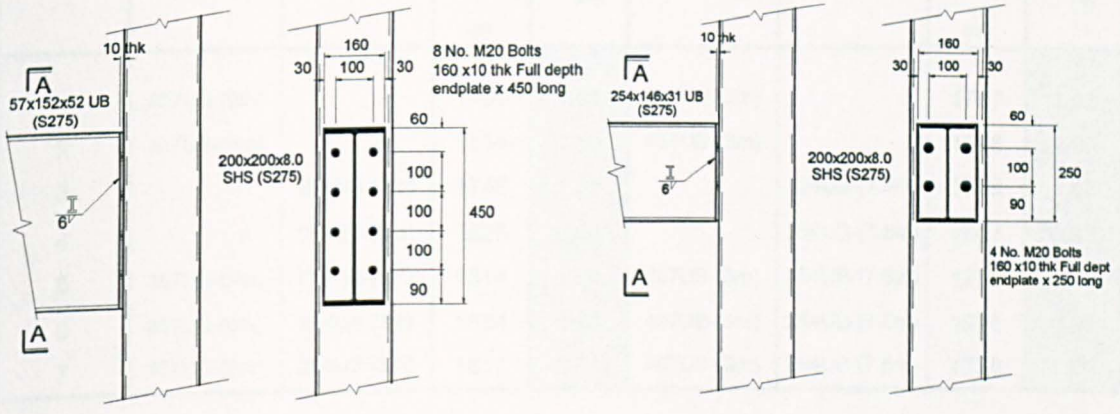

457 UB- Joint test no. 2

254 UB- Joint test no. 10

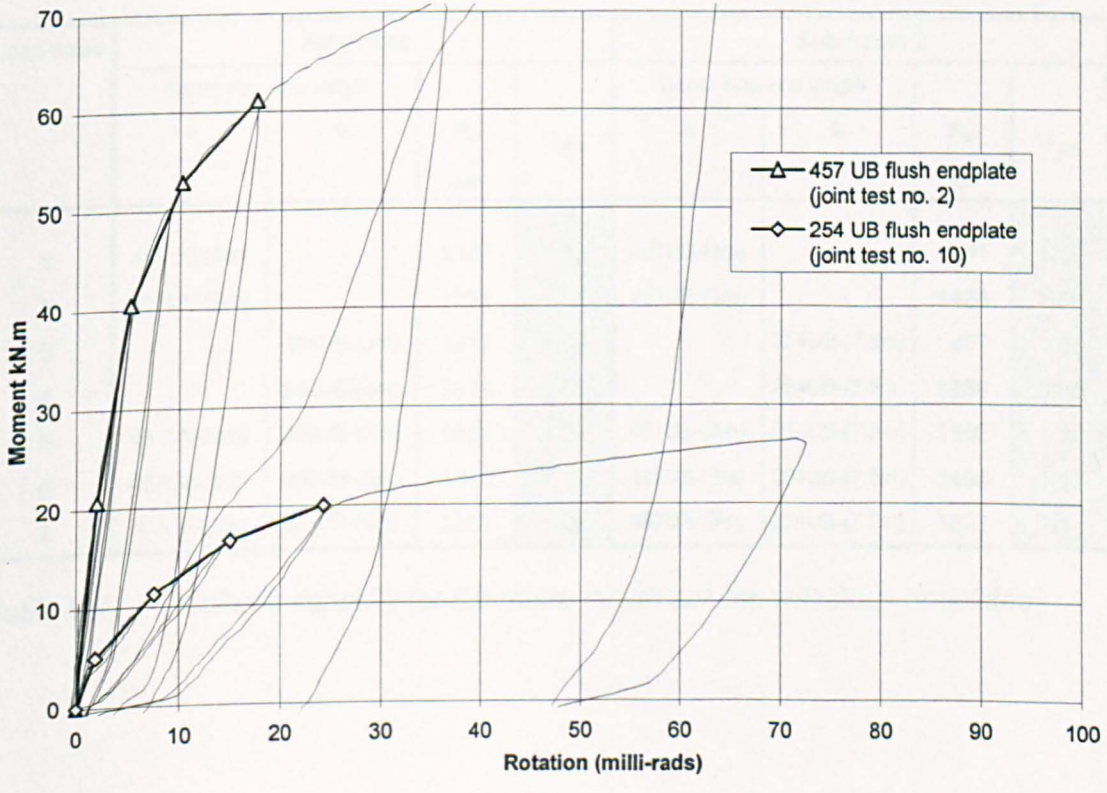

Figure 9.8 Details of moment-rotation characteristics for flush endplates

Tables 9.6 and 9.7 present the results of the analysis for both the 4m and 6.5m column lengths respectively. The alpha pin values shown highlighted are the column capacity divided by the capacity of the pin ended values determined previously and noted in Table 9.3.

Load case	Sub-frame 1				Sub-frame 2			
	Beam size and length		P_{sr} (kN)	α_{pin}	Beam size and length		P_{sr} (kN)	α_{pin}
	A	B			A	B		
1	457UB-(9m)	-	1790	**1.04**	457UB-(3m)	-	1767	**1.02**
2	457UB-(9m)		1514	0.88	457UB-(3m)		1648	0.95
3		254UB-(3m)	1746	**1.01**		254UB-(7.5m)	1755	**1.02**
4		254UB-(3m)	1625	0.94		254UB-(7.5m)	1607	0.93
5	457UB-(9m)	254UB-(3m)	1814	**1.05**	457UB-(3m)	254UB-(7.5m)	1781	**1.03**
6	457UB-(9m)	254UB-(3m)	1554	0.90	457UB-(3m)	254UB-(7.5m)	1673	0.97
7	457UB-(9m)	254UB-(3m)	1617	0.94	457UB-(3m)	254UB-(7.5m)	1728	1.00

Table 9.6 Column capacity for 4.0 metre length column with flush endplates

Load case	Sub-frame 1				Sub-frame 2			
	Beam size and length		P_{sr} (kN)	α_{pin}	Beam size and length		P_{sr} (kN)	α_{pin}
	A	B			A	B		
1	457UB-(9m)	-	1461	**1.12**	457UB-(3m)	-	1541	**1.19**
2	457UB-(9m)		1268	0.98	457UB-(3m)		1406	1.08
3		254UB-(3m)	1412	**1.09**		254UB-(7.5m)	1407	**1.08**
4		254UB-(3m)	1274	0.98		254UB-(7.5m)	1268	0.98
5	457UB-(9m)	254UB-(3m)	1601	**1.23**	457UB-(3m)	254UB-(7.5m)	1560	**1.20**
6	457UB-(9m)	254UB-(3m)	1315	1.01	457UB-(3m)	254UB-(7.5m)	1458	1.12
7	457UB-(9m)	254UB-(3m)	1381	1.06	457UB-(3m)	254UB-(7.5m)	1522	1.17

Table 9.7 Column capacity for 6.5 metre length column with flush endplates

9.4.1 Discussion of results

The analysis of column capacities for the flush endplates presents an identical pattern of results to that of the partial depth endplates reported in 9.3.1. The only difference being increased column capacities and subsequent alpha pin values.

For the load cases where the beams are not loaded (load cases 1, 3 and 5), the restraint afforded by the connection to the 4m length of column resulted in alpha pin values above unity with a maximum value of 1.05 recorded. For column lengths of 6.5m the alpha pin value was increased to 1.23, which results in significant increase in column strength for higher ranges of column slenderness.

When the beams are loaded then the alpha pin values are generally less than unity for the 4m column length with a minimum value of 0.88 observed for load case 2. The factors are improved when the 6.5m long column is analysed resulting in minimum and maximum factors of 0.98 and 1.17, respectively. This is the only situation where the connection restraint has been shown to outweigh the detrimental effect imposed by the connection moment. However, the advantages shown for the 6.5m column is not a realistic column length. The 4m column length is more representative of practical storey heights.

9.4.2 Overall comments on the behaviour of subframes using both partial depth and flush endplates

The parametric study presented in this chapter was developed in a relatively short timescale to examine the ways in which flowdrill connections influence column subframe behaviour. It was observed during the study that unexpected low alpha pin values were encountered for the edge column configurations. The reduction of the column's axial load in these instances was shown to reflect cases where the column slenderness was stocky and moment had been applied at the column head. The most onerous subframe analysed was the result of the 457UB edge beam connected to a 4m long column with a partial depth endplate. This subframe resulted in an alpha pin value of 0.85. The replacement of the partial depth endplate with the flush endplate increased the column's capacity to an alpha pin ratio of 0.95.

The low alpha pin values found from this study have contradicted those of previous studies using open section subframes, where the limited restraint afforded by simple

connections was shown to be beneficial to column design. A possible reason for this apparent difference can be explained by the type of section used in the studies. The SHS column will, as a general rule, result in a more structurally efficient design, presenting column sections that are less slender than their open section equivalents. It was noticed in previous studies that the beneficial effect of the connection restraint has less effect on the stocky column capacity [83] . The results of these previous studies reflect the findings shown in the author's own study. However the increased severity of the results observed in the author's own study causes some concern about the reliability of the output, considering the limited time available to fully investigate the results.

Another possible reason for the greater reduction observed in the column capacity may have been the mode of the column's failure and the connection detail adopted. The connections used in the subframe analysis can be considered as significantly more flexible than their open section equivalents. The amount of restraint generated by either the partial depth or flush endplate is negligible, as observed from the modest increases in column capacity. Similarly the loads applied to the beams were substantially greater than those assumed for the previous studies. In some instances the loads which were applied to the 457UB, spanning 3m, were unrepresentative of those occurring in practice. When the beam's shear reaction is applied to the column's face, a substantial 'out of balance' moment is applied to the column edge subframes. These effects, combined with the stocky column, induce limited rotation at the column head which is unlikely to deform by appreciable amounts to enable sufficient restraint to be mobilised from the connection. The column is therefore more likely to fail from plasticity than from instability. Column failure in all the subframes examined was associated with plasticity occurring at mid-height of the column.

When comparing directly the two different connection details, it is apparent that the unloaded beam cases for the flush endplates relating to the stocky 4m column results in only a small percentage increase in column capacity when compared to that of the partial depth endplate; the restraint generated from the connection is limited. The column in these instances could realistically be assumed pinned ended and designed with an effective length of $1.0xL_c$. However, traditional simple design for the column often assumes that the flush endplate connection provides some rotational restraint to allow an effective length of $0.85xL_c$ to be adopted. Clearly, there is an error in this assumption for relatively stocky column sections.

Column design also assumes that the end reaction of an assumed simply supported beam is applied at 100mm from the face of the column. Thus, a nominal moment is applied to the column head to account for connection rigidity. Although the results are not presented, it was observed during the sub-frame analysis that actual moments varied depending on the beam end rotations. For relatively stiff beams of short span the end rotations were limited and smaller moments were applied to the column head than that assumed from traditional design. An opposite situation existed for beams with large end rotations where substantially more moment was applied than that assumed by traditional design. These observations were with a comparison of moments at the centre line of the column at applied service loading. In all the load cases analysed, the column moment always reached a maximum at serviceability level. As the column began to load, the moment reduced through the direct action of moment shedding at the column head.

Both the observations of column restraint and moment transferred at the joint, have in the past been linked to connection restraint, and more often the type of connection details. In this study, two very different connections have been used at the opposite ends of the connection stiffness spectrum. Current arguments for the flexible connection have been that the detail best simulates the condition of the pin and is therefore suited to simple construction. However, use of the flush endplate is widespread and sometimes frowned upon when used as a direct replacement for the flexible endplate. It would appear from the results that using the flush endplate presents higher and more beneficial results than the flexible endplate in all situations when the column is designed with identical effective lengths. It is the author's opinion that there is no justification, based on these results, to dismiss the flush endplate when used for simple construction on the grounds that its stiffness is detrimental or damaging to the structure's performance.

From this study, a conservative column design would assume an effective length equal to its system length. It would appear that any future studies should concentrate on a procedure for calculating the actual moment at the column head, using the joint model developed in the previous chapter. Further studies can be conducted with slender column sections, although the nature of SHS column design generally results in stocky sections, indicating that there is little to be gained from a reduced effective length, and possibly a more accurate prediction of column moment considering the effects of moment shedding may present more accurate assessment of column design.

9.5 Chapter summary

A series of computer sub-frame analyse using real connection response has been performed to examine the performance of the column member. All the sub-frames represented typical section sizes and frame configurations. The results of the study showed that;

1. The flush endplate had distinct advantages over partial depth endplates with regard to column capacity.

2. Some alpha pin factors were less than unity, indicating that the restraint provided to the column did not outweigh the detrimental effect of moment being transferred into the column. This is at variance with the extensive studies on open section columns and requires more detailed investigation than this project has provided.

3. Considering the timescale of the study, it would be prudent to accept that there may be some discrepancies in the final results, until a more comprehensive study can be undertaken. Emphasise of research should be directed towards the moment applied at the joint, and the effect which this may cause to stocky columns.

Chapter 10

Economic comparison of tubular columns

Weight for weight a tubular column is more expensive than an open rolled section but it is structural more efficient. The difficulty of the fabrication of joints has been a further disincentive to the use of tubular columns. Before commencing the joint tests an economic comparison was conducted to assess the economics of using tubular columns.

10.1 Column comparison

A previous economic investigation comparing the use of tubular and open section columns has been conducted by the SCI [88]. The comparison was based on the case of the braced internal column taking no account of the out of balance moments generated from either edge columns or dissimilar beam loads. The column was also assumed to be six storeys high and subjected to axial loads applied by beam members of either six or twelve metre spans. Column size was determined at three positions. The survey conducted by the SCI found advantages in using tubular columns but was limited by taking no account of either the building geometry or the type of frame.

To rectify this deficiency, an economic comparison was constructed using an imaginary low rise multi-storey building which modelled a typical UK office type development. The comparison considered the whole building by including both internal columns subjected to pure axial load and also edge columns. The comparison also accounted for the different design assumptions commonly used for frame design, which included the following;

(1) Braced construction; horizontal wind loads being resisted by strong points such as concrete lift shafts, bracing, masonry shear walls etc.

(2) Unbraced construction in the major axis direction- braced in the minor axis direction; horizontal loads being resisted by frame action in the major axis and strong points similar to (1) being provided in the minor axis direction.

(3) Unbraced construction about both axes of the frame; horizontal loads resisted by frame action in both the major and minor axes of the column.

Under these three categories of frame design the column members were designed either as open-sections, SHS or concrete filled composite SHS using current conventional UK practice.

10.2 Selection of an appropriate building

To aid in the development of building geometry, a survey[89] indicated that 77% of multi-storey office floor area during the period of 1993 was attributed to two, three and four storey buildings. Of that total, steel frames accounted for three-quarters of the two storey market and over half of the three to four stories. With the majority of buildings typically less than four stories, it was considered appropriate to restrict the economic assessment to low rise construction of less than four storeys. In this section, the term low-rise multi-storey construction, relates to buildings of less than four storeys.

An appropriate building for the author's own survey therefore needed to be selected from a two, three or four storey geometry. For two storey buildings, UK national building regulations would require that the column members have a half hour fire resistance, which compares to the one hour fire resistance for three stories. A half hour fire rating would give an unfair advantage to the composite designed tubular column which would require no special protection to attain this level of fire resistance. In the case of the four storey building, then sway deflection would be the design criteria and would provide a distorted comparison between braced and unbraced construction. As a compromise, a building having three storeys was selected. Figures 10.1 and 10.2 show the overall plan layout and the elevation of the building respectively.

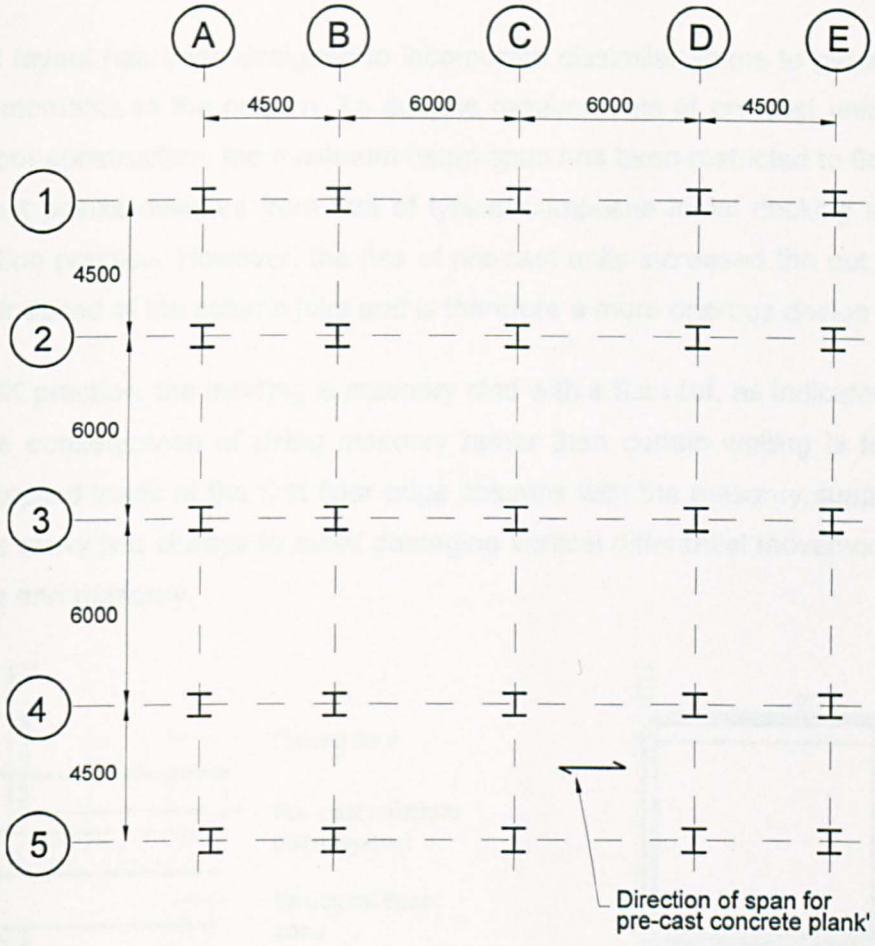

Figure 10.1 Plan layout of building columns

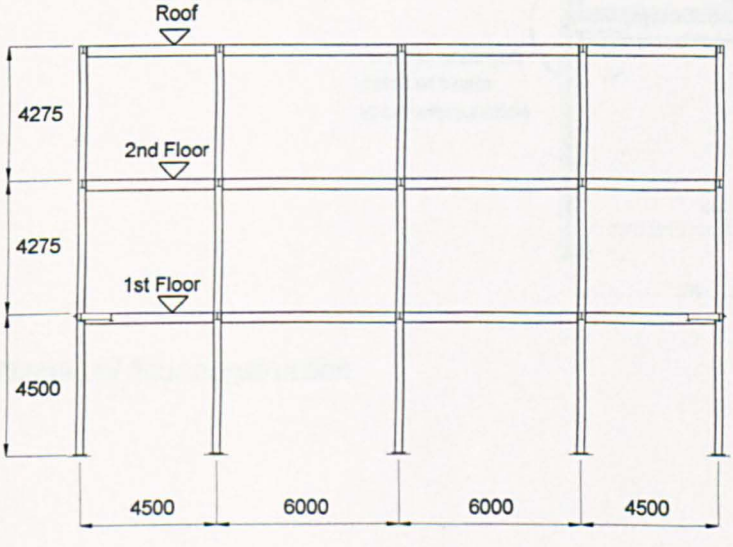

Figure 10.2 Elevation of steel frame along grid line 'C'

The plan layout has been designed to incorporate dissimilar spans to generate out of balance moments to the column. To suit the requirements of pre-cast units specified for the floor construction, the maximum beam span has been restricted to 6m. The use of pre-cast planks deviates from that of typical composite metal decking used in UK construction practice. However, the use of pre-cast units increased the out of balance moment induced at the column joint and is therefore a more onerous design criterion.

To suit UK practice, the building is masonry clad with a flat roof, as indicated in Figure 10.3. The consequence of using masonry rather than curtain walling is to generate greater applied loads at the first floor edge columns with the masonry supported from the frame every two storeys to avoid damaging vertical differential movement between the frame and masonry.

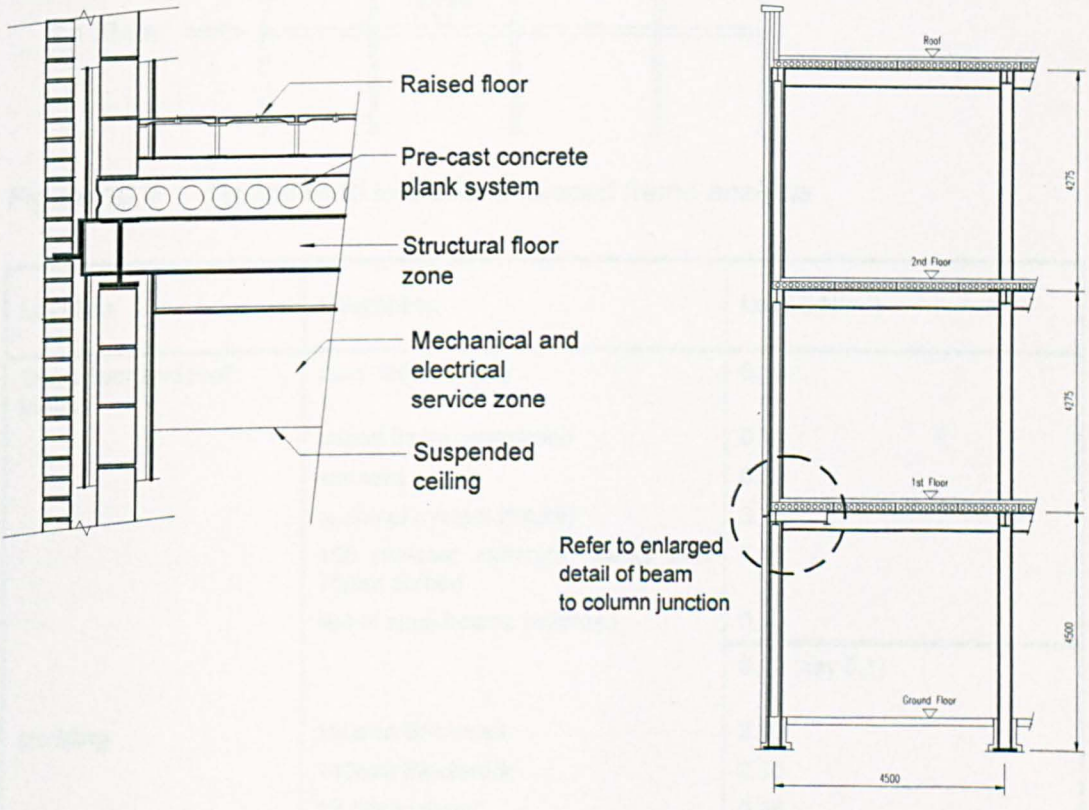

Figure 10.3 Details of floor construction

10.3 Applied Loading

All imposed and dead loadings are derived from BS6399: part 1 [90]. A summary and break down of actual floor loads is presented in Table 10.1.

A wind pressure coefficient derived from CP3:Chapter V: Part 2:1972 [91] is used which represents a building situated on the outskirts of Sheffield. The floor in this case acts as a stiff plate distributing the wind loads as shown in Figure 10.4.

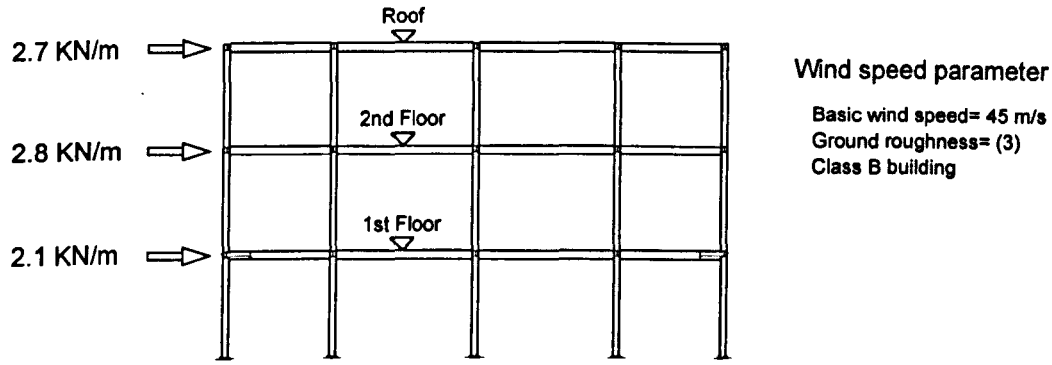

Figure 10.4 Typical wind loads for unbraced frame analysis

Location	Description	Load (kN/m^2)
Dead floor and roof loads	suspended ceiling	0.10
	raised floor construction	0.15
	services	0.30
	sprinkler system (future)	0.10
	150 pre-cast concrete planks with 75mm screed	4.13
	swt of steel beams (approx.)	0.35
		5.13 (say 5.1)
cladding	100mm Brickwork	2.00
	140mm Blockwork	2.80
	12.5mm plaster	0.25
		5.05 per Wall area (say 5.1)
Imposed floor loads	office load	4.0
	partition loading	1.0
		5.0
Imposed roof load	Maintenance and access only	1.5
		1.5

Table 10. 1 Summary of applied floor and cladding used

10.4 Frame design

A different structural design was required for the three cases of braced and unbraced frames mentioned at the beginning of the chapter. All open and closed formed sections were designed to BS5950:Part 1:1990 [78], with the composite SHS designed to the recommendations of the British Steel publication 'Design manual for concrete filled columns' [92]. The member design for each frame, either braced or unbraced, assumed a constant section size throughout the height of the building. The maximum length of tubular columns from the steel mill is 14.6 metres which accommodates the three storeys of the building without the added expense of introducing a splice detail.

For the braced frame an effective length for the columns was taken to be $1.0xL_c$. A reduced effective length which allowed for connection restraint was not used. All steelwork was designed with S355 grade of steel and grade C40 concrete for the SHS concrete filled columns. Typical section sizes designed for the 'braced' frame are shown for grids A-B/1-3 in Figure 10.5.

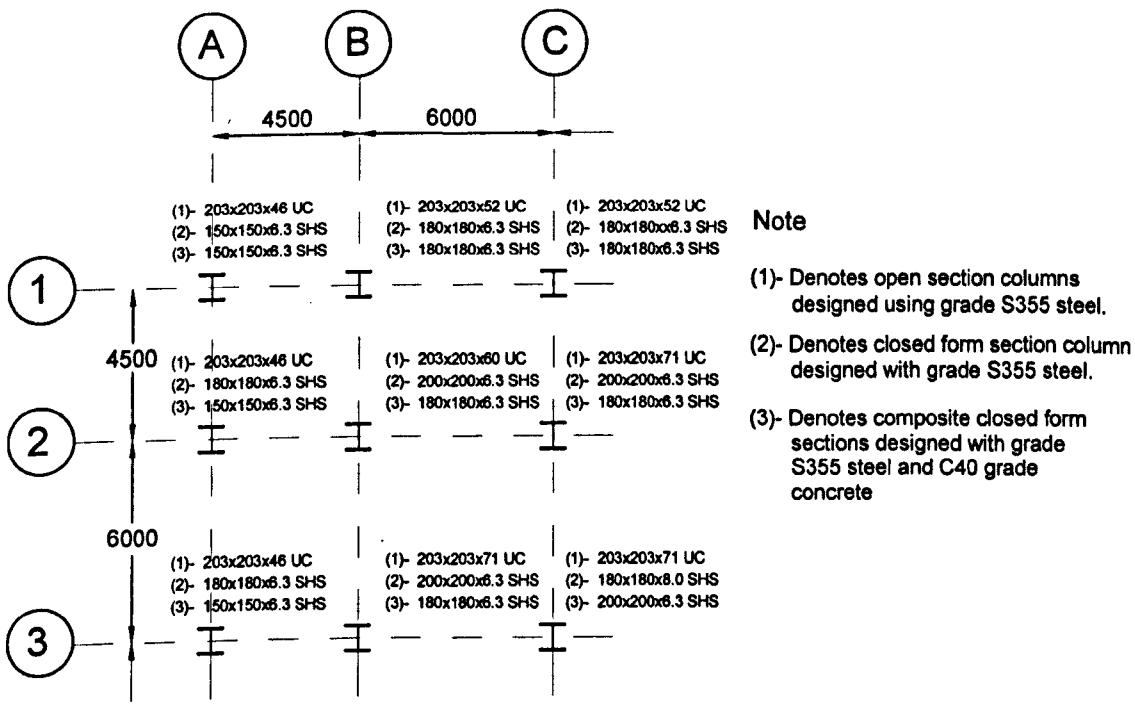

Figure 10.5 Column member sizes for BRACED frame construction

The design of the unbraced frames used the 'Wind moment method' as documented in SCI publication by Anderson et al [93]. This method assumes that the beams are pinned for gravity load but rigid when lateral loads are applied. This particular method has been used over a number of years as a simplified rigid design for unbraced frames.

The origin of such an analysis is empirical and is not a true semi-rigid design even though some justification is presented [93]. However over the years it has provided safe structures for frames less than eight storeys and is a proven design method.

The wind moment method requires the column to be designed for an effective length of $1.5xL_c$ in the plane of the frame. This value is used to allow for the P-delta effect. Again the value is empirical and known to be safe. Within BS5950 [78] guidance is also provided for braced semi-rigid frames rather than unbraced frames. The code suggests that a restraint moment of '10' percent of the maximum beam moment be applied at the connection. This clause together with the adoption of patterned loading and a beam reaction assumed at 100mm eccentricity from the face of the column is recommended by Anderson et al. [93]. The design moments applied to the column partly offset the problem of the column being under designed and beams overdesigned.

The grade of steel adopted in the calculations was grade S275. Figure 10.6 indicates the calculated section sizes from the frame analysis.

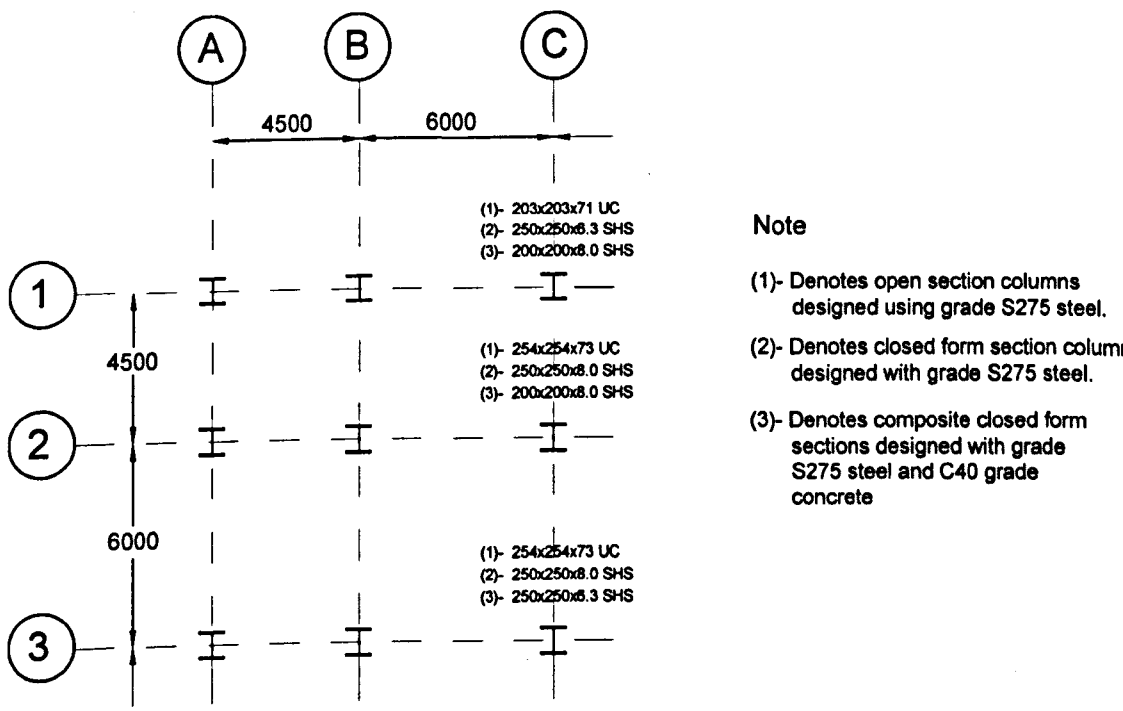

Figure 10.6 Column sizes for UNBRACED frame about the MAJOR axis, BRACED about the MINOR axis

The application of the wind moment method is only recommended for unbraced frames about the major axis of the column [93] as the stiffness developed from minor axis beam to column connections is considerably less than that of the major axis without introducing stiffening. Such a restriction to the SHS appears unjustified as the columns exhibit equal structural performance about both axes. For this reason the method has been applied to a frame unbraced about both axes of the SHS column and for comparison purposes 'only' applied to the open section minor axis assuming appropriate stiffening at the beam-to-column connection. Figure 10.7 presents the calculated section sizes.

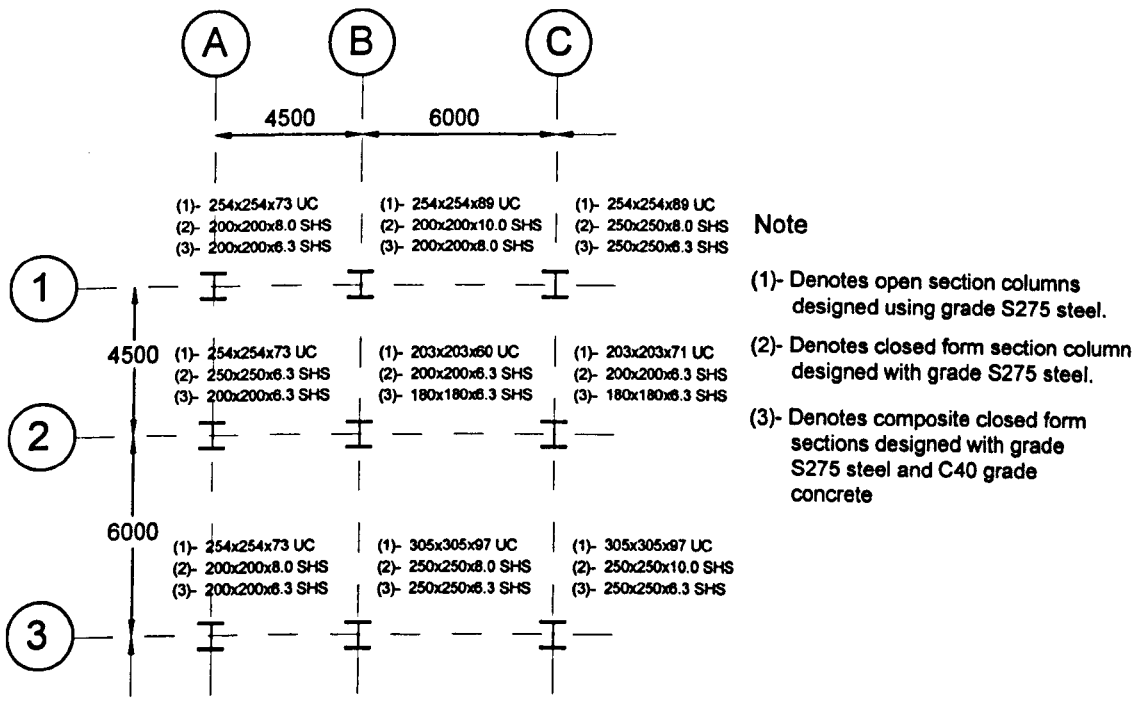

Figure 10.7 Column member sizes for UNBRACED construction in both directions

Recommendations for the design of unbraced frames also require the frame to be checked for sway deflection. An elastic analysis is performed on the frame assuming the connections are rigid. To allow for the semi-rigid nature of the joint the deflections are arbitrarily increased by 50 percent [93]. The deflection should not exceed the storey height divided by 300. The results of the elastic analysis performed on both the member sizes adopted for grid line 'C' in Figure 10.6 and also grid line '3' in Figure 10.7 are presented in Table 10.2.

Storey	UC		SHS		COMPOSITE SHS	
	Major axis deflection					
Roof	1/1359	pass	1/1019	pass	1/1019	pass
2nd	1/921	pass	1/607	pass	1/582	pass
1st	1/1000	pass	1/545	pass	1/536	pass
	Minor axis deflection					
Roof	1/519	pass	1/519	pass	1/528	pass
2nd	1/288	fail	1/294	fail	1/303	pass
1st	1/309	pass	1/322	pass	1/330	pass

Note: Deflection limit based on storey height over 300

Table 10.2 Unbraced frame deflections for lateral loading

The frame deflections shown in Table 10.2, indicate that the amount of lateral deflection in the minor axis of the column at the second storey level for both the UC and SHS cases fails the criteria, even though the bases have been assumed to be fixed. Assessment of sway is important for both the stability of the frame and to avoid serviceability cracks in masonry. In this instance the margin of failure is relatively small and would normally be allowed in practice, considering the arbitrary nature of the analysis which allowed for connection flexibility. Therefore the sections determined for the three cases are used for the economic comparison.

10.5 Pricing system

The pricing system adopted is based upon the one previously used by SCI [88]; where fabrication, steel sections, fire protection, steelwork erection, transportation and concrete filling are included in the column cost. However, the final pricing structure for the fabrication and material costs deviates from the global figure used by the SCI to account for both items by costing them separately. A 'fabrication' cost of £350 /tonne is therefore used which is applied to the open section column. The total cost determined is then assumed for the SHS columns as well, regardless of the SHS total weight. This results in equal total fabrication costs to both the open and SHS columns. The reason for this approach is that the flowdrill system is assumed to produce equal manufacturing costs compared to that of normal drilling. Any slight disadvantage which the flowdrill has will be offset by the simpler and standardised connection details resulting from its use. Table 10.3 lists the base costs applied to the columns.

The problem encountered with this pricing regime is the fluctuation of prices over a brief period of time. This comparison was completed in 1994, undoubtedly the base costs would have increased, implying that the outcome maybe somewhat different to that presented in the results. However, the actual section sizes calculated will not change, only the price. Any errors will therefore be applied to both sections, with only the total cost of the column subject to change.

Steel costs	As per price list: British Steel; Effective 2nd January 1994.	
Fabrication costs	Drill, plate and transport	£350 /tonne
Fire protection	British Gypsom, Glasroc S board system	£22.90 /m^2
Concrete filling	Grade C40	£150 /m^3

Table 10.3 Costing data used

10.6 Results of economic comparison

The total column costs are calculated using the above prices of Table 10.3 and the section sizes noted in Figures 10.5, 10.6 and 10.7. A summary of all the column costs are presented in Table 10.4.

	UC		SHS		COMPOSITE SHS	
(1) Braced Frame						
Column (Internal)	£901	1.00	£926	1.03	£903	1.00
Column (Edge)	£812	1.00	£809	1.00	£825	1.02
(2) Unbraced Frame						
(major axis only)						
Column (Internal)	£1,055	1.17	£1,212	1.35	£1,210	1.34
Column (Edge)	£1,009	1.24	£1,152	1.42	£1,102	1.36
(3) Unbraced Frame						
(both axis)						
Column (Internal)	£1,265	1.40	£1,271	1.41	£1,220	1.35
Column (Edge)	£1,196	1.47	£1,209	1.49	£1,167	1.44

Table 10.4 Summary of relative column costs for actual material pricing scheme

The values listed in Table 10.4 represent the average total column cost for each frame design. Each column cost is compared to the initial braced frame designed with open section members. This value is subsequently denoted as the ratio of 1.00 and highlighted in the table. Thus a simple presentation of relative costs between different design assumptions is available.

Although every effort has been made to be impartial and fair, discrepancies will arise either through the selection of basic prices or from the over design of column members from a finite section size range. To reduce these discrepancies, all the total costs for the columns have been averaged according to there respective categories of internal or edge columns; the internal column selection representing pure axial loading whereas the edge columns represent column with moments applied through the joint.

The overall results from Table 10.4 indicate that the use of structural hollow sections in braced frames as a direct replacement for open sections results in marginally increased costs of 3 percent. For unbraced frames where the minor axis is braced (the most common form of unbraced frame) results in cost penalties of 17 percent above that of the UC section. This is not surprising considering that the beneficial asymmetric properties of open sections will favour this type of construction compared to the all round properties exhibited by the SHS. The adoption of rectangular sections may in some way reduce this penalty. In cases of unbraced frames in both directions the SHS shows similar costs with the UC sections while composite SHS sections average costs 5 percent lower. This is not surprising as in this instance the efficiency of the SHS shows greater performance to the minor axis open sections which accommodates relatively high slenderness ratios produced by the $1.5xL_c$ effective length of the minor axis.

All the results presented so far have been based on total column costs where the benefits of reduced fire protection benefit the SHS by virtue of a smaller cross sectional area. Table 10.5 presents the steel costs alone on actual steel section prices. Apart from the composite SHS designed column the closed form section exhibits a higher purchase cost. The construction trend is to tender individual parts of a contract where the steel fabrication is treated separately from that of fire protection. Hence the fabricator would be reluctant to select the more expensive box sections on a weight for weight basis over traditional UC sections. The advantages of reduced fire protection therefore account for the comparative performance between open and SHS columns.

	UC		SHS		COMPOSITE SHS	
Braced Frame						
Column (Internal)	£331	1.00	£380	1.14	£316	1.05
Column (Edge)	£288	1.00	£334	1.16	£302	1.05
Unbraced Frame (major axis only)						
Column (Internal)	£376	1.14	£544	1.64	£432	1.31
Column (Edge)	£367	1.27	£488	1.69	£432	1.50
Unbraced Frame (both axis)						
Column (Internal)	£475	1.44	£550	1.66	£402	1.21
Column (Edge)	£455	1.58	£527	1.83	£402	1.40

Table 10.5 Summary of steel costs separate from fire protection and concrete filling.

10.7 Chapter summary

The economic comparison for buildings of less than four storeys using SHS columns has indicated marginally increased costs over their open section equivalents. The benefit of using tubular columns has been through the reduced cost of fire protection.

The survey has highlighted the possibility for unbraced frames using the flowdrill connector in both directions of the column's axis. Although three storeys appeared to be the limit for deflection, increased storey heights could be accommodated by a more appropriate floor system which allows the second moment of area of the secondary floor beams to be increased in size, reducing lateral deflection of the frame.

Chapter 11

Conclusions

This thesis has presented the results of 35 full scale cantilevered joint tests where open section beams were connected to SHS columns. The majority of the connections were made with the Flowdrill blind bolting connector. The objective of the work was to investigate joint performance for welded endplate details, over the full range of connection stiffness. These included the simple connections of the partial depth and full depth endplates, to the more rigid connections incorporating extended endplates.

The principal conclusions and observations of those tests are as follows;

1. For all the flowdrill joint tests, the principal failure mechanism of the joint was through excessive column face deformation. The joints exhibited high flexibility, greater than those of equivalent open sections. In the majority of joint tests the loading was stopped through excessive rotation rather than any structural failings, significantly beyond the serviceability limit. Only in the more extreme tests conducted with extended endplates did the connector strip its thread and pull out. Again this was beyond the serviceability limit of the joint.

2. The joint's moment-rotation curve showed highly non-linear characteristics at the very start of loading. In the majority of cases no upper limit to the moment carrying capacity was defined, only a reduced stiffness which was developed from both strain hardening and membrane forces mobilised after severe column face yielding. All the simple joints that were subjected to cyclic loading, recorded a hysteresis moment-rotation characteristics which showed a sudden reduction in stiffness as zero moment was approached in the cycle of load. The path developed in the moment-rotation curve did however eventually rejoin and follow its original monotonic curve.

3. Tests on identical concrete filled joints showed excellent increases in initial stiffness and moment capacity over unfilled sections. The compression zone of the joint had clearly benefited from the concrete fill, with no visible deformation to the column. In

unfilled joint tests the compression zone was identified as governing the final failure as the side walls began to yield and lose their stiffness.

4. The presence of column axial load had an effect of reducing the ultimate strength of the connection. A reduced post yielded stiffness was noticed, resulting in one case of zero stiffness corresponding to column loads which were typical of serviceability limit state.

5. Actual theoretical calculated flowdrill bolt loads at failure indicated that the values for the 8mm or less thickness of wall were unsafe when compared to published connector capacities. It is recommended that moment connections be designed with either a minimum tube wall thickness equal to or greater than 8mm, or some other reduction factor be incorporated. Tests on connections assumed to be pinned are not subjected to this restriction. Joint tests with equivalent Hollo-bolt connectors resulted in a similar moment-rotation characteristic to the nominally identical flowdrill joints, even though the holes drilled in the column removed a substantial portion of the columns steel to accommodate the increased bolt diameter. There was, however, a serious occurrence with bolt pullout when the bolts were subjected to tension. At the limit of manufacturer's recommended minimum depth of bolt insert, it was found that the bolts were unable to expand fully and adequately clamp the endplate to the face of the column resulting in the bolt failing at low and unsafe capacities under tension.

6. A joint model for the connection (Chapter 8) has been proposed. This model defines the full moment-rotation of the joint in cases where the column face predominantly determines the majority of the overall joint's rotation. A method to incorporate endplate flexibility (Chapter 7) was not successful, indicating that endplate stiffness had influenced the overall response of the joint. The two effects cannot be treated separately. However, because the column face will, in the majority of cases form the principal failure, the accuracy of the model has been shown to be reasonable for all the moment-resisting joint tests and connections where the endplate flexibility is sufficiently small to be ignored.

7. The principal mode of failure for the joint model was based on yield lines developing in both the tension and compression zones of the joint. The curve used in the model adopts a modified Ramberg-Osgood function. The joint rotation is calculated by assuming both a rotation axis for the joint, and a new proposed deformation limit to the bolts which is based on the slope of the column face rather than any fixed

deformation limit. A similar criterion of face deformation is also used to determine the bolts final pull out. Between these two limits a procedure has been developed to incorporate the effects of strain hardening into the joint model. The use of deformation limits in this way have, for the first time, indicated the boundaries to which the yield model for the tension zone can safely migrate down the depth of the connection.

8. The joint models for simple connections of partial depth and flush endplates have been incorporated into a parametric sub-frame study of braced frames (Chapter 9). The results have indicated that both these connections influence column performance. It has been found that the restraint developed by the joint detail to the column does not always outweigh the detrimental effect of moment transfer. The moment transferred into the column usually being greater than that determined from a nominal 100mm eccentricity of load specified in BS5950.

9. An economic comparison between open section and SHS columns has resulted in only marginal increases in cost. The benefit of the SHS primarily resulted in reduced cross sectional area and lower fire protection costs. It was assumed that the fabrication costs of both open and closed form sections would be approximately equal. This was justified by the fact that the introduction of the flowdrill connectors would have resulted in significant standardisation.

11.1 Proposed future work and observations on programme

The majority of the work conducted in this project has been through the experimental investigation of full scale joints. The data generated from the tests have been invaluable in constructing and validating the joint model proposed. There are some areas indicated by this programme of joint tests which have been shown to require some further investigation.

11.1.1 Further work on the Flowdrill connectors performance

The performance of the Flowdrill connector was previously determined from external investigations prior to the start of this programme by a series of isolated bolt pull out tests on undeformed flowdrill thread specimens. It was clear that during the joint tests the thread was being subjected to both excessive deformation and combined shear and tension bolt loads, which had clearly not been allowed for in the previous investigations of bolt capacity.

Considering the concern expressed by the author on the published bolt capacities of Flowdrill connectors in steel less than 8mm, it would be worth while to conduct a further series of simple one bolt connector tests in which the thread had been purposely deformed. At a known deformation limit imposed, the thread can be clamped into position and subjected to both shear and tension combinations. The level of deformation imposed on the thread can be based on the author's proposed deformation limits of Chapter 8. These additional simple bolt tests would provide a more realistic mode of failure imposed on the bolt and provide greater confidence of the connector's structural integrity.

11.1.2 Compression zone failure of the joint

An important area which was found to be deficient of adequate guide lines is the mode of failure for the joint's compression zone. This particular area of the joint's failure is unique as there appears to be insufficient experimental knowledge relating to the endplate bearing onto the SHS column. Previously the problem has been largely investigated with branch plates which simulate a beam flange welded to the column face. However, a different situation will exist when bolted endplates are used where the effects of both non-uniform distribution under the plate and punching shear will now play a part in overall failure.

The capacity of the compression zone is usually determined by either flexural failure of the column face or from the buckling capacity of the side walls. These two failure mechanisms depend largely on the relative width of the endplate to that of the column. The dividing line commonly used to separate the two failures has usually been assumed when the endplate width is 0.85 times the column width. When the endplate is greater than this limit, an interaction of the two modes of failure is usually assumed.

To a certain extent the joint tests conducted previously go some way to investigate these effects, with both the ratio of endplate to column varied throughout the programme, thereby creating different distributions of load under the compression flange of the joint. The joint model proposed provides some guidance on the compression zone design. However, without isolating each individual contribution from the joint, the compression zone failure could not be totally investigated. It is therefore recommended that a series of simple tests on SHS members which recreate the conditions of the endplate's rotation in the compression zone are conducted. The isolation of such tests may lead to a greater understanding and simpler design guidance.

11.1.3 Further full scale testing

All the joint tests conducted in the previous test programme concentrated on the two dimensional behaviour of in-plane response. A further test programme could be expanded to the more complex problem of multi-planar flowdrill joints. Previous work in this field has been from the joint tests conducted with open section beams welded to tubular columns. Although the flowdrill joint tests would, by their nature, be more complicated than those previously conducted, there is presently no known data to exist for these type of joints.

A further investigation could also be directed towards composite construction. Joint tests with composite beams could be constructed, identical to the unfilled ones previously tested, to provide the necessary moment-rotation data to allow further parametric studies into frame behaviour. The tests could also be expanded to include composite columns which, considering the increased strength and stiffness achieved in the author's test programme, may well lead to substantial benefits in the joint's rigidity with use of adequate concrete reinforcement.

In the main thesis, parametric studies have been reported on sub-frame behaviour. This theoretical work could be expanded into actual experimental testing, similar to those conducted with open sections. As indicated in the main text of the thesis, there has been very little experimental work conducted on the effect of joint behaviour has on SHS column capacity. The situation is more interesting with the preliminary results of the parametric study implying that the connection is detrimental to the column's performance. Further evidence, both experimental and parametric, is required before any firm conclusions can be drawn from a relatively small study.

11.1.4 Numerical modelling

A cost effective way of investigating joint response is by the direct application of the Finite Element Model. Over the period of this project, it has been noticed that these models are becoming increasingly more sophisticated and popular. The majority of the models have shown to predict reasonable accuracy for cases where open sections are welded directly to SHS columns. High accuracy is usually achieved when the flexural response governs the joints overall failure. However, in cases of punching shear, this accuracy diminishes. The lack of accuracy in these cases is a result of using shell elements in areas where the stress in the column needs to be determined through the

thickness of the tube. The model therefore needs to incorporate 3D effects of the column.

Incorporating the thickness of the wall into a F.E. model, which can accommodate the 3D effect, increases the complexity of the numerical model considerably and, more importantly, the solution time for the computer to analysis the problem. With the advancement of computer processing power, this problem will gradually reduce. It is therefore recommended that a numerical model should be developed to investigate the compression zone of the joints to understand the complex interaction which develops directly under the compression flange of the beam. The validation of the model could be combined with future experimental tests described in section 11.1.2. If these tests are not available then the joint test data collated in appendix A of this thesis provides ideal material for future reference and validation.

Another use for numerical models is that of investigating the global behaviour of steelwork frames examined briefly in Chapter 9. One area which requires further investigation highlighted from this study is that of moment transfer to the column at ultimate failure. The analytical joint model presented in this thesis will allow the relatively small parametric study conducted by the author to be expanded to other combination of member sizes rather than limiting the parametric study to those of the actual joint test sizes referenced in appendix A. Further extension of the study can also be expanded to unbraced frame behaviour, although concern is expressed with the frame models used for global analysis. The problem is concerned with local deformation and plasticity in the column. As the joint yields, there is a certain amount of inelasticity present in the column from an early stage in the joint loading, well before the column's moment capacity is reached. The presence of yielding reduces the elastic core and hence column stiffness at the position of the joint. The absence of these effects in the column element will inevitably lead to the full section properties to be relied upon in a elastic-plastic analysis, and result in a excessively high frame capacity for unbraced frames.

Accounting for the local deformations in braced frames would not affect the final column capacity as the column is laterally restrained at its ends. This cannot be said for the case of unbraced frames where stiffness of the column at this point is important to frame stability. This problem is remarkably similar to accounting for residual stresses, although the column stresses induced are varying throughout the columns loading sequence.

Chapter 12

References

[1] Wilson, W. M. & Moore, H. F., 'Tests to determine the rigidity of riveted joints in steel structures'. University of Illinois, Engineering Experimental Station, Bulletin No. 104, Urbana, USA. 1917.

[2] Sherman, D. R., 'Evaluation of flowdrilled holes for bolted connections in structural tubes'. University of Wisconsin-Milwaukee, USA. July, 1989.

[3] Eurocode 3: Design of Steel Structures. Part 1.1 General rules and rules for buildings-Annex K. DD ENV 1993-1-1 : 1992.

[4] Giddings, T. W., 'Welded joints in tubular construction'. *Proc. Joints in structural steelwork.* Cleveland, England. 6-9th April 1981. London: Pentech Press. pp 4.3-4.24.

[5] CIDECT Monograph No. 6., 'The strength and behaviour of statically loaded welded connections in structural hollow sections'-ed. Giddings, T. W. & Wardenier, J. 1986.

[6] SCI., 'Survey of existing connection types and design methods using hollow sections'. Steel Construction Institute. Report SCI-RT224. July, 1991.

[7] White, R. N. & Fang, P. J., 'Framing connections for square structural tubing'. *ASCE, Journal of the Structural Division.* Vol. 92, No. ST2. April 1966. pp. 175-194.

[8] Ales Jr, J. M., 'The design of shear tabs welded to tubular columns'. *M.Sc. Thesis.* University of Wisconsin, Milwaukee, USA. 1990.

[9] Moore, D. B. & Owens, G. W., 'Verification of design methods for finplate connections'. *The Structural Engineer.* Vol. 70, No. 3. February, 1992. pp. 46-53.

[10] Haslam, C. A., 'The capacities of tubular columns with shear tab beam connections'. *M.Sc. Thesis.* University of Wisconsin, Milwaukee, USA. 1993.

[11] Kato, B., 'Beam-to-column connection research in Japan'. *ASCE, Journal of the Structural Division.* Vol. 108, No. ST2.. February, 1982. pp. 343-360.

[12] Szlendak, J & Ligocki, I., 'Strength of T-joints of type RR-I in rectangular hollow section frames'. *Stavenvnicky Casopis.* Vol. 37, no. 3, VEDA, Bratislava, 1989. pp. 175-189.

[13] Tsai, K. C., Lin, K. C. & Liu, M. C., 'Seismic behaviour of steel beam-to-box column connections.' *Proc. Earthquake Engineering, Tenth World Conference.* Rotterdam: A. A. Balkema. 1992. pp. 2903-2909.

[14] Lu, L. H., & Wardenier, J., 'The static strength of uniplanar and multiplanar connections between I-beams and RHS columns loaded by axial compression'. *Proc. 14th International Conference on Off-shore Mechanics & Artic Engineering:* ASME Vol. III : 1995. pp 173-179.

[15] Mehrotra, B. L., 'Stiffening in tubular junctions-some new concepts'. *ASCE, Journal of the Structural Division.*, Vol. 97, No. ST9. 1971. pp. 2453-2457.

[16] Dawe, J. L. & Grondin, G. Y., 'W-Shape beam to RHS column connections'. *Canadian Journal of Civil Engineering.* Vol. 17. 1990. pp. 788-797.

[17] Picard, A. & Giroux, Y.-M., 'Moment connection between wide flange beams and square tubular columns'. *Canadian Journal of Civil Engineering.*, Vol. 3. 1976. pp. 174-185.

[18] Shanmugam, N. E., Ting, L. C. & Lee, S. L., 'Behaviour of I-beam to box-column connections stiffened externally and subjected to fluctuating loads'. *Journal of Constructional Steel Research.* Vol. 20. 1991. pp 129-148.

[19] Shanmugam, N. E., Ting, L. C. & Lee, S. L., 'Static behaviour of I-beam to box-column connections with external stiffeners'. *The Structural Engineer.* Vol. 71, No. 15. August, 1993. pp. 269-275.

[20] Kanatani, H., Tabuchi, M., Kamba, T., Hsiaolien, J. & Ishikawa, M., 'A study on concrete filled RHS column to H-beam connections fabricated with HT bolts in rigid frames'. *Proc. Engineering Foundation Conference on Composite Construction in Steel and Concrete.* 1987. pp. 614-635.

[21] Maquoi, R., Naveau, X. & Rondal, J., 'Beam-column welded stud connections'. *Journal of Constructional Steel Research.* Vol. 4. 1984. pp. 3-26.

[22] Vandegans, D., 'Liaison entre poutres metalliques et colonnes en profils creux remplis de beton, basee sur la technique du goujonnage. (goujons filetes)'. *CRIF.* Report MT 193. October, 1995.

[23] Kato, B., 'Bolted beam-to-column moment connection'. *Proc. International Colloquium on Bolted and Special Structures.* Moscow, USSR. 15-20th May, 1989. pp. 29-38.

[24] Ghobarah, A., Mourad, S. & Korol, R. M., 'Behaviour of blind bolted connections for HSS columns'. *Tubular Structures V, Proc. Fifth International Symposium.* Coutie, M. G. et al ed. London: E & FN Spon. 1993. pp. 125-132.

[25] Mourad, S., Korol, R. M. & Ghobarah, A., 'Design of extended end-plate connections for hollow section columns'. *Canadian Journal of Civil Engineering.* No. 23. 1996. pp. 277-286.

[26] Korol, R. M., Ghobarah, A. & Mourad, S., 'Blind bolting W-shape beams to HSS columns'. *ASCE Journal of Structural Engineering.* Vol. 119, No. 12. December, 1993. pp. 3463-3481.

[27] Tabuchi, M., Kanatani, H., Tanaka, T., Fukuda, A., Furumi, K., Usami, K. & Murayama, M., 'Behaviour of SHS column to H beam moment connections with one side bolts'. *Proc. Sixth International Symposium on Tubular Structures.* Grundy, P. et al ed. Rotterdam: A. A. Balkema. 1994. pp. 389-396.

[28] Sadri, S. M. & Wang, H-T., 'Advanced technique for jointing hollow steel structures'. *Proc. Nordic Steel Construction Conference 95',* Vol. II. 1995 . pp. 757-764.

[29] Tanaka, T., Tabuchi, M., Murayama, M., Furumi, K., Morita, T., Usami, K. & Matsubara, Y., 'Experimental study on end-plate to SHS column connections reinforced by increasing wall thickness with one side bolts'. *Tubular Structures VII, Proc. Seventh International Symposium.* Farkas, J. et al ed. Rotterdam: A. A. Balkema. Miskolc, Hungary. 1996. pp. 253-260.

[30] Dekkers, G. J., 'Flowdrill Technical Guide'. *Flowdrill B. V.*, Holland. April, 1993.

[31] Sherman, D. R., 'Framed connections to HSS columns'. *Tubular Structures V, Proc. Fifth International Symposium.* Coutie, M. G. et al ed. London: E & FN Spon. 1993. pp. 241-248.

[32] Banks, G., 'Flowdrilling for tubular structures'. *Tubular Structures V, Proc. Fifth International Symposium.* Coutie, M. G. et al ed. London: E & FN Spon. 1993.. pp. 117-124.

[33] Flowdrill jointing with Hollow sections, Interim report. British Steel Tubes & Pipes-TD366A/E/. October 1993.

[34] Ballerini, M., Piazza, M., Bozzo, E. & Occhi, F., 'Shear capacity of blind bolted connections for RHS steel structural elements'. *Tubular Structures VII, Proc. Seventh International Symposium.* Farkas, J. et al ed. Rotterdam: A. A. Balkema. Miskolc, Hungary. 1996. pp. 99-106.

[35] Ballerini, M., Bozzo, E., Occhi, F. & Piazza, M., 'The Flowdrill system for the bolted connection of steel hollow sections. Part 1-The drilling process and the technological aspects'. *Costruzioni Metalliche*, No. 4. 1995.

[36] Yeomans, N. F., 'I-beam/rectangular hollow section column connections using the Flowdrill system'. *Tubular Structures VI, Proc. Sixth International Symposium.* Grundy, P. ed. Rotterdam: A. A. Balkema. 1994.. pp. 381-388.

[37] Yeomans, N. F. '"Flowdrill" bolted connections in RHS'. *Technical note TCH 90/914.* Corby Technical Centre, England. December, 1990.

[38] Kirby, P. A., Zandonini, R., & Davison, J. B., 'On the determination of moment-rotation characteristics of beam-to-column joints'. *Testing of metal structures.* Mazzolani, F. M. ed. London: E & F. N. Spon. 1992.

[39] Davison, J. B., 'Strength of beam columns in flexibly connected steel frames'. *Ph.D. Thesis.* Department of Civil and Structural Engineering, University of Sheffield, England. June, 1987.

[40] Gibbons, C., 'The strength of biaxially loaded columns in flexibly connected steel frames'. *Ph.D. Thesis.* Department of Civil and Structural Engineering, University of Sheffield, England. December, 1990.

[41] Lam, D., 'Influence of composite flooring on steel beam-column connections'. *M.Phil. Thesis.* Department of Civil and Structural Engineering, University of Sheffield, England. 1989.

[42] Surtees, J. O. & Ibrahim, M. E., 'Bolt tension measurement from head strain data'. *ASCE, Journal of the Structural Division.* Vol. 106, No. ST2. 1980. pp. 477-490.

[43] Jenkins, W. M., Tong, C. S. & Prescott, A. T., 'Moment-transmitting endplate connections in steel construction, and proposed basis for flush endplate design'. *The Structural Engineer.* Vol. 64a, No. 5. May, 1986. pp 121-132.

[44] Owens, G. W. & Moore, D. B., 'Steelwork connections- The robustness of simple connections'. *The Structural Engineer.* Vol. 70, No. 3. February, 1992. pp 37-46.

[45] Celikag, M., 'Moment-rotation behaviour of steel beam-to-column connections.' *Ph.D. Thesis.* Department of Civil and Structural Engineering, University of Sheffield, England. February, 1990.

[46] Joints in Simple construction. Vol. 1: Design methods. SCI/ BCSA. 1991.

[47] Eurocode 3: Design of Steel Structures. Part 1.1 General rules and rules for buildings. DD ENV 1993-1-1 : 1992.

[48] France, J. E., Davison, J. B., & Kirby, P. A., 'Experimental testing of flowdrill connectors with concrete-filled SHS columns'. *Tubular Structures VII, Proc. Seventh International Symposium.* Farkas, J. et al ed. Rotterdam: A. A. Balkema. Miskolc, Hungary. 1996. pp. 333-340.

[49] SHS Jointing-Flowdrill & Hollo-bolt, British Steel Tubes & pipes publication-TD384.12E.95.

[50] Zhao, X-L. & Hancock, G. J., 'T-joints in rectangular hollow sections subject to combined actions'. *ASCE, Journal of Structural Engineering.* Vol. 117, No. 8. August, 1991. pp. 2258-2277.

[51] Yu, Y. & Wardenier, J., 'Influence of chord bending moments on the ultimate load capacity of x-joints in rectangular hollow sections'. *Tubular Structures VII, Proc. Seventh International Symposium.* Farkas, J. et al ed. Rotterdam: A. A. Balkema. Miskolc, Hungary. 1996. pp. 205-212.

[52] Bergmann, R., Matsui, C., Meinsma, C., & Dutta, D. 'Design guide for concrete filled hollow section columns under static & seismic loading'. CIDECT. 1995.

[54] Tschemmernegg, F. & Queiroz, G., 'Mechanical modelling of semi-rigid joints for the analysis of framed steel and composite structures'. *AISC, Proc. Third International Workshop on connections in Steel Structures.* University of Trento, Italy. May, 1995.

[55] Bahaari, M. R. & Sherbourne, A. N., 'Structural behaviour of end-plate bolted connections to stiffened columns'. *ASCE, Journal of Structural Engineering.* Vol. 122, No. 8. August, 1996. pp 926-935.

[56] Krishnamurthy, N., Huang, H. T., Jeffrey, P. K. & Avery, L. K., 'Analytical moment-rotation curves for endplate connections'. *ASCE, Journal of the Structural Division.* Vol. 105, No.ST1. January, 1979. pp 133-145.

[57] Lothers, J. E., 'Elastic restraint equations for semi-rigid connections'. *ASCE Transactions.* Vol. 116. 1951. pp 480-502.

[58] Tarpy, T. S. & Cardinal, J. W., 'Behaviour of semi-rigid beam-to-column end-plate connections'. *Proc. Joints in structural steelwork.* Cleveland, England 6-9th April, 1981. London: Pentech Press. pp 2.3-2.25

[59] Johnson, R. P. & Law, C. L. C., 'Semi-rigid joints for composite frames'. *Proc. Joints in structural steelwork.* London: Pentech Press. Cleveland, England 6-9th April 1981. pp 3.3-3.19

[60] Maxwell, S. M., Jenkins, W. M., & Howlett, J. H., 'A theoretical approach to the analysis of connection behaviour'. *Proc. Joints in structural steelwork.* London: Pentech Press. Cleveland, England. 6-9th April, 1981. pp 2.49-2.70

[61] Sommer, W. H., 'Behaviour of welded header plate connections'. *M.Sc. Thesis.* University of Toronto, Ontario. 1969.

[62] Jones, S. W., Kirby, P. A. & Nethercot, D. A., 'Modelling of semi-rigid connection behaviour and its influence on steel column behaviour'. *Proc. Joints in structural steelwork.* London: Pentech Press. Cleveland, England 6-9th April, 1981. pp 5.73-5.87

[63] Ang, K. M. & Morris, G. A., 'Analysis of three-dimensional frames with flexible beam-column connection'. *Canadian Journal of Civil Engineering.* Vol. 11. 1984. pp 245-254

[64] Ramberg, W. & Osgood, W. R., 'Description of stress-strain curves by three parameters'. National Advisory Commitee for Aeronautics. Technical Report no. 902. 1943.

[65] Kishi, N. & Chen, W. F., 'Moment-rotation relationships of semi-rigid connections with angles'. *ASCE, Journal of Structural Engineering.* Vol. 116, No. 7. 1990. pp 1813-1834.

[66] International Institute of Welding 'Design recommendations for Hollow section joints-Predominantly statically loaded'. IIW Document no. xv-701-89, 2nd Edition. September, 1989.

[67] Yura, J. A., Zettlemoyer, N. & Edwards, I. F., 'Ultimate capacity equations for tubular joints'. *OTC Proceedings.* Vol. 1, No. 3690. 1980.

[68] Lu, L. H., Winkel, G. D. de., & Wardenier, J., 'Deformation limit for the ultimate strength of Hollow section joints'. *Proc. Sixth International Symposium on Tubular Structures.* Grundy, P. et al ed. Rotterdam: A. A. Balkema. 1994,. pp. 341-347.

[69] Prager, W. & Hodge, P. G., 'Theory of perfectly plastic solids'. New York: John Wiley & Sons. 1951.

[70] Packer, J. A., Morris, G. A. & Davies, G., ' A limit states design method for welded tension connections to I-section webs'. *Journal of Constructional Steel Research.* Vol. 12. 1989. pp 33-53.

[71] Kim, Y. W., 'The behaviour of beam-to-column web connections with flush endplates'. *M.Sc. Thesis.* University of Warwick, England. July, 1988.

[72] Gomes, F. C. T., Jaspart, J. -P. & Maquoi, R., 'Behaviour of minor-axis joints and 3-D joints'. *COST C1, Proc. 2nd State of the art workshop.* Prague. 26th-28th October, 1994. pp 111-121.

[73] Vandegans, D., 'Application of the component method according to Eurocode 3 to connections with threaded studs'. COST C1. 1995.

[74] Wood, R. H., 'Plastic and Elastic design of slabs and plates'. London: Thames & Hudsons. 1967.

[75] Coates, R. C., Coutie, M. G., & Kong, F. K. 'Structural Analysis'. Van Nostrand Reinhold Co. Ltd., Third Edition, England. 1988.

[76] Packer, J. A., Wardenier, J., Kurobane, Y., Dutta, D., & Yeomans, N., 'Design guide for rectangular Hollow section (RHS) joints under predominantly static loading'. *CIDECT.* 1992.

[77] Davies, G. & Packer, J. A., 'Predicting the strength of branch plate-RHS connections for punching shear'. *Canadian Journal of Civil Engineering.* Vol. 9. 1982. pp 458-467.

[78] BS 5950: Part 1: 1990., 'Structural use of steelwork in building-code of practise for design in simple and continuous construction: hot rolled sections'. British Standards Institution.

[79] Steelwork Design Guide to BS5950:Part 1: 1985, Vol. 1 Section Properties, Member Capacities: 2nd Edition. SCI.

[80] Morrell, P. J. B., 'Beams in RHS: The effective line of action of loads applied uniformly over the flanges of RHS beams'. *Constructional steelwork Metal & Materials.* March, 1972.

[81] Szlendak, J., 'Classification system for I-beam-to-RHS column connections'. *Tubular Structures VII, Proc. Seventh International Symposium.* Farkas, J. et al ed. Rotterdam: A. A. Balkema. Miskolc, Hungary. 1996.. pp. 245-252.

[82] Beer, H. & Schulz, G. W., 'Theoretical bases of the European column buckling curves'. *Construction Metallique.* Paris, France. (3), 1970. pp 37-55 (in French).

[83] Jones, S. W., Kirby, P. A. & Nethercot, D. A., 'Effect of Semi-rigid connections on steel frames'. Journal of Constructional Steel Research. Vol. 1, No. 1. September, 1980. pp 38-46.

[84] Carr, J. F., 'A simplified approach to the design of semi-rigidly connected columns in multi-storey non-sway steel framed buildings'. *M.Phil. Thesis.* Department of Civil and Structural Engineering, University of Sheffield, England. May, 1993.

[85] Poggi, C., 'A finite element model for the analysis of flexibly connected steel frames'. *International Journal for Numerical methods in Engineering.* vol. 26. 1988. pp 2239-2254.

[86] Bjorhovde, R., 'Compression Members'. *Constructional Steel Design- An International Guide.* Dowling, P. J., Harding, J. E. & Bjorhovde, R. ed. Elsevier Applied Science. Chapter 2.3. 1992. pp 67-89.

[87] Sherman, D. R., 'Tubular Members'. *Constructional Steel Design- An International Guide.* Dowling, P. J., Harding, J. E. & Bjorhovde, R. ed. Elsevier Applied Science. Chapter 2.4. 1992. pp 91-104.

[88] SCI., 'Column cost comparison'. Steel Construction Institute-Report RT358, 1993.

[89] New Steel Construction. 'Steel framing's share of multi-storey building reaches new peak'. *ICE New Steel Construction Publication.* Vol. 2., No. 2:8. 1994.

[90] BS 6399 : Part 1 : 1984, 'Design loading for buildings, Part 1. Code of practise for dead and imposed loads'. British Standards Institution.

[91] CP3 : Chapter V : Part 2 : 1972., 'Basic data for the design of buildings-Part 2. Wind loads'. British Standards Institution.

[92] 'Design manual for concrete filled columns'. Part 1. British Steel.-TD 296:Part 1/3E/92.

[93] Anderson, D., Reading, S. J. & Kavianpour, K., 'Wind-moment design for unbraced frames'. Steel Construction Institute, Publication 082. 1991.

[94] BS EN 10002-1 : 1990., 'Tensile testing of metallic materials, Part 1. Method of test at ambient temperature', British Standards Institution.

[95] Brockenbrough, R. L., 'Material properties'. *Constructional Steel Design- An International Guide.* Dowling, P. J., Harding, J. E. & Bjorhovde, R. ed. Elsevier Applied Science. Chapter 1.2. 1992. pp 17-32.

[96] Galambos, T. V., 'Properties of steel for use in LRFD'. *ASCE, Journal of Structural Engineering.* Vol. 104, No. ST9. September, 1978.

[97] Surtees, J. O., & Mann, A. P., 'End plate connections in plastically designed structures'. *Conference on joints in structures*, University of Sheffield, UK. 1970.

[98] Gent, A. R. & Milner, H. R., 'The ultimate load capacity of elastically restrained H-columns under biaxial bending'. *Proc. Inst. Civil Engineers.*, No. 41, 1968, pp 685-704.

Appendix A

Moment-rotation curves for Flowdrill joints

This appendix contains all the moment rotation data for the flowdrill joint tests numbered 1 to 33 inclusive. A complete listing of each test can be located in the main thesis.

The data has been arranged to provide a concise reference for future investigations. Each individual test is presented on one A4 data sheet, which includes both the geometrical details of the joint and the complete moment rotation characteristic that shows the load path of the joint.

To simplify the data presented, each moment-rotation curve was reduced to a multi-linear characteristic by selecting representative points along the original curve. In situations where cyclic loading was used, the points selected represented the maximum point of rotation and corresponding moment for each cycle of load applied to the joint. For each joint, the multi-linear characteristic has been superimposed onto the full curve for reference. Tabulated values which construct the multi-linear characteristic are also included.

A diagram of the joint completes each data sheet which provides details of endplate thickness, member sizes, bolt locations, weld size and type of connection. The diagram is so drawn that the positive moment of the corresponding moment-rotation characteristic will always represent the action of a downward acting force applied to the top flange of the beam.

The material strength and geometrical survey of the column specimens used in the series of tests can be found in appendix B of this thesis.

Experimental Moment-Rotation curve for Joint Test No. 1

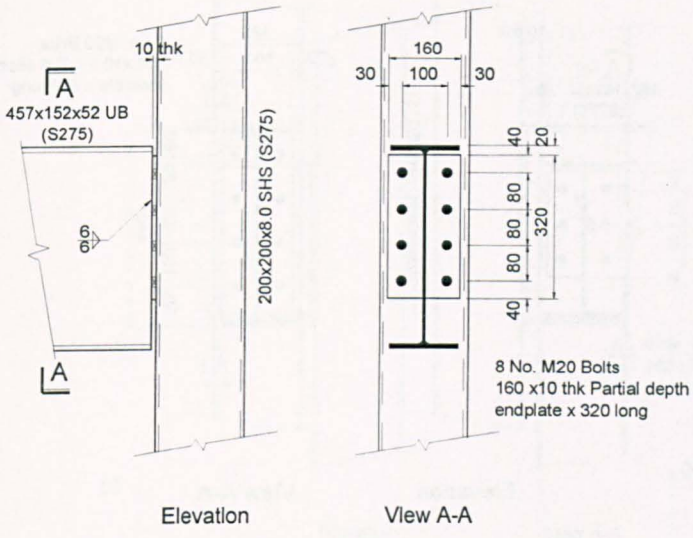

Elevation View A-A

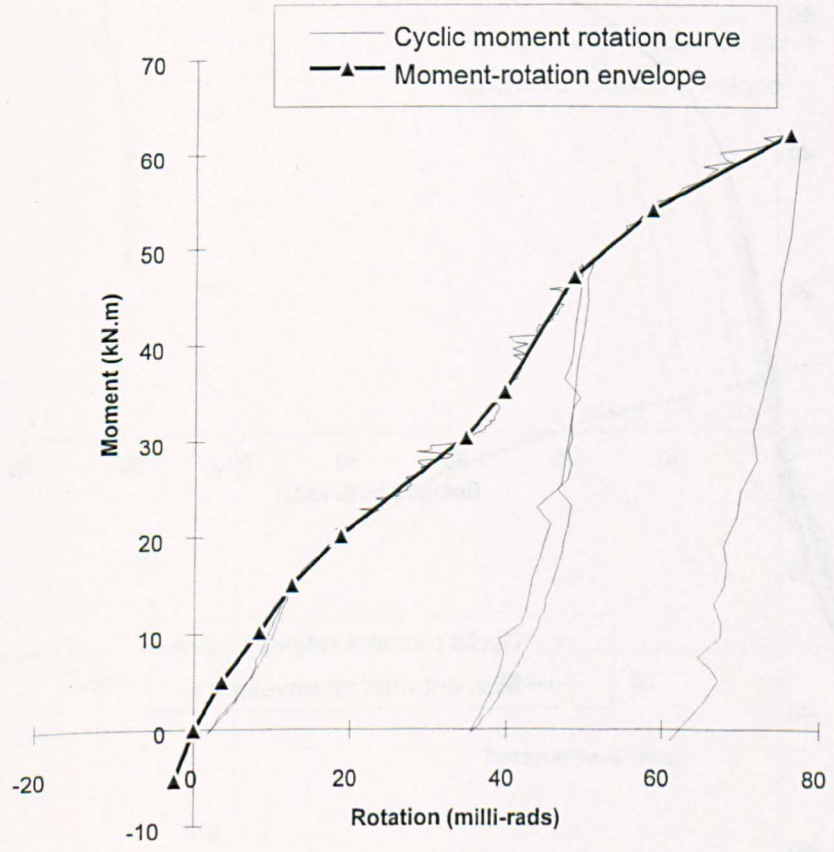

Moment rotation envelope :											
Moment (kN.m)	-5.2	0	5.1	10.3	15.2	20.3	30.4	35.3	47.1	54.2	62.3
Rotation (milli-rads)	-2.4	0	3.6	8.4	12.5	18.7	34.7	39.6	48.5	58.6	76.1

Experimental Moment-Rotation curve for Joint Test No. 2

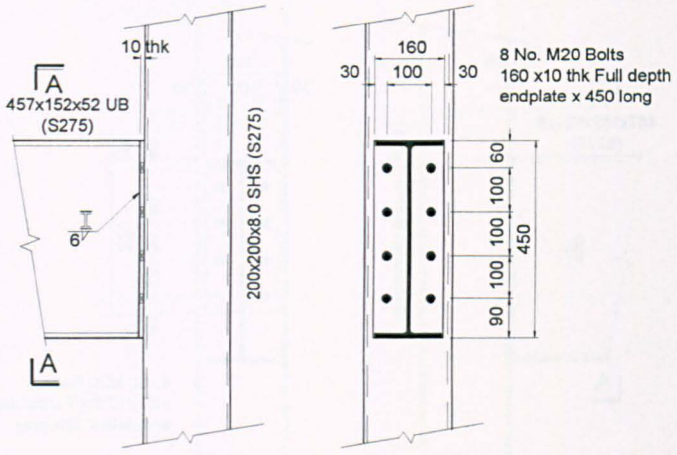

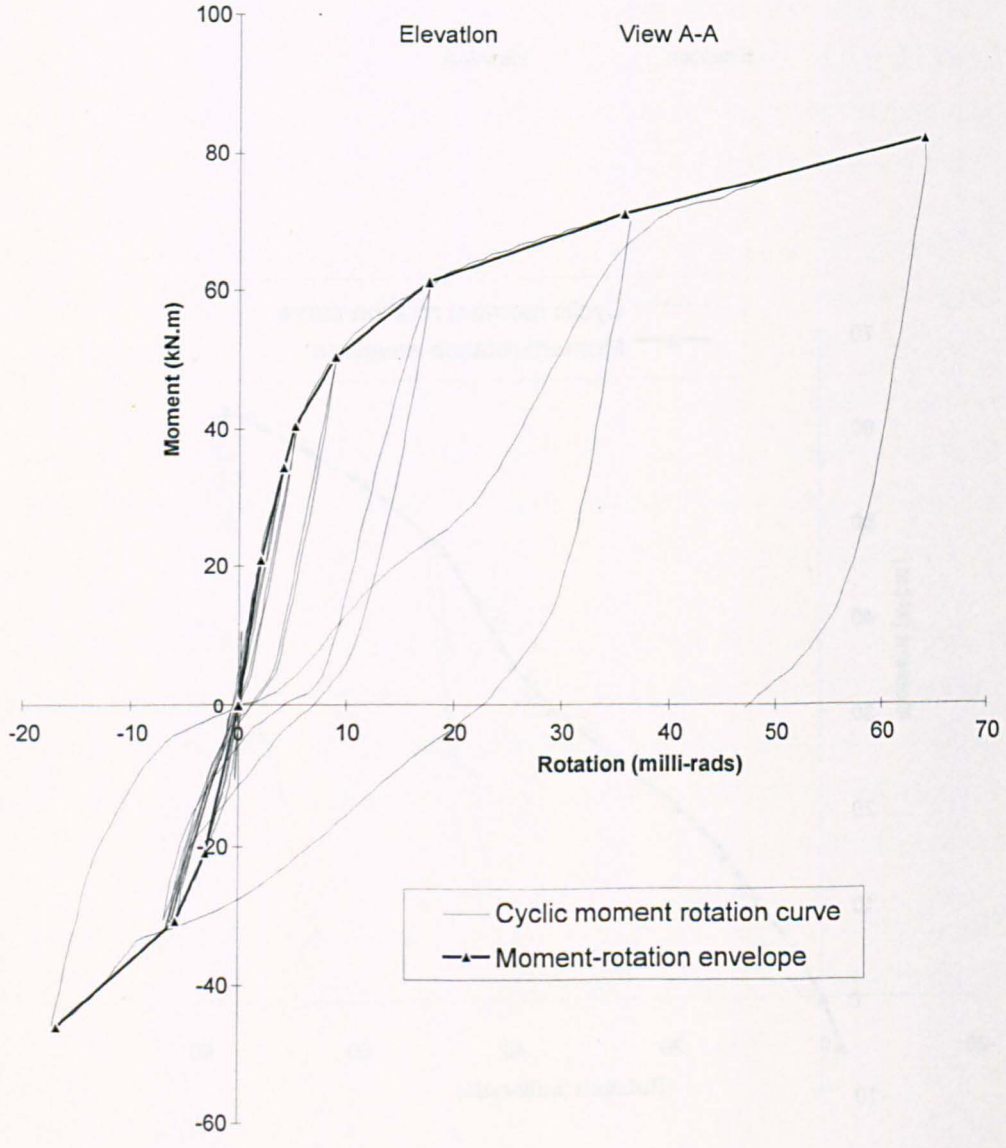

Moment rotation envelope :											
Moment (kN.m)	-46.2	-30.7	-20.9	0	20.9	34.4	40.5	50.4	61.1	71.1	82.1
Rotation (milli-rads)	-16.8	-5.8	-3.0	0	2.1	4.1	5.2	9.0	17.7	35.9	64.1

Experimental Moment-Rotation curve for Joint Test No. 3

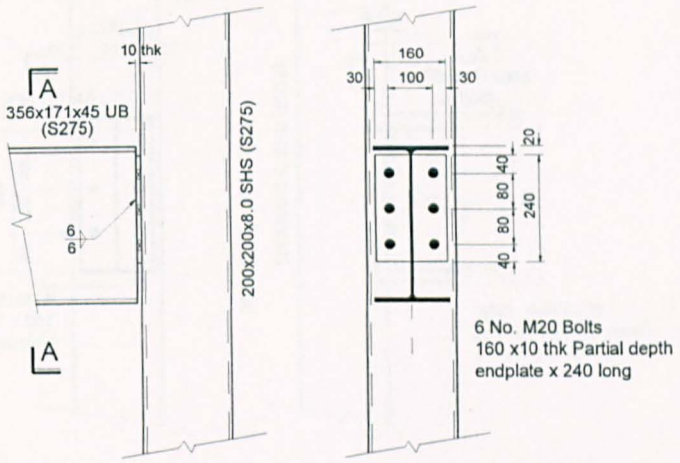

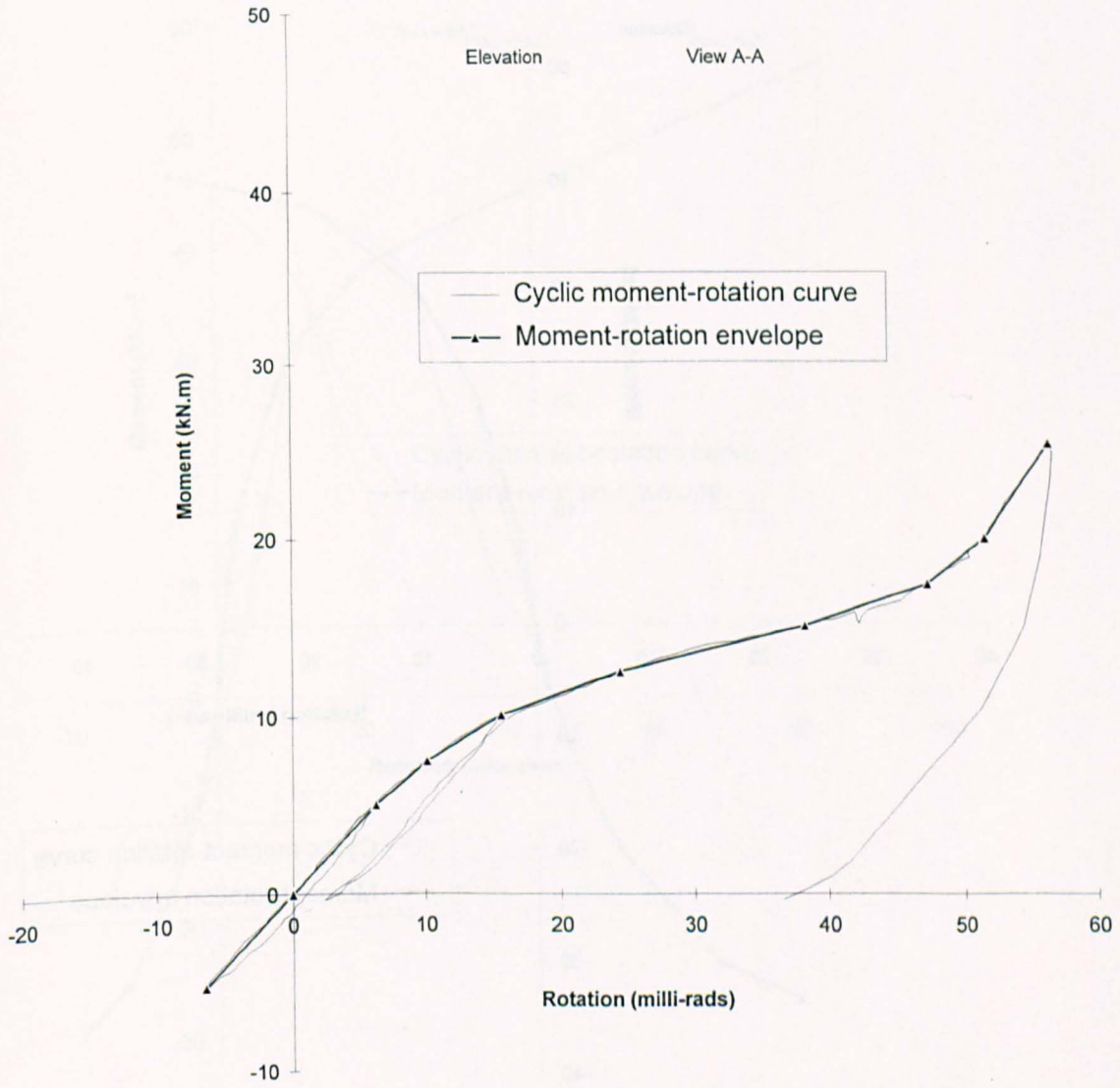

Moment rotation envelope :										
Moment (kN.m)	-5.2	0	5.1	7.6	10.1	12.5	15.1	17.4	20.1	25.5
Rotation (milli-rads)	-6.5	0	6.3	10.2	15.7	24.5	38.3	47.4	51.7	56.6

Experimental Moment-Rotation curve for Joint Test No. 4

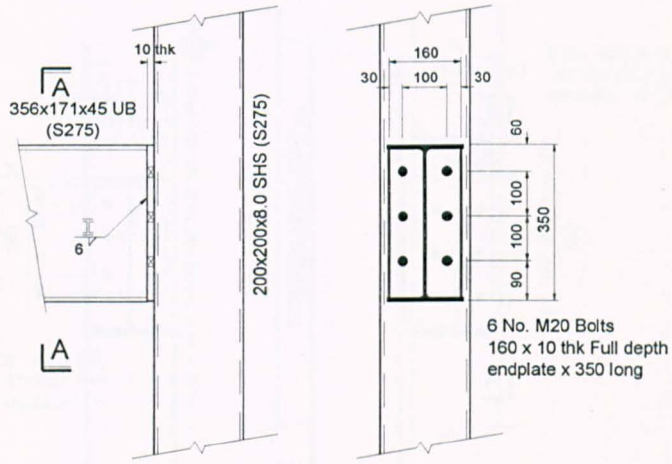

Elevation View A-A

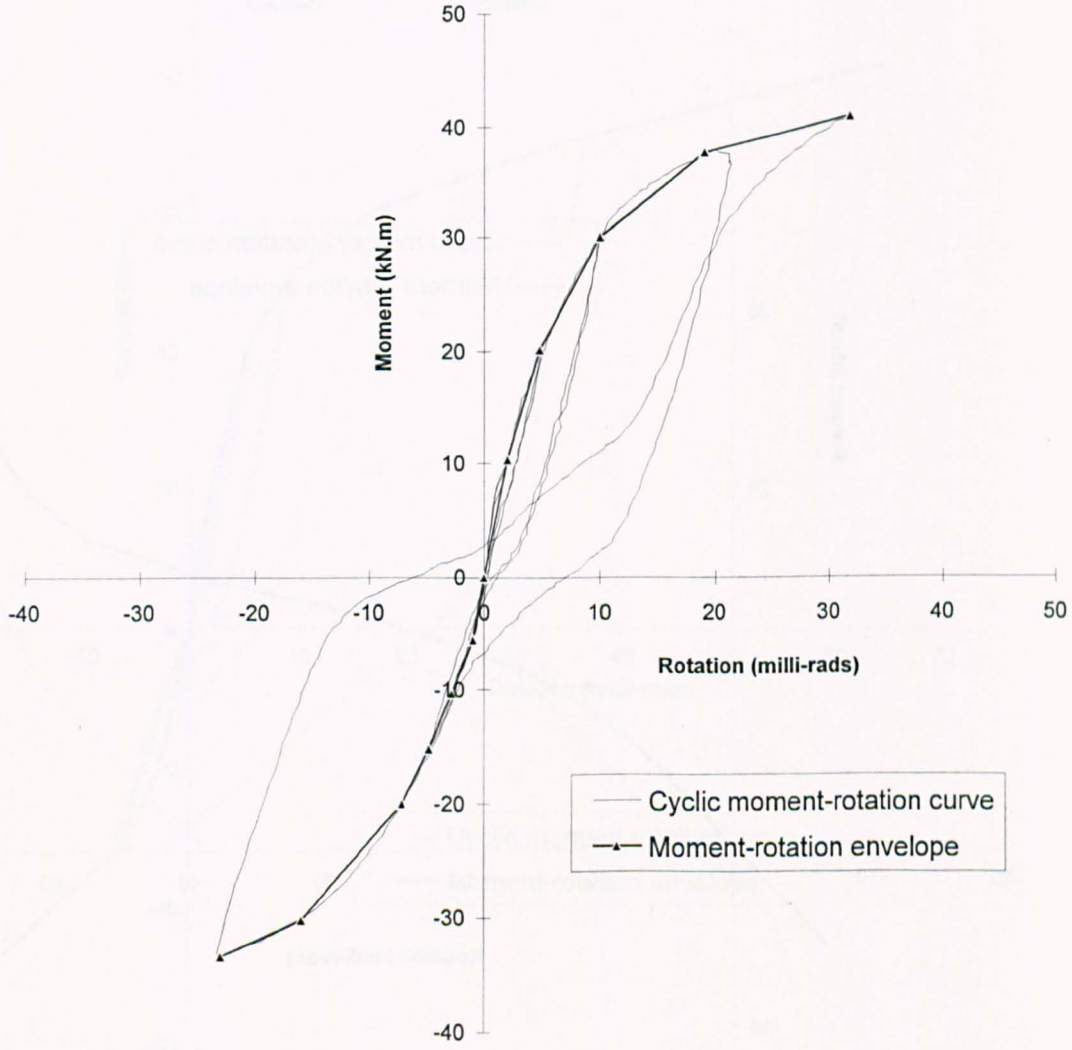

Moment rotation envelope :												
Moment (kN.m)	-33.3	-30.2	-20.2	-15.3	-10.3	-5.4	0	10.3	20.1	30.1	37.7	40.9
Rotation (milli-rads)	-23.0	-16.0	-7.3	-4.9	-2.8	-1.0	0	1.9	4.8	10.0	19.2	31.9

Experimental Moment-Rotation curve for Joint Test No. 5

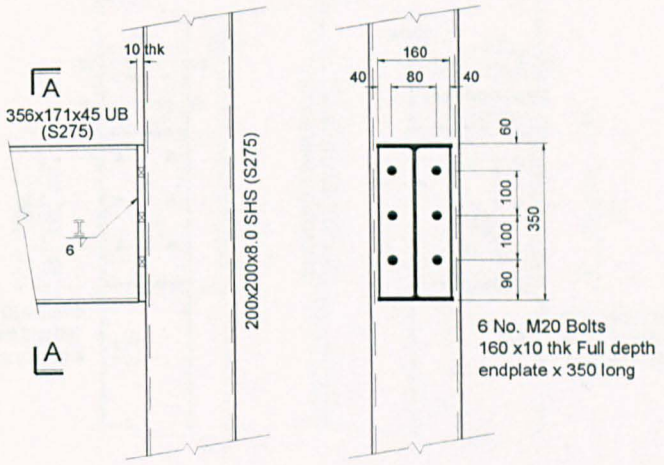

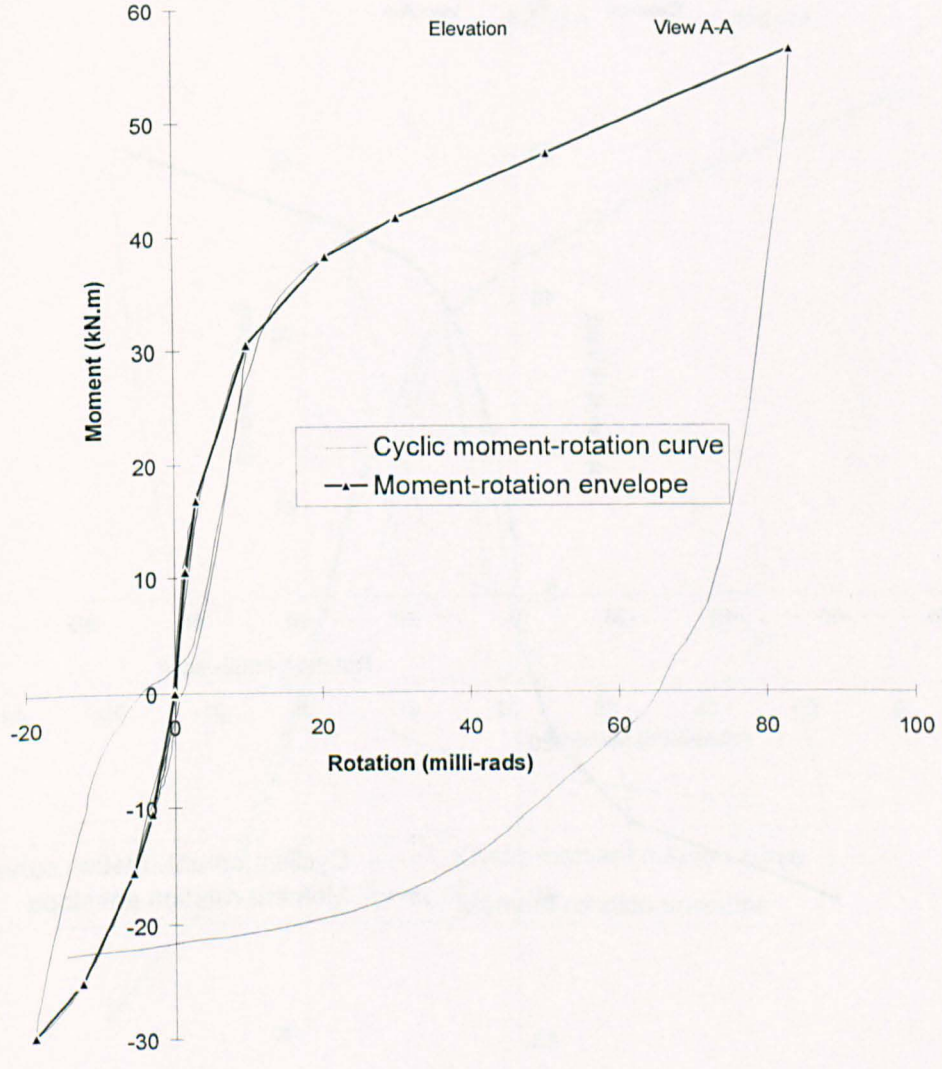

Moment rotation envelope :												
Moment (kN.m)	-29.5	-24.9	-15.4	-10.5	0	10.6	16.9	30.5	38.2	41.6	47.2	56.3
Rotation (milli-rads)	-18.9	-12.5	-5.6	-3.0	0	1.4	2.9	9.9	20.7	30.3	50.7	83.7

Experimental Moment-Rotation curve for Joint Test No. 6

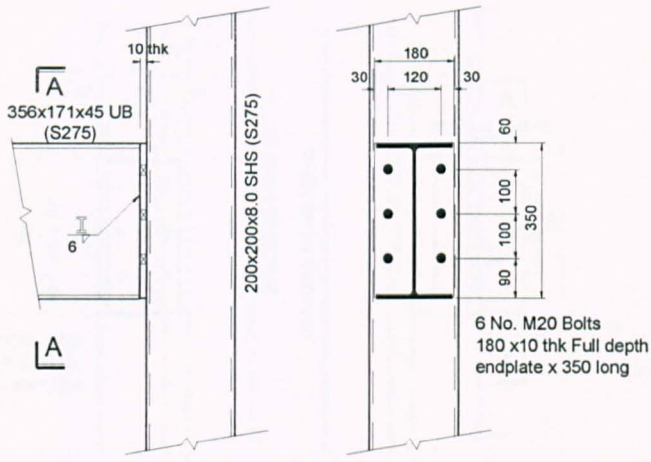

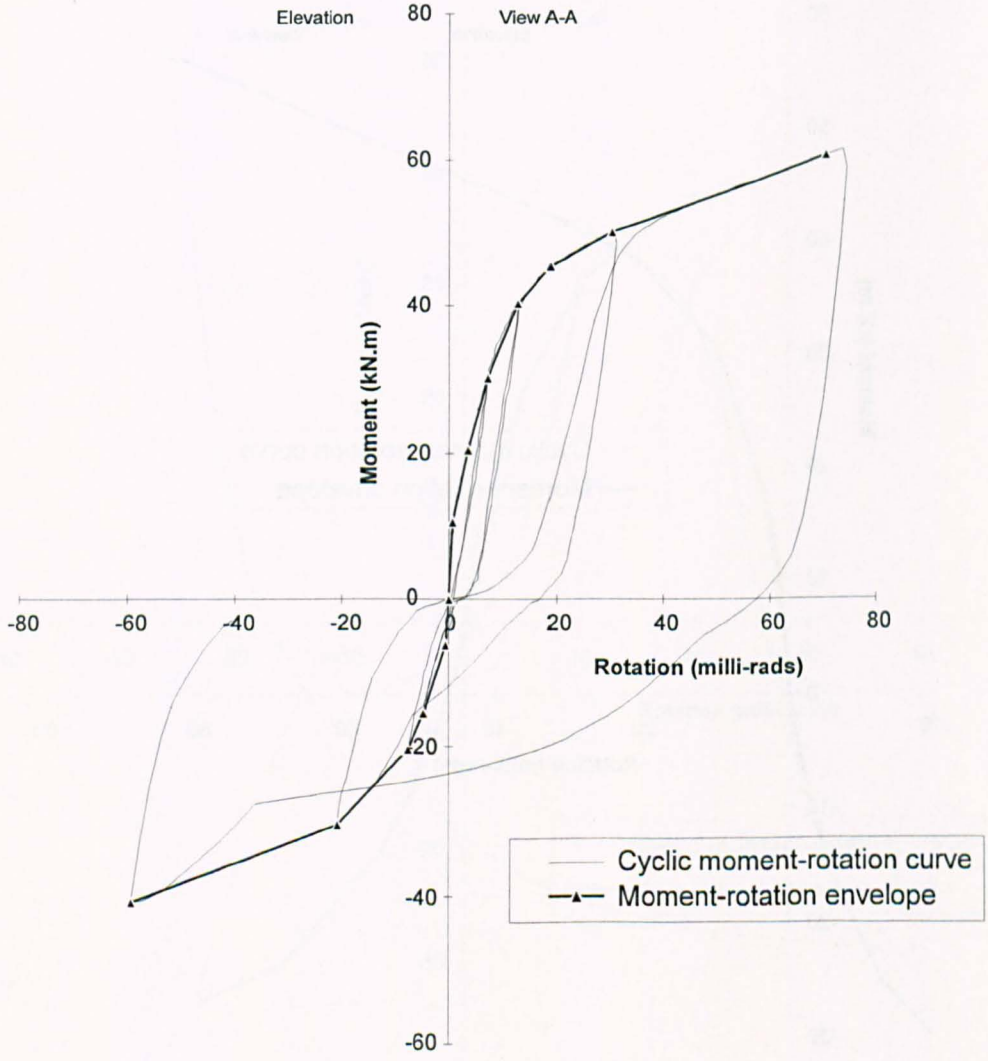

Moment rotation envelope :											
Moment (kN.m)	-40.7	-30.4	-20.4	-15.5	-6.2	0	10.5	20.5	30.2	40.2	45.3
Rotation (milli-rads)	-59.1	-20.7	-7.6	-4.7	-0.7	0	0.8	3.5	7.2	12.9	18.9

Moment rotation envelope con'd:		
Moment (kN.m)	50.1	60.8
Rotation (milli-rads)	30.3	70.5

Experimental Moment-Rotation curve for Joint Test No. 7

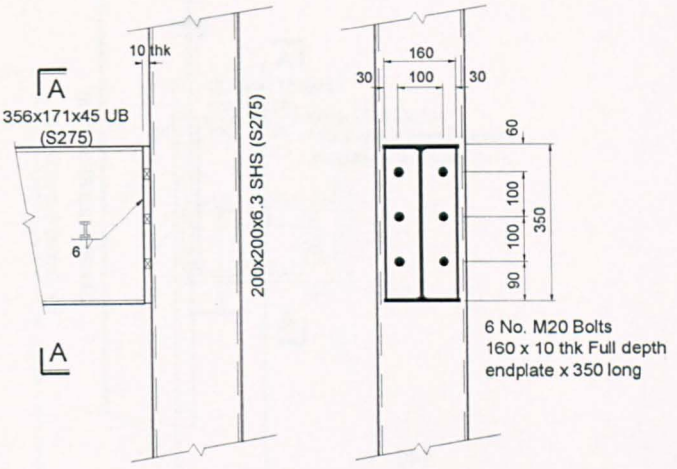

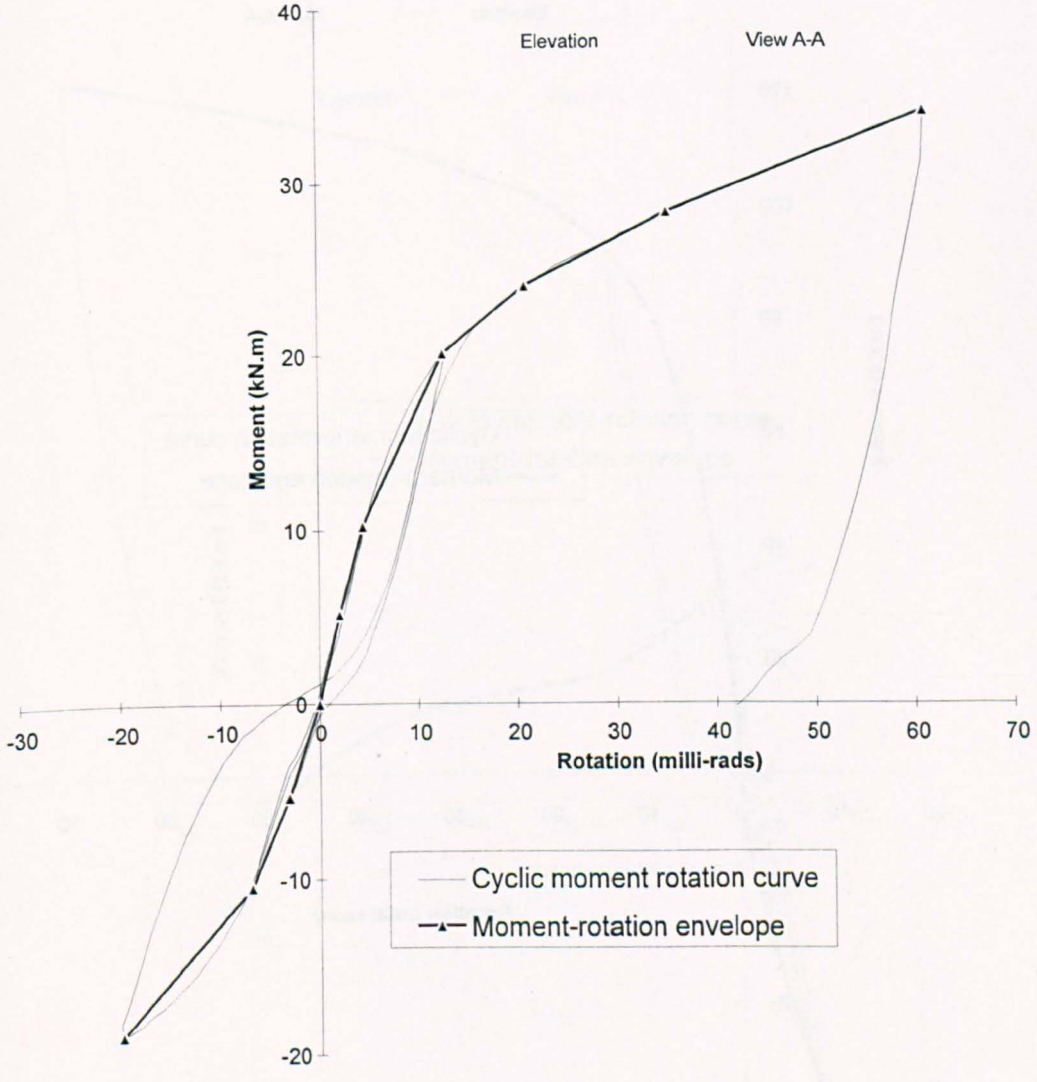

Moment rotation envelope :										
Moment (kN.m)	-18.9	-10.4	-5.8	0	5.1	10.3	20.1	24.0	28.3	34.1
Rotation (milli-rads)	-19.9	-6.9	-3.2	0	2.1	4.5	12.6	21.0	35.3	61.2

Experimental Moment-Rotation curve for Joint Test No. 8

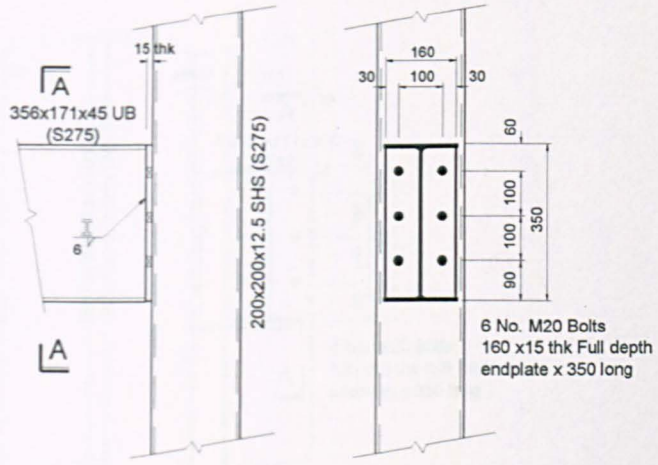

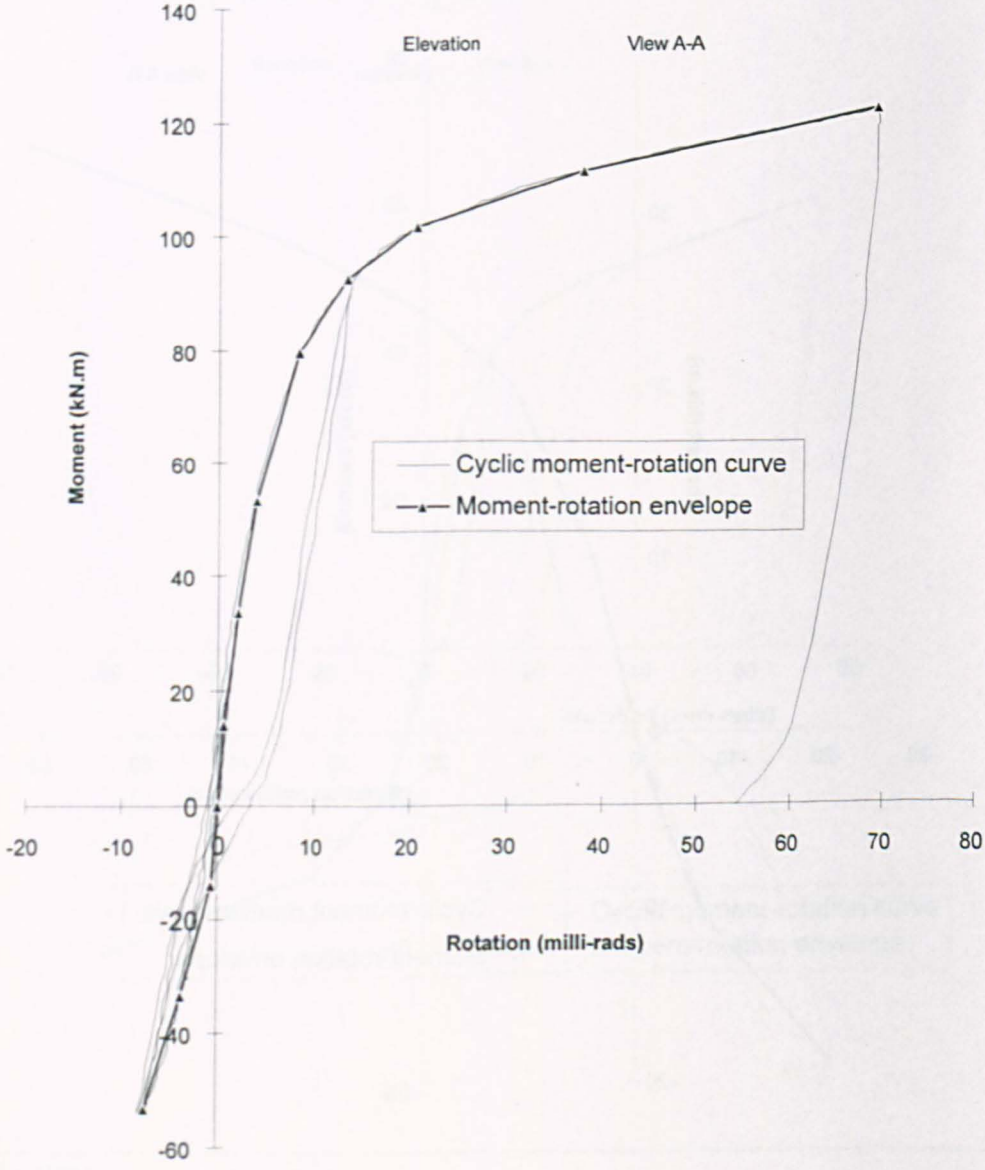

Moment rotation envelope :												
Moment (kN.m)	-53.3	-33.6	-14.1	0	14.0	33.5	53.2	79.7	92.5	101.7	111.8	122.5
Rotation (milli-rads)	-7.4	-3.8	-0.7	0	0.6	2.1	3.9	8.4	13.3	20.6	37.9	69.4

Experimental Moment-Rotation curve for Joint Test No. 9

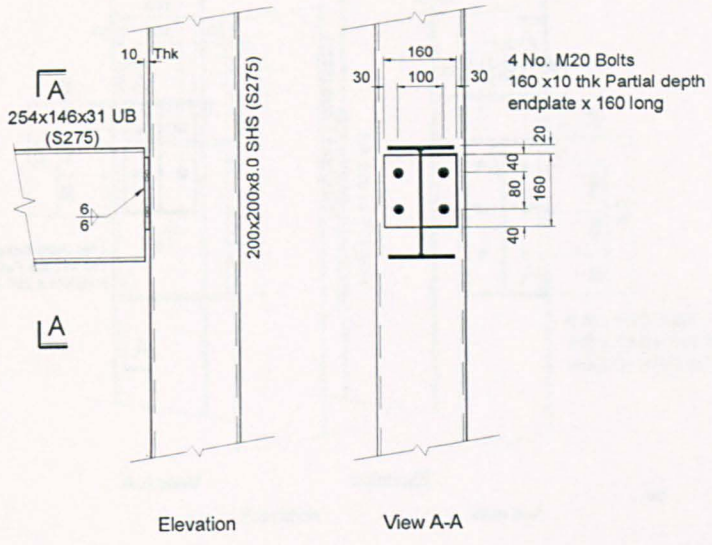

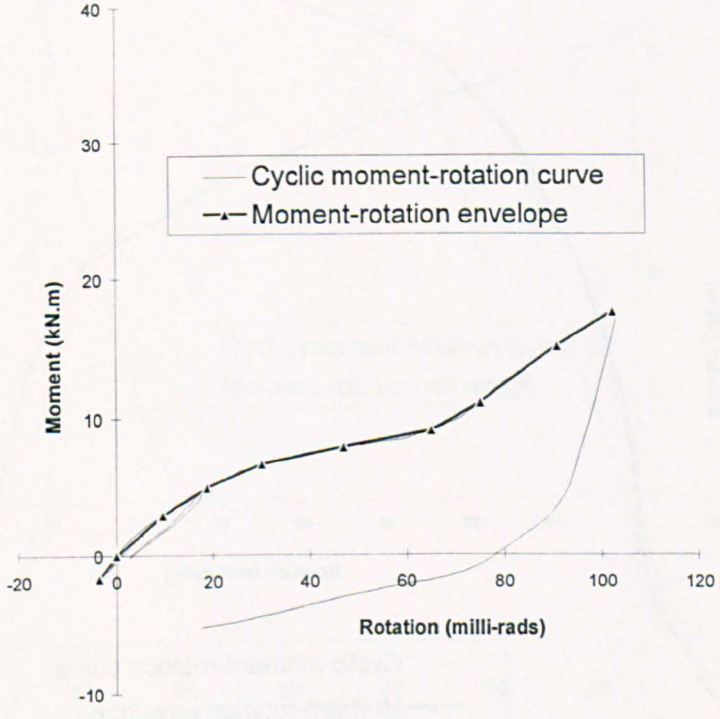

Moment rotation envelope :										
Moment (kN.m)	-1.7	0	2.9	4.9	6.6	7.8	9.1	11.0	15.1	17.5
Rotation (milli-rads)	-3.5	0	9.6	18.7	30.1	47.1	65.1	75.1	91.1	102.5

Experimental Moment-Rotation curve for Joint Test No. 10

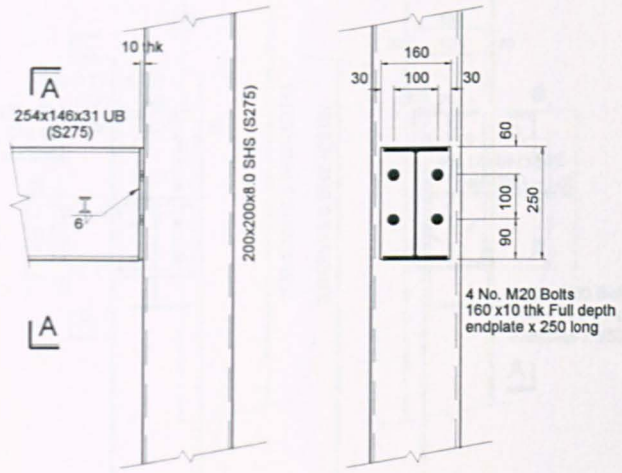

Elevation View A-A

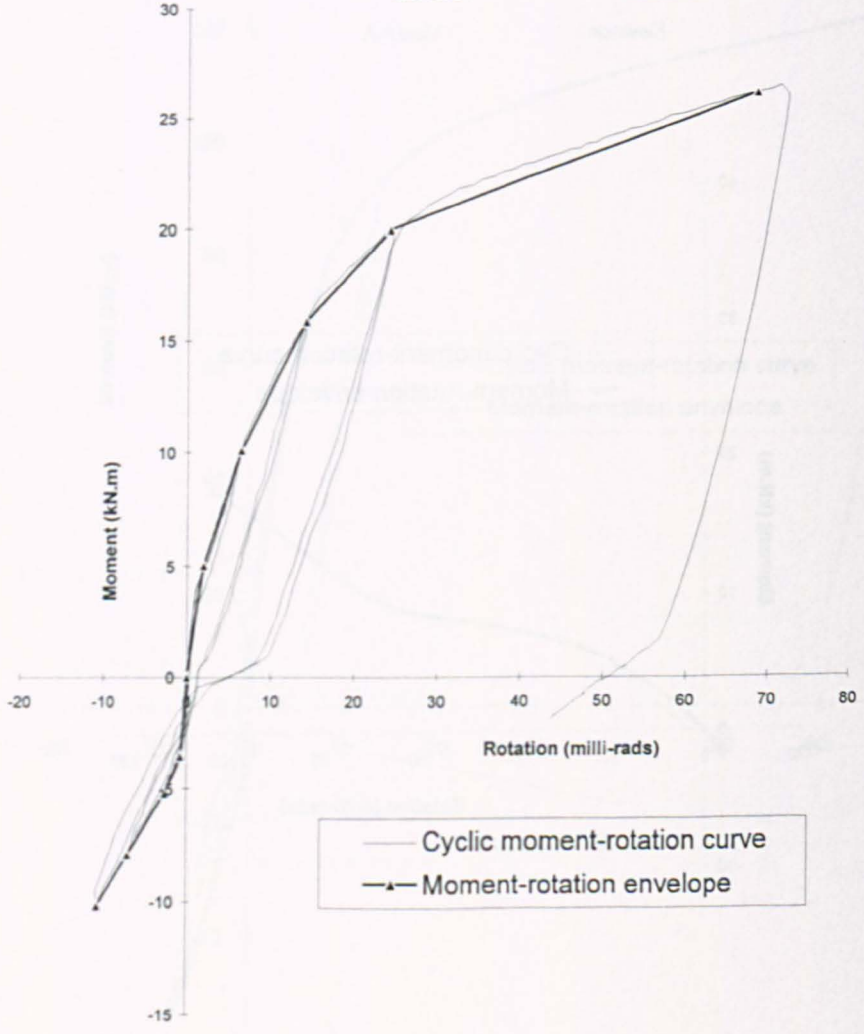

Moment rotation envelope :										
Moment (kN.m)	-10.2	-7.9	-5.2	-3.5	0	5.0	10.1	15.9	20.0	26.2
Rotation (milli-rads)	-10.7	-7.0	-2.5	-0.8	0	2.0	6.4	14.1	24.3	68.7

Experimental Moment-Rotation curve for Joint Test No. 11

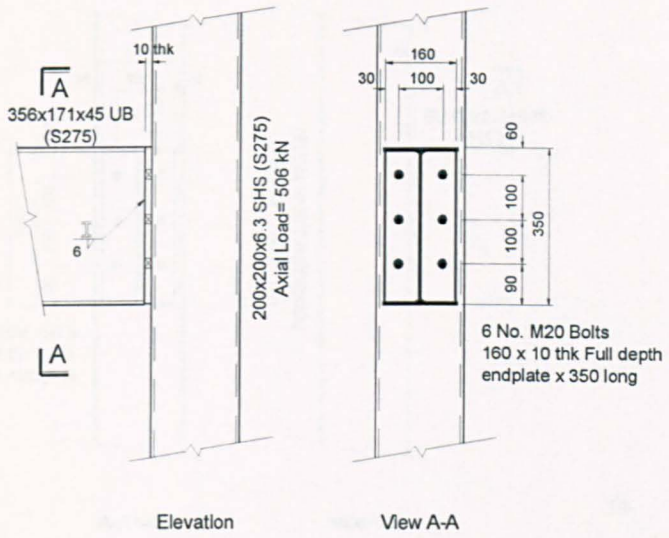

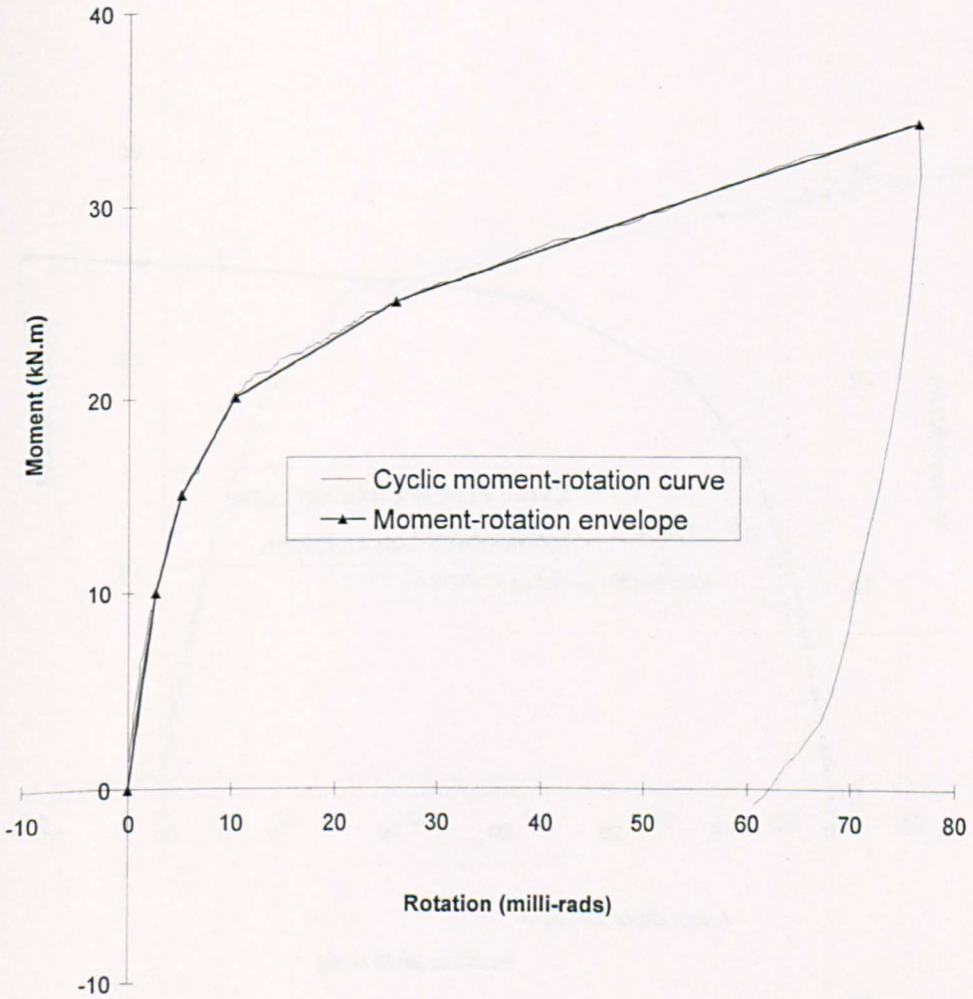

Moment rotation envelope :						
Moment (kN.m)	0	10.0	15.0	20.2	25.0	34.4
Rotation (milli-rads)	0	2.8	5.3	10.4	25.8	76.5

Experimental Moment-Rotation curve for Joint Test No. 12

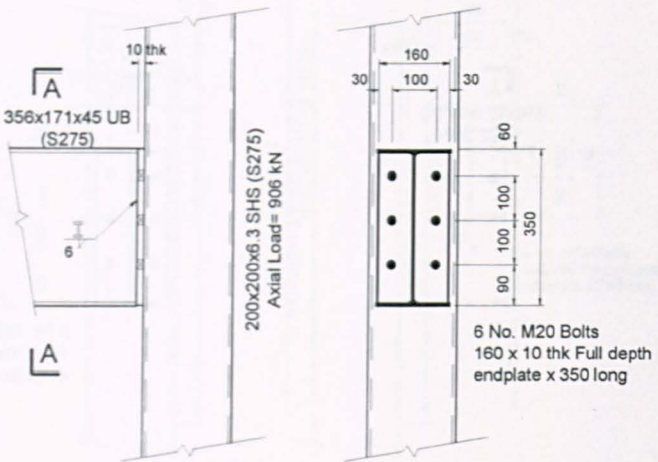

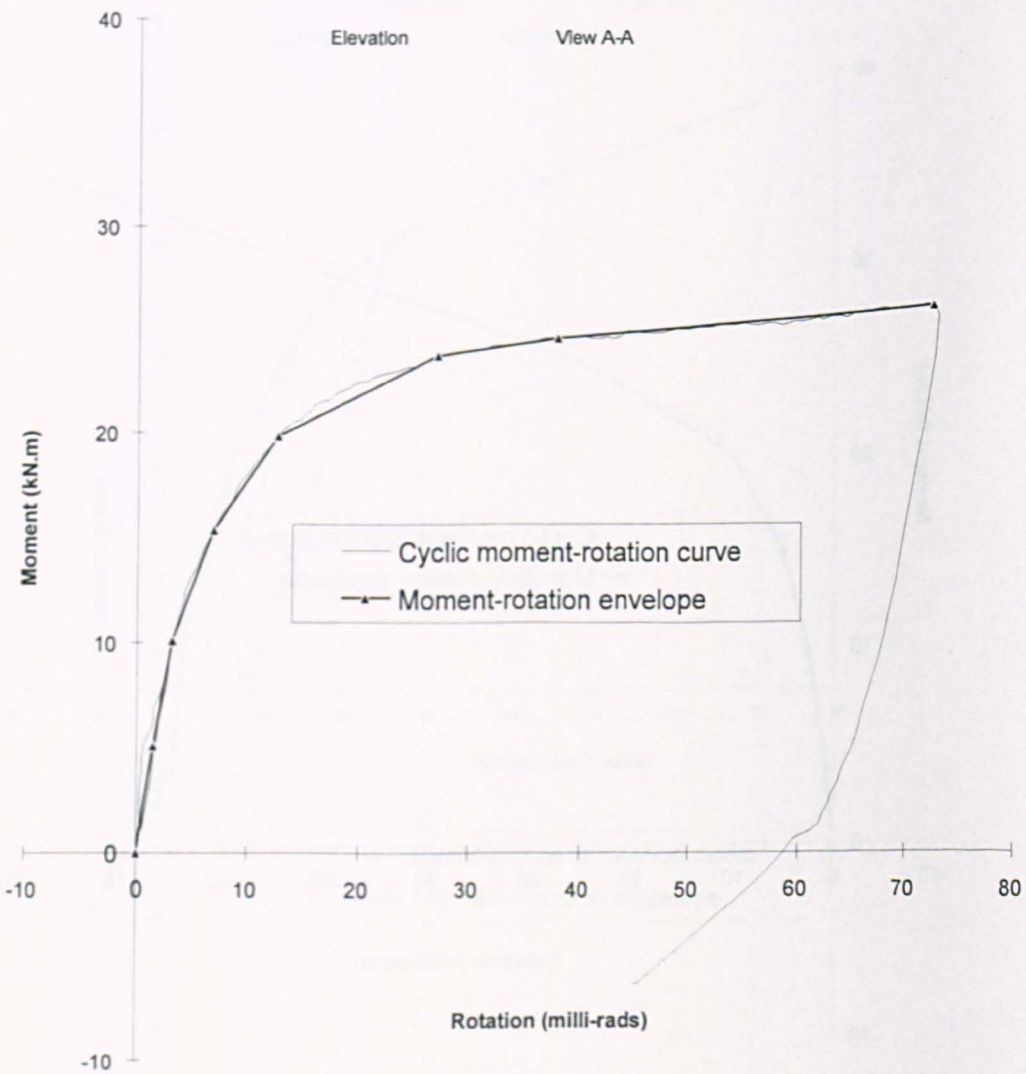

Moment rotation envelope :								
Moment (kN.m)	0	5.1	10.1	15.4	19.9	23.8	24.6	26.2
Rotation (milli-rads)	0	1.6	3.2	6.9	12.7	27.0	37.9	72.6

Experimental Moment-Rotation curve for Joint Test No. 13

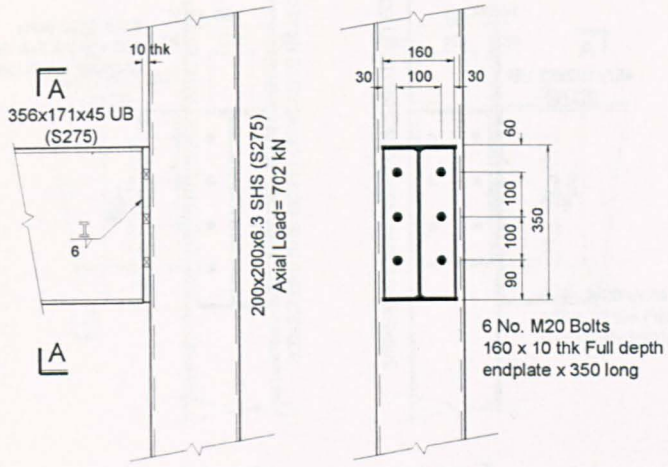

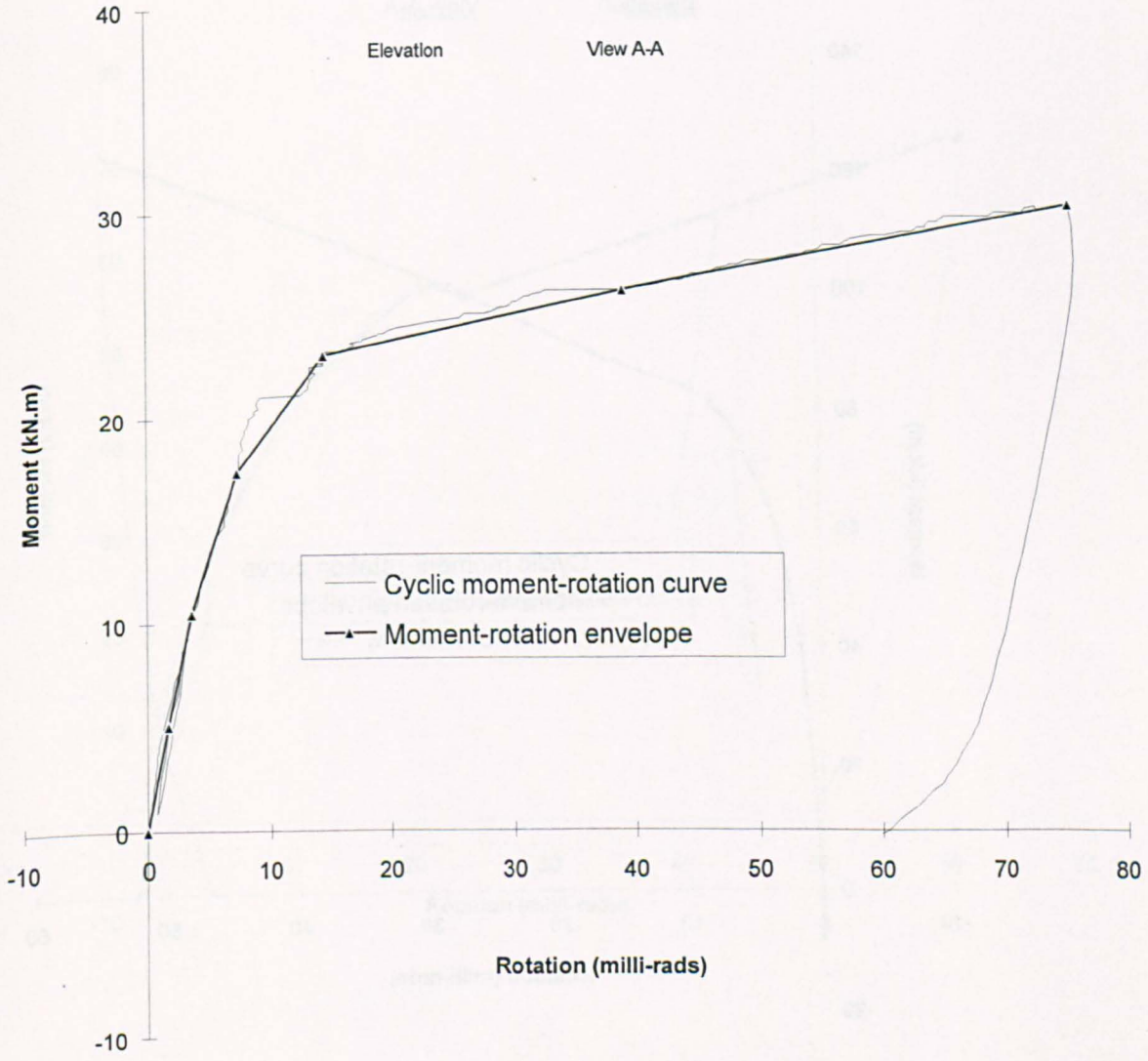

Moment rotation envelope :							
Moment (kN.m)	0	5.0	10.5	17.3	23.1	26.2	30.4
Rotation (milli-rads)	0	1.7	3.6	7.3	14.4	39.1	75.4

Experimental Moment-Rotation curve for Joint Test No. 14

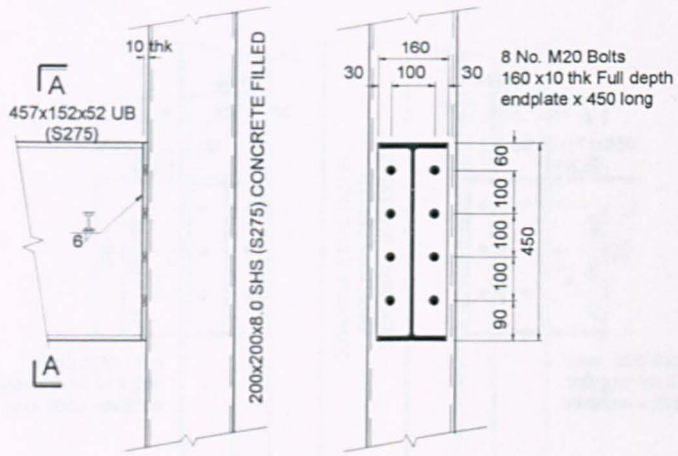

Elevation View A-A

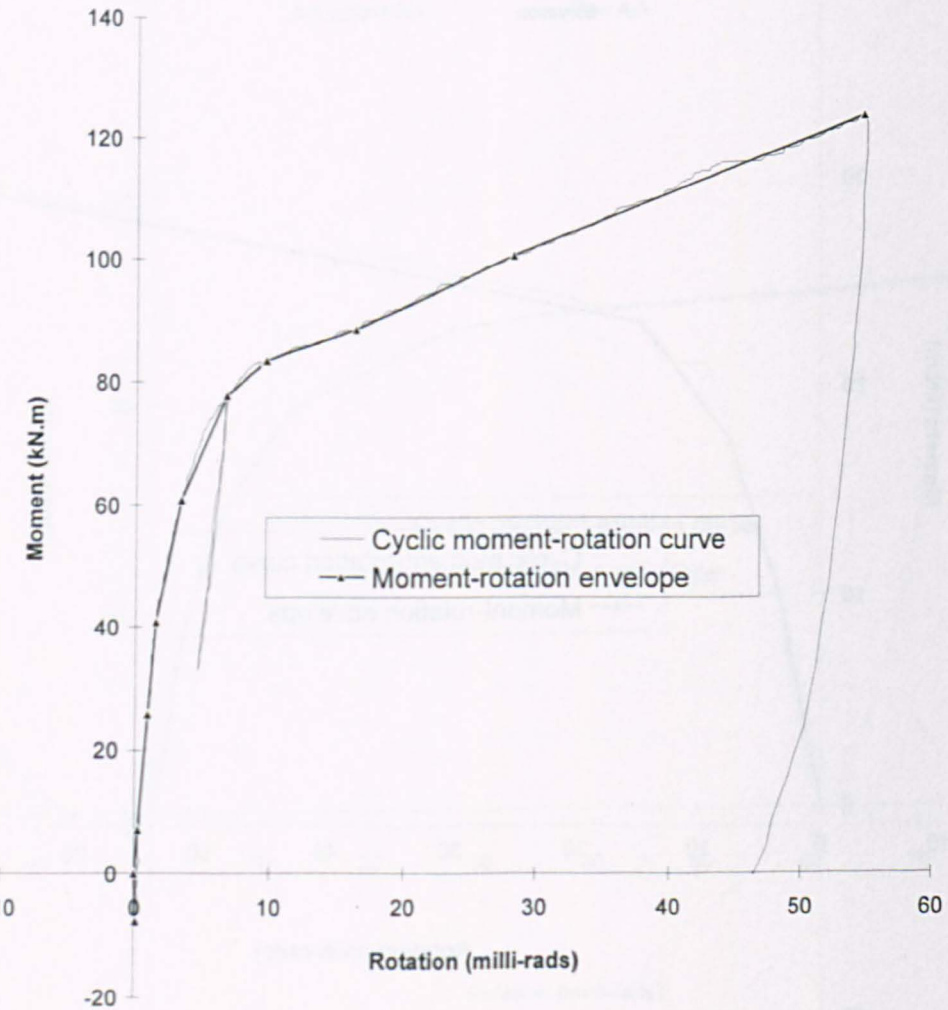

Moment rotation envelope :											
Moment (kN.m)	-7.8	0	7.2	25.7	41.0	60.9	77.7	83.5	88.7	100.5	124.1
Rotation (milli-rads)	0.2	0	0.3	0.9	1.6	3.4	6.7	9.7	16.3	28.2	54.7

Experimental Moment-Rotation curve for Joint Test No. 15

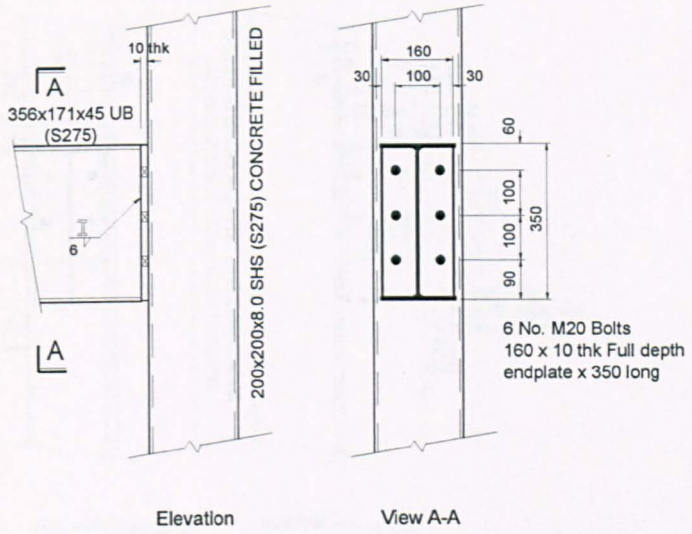

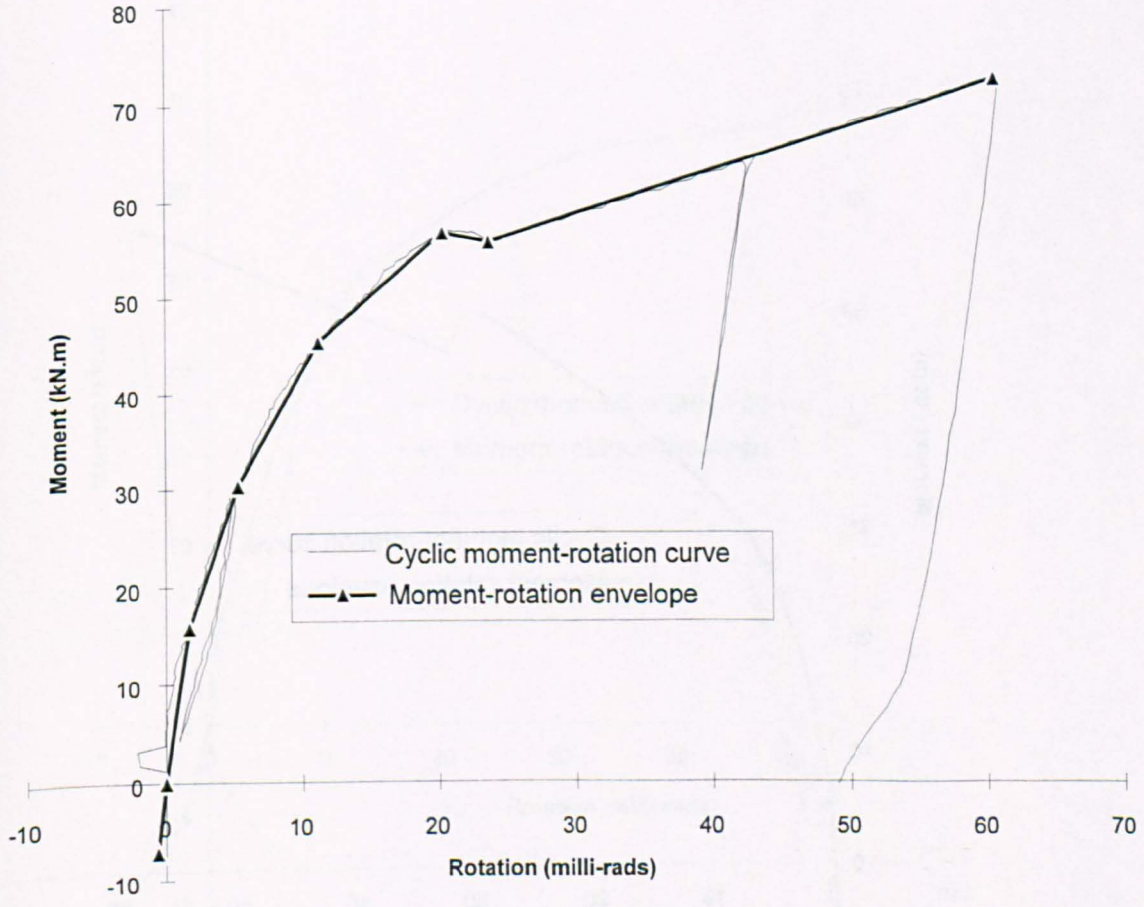

Moment rotation envelope :								
Moment (kN.m)	-7.1	0	15.8	30.3	45.4	56.7	55.8	72.7
Rotation (milli-rads)	-0.6	0	1.7	5.3	11.2	20.3	23.7	60.7

Experimental Moment-Rotation curve for Joint Test No. 16

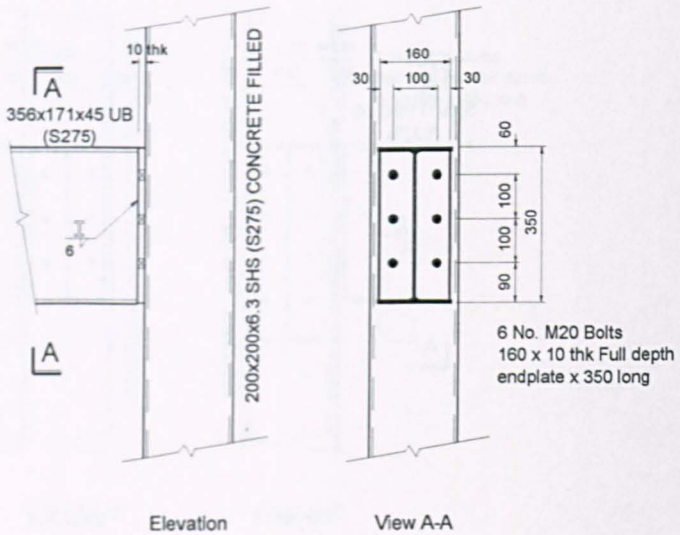

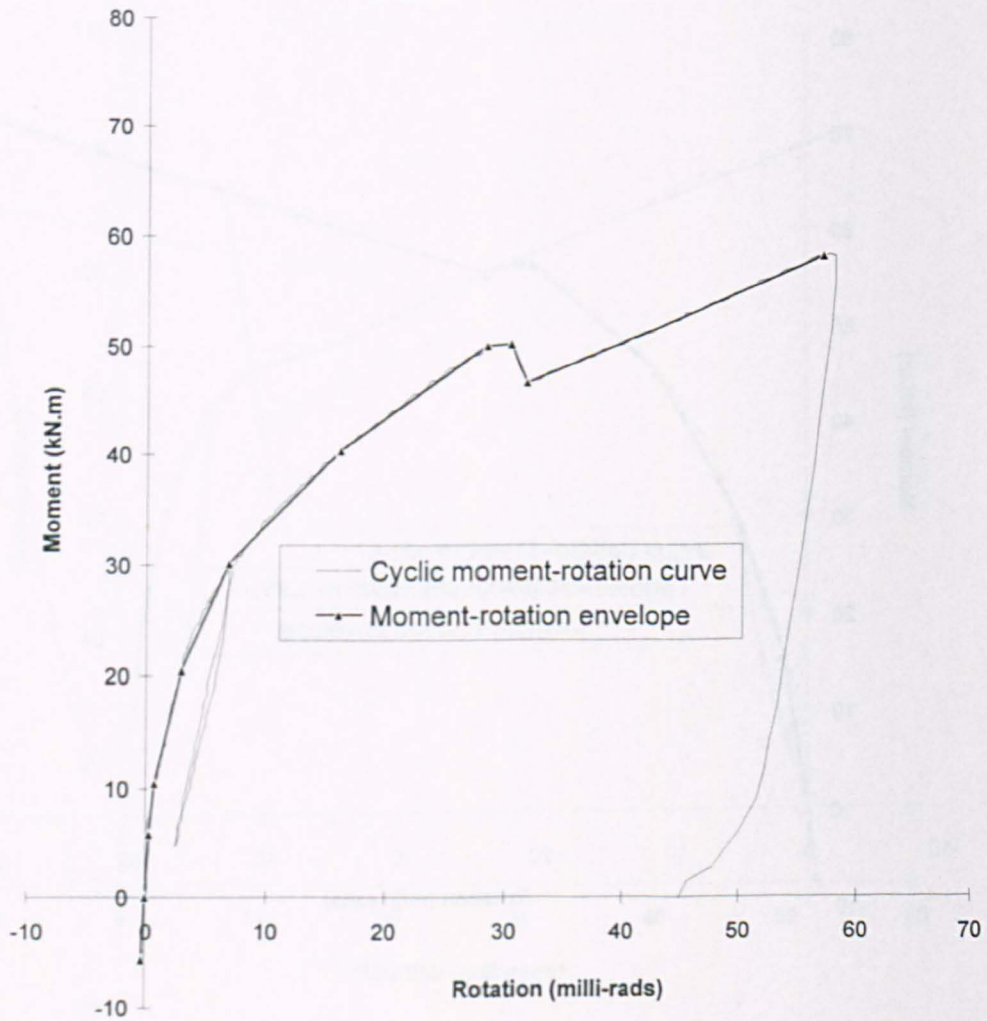

Moment rotation envelope :											
Moment (kN.m)	-5.7	0	5.8	10.5	20.5	30.2	40.3	49.9	50.1	46.7	58.2
Rotation (milli-rads)	-0.4	0	0.2	0.7	2.8	6.8	16.3	28.4	30.5	31.8	57.2

Experimental Moment-Rotation curve for Joint Test No. 17

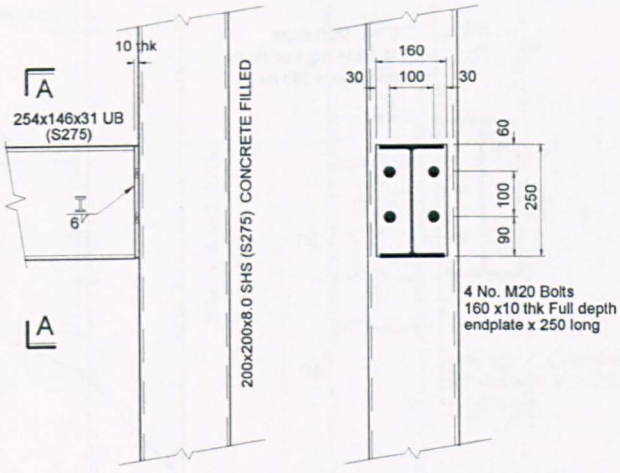

Elevation View A-A

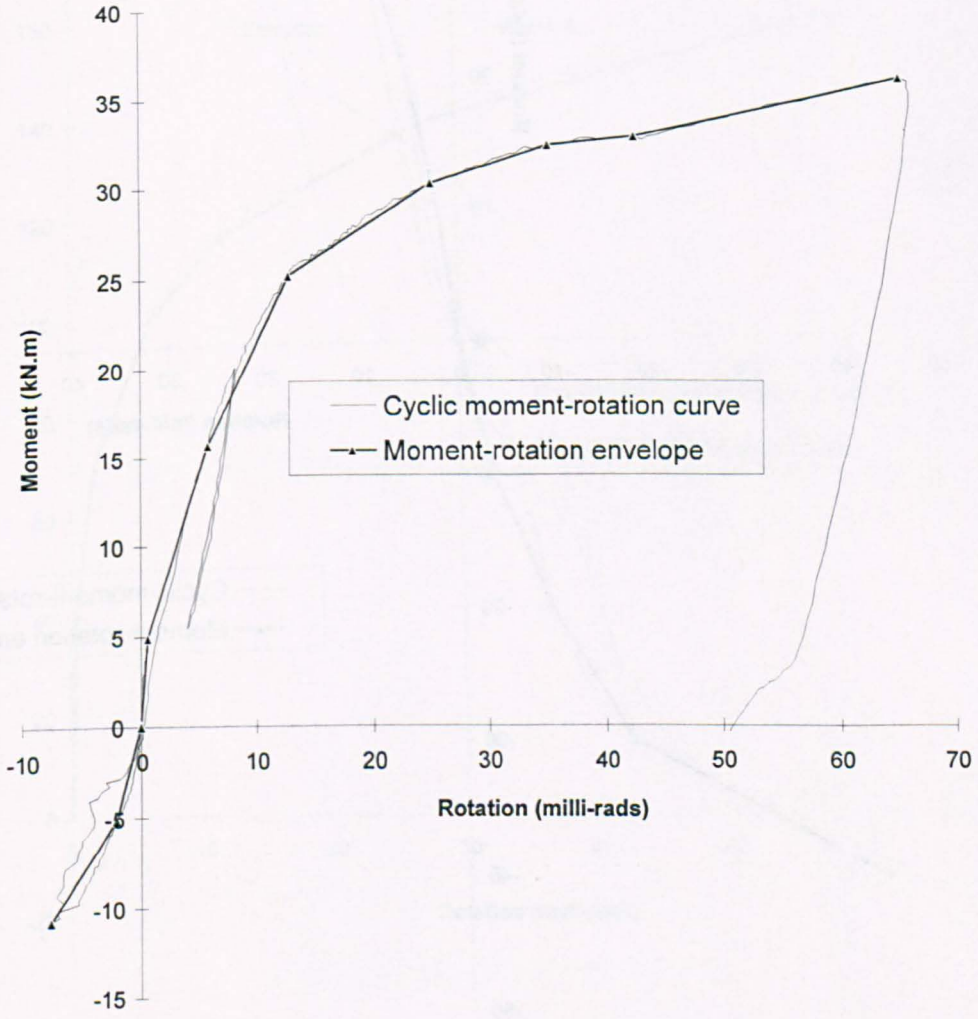

Moment rotation envelope :										
Moment (kN.m)	-10.7	-5.1	0	4.9	15.7	25.2	30.3	32.4	32.9	36.2
Rotation (milli-rads)	-7.6	-1.9	0	0.7	5.8	12.9	25.2	35.2	42.5	65.3

Experimental Moment-Rotation curve for Joint Test No. 18

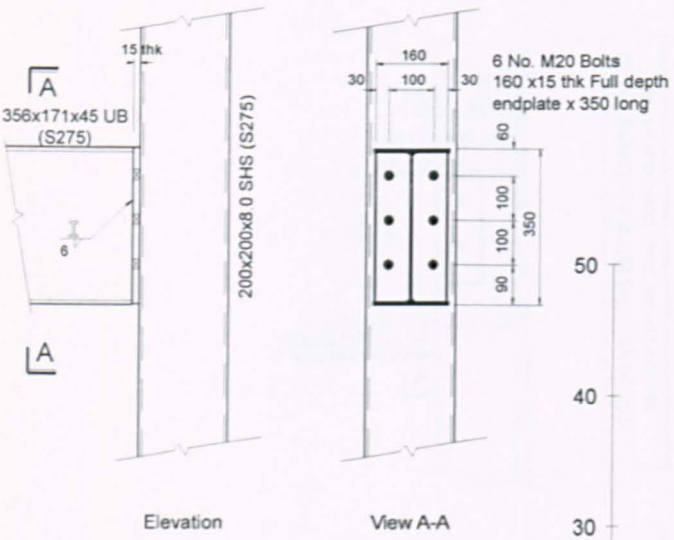

Moment rotation envelope :										
Moment (kN.m)	-40.4	-30.2	-19.8	-10.1	0	10.7	20.3	30.1	40.1	49.9
Rotation (milli-rads)	-42.9	-17.2	-8.8	-3.3	0	2.2	4.9	8.9	20.8	48.9

Experimental Moment-Rotation curve for Joint Test No. 19

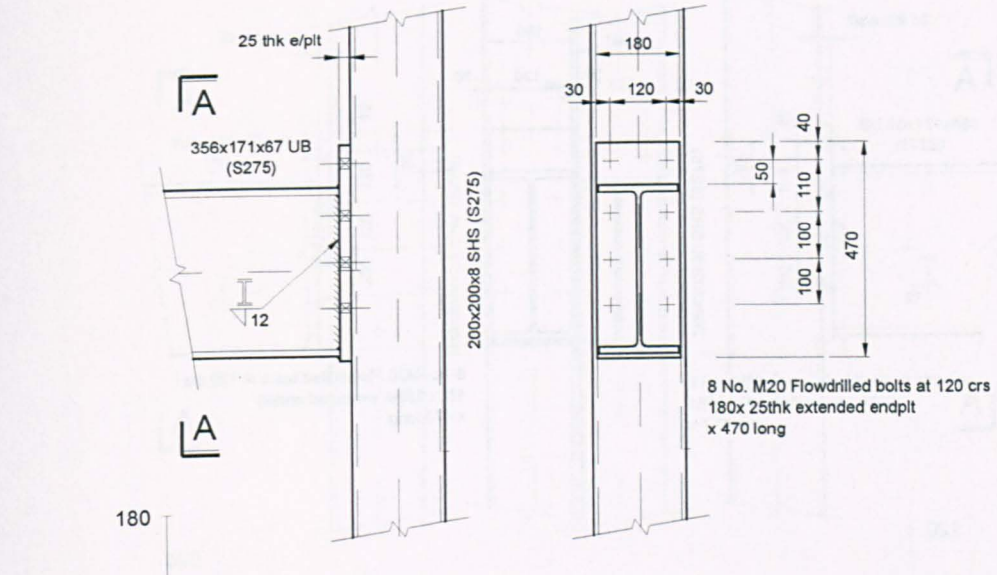

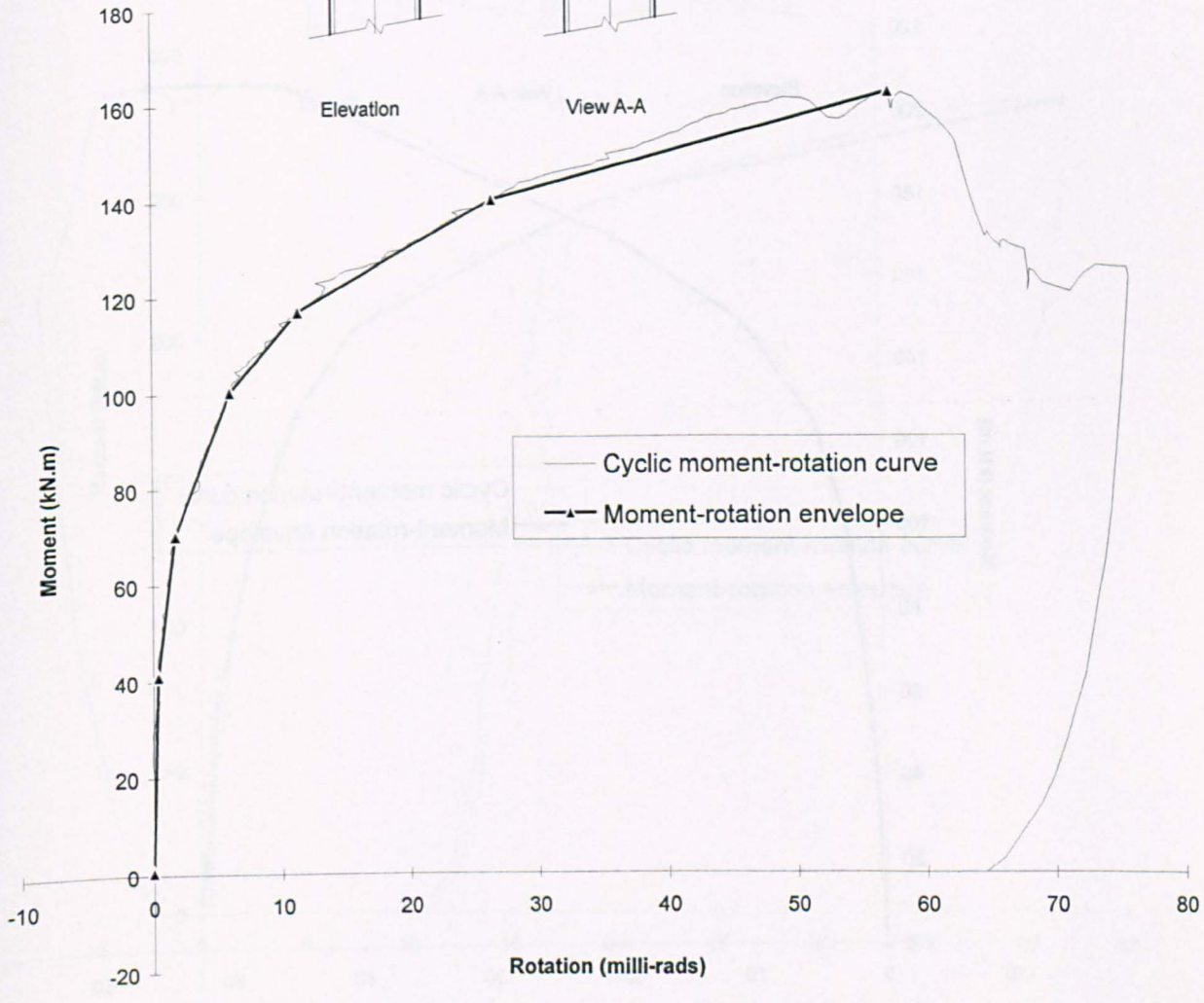

Moment rotation envelope :							
Moment (kN.m)	0	41.1	70.3	100.3	116.9	140.1	162.1
Rotation (milli-rads)	0	0.4	1.7	6.0	11.3	26.5	57.3

Experimental Moment-Rotation curve for Joint Test No. 20

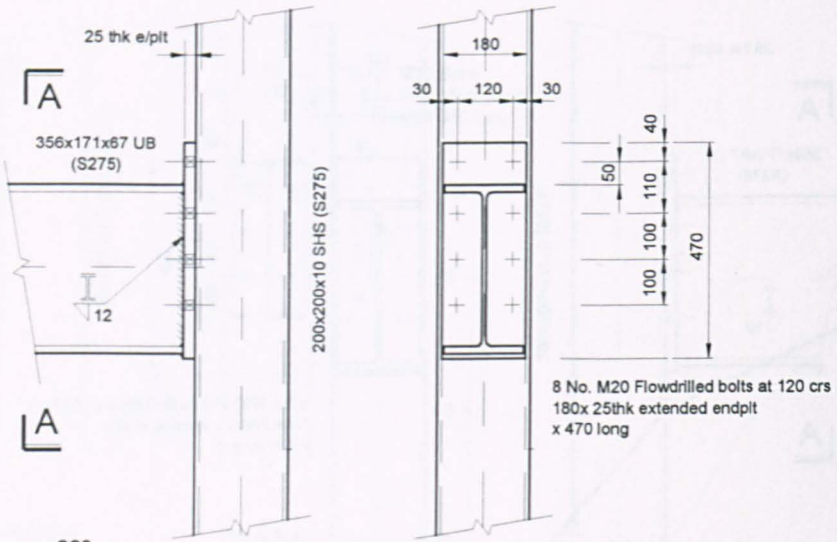

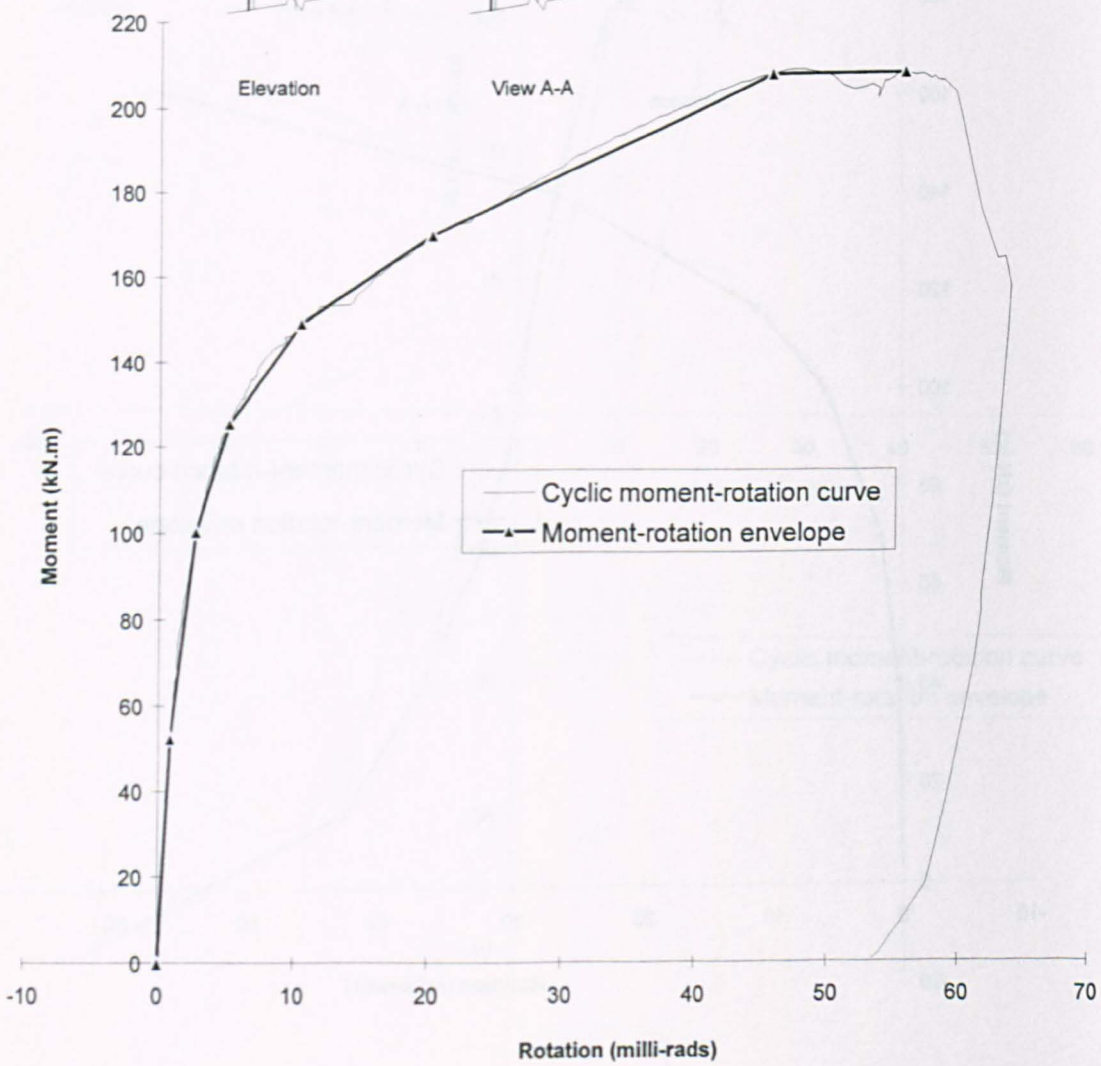

Moment rotation envelope :								
Moment (kN.m)	0	52.3	100.2	125.4	149.1	170.0	208.0	208.3
Rotation (milli-rads)	0	0.9	2.7	5.1	10.5	20.3	45.8	55.9

Experimental Moment-Rotation curve for Joint Test No. 21

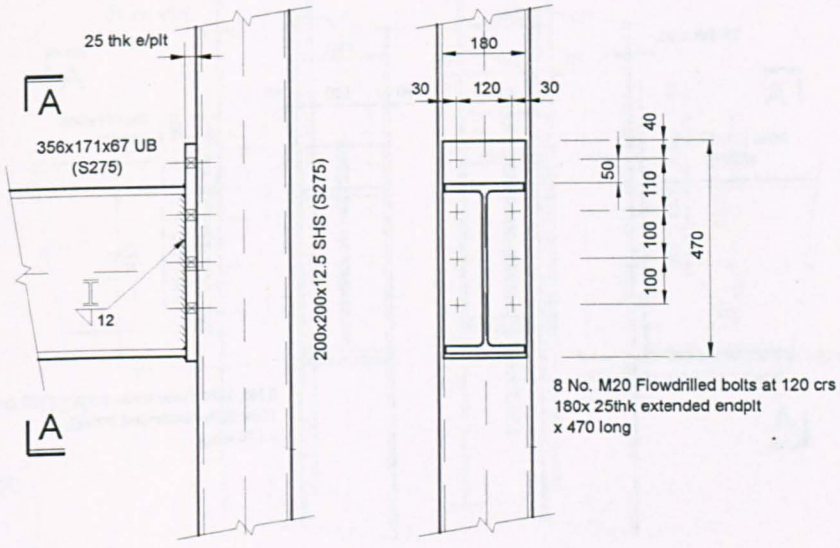

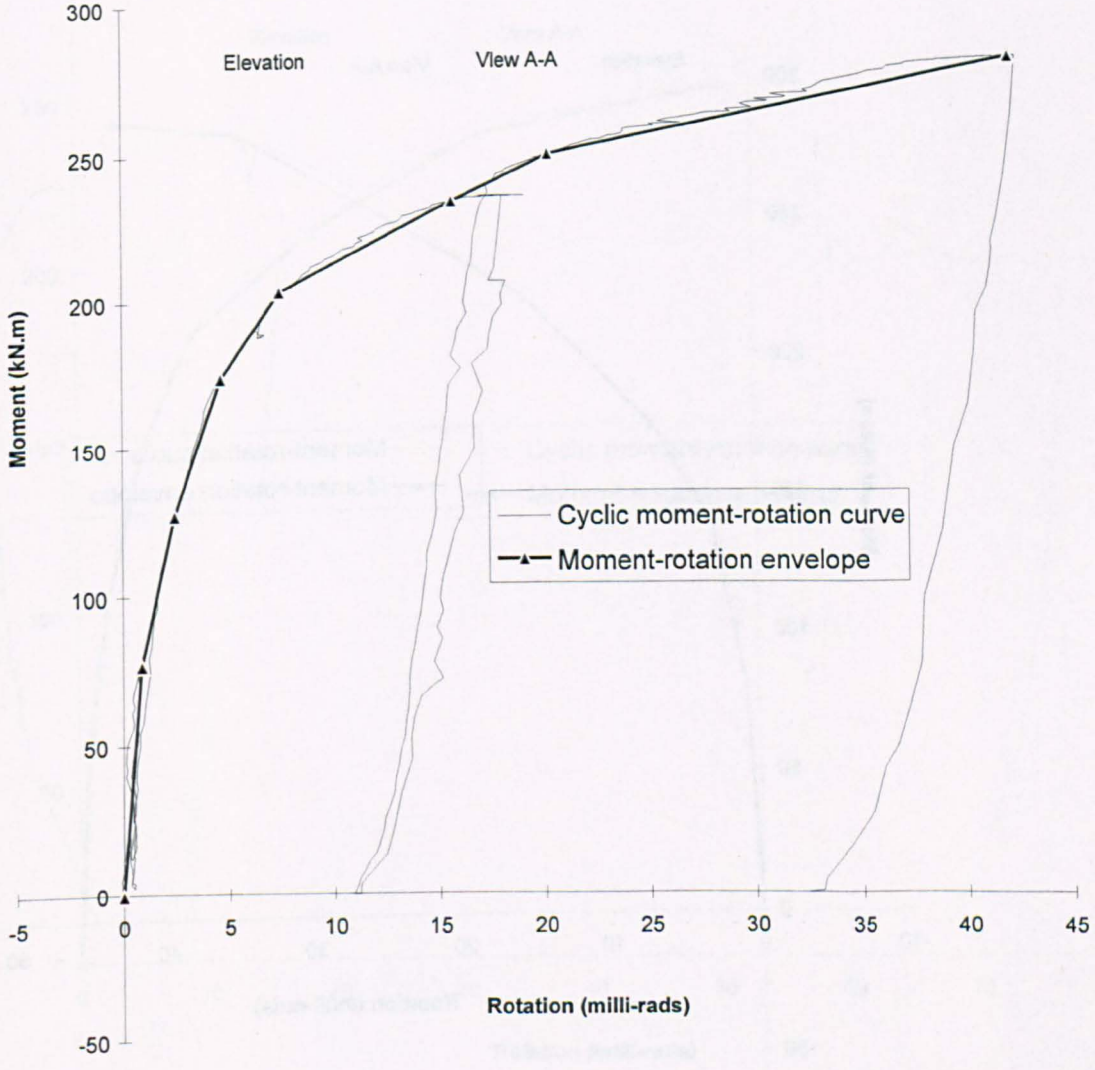

Moment rotation envelope :								
Moment (kN.m)	0	76.6	127.0	173.8	203.3	234.4	250.7	282.9
Rotation (milli-rads)	0	0.9	2.5	4.6	7.4	15.7	20.3	42.1

Experimental Moment-Rotation curve for Joint Test No. 22

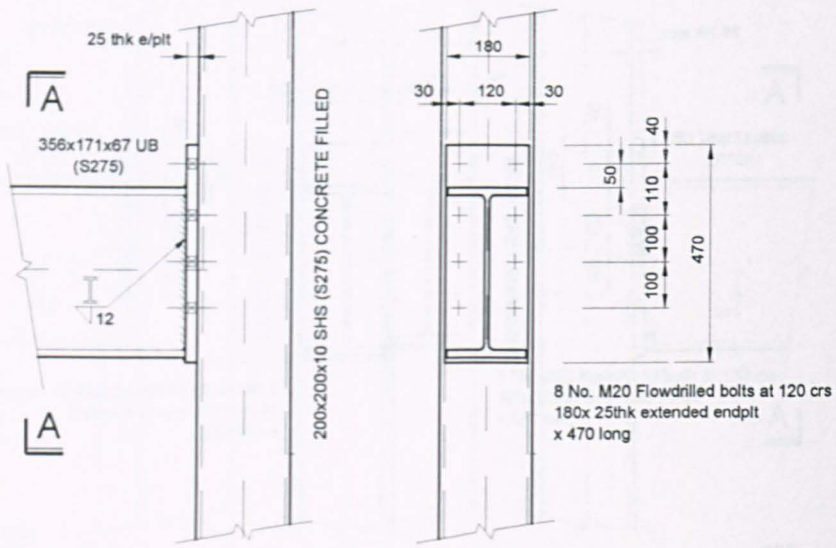

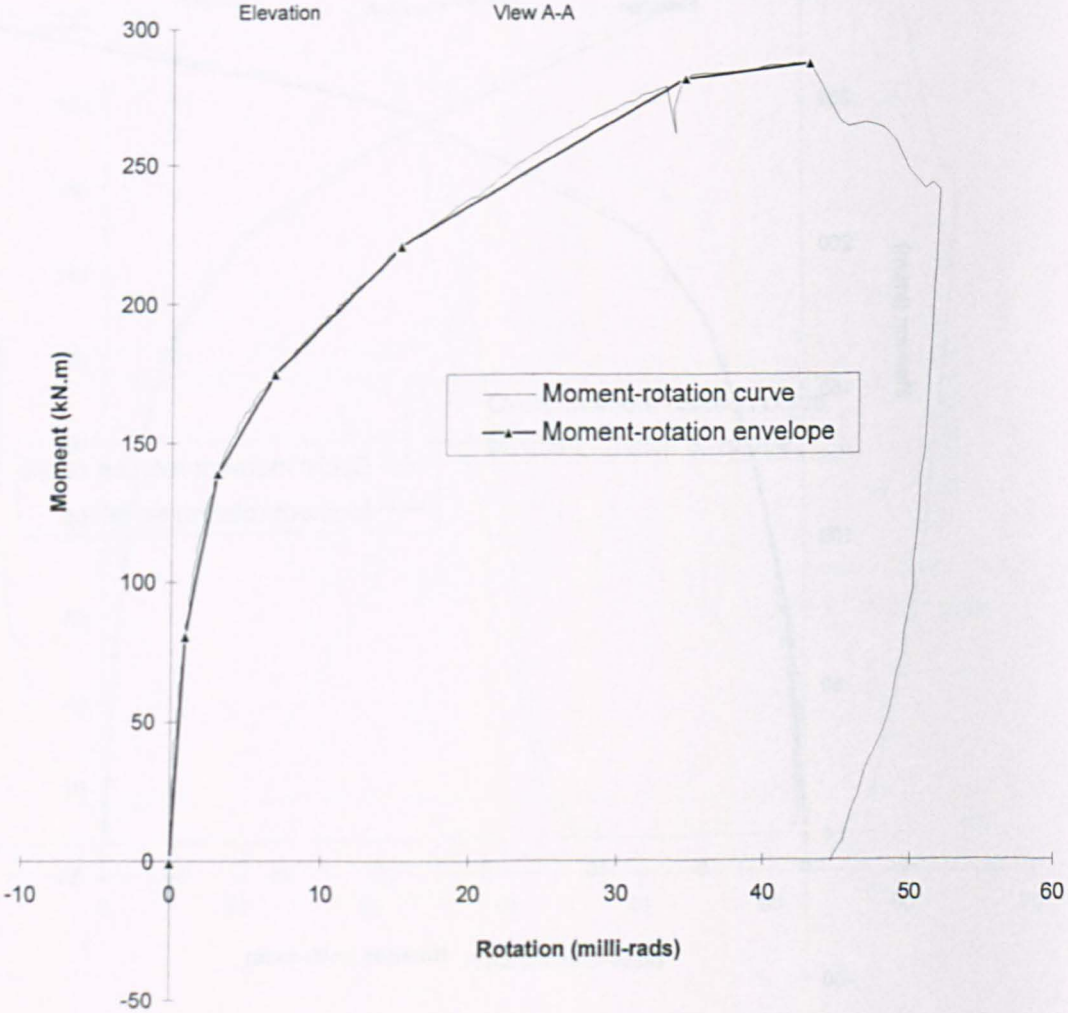

Moment rotation envelope :							
Moment (kN.m)	0	80.5	139.4	175.0	221.3	281.7	287.9
Rotation (milli-rads)	0	0.9	3.1	6.9	15.4	34.5	43.0

Experimental Moment-Rotation curve for Joint Test No. 23

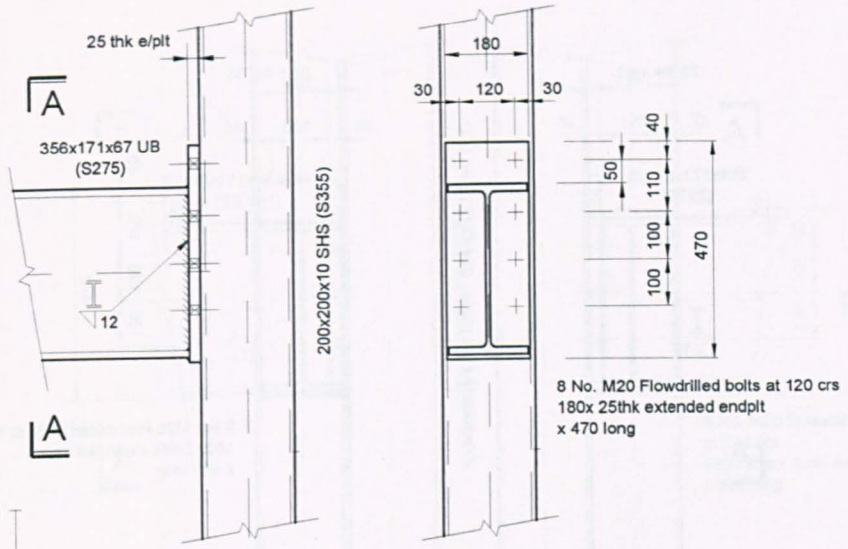

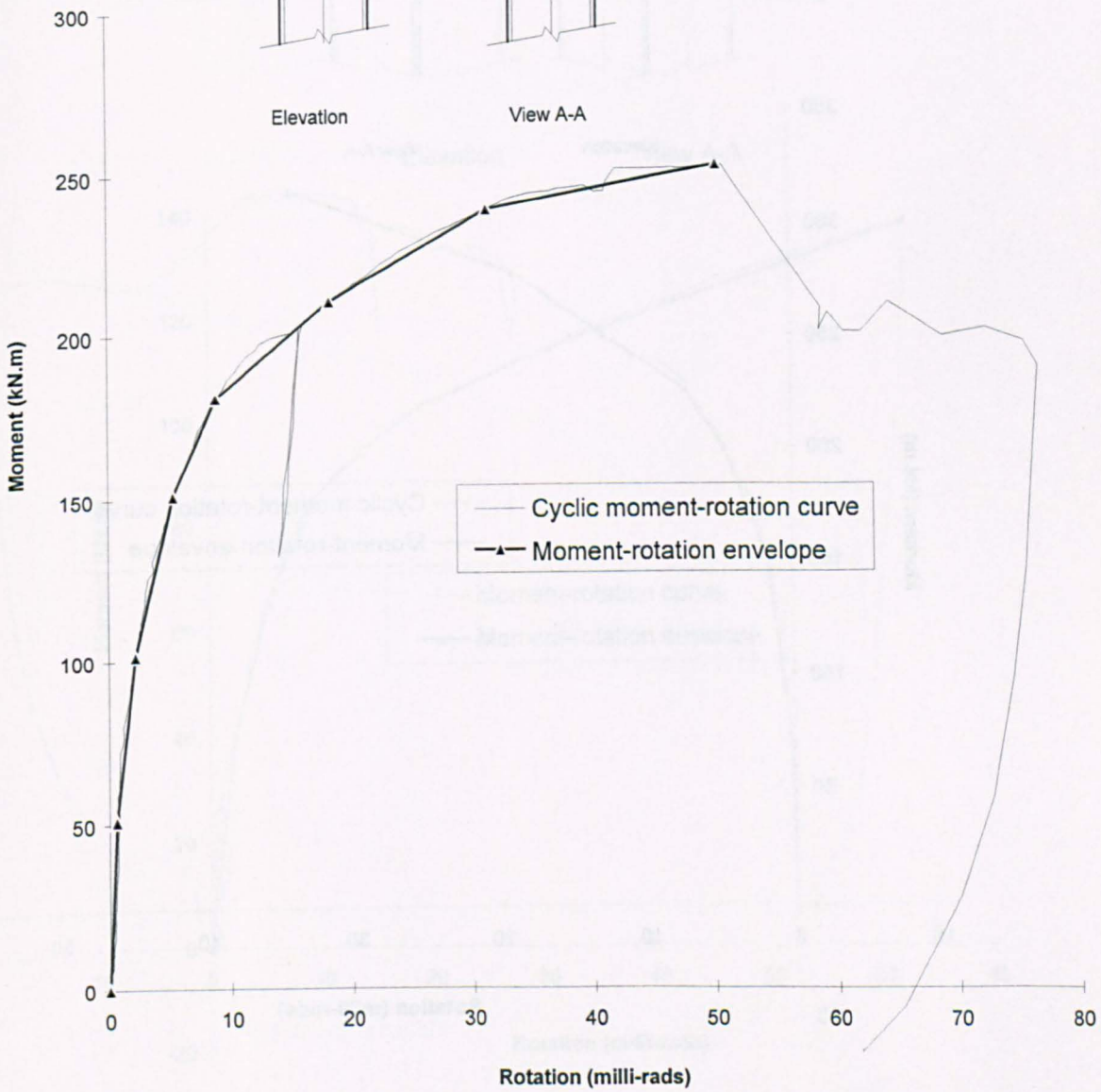

Moment rotation envelope :								
Moment (kN.m)	0	51.0	101.4	151.0	180.9	210.3	239.3	252.6
Rotation (milli-rads)	0	0.6	2.2	5.3	8.9	18.4	31.3	50.4

Experimental Moment-Rotation curve for Joint Test No. 24

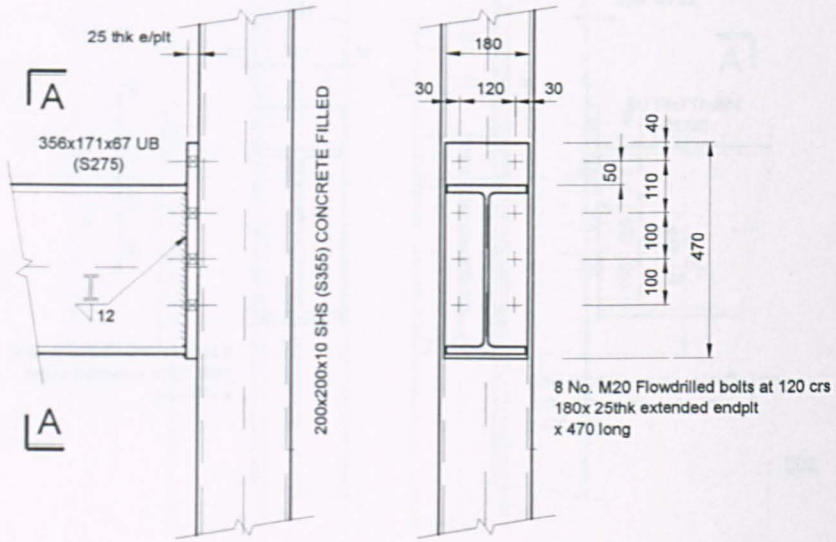

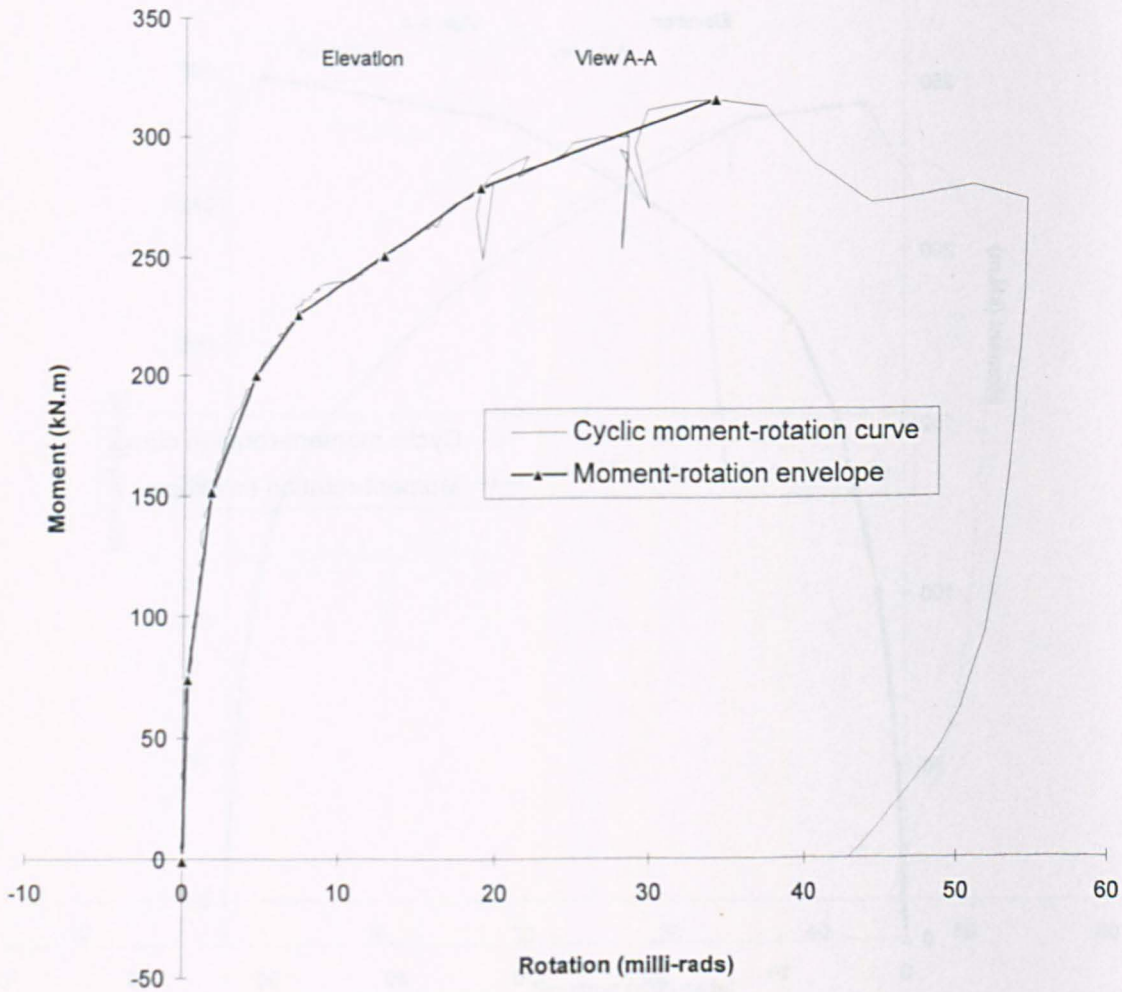

Moment rotation envelope :								
Moment (kN.m)	0	74.5	151.3	200.1	225.9	250.4	279.1	316.3
Rotation (milli-rads)	0	0.3	1.8	4.6	7.3	12.8	18.9	34.2

Experimental Moment-Rotation curve for Joint Test No. 25

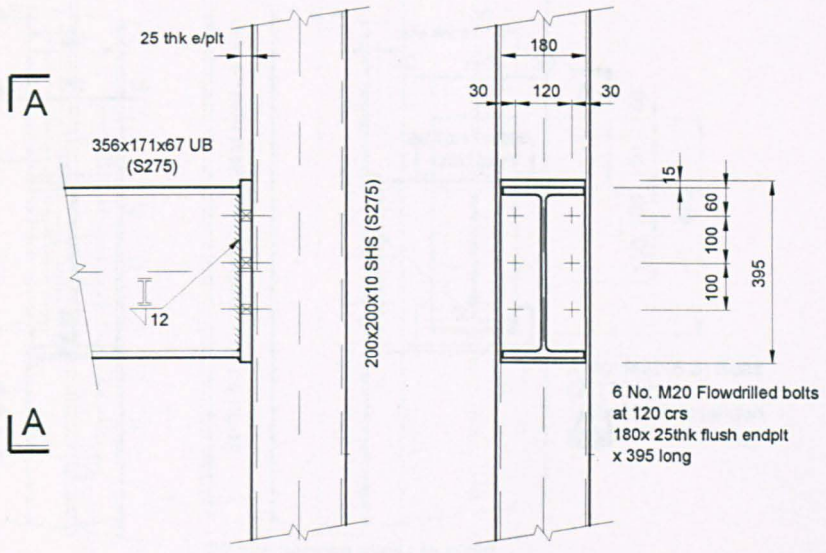

Elevation View A-A

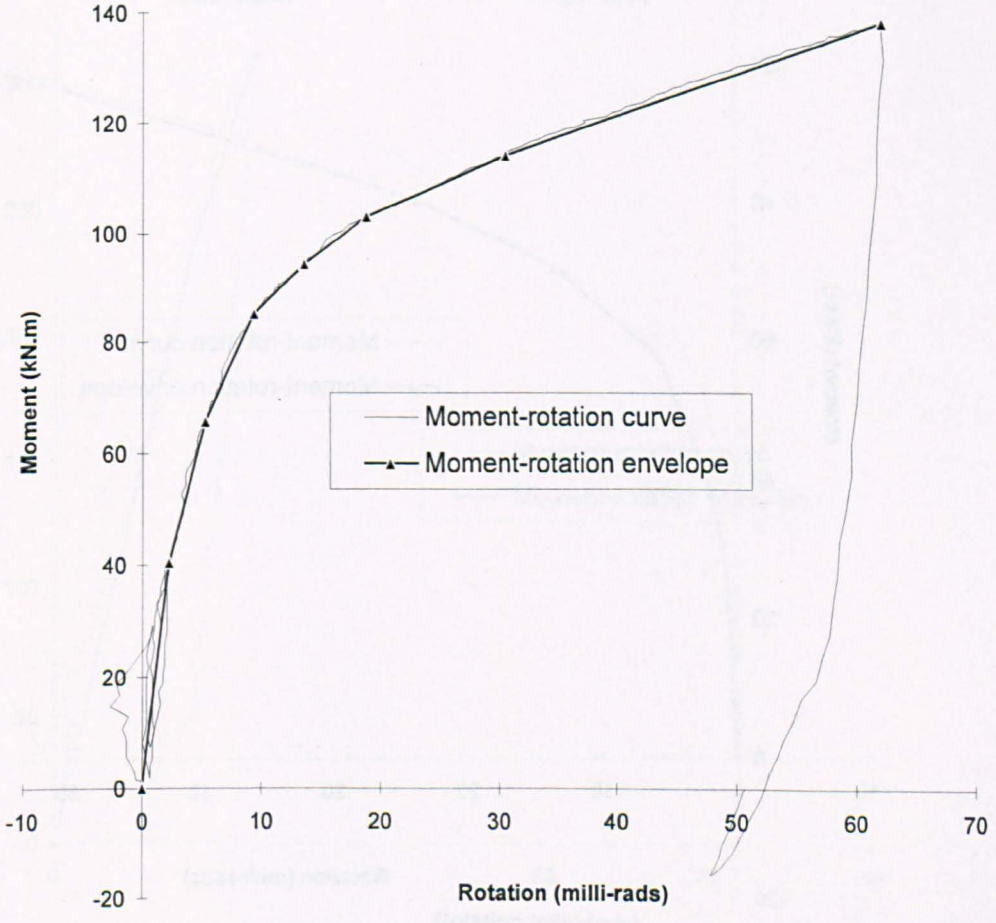

Moment rotation envelope :								
Moment (kN.m)	0	40.4	65.5	85.0	94.3	102.8	114.1	138.0
Rotation (milli-rads)	0	2.3	5.2	9.4	13.6	18.9	30.6	62.2

Experimental Moment-Rotation curve for Joint Test No. 26

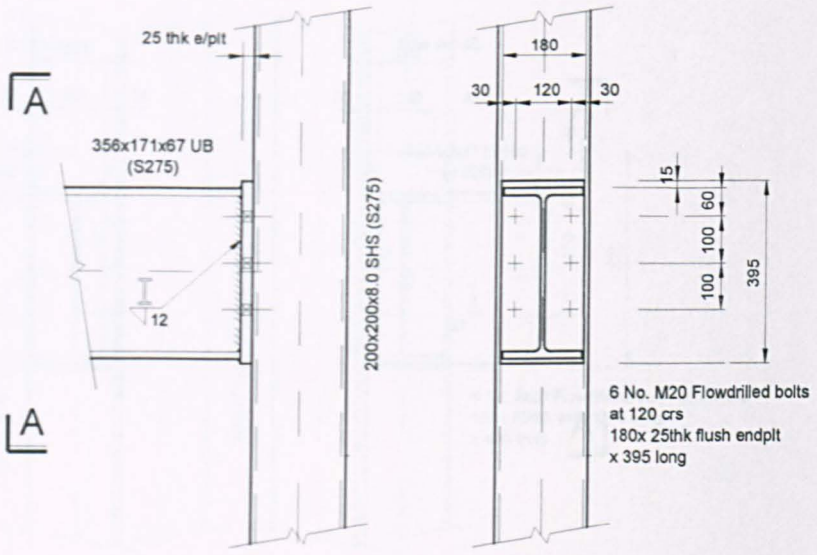

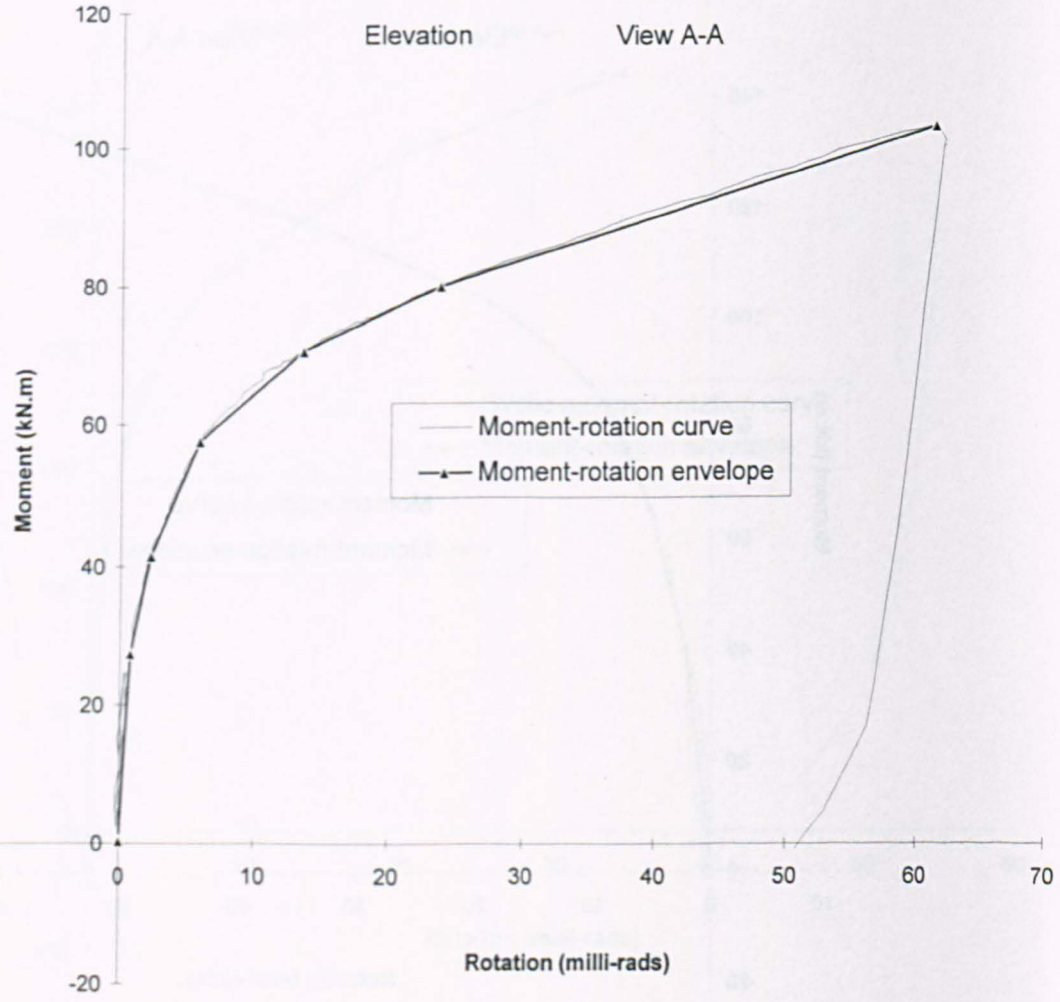

Moment rotation envelope :							
Moment (kN.m)	0	27.3	41.5	57.7	70.6	80.4	103.7
Rotation (milli-rads)	0	0.7	2.2	5.8	13.5	23.8	61.6

Experimental Moment-Rotation curve for Joint Test No. 28b

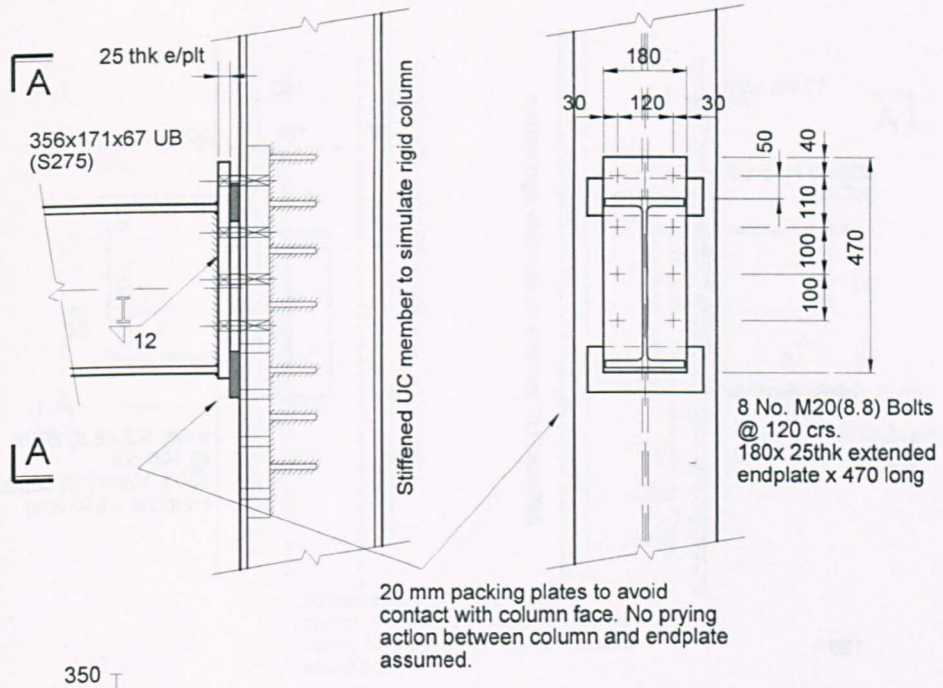

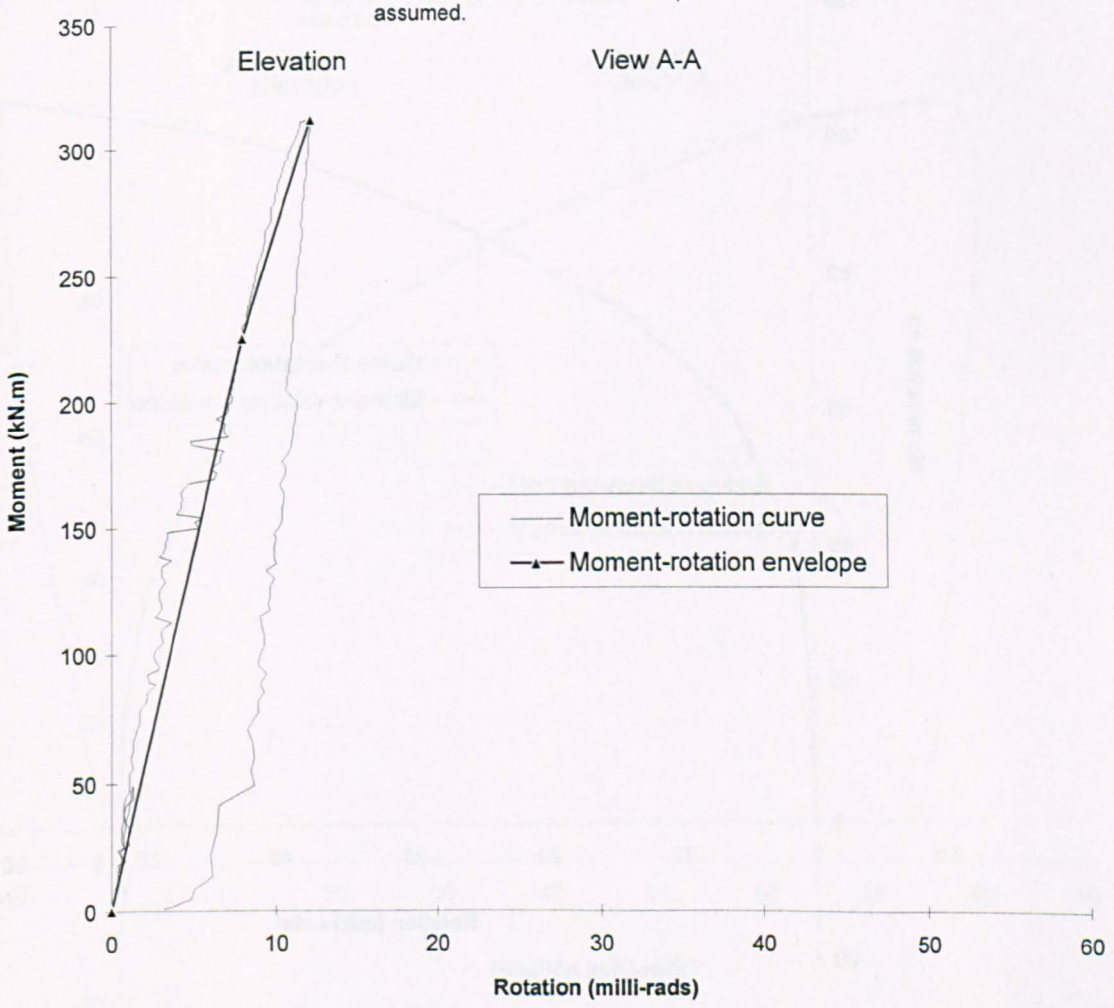

Moment rotation envelope :			
Moment (kN.m)	0	225.3	311.9
Rotation (milli-rads)	0	8.0	12.2

Experimental Moment-Rotation curve for Joint Test No. 29a

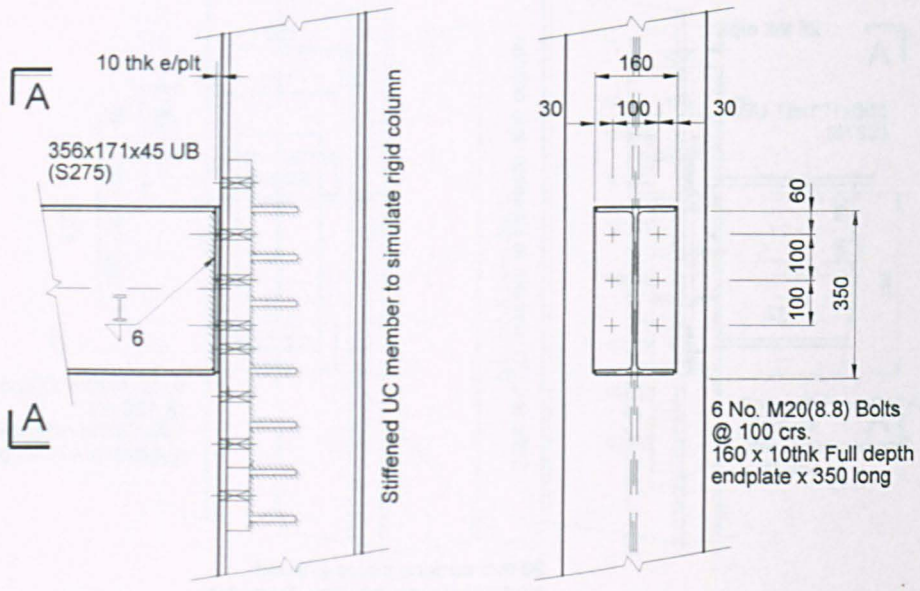

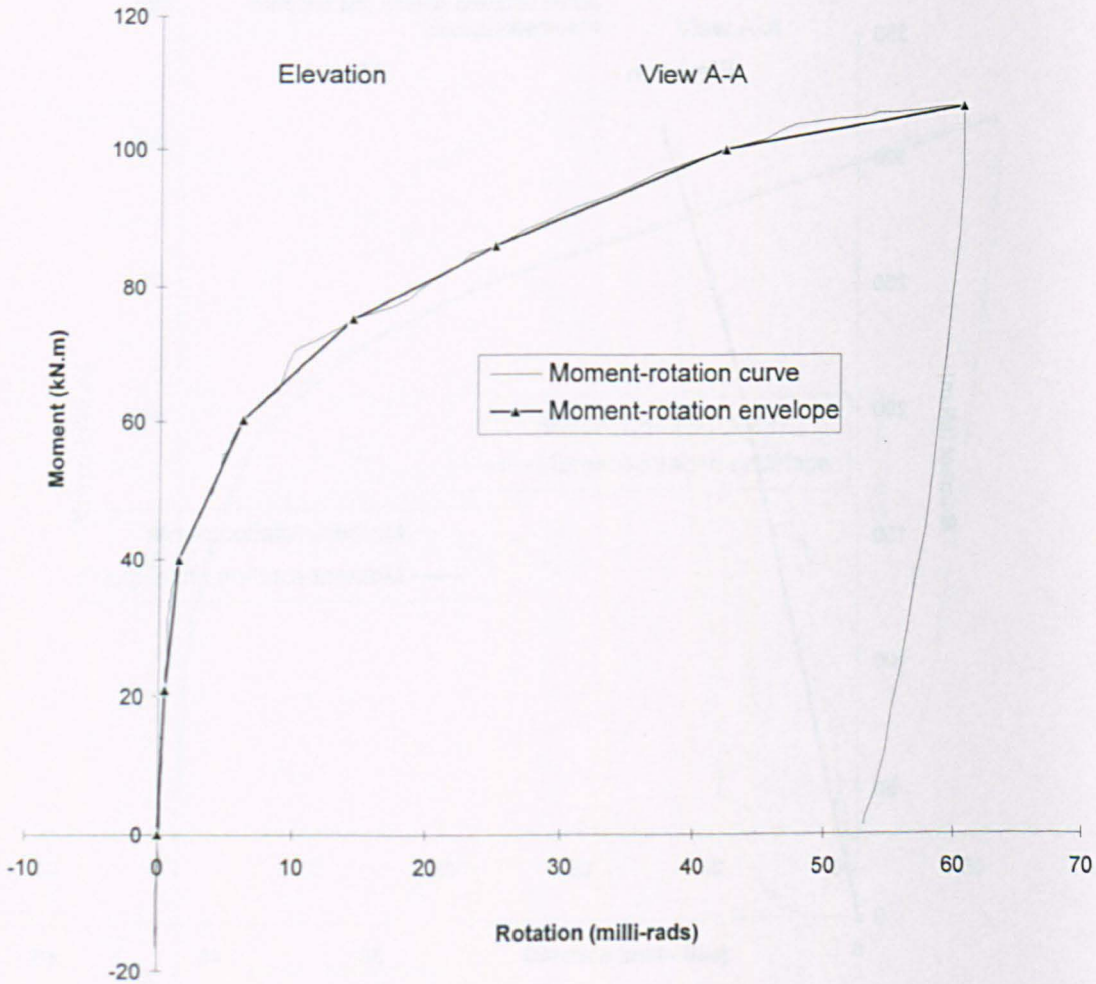

Moment rotation envelope :								
Moment (kN.m)	0	21.0	40.1	60.5	75.4	86.0	100.1	106.6
Rotation (milli-rads)	0	0.4	1.5	6.1	14.3	25.1	42.5	60.8

Experimental Moment-Rotation curve for Joint Test No. 29b

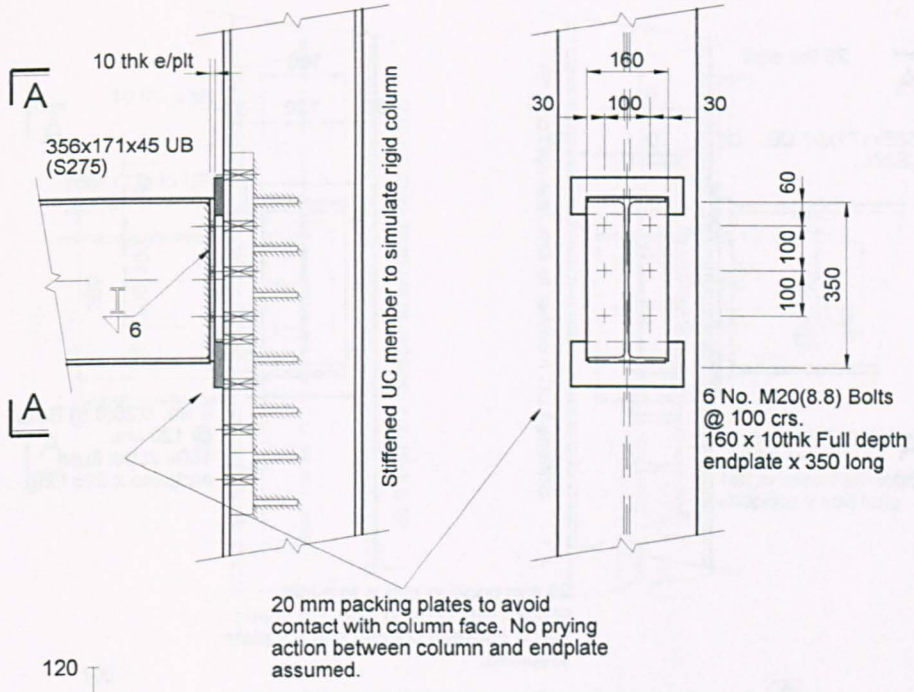

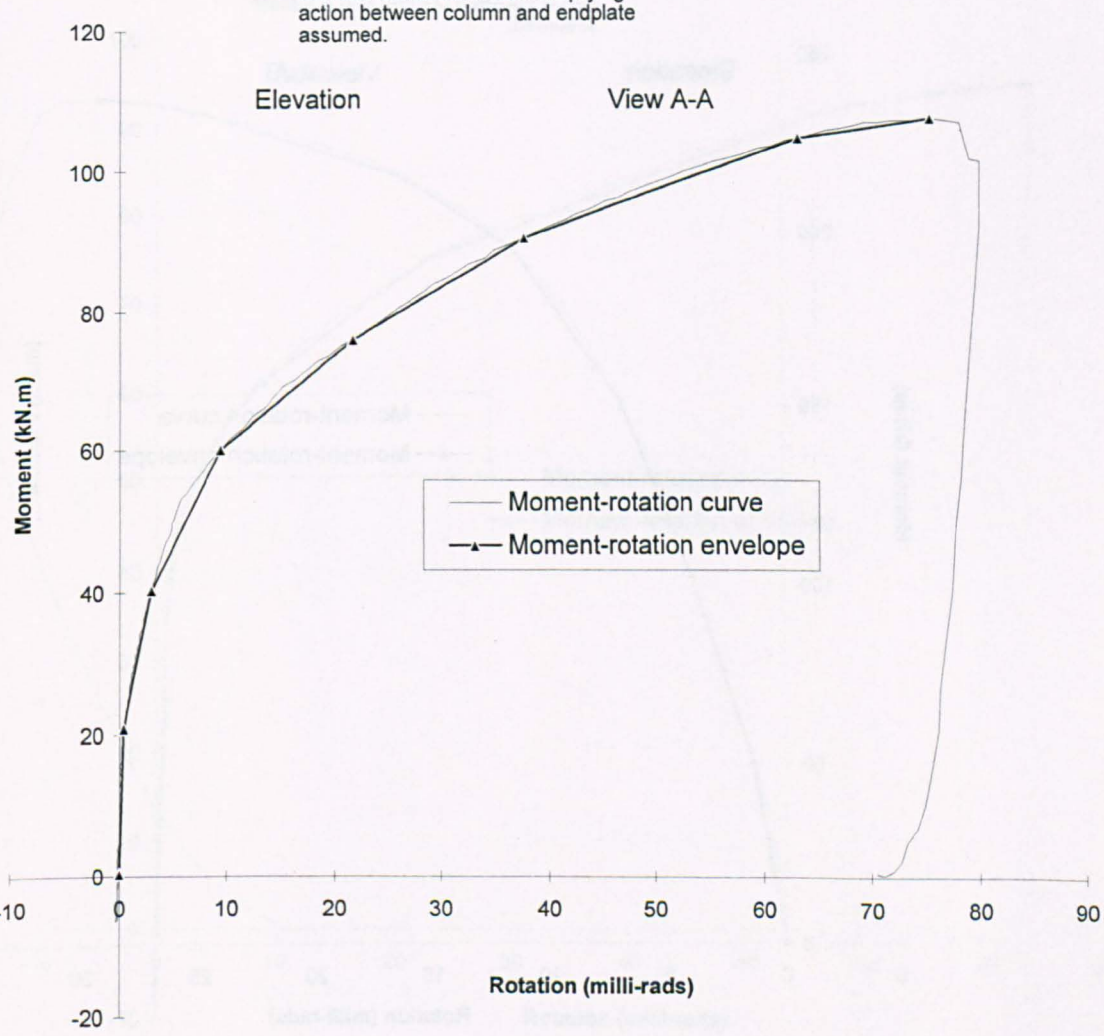

Moment rotation envelope :									
Moment (kN.m)	0	20.8	40.4	60.1	75.9	90.5	104.9	107.6	107.6
Rotation (milli-rads)	0	0.5	2.9	9.4	21.7	37.6	63.2	75.5	75.5

Experimental Moment-Rotation curve for Joint Test No. 30b

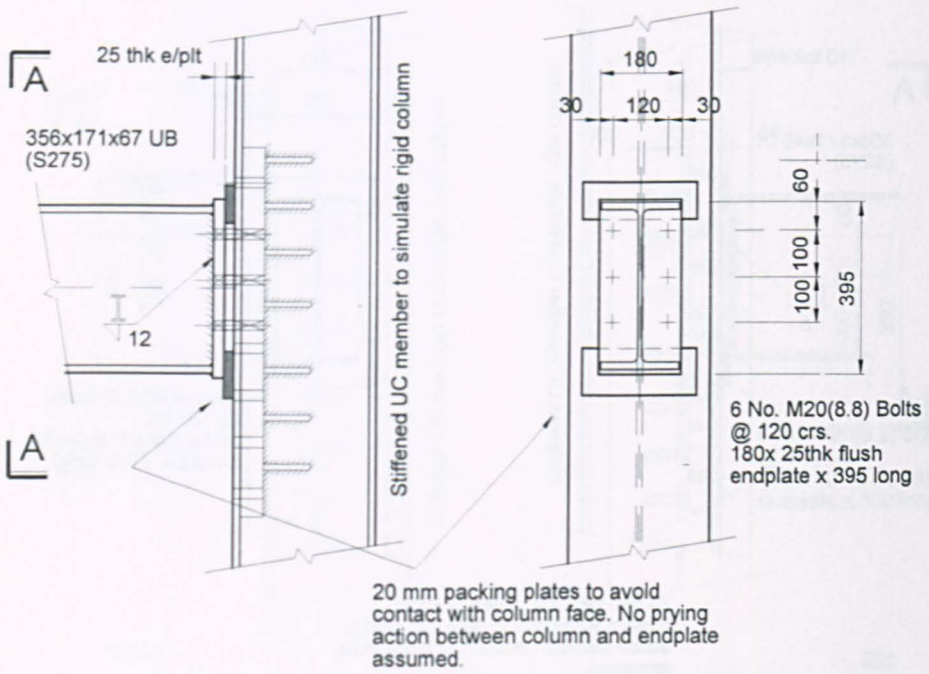

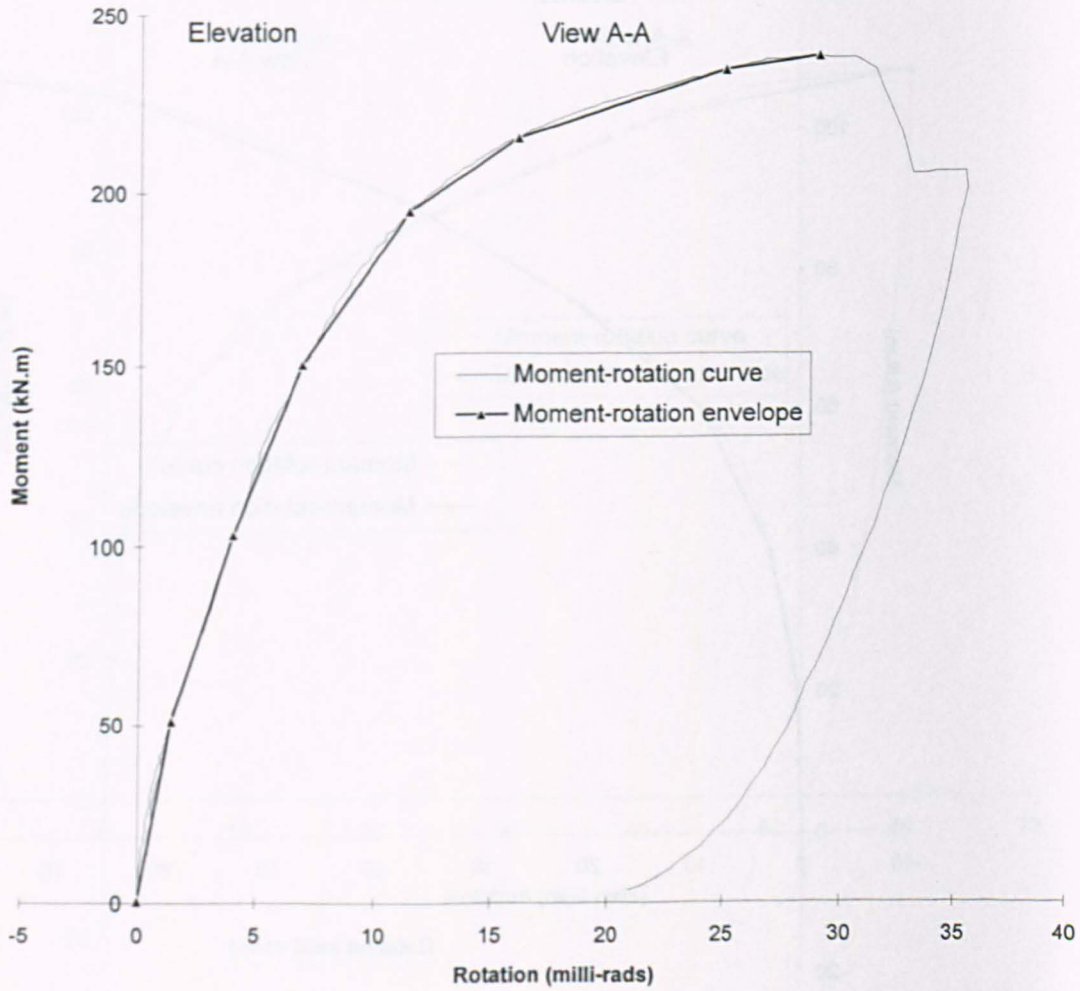

Moment rotation envelope :								
Moment (kN.m)	0	51.3	103.3	150.9	194.9	215.7	234.8	238.6
Rotation (milli-rads)	0	1.4	4.0	6.9	11.4	16.1	25.1	29.1

Experimental Moment-Rotation curve for Joint Test No. 31a

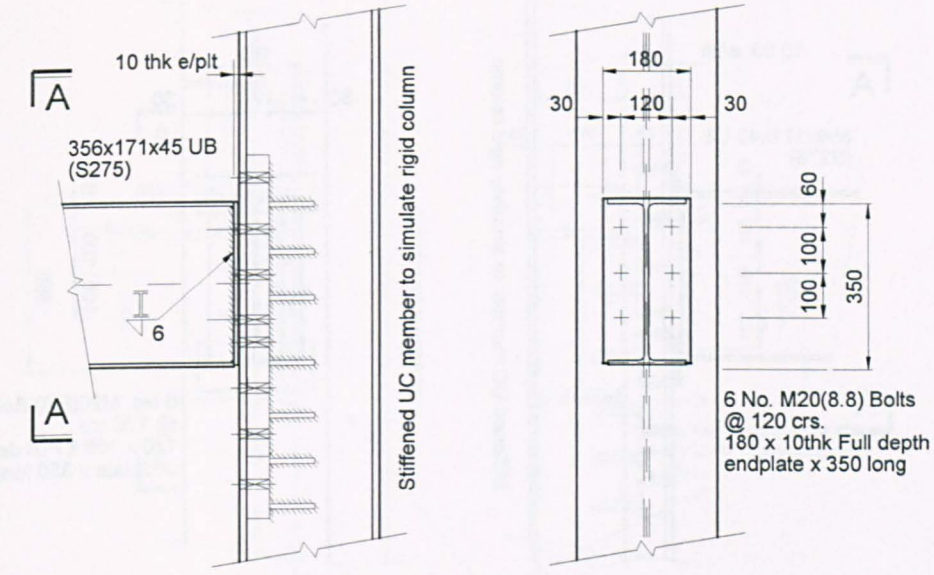

Elevation View A-A

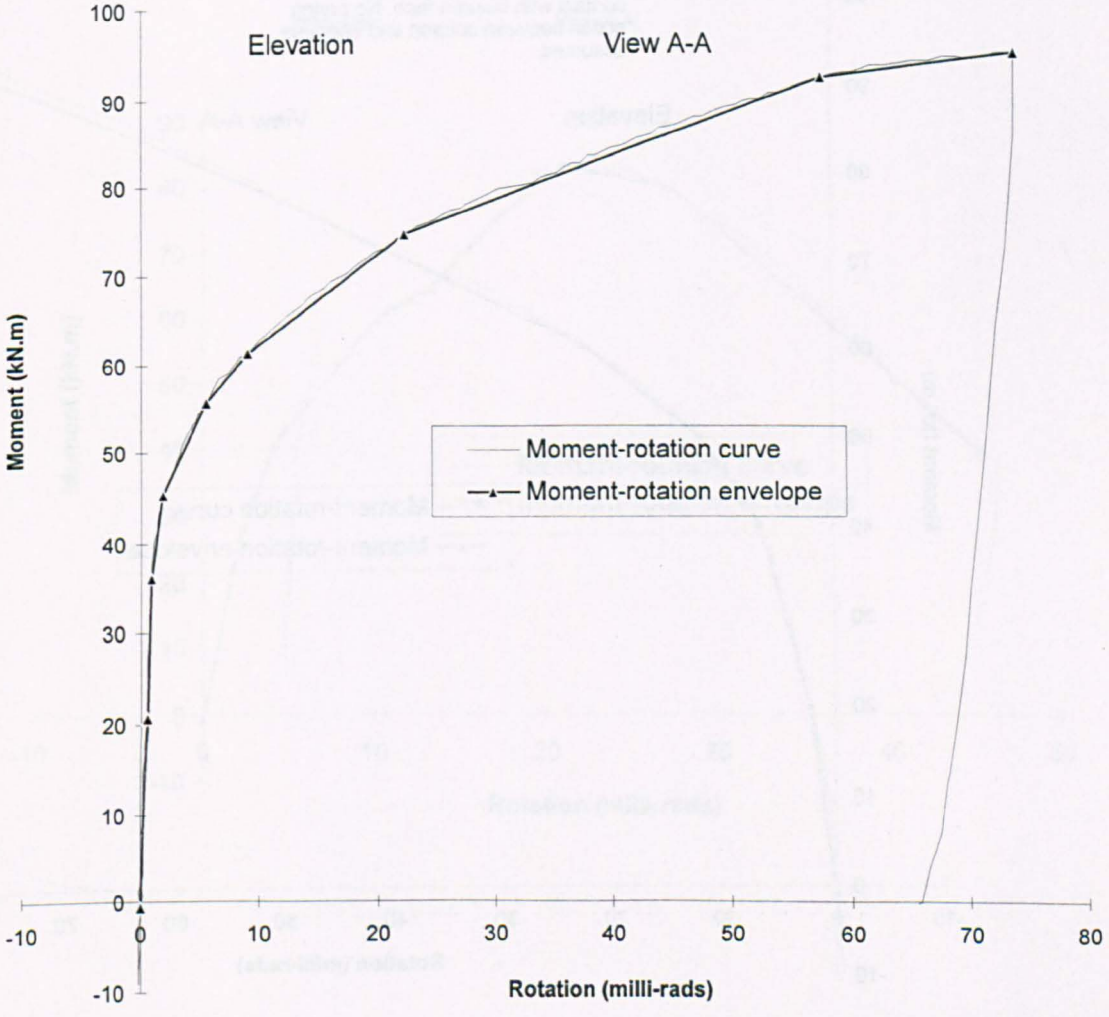

Moment rotation envelope :									
Moment (kN.m)	0	20.6	36.2	45.3	55.7	61.3	74.6	92.6	95.3
Rotation (milli-rads)	0	0.4	0.8	1.8	5.4	9.0	22.3	57.4	73.7

Experimental Moment-Rotation curve for Joint Test No. 31b

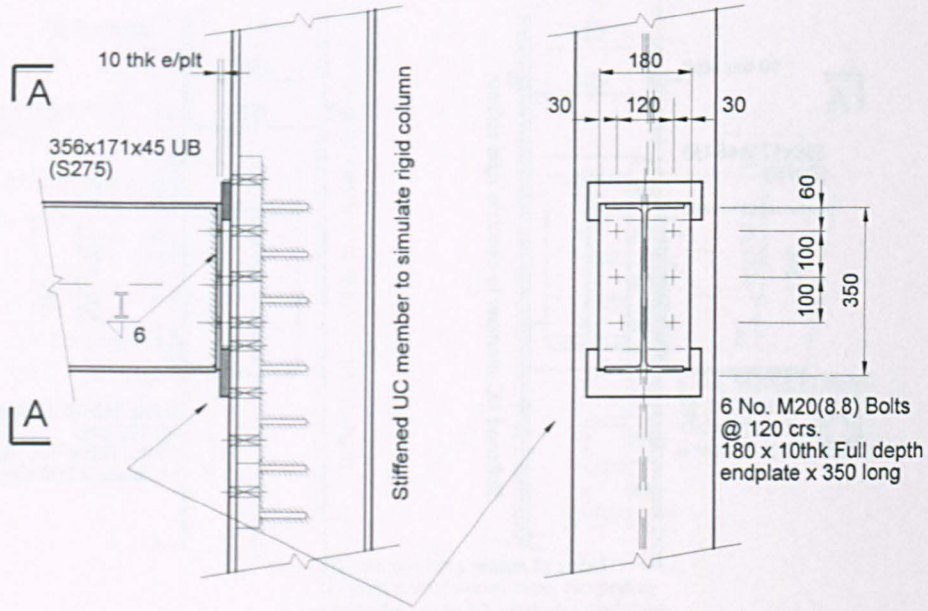

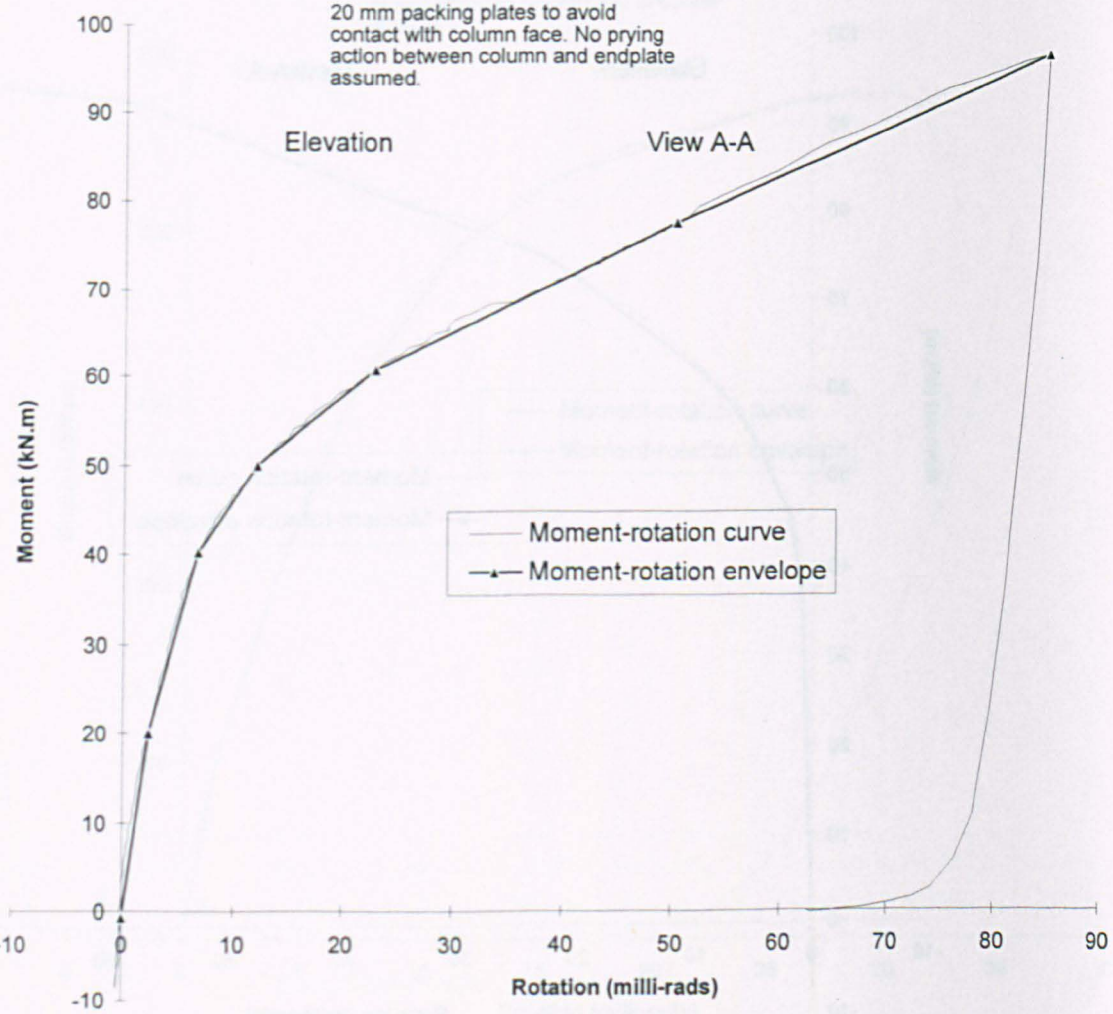

Moment rotation envelope :							
Moment (kN.m)	0	20.1	40.2	50.1	60.6	77.5	96.3
Rotation (milli-rads)	0	2.3	6.8	12.1	22.9	50.4	85.4

Experimental Moment-Rotation curve for Joint Test No. 32a

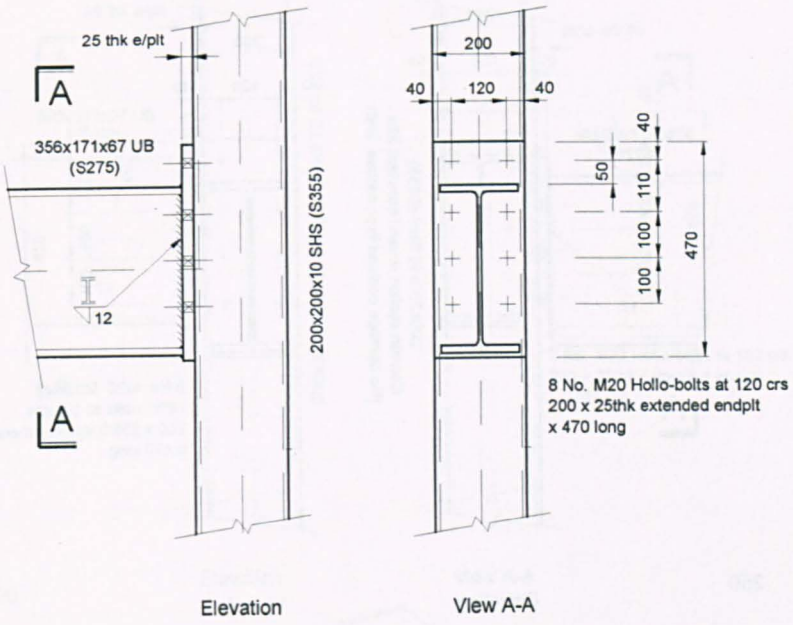

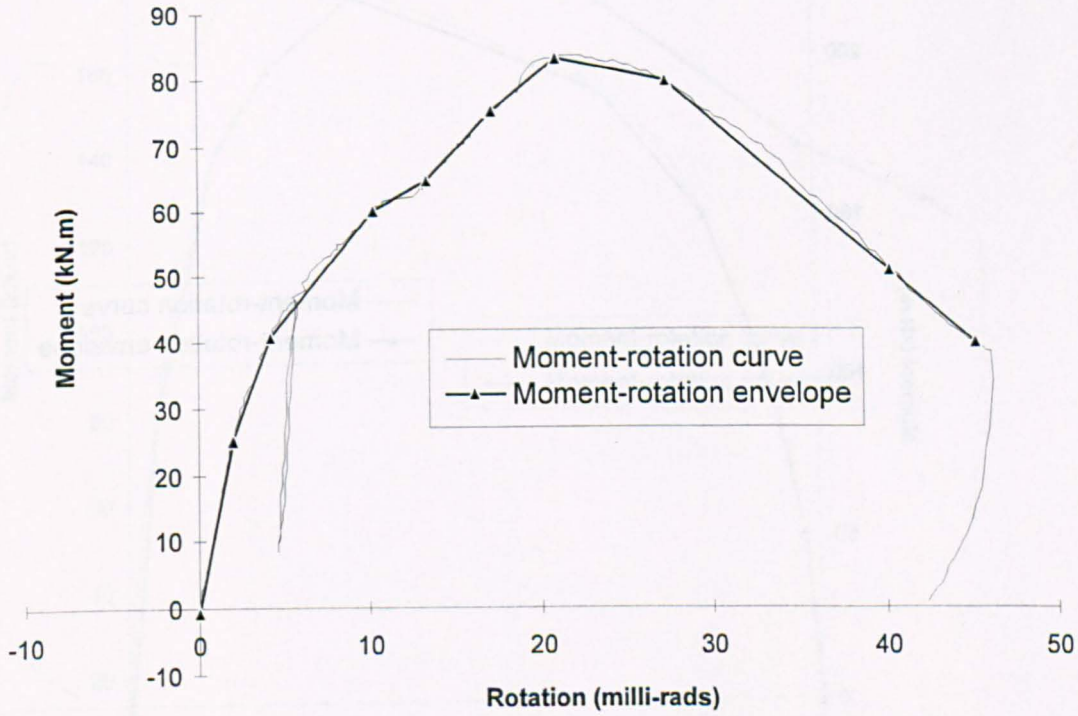

Moment rotation envelope :										
Moment (kN.m)	0	25.1	40.6	60.3	64.5	75.1	83.1	79.6	50.9	39.6
Rotation (milli-rads)	0	2.0	4.3	10.3	13.4	17.2	21.0	27.4	40.4	45.3

Experimental Moment-Rotation curve for Joint Test No. 32b

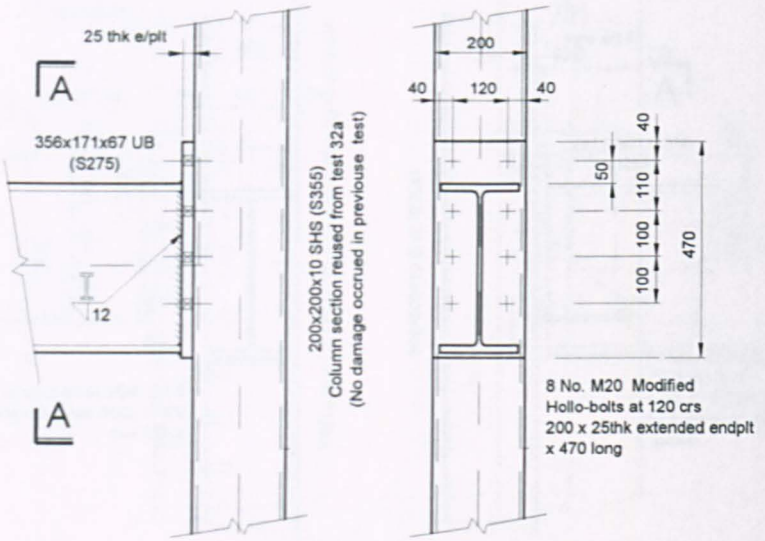

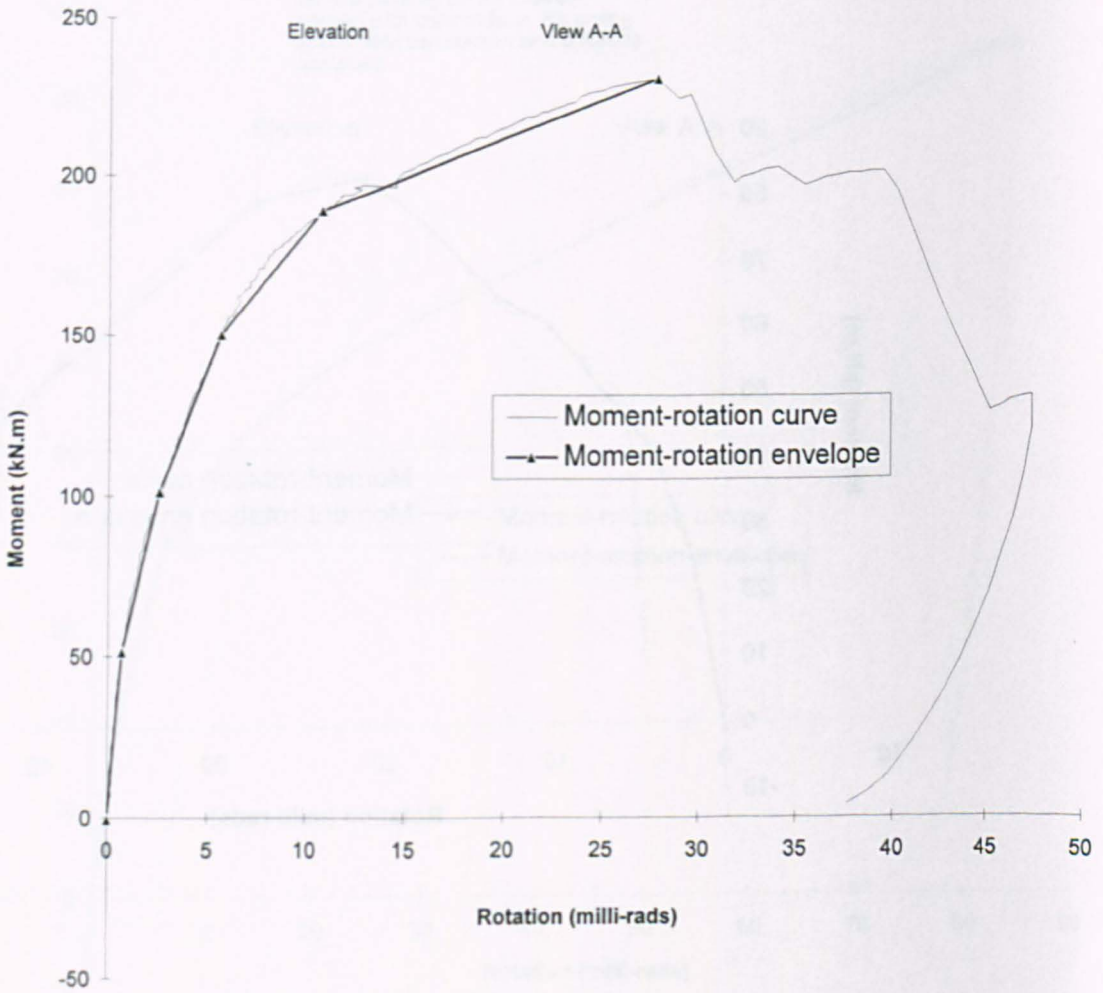

Moment rotation envelope :						
Moment (kN.m)	0	51.1	101.2	150.3	188.7	230.3
Rotation (milli-rads)	0	0.7	2.6	5.6	10.7	27.8

Experimental Moment-Rotation curve for Joint Test No. 33

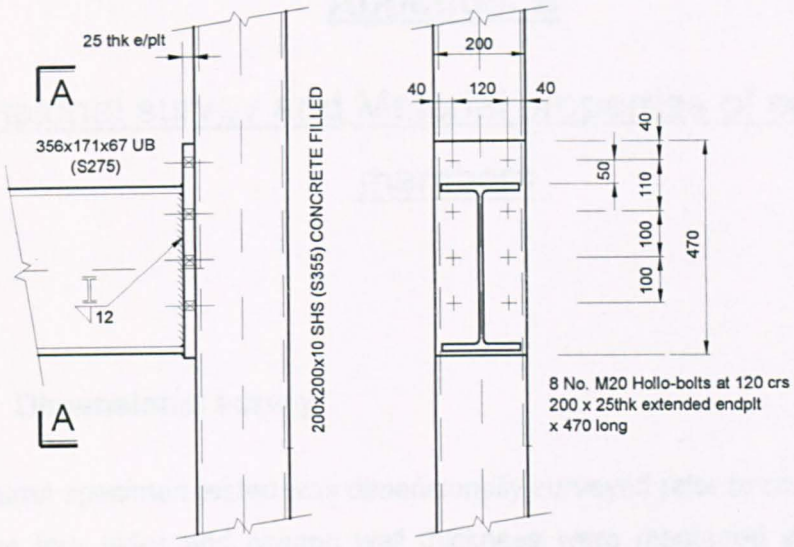

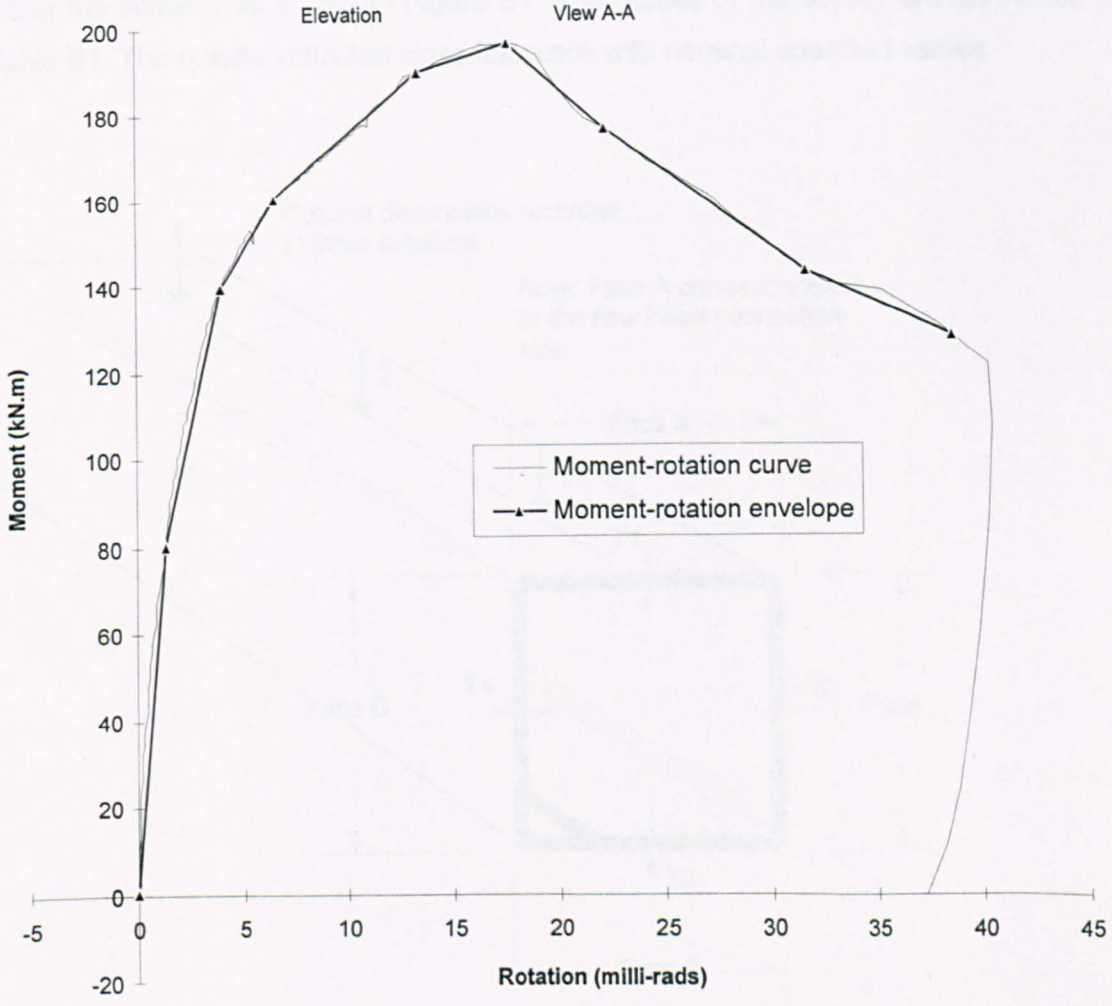

Moment rotation envelope :									
Moment (kN.m)	0	80.5	139.5	160.6	189.9	196.7	176.7	143.6	128.3
Rotation (milli-rads)	0	1.4	4.0	6.6	13.4	17.6	22.3	31.7	38.7

Appendix B

Dimensional survey and Material properties of column SHS members

B.1 Dimensional survey

Each column specimen tested was dimensionally surveyed prior to conducting the joint tests. The four sides and column wall thickness were measured at three locations along the section, as shown in Figure B1. The results of the survey are presented in Table B1. The results indicated close tolerance with nominal specified values.

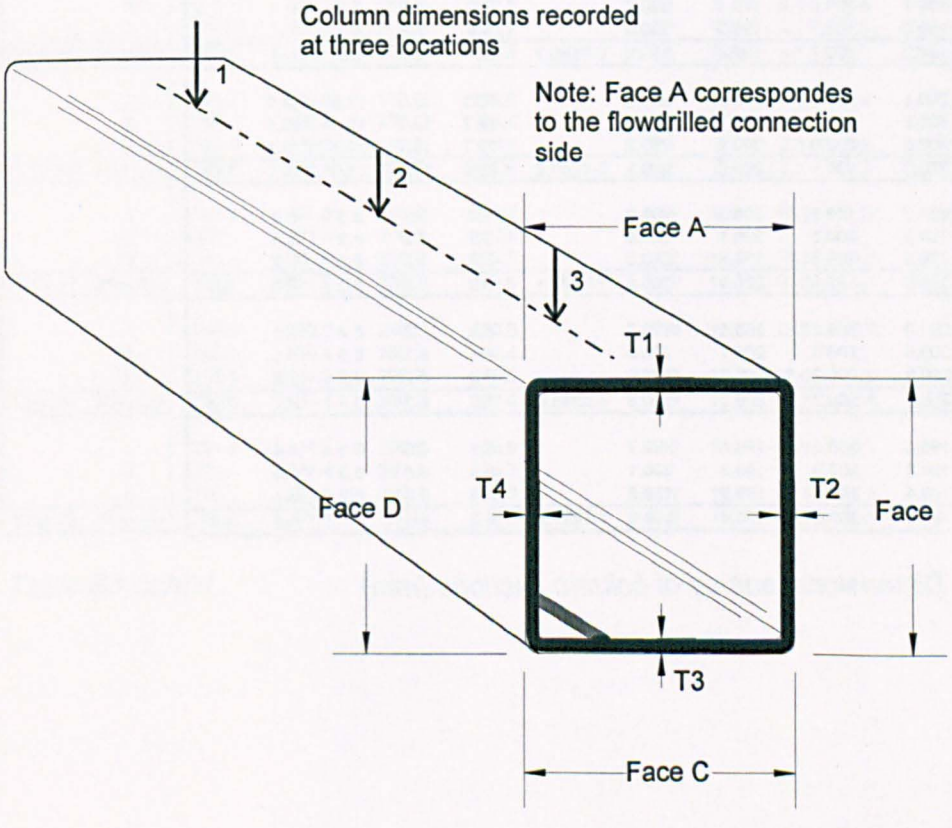

Figure B1 *Reference positions for dimensional survey conducted on column sections*

		Face reference									
		A	B	C	D		T1	T2	T3	T4	
	1	199.9	200.0	199.3	200.1		8.2	8.3	8.2	8.5	
	2	200.3	200.0	200.0	200.2		8.5	8.5	8.1	8.5	
	3	200.2	200.1	199.5	200.2		8.2	8.4	8.1	8.5	
Test 1	Average	200.1	200.0	199.6	200.2	200.0	8.3	8.4	8.1	8.5	8.3
	1	200.2	200.0	199.7	200.3		8.6	8.4	8.2	8.4	
	2	200.3	199.9	200.1	200.1		8.3	8.3	8.2	8.3	
	3	200.2	199.9	199.6	199.8		8.2	8.3	8.2	8.3	
Test 2	Average	200.2	199.9	199.8	200.1	200.0	8.4	8.3	8.2	8.3	8.3
	1	200.2	200.1	199.7	200.2		8.5	8.5	8.2	8.5	
	2	200.9	200.3	200.1	200.0		8.6	8.5	8.1	8.3	
	3	200.3	200.0	200.2	200.3		8.5	8.4	8.3	8.3	
Test 3	Average	200.5	200.1	200.0	200.2	200.2	8.5	8.5	8.2	8.4	8.4
	1	200.3	200.3	200.1	200.4		8.4	8.4	8.3	8.4	
	2	200.2	200.6	200.1	200.1		8.4	8.1	8.2	8.2	
	3	199.9	200.2	200.1	200.2		8.3	8.2	8.2	8.2	
Test 4	Average	200.1	200.4	200.1	200.2	200.2	8.4	8.2	8.2	8.3	8.3
	1	200.5	200.1	200.0	200.6		8.3	8.3	8.4	8.3	
	2	200.1	200.4	200.2	200.4		8.3	8.2	8.3	8.3	
	3	200.0	200.6	199.8	200.5		8.2	8.4	8.2	8.2	
Test 5	Average	200.2	200.4	200.0	200.5	200.3	8.3	8.3	8.3	8.3	8.3
	1	199.9	199.9	200.4	200.5		8.2	8.3	8.2	8.3	
	2	200.0	200.5	199.9	200.6		8.3	8.3	8.3	8.4	
	3	200.1	200.3	200.0	200.4		8.3	8.3	8.2	8.3	
Test 6	Average	200.0	200.2	200.1	200.5	200.2	8.3	8.3	8.2	8.3	8.3
	1	199.5	199.7	199.8	199.6		6.3	6.6	6.3	6.4	
	2	199.7	199.8	199.1	200.0		6.6	6.4	6.2	6.4	
	3	199.8	199.7	199.3	200.0		6.3	6.3	6.2	6.4	
Test 7	Average	199.7	199.7	199.4	199.9	199.7	6.4	6.4	6.2	6.4	6.4
	1	200.1	200.2	200.2	200.2		13.1	13.1	12.9	13.1	
	2	200.2	200.2	200.5	200.3		12.7	12.7	13.1	13.1	
	3	200.5	200.0	200.1	200.2		12.7	13.1	13.1	13.1	
Test 8	Average	200.3	200.1	200.3	200.2	200.2	12.8	13.0	13.0	13.1	13.0
	1	200.2	199.6	200.3	201.0		8.2	8.3	8.3	8.3	
	2	199.8	200.3	200.1	200.8		8.2	8.2	8.3	8.3	
	3	199.8	199.5	199.9	200.0		8.3	8.2	8.3	8.2	
Test 9	Average	199.9	199.8	200.1	200.6	200.1	8.2	8.2	8.3	8.3	8.3
	1	200.0	200.2	200.1	199.7		8.3	8.2	8.4	8.3	
	2	200.3	200.3	200.1	200.0		8.4	8.1	8.5	8.1	
	3	200.0	200.2	200.0	199.6		8.2	8.2	8.2	8.2	
Test 10	Average	200.1	200.2	200.1	199.8	200.0	8.3	8.2	8.4	8.2	8.3
	1	199.4	200.0	199.4	199.7		6.3	6.5	6.3	6.4	
	2	199.3	200.0	199.3	200.1		6.4	6.4	6.3	6.4	
	3	199.4	199.9	199.5	199.8		6.3	6.3	6.2	6.4	
Test 11	Average	199.4	200.0	199.4	199.9	199.7	6.3	6.4	6.3	6.4	6.4

Table B1 Dimensional survey of column sections (mm)

		Face reference A	B	C	D		T1	T2	T3	T4	
	1	199.2	199.9	199.2	199.6		6.3	6.3	6.3	6.4	
	2	199.4	199.9	199.3	200.2		6.3	6.4	6.4	6.4	
	3	199.1	199.8	199.2	199.7		6.4	6.5	6.3	6.5	
Test 12	Average	199.2	199.9	199.2	199.8	**199.5**	6.3	6.4	6.3	6.4	**6.4**
	1	199.5	200.0	199.3	199.9		6.3	6.4	6.5	6.6	
	2	199.3	199.9	199.4	199.9		6.4	6.5	6.3	6.5	
	3	199.6	200.0	199.3	199.8		6.3	6.4	6.3	6.5	
Test 13	Average	199.5	200.0	199.3	199.9	**199.7**	6.3	6.4	6.4	6.5	**6.4**
	1	200.6	200.1	200.0	200.4		8.8	8.3	8.1	8.2	
	2	200.6	200.1	200.2	200.6		8.2	8.3	8.1	8.5	
	3	200.7	200.0	200.6	200.3		8.5	8.4	8.1	8.5	
Test 14	Average	200.6	200.1	200.3	200.4	**200.4**	8.5	8.3	8.1	8.4	**8.3**
	1	200.4	200.4	199.9	200.3		8.3	8.4	8.2	8.3	
	2	200.6	200.3	200.2	200.0		8.6	8.4	8.2	8.5	
	3	200.6	200.2	200.1	199.9		8.3	8.4	8.9	8.5	
Test 15	Average	200.5	200.3	200.1	200.1	**200.2**	8.4	8.4	8.4	8.4	**8.4**
	1	199.2	199.8	199.4	199.9		6.5	6.5	6.4	6.6	
	2	199.6	200.4	199.6	200.0		6.3	6.4	6.4	6.4	
	3	199.7	200.0	200.0	200.0		6.4	6.4	6.3	6.6	
Test 16	Average	199.5	200.1	199.7	200.0	**199.8**	6.4	6.4	6.4	6.5	**6.4**
	1	200.0	200.2	200.3	200.1		8.2	8.1	8.2	8.2	
	2	200.5	200.6	200.0	200.4		8.3	8.3	8.1	8.2	
	3	200.2	200.1	200.2	199.8		8.4	8.1	8.2	8.3	
Test 17	Average	200.2	200.3	200.2	200.1	**200.2**	8.3	8.2	8.2	8.2	**8.2**
	1	200.5	200.1	199.8	200.4		8.3	8.3	8.1	8.3	
	2	200.7	200.4	200.2	200.0		8.3	8.4	8.1	8.5	
	3	200.7	200.9	200.1	200.2		8.2	8.3	8.1	8.3	
Test 18	Average	200.6	200.5	200.0	200.2	**200.3**	8.3	8.3	8.1	8.4	**8.3**
	1	199.7	199.8	199.9	199.6		8.2	8.4	7.9	8.2	
	2	199.4	199.9	199.5	199.4						
	3	199.5	199.6	199.7	199.4		8.3	8.3	8.3	8.2	
Test 19	Average	199.5	199.8	199.7	199.5	**199.6**	8.2	8.4	8.1	8.2	**8.2**
	1	201.0	201.3	200.8	200.7		10.1	10.0	10.2	9.9	
	2	201.4	201.3	200.0	200.5						
	3	201.2	201.4	200.7	200.5		10.2	10.3	10.1	10.0	
Test 20	Average	201.2	201.3	200.5	200.6	**200.9**	10.1	10.1	10.2	10.0	**10.1**
	1	200.4	200.5	200.5	200.6		12.9	12.8	12.8	12.7	
	2	200.3	200.4	200.2	200.4						
	3	200.3	200.3	200.3	200.3		12.8	12.8	12.6	12.5	
Test 21	Average	200.3	200.4	200.3	200.4	**200.4**	12.9	12.8	12.7	12.6	**12.7**
	1	201.4	201.6	200.6	200.9		10.2	10.2	10.1	10.1	
	2	201.0	201.4	201.1	200.7						
	3	201.1	201.5	200.7	200.8		10.1	10.1	10.1	10.3	
Test 22	Average	201.2	201.5	200.8	200.8	**201.1**	10.2	10.1	10.1	10.2	**10.2**

Table B1 cont'd

		Face reference A	B	C	D		T1	T2	T3	T4	
	1	200.3	200.5	200.4	200.1		10.2	10.2	10.3	10.2	
	2	200.5	200.4	200.5	200.1						
	3	200.0	200.2	200.4	200.0		10.2	10.0	9.9	10.2	
Test 23	Average	200.3	200.4	200.4	200.1	200.3	10.2	10.1	10.1	10.2	10.1
	1	200.3	200.3	200.4	200.0		10.2	10.2	10.3	10.1	
	2	200.5	200.5	200.5	200.2						
	3	200.4	200.7	200.5	200.1		10.2	10.2	10.1	10.3	
Test 24	Average	200.4	200.5	200.5	200.1	200.4	10.2	10.2	10.2	10.2	10.2
	1	201.0	201.3	200.7	200.6		10.1	10.0	10.3	9.9	
	2	200.7	201.4	200.4	200.5						
	3	201.3	201.0	201.3	200.7		10.2	10.3	10.2	10.2	
Test 25	Average	201.0	201.2	200.8	200.6	200.9	10.2	10.2	10.3	10.1	10.2
	1	199.6	199.8	199.7	199.3		7.9	8.3	7.9	8.1	
	2	199.6	199.7	199.7	199.7						
	3	199.7	199.7	199.8	199.4		8.0	8.4	8.0	8.1	
Test 26	Average	199.6	199.7	199.7	199.5	199.6	7.9	8.3	7.9	8.1	8.1
	1	200.9	201.4	200.7	200.7		10.1	10.2	10.4	9.9	
	2	201.6	201.4	200.7	200.5						
	3	200.6	201.3	200.7	200.5		10.2	10.2	10.3	10.0	
Test 27	Average	201.0	201.4	200.7	200.6	200.9	10.1	10.2	10.4	10.0	10.2
	1	200.2	200.2	200.3	200.0		10.1	10.1	10.1	10.2	
	2	200.7	200.2	200.6	200.2						
	3	200.3	200.2	200.3	199.9		10.2	10.2	10.2	10.2	
Test 32a	Average	200.4	200.2	200.4	200.0	200.3	10.1	10.1	10.1	10.2	10.1
	1	200.2	200.2	200.3	200.0		10.1	10.1	10.1	10.2	
	2	200.7	200.2	200.6	200.2						
	3	200.3	200.2	200.3	199.9		10.2	10.2	10.2	10.2	
Test 32b	Average	200.4	200.2	200.4	200.0	200.3	10.1	10.1	10.1	10.2	10.1
	1	200.7	200.2	200.4	200.0		10.1	10.1	10.3	10.2	
	2	200.6	200.1	200.6	200.0						
	3	200.4	200.2	200.2	200.2		10.3	10.2	10.0	10.1	
Test 33	Average	200.6	200.2	200.4	200.1	200.3	10.2	10.1	10.2	10.2	10.2

Table B1. cont'd

B.2 Tensile coupon tests

The coupon tests were conducted under the recommendations of BS EN 10002-1:1990 [94]. There were six coupons cut from each batch of steel as indicated in Figure B.2. Three coupons were selected to determine the longitudinal properties while three were cut transversely across the section to determine if any differences in the yield strength exist. As seen from Figure B.2 only three sides of the column produced the coupon specimens, with the face containing the weld seam not being used. The geometry of the coupons were machined to the dimensions shown, which complied with the recommendations of BS EN 10002-1 annex C [94].

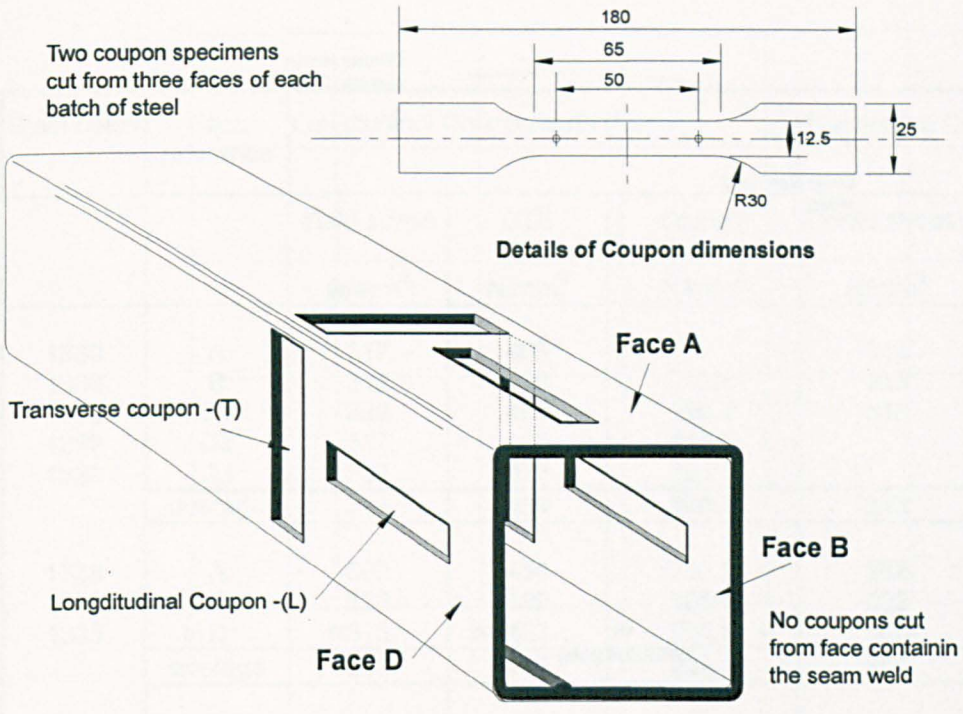

Figure B.2 Position of coupon specimens removed from column sections

Each of the coupons was tested on a 100 kN universal testing machine under deflection control to determine the static yield strength, Young's modulus and ultimate tensile strength. An extensonmeter calibrated to an accuracy of 0.002 mm was attached to the reduced part of the specimen to measure the elongation over a gauge length of 50mm. The direct reading of the coupon's elongation allowed the Young's modulus to be determined. All the coupons were strained at 0.00033 /s within the elastic range and increased to 0.003 /s after yield. Figure B.3 indicates a typical stress strain relationship produced.

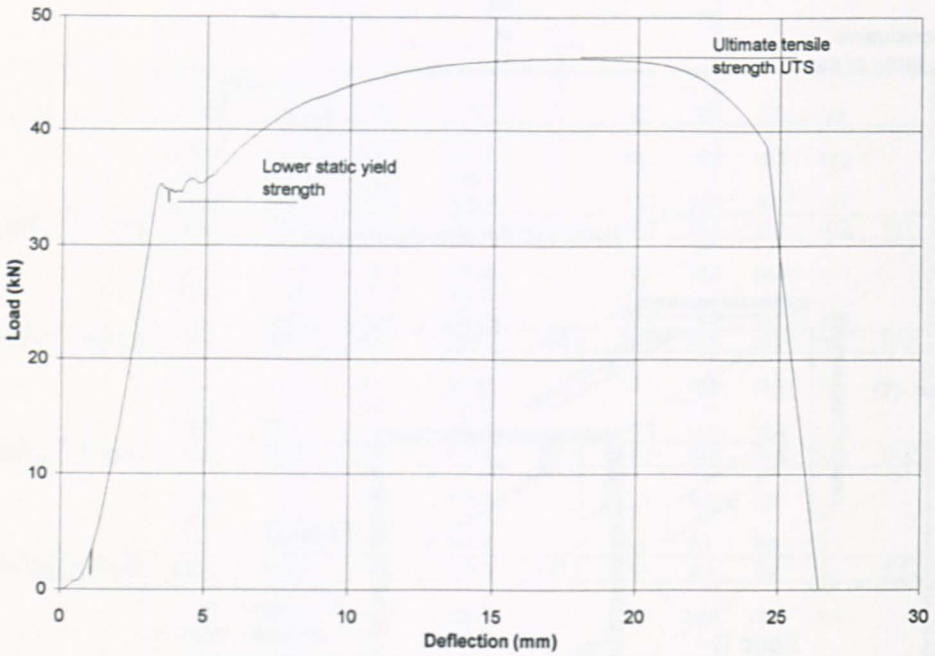

Figure B.3 Typical load vs. deflection plot for coupon specimens

Previous coupon tests have indicated that the loading rate influences the final measured stress [95]. A high loading rate applied to the specimen will generally increase the yield strength. By maintaining the level of strain for two minutes, directly after the upper yield point is reached, the lower 'static' yield was obtained as indicated in Figure B.3. The results of the tensile coupon tests for all the batches of column steel used in the complete test programme showing the lower yield strength, the ultimate tensile strength and Young's modulus, are presented in Table B.2. Table B.3 provides a summary of the yield strengths together with British Steels own test certificates values which are shown to be generally 20 N/mm^2 higher than those tested. An explanation for the increased yield maybe through the use of a higher rate of strain applied to the specimen as previously observed by Galambos [96].

Steel batch	Face reference	Longitudinal Coupon tests (L)			Transverse Coupon tests (T)	
		Yield stress N/mm^2	UTS N/mm^2	Young's Modulus N/mm^2	Yield stress N/mm^2	UTS N/mm^2
1339	A	317	468	-	314	465
1339	B	312	459	202.8	313	453
1339	D1	322	467	199.7	313	469
1339	D2	317	466	196.6		
1339	D3	323	472	203.8		
	average	**318**	**466**	**200.7**	**313**	**462**
1338	A	302	454	202.3	282	454
1338	B	323	469	199.6	322	468
1338	D	313	462	201.5	300	460
	average	**313**	**462**	**201.1**	**301**	**461**
1712	A	343	475	208.1	324	471
1712	B	330	480	206.6	338	487
1712	D	336	481	200	326	481
	average	**336**	**479**	**204.9**	**329**	**480**
2096	A	305	455	207.1	303	455
2096	B	-	-	-	308	449
2096	D	308	448	207.8	300	448
	average	**307**	**452**	**207.5**	**304**	**451**
3325	A	347	486	209.7	336	479
3325	B	347	493	204.3	353	487
3325	D	344	488	202.6	342	486
	average	**346**	**489**	**205.5**	**344**	**484**
7041	A	-	466	208.7	307	461
7041	B	336	489	212.3	327	474
7041	D	322	475	211.7	319	476
	average	**329**	**477**	**210.9**	**318**	**470**
3012	A	426	554	204.9	422	548
3012	B	421	565	239	435	561
3012	D	434	562	206.1	429	559
	average	**427**	**560**	**216.7**	**429**	**556**

Table B2 Material properties of column steel

Test no.	Steel batch	Section	Grade	Yield		UTS[3]		Young's modulus
				(1) N/mm2	(2) N/mm2	(1) N/mm2	(2) N/mm2	kN/mm2
1	1338	200x200x8.0 SHS	S275	313	331	462	474	201.1
2	1338	200x200x8.0 SHS	S275	313	331	462	474	201.1
3	1338	200x200x8.0 SHS	S275	313	331	462	474	201.1
4	1338	200x200x8.0 SHS	S275	313	331	462	474	201.1
5	1339	200x200x8.0 SHS	S275	318	331	466	474	200.7
6	1339	200x200x8.0 SHS	S275	318	331	466	474	200.7
7	1712	200x200x6.3 SHS	S275	336	360	479	500	204.9
8	2096	200x200x12.5 SHS	S275	307	316	452	484	207.5
9	1339	200x200x8.0 SHS	S275	318	331	466	474	200.7
10	1339	200x200x8.0 SHS	S275	318	331	466	474	200.7
11	1712	200x200x6.3 SHS	S275	336	360	479	500	204.9
12	1712	200x200x6.3 SHS	S275	336	360	479	500	204.9
13	1712	200x200x6.3 SHS	S275	336	360	479	500	204.9
14	1338	200x200x8.0 SHS	S275	313	331	462	474	201.1
15	1339	200x200x8.0 SHS	S275	318	331	466	474	200.7
16	1712	200x200x6.3 SHS	S275	336	360	479	500	204.9
17	1339	200x200x8.0 SHS	S275	318	331	466	474	200.7
18	1338	200x200x8.0 SHS	S275	313	331	462	474	201.1
19	3325	200x200x8.0 SHS	S275	346	367	489	494	205.5
20	7041	200x200x10 SHS	S275	329	337	477	470	210.9
21	2096	200x200x12.5 SHS	S275	307	316	452	484	207.5
22	7041	200x200x10 SHS	S275	329	337	477	470	210.9
23	3012	200x200x10 SHS	S355	427	448	560	561	216.7
24	3012	200x200x10 SHS	S355	427	448	560	561	216.7
25	7041	200x200x10 SHS	S275	329	337	477	470	210.9
26	3325	200x200x8.0 SHS	S275	346	367	489	494	205.5
27	7041	200x200x10 SHS	S275	329	337	477	470	210.9
32a	3012	200x200x10 SHS	S355	427	448	560	561	216.7
32b	3012	200x200x10 SHS	S355	427	448	560	561	216.7
33	3012	200x200x10 SHS	S355	427	448	560	561	216.7

Notes (1) values obtained from coupon tests
(2) values from British steel test certificates
(3) UTS -Ultimate tensile strength

Table B3 Summary of longitudinal column properties for individual joint tests

During the manufacturing process of open sections, large residual stresses are developed of either a compressive or tensile nature, which vary over the cross section as a direct result of differential cooling. A way of accounting for the residual stresses and to provide a representative stress over the complete cross section is to conduct a stub column test. In the case of the hot rolled tubular member, residual stresses are not present to the same extent within the section due to its uniform profile that allows much more even cooling to develop. As a consequence, stub column tests were not conducted and the average tensile coupon results presented in Table B.3 are taken to be representative of the average yield strength of the cross-section.